

University of Alberta

The Phase Behavior of Asphaltene + Polystyrene + Toluene Mixtures at
293 K

by

Merouane Khammar

A thesis submitted to the Faculty of Graduate Studies and Research
in partial fulfillment of the requirements for the degree of

Doctor of Philosophy
in
Chemical and Materials Engineering

Department of Chemical and Materials Engineering

©Merouane Khammar
Spring 2011
Edmonton, Alberta

Permission is hereby granted to the University of Alberta Libraries to reproduce single copies of this thesis and to lend or sell such copies for private, scholarly or scientific research purposes only. Where the thesis is converted to, or otherwise made available in digital form, the University of Alberta will advise potential users of the thesis of these terms.

The author reserves all other publication and other rights in association with the copyright in the thesis and, except as herein before provided, neither the thesis nor any substantial portion thereof may be printed or otherwise reproduced in any material form whatsoever without the author's prior written permission.

Examining Committee

John M. Shaw, Chemical and Materials Engineering, University of Alberta

Murray R. Gray, Chemical and Materials Engineering, University of Alberta

Phillip Y. K. Choi, Chemical and Materials Engineering, University of Alberta

Hongbo Zeng, Chemical and Materials Engineering, University of Alberta

Rick Chalaturnyk, Civil and Environmental Engineering, University of Alberta

Jérôme Pauly, Laboratoire des Fluides Complexes et Leurs Reservoirs, Université
de Pau, France

Dedication

This thesis is dedicated to my parents Hassen and Malika, my brother Hichem, my sisters Wafaa and Habiba and to all my family.

Abstract

Polymers of various types are added to crude oils and oil products to prevent wax deposition, break water-in-oil emulsions, reduce drag in pipelines and to stabilize asphaltenes. In mixtures where a polymer does not adsorb on colloids, two stable liquid phases can arise due to depletion flocculation. Asphaltenes in heavy oils and toluene mixtures form sterically stabilized colloidal particles. In this work, the addition of a non-adsorbing polymer (polystyrene) to C₅ Maya asphaltene + toluene mixtures was investigated experimentally and theoretically. As concentrated asphaltene + toluene mixtures are opaque to visible light, phase volumes and compositions were detected using ultrasound. The sensors comprised two commercial 64 element phased-array acoustic probes. The operation of the view cell, and kinetic and equilibrium data processing procedures were validated using mixtures of methanol + alkanes. Acoustic speed and attenuation profiles were found to provide independent measures of phase separation. At equilibrium, acoustic speed profiles are uniform in each phase with a step change at the interface. Acoustic wave attenuation profiles exhibit a sharp peak/spike at liquid-liquid interfaces. Mixtures of asphaltenes + polystyrene + toluene are shown to exhibit liquid-liquid phase behavior over broad ranges of composition. This is the first report of liquid-liquid phase behavior for such mixtures. One phase is asphaltene rich and the other phase is polystyrene rich. Liquid-liquid critical

points were also identified along the liquid-liquid/liquid phase boundary for mixtures with two mean molar masses of polystyrene.

Compositions of co-existing phases were computed using phase volume variations along dilution lines [1], acoustic speed data and a mass balance model. A parameter was introduced to improve the agreement between calculated and experimental speeds of sound. The results of the model indicate that more than half of the asphaltenes, by volume, participate in the depletion flocculation process. Phase compositions were measured independently using UV-visible spectrophotometry. The nominal size of asphaltene colloidal particles participating in the phase separation mechanism was estimated by comparing calculated phase boundaries with the experimental phase diagram. The estimated size of asphaltene colloidal particles is in agreement with the expected size of asphaltenes in toluene mixtures obtained exogenously.

1. Bodnar, I. & Oosterbaan, W. (1997) Indirect determination of the composition of the coexisting phases in a demixed colloid polymer mixture. *Journal of Chemical Physics* 106, 7777-7780.

Aknowledgements

I would like to express my gratitude to my supervisor Prof. Shaw for giving me the opportunity to work on my PhD research project in the petroleum thermodynamics research laboratory and for his continious help, support and encouragements to develop and pursue new ideas. This work could not have been completed without those encouragements. I m also grateful for the time and the effort the members of the supervisory and examining committees have spent on reviewing this thesis. Gratitude is also extended to Dr. Masliyah and Dr. Xu for the insightful discussions.

I would like to thank my parents Hassen and Malika, my brother Hichem and my sisters Wafaa and Habiba for their continious and unlimited support. I would also like to thank all the friends who made the long experience of graduate school more manageable.

I would like to thank Mildred Becerra, our lab manager, Pat Ajas, Kevin Heidebrecht and the technicians Bob Smith, Dave Parlin, James Mckinnon, Clark Bicknell, Bob Barton and Jack Gibeau for their help throughout all the stages of this project and for their positive energy.

Table of Contents

1. Introduction

1.1. Background	1
1.1.1. Mixtures of colloids + non-adsorbing polymers	1
1.1.2. Colloidal nature of asphaltene and the effect of polymer addition	2
1.2. Thesis outline.....	3
References.....	3

2. Literature Review

2.1. Asphaltenes as colloids.....	6
2.2. Chemical and polymeric additions to asphaltene solutions.....	8
2.3. Phase behaviour of polymer + polystyrene mixtures and phase separation by depletion flocculation.....	9
2.4. Mixtures of colloidal particles + non-adsorbing polymers.....	12
2.4.1. Phase separation by depletion flocculation and the free volume fraction...	13
2.4.2. Thermodynamic model for a mixture of mono-dispersed colloidal particles + non-adsorbing polymer.....	15
2.4.2.1. Phase diagram calculation.....	15
2.4.2.2. Effect of polymer radius of gyration and colloidal particle size on the predicted phase diagram.....	18
2.4.2.3. Comparison between predicted and experimental critical points.....	20
2.4.3. Experimental determination of phase composition.....	22
2.4.4. Experimental measurements of phase separation for mixtures of colloidal particles + polystyrene + toluene.....	28
2.5. Objective.....	30
References.....	32

3. Phase Behaviour and Phase Separation Kinetics Measurement

Using Acoustic Arrays

3.1. Introduction	35
3.2. Experimental methodology	36

3.2.1. Experimental apparatus	36
3.2.2. Measurement methodology and calibration.....	38
3.2.3. Materials.....	43
3.3. Results and discussion.....	44
3.3.1. Acoustic measurements of liquid-liquid separation in organic mixtures.....	44
3.3.1.1. Speed of sound vs composition	44
3.3.1.2. Acoustic property profiles and the kinetics of phase separation in liquid mixtures.....	46
3.3.2. Acoustic measurements in porous media	50
3.3.3. Two dimensional acoustic mapping.....	50
References.....	52
4. Phase Behavior of Asphaltenes + Polystyrene + Toluene	
Mixtures at 293 K, Part One: Results and Discussion	
4.1. Introduction.....	54
4.2. Experimental methodology.....	57
4.2.1. Chemicals and solution preparation.....	57
4.2.2 Experimental apparatus and measurements.....	57
4.3. Dependence of the speed of sound and acoustic wave attenuation on the volume fraction of asphaltenes and polystyrene in toluene.....	59
4.4. Results and discussion.....	64
4.4.1. Effect of adding a solution of polystyrene in toluene to a mixture of asphaltene in toluene.....	64
4.4.2. Reproducibility of phase separation.....	71
4.4.3. Effect of adding toluene to a mixture of asphaltene + polystyrene + toluene.....	75
4.4.4. Phase separation kinetics.....	79
4.5. UV-Visible spectrophotometry measurements of asphaltene composition in the separated phases.....	84
4.6. Conclusions.....	88
References.....	90

5. Phase Behavior of Asphaltenes + Polystyrene + Toluene Mixtures at 293 K, Part Two: Data Analysis	
5.1. Introduction.....	92
5.2. Evaluation of binodal compositions.....	94
5.2.1. Phase volume, mass balance and UV spectrophometry data.....	94
5.2.2. Speed of sound data and the fraction of asphaltenes participating in the phase separation mechanism.....	97
5.2.3. Comparison between experimental phase boundaries, critical points and the depletion flocculation theory.....	114
5.3. Conclusion.....	119
References.....	122
6. Conclusions and Recommendations	
6.1. Phased array acoustic cell.....	124
6.2. Measurements of phase behaviour of mixtures of asphaltene + polystyrene + toluene.....	125
6.3. Future work and recommendations.....	127
References.....	128
Appendix A. Acoustic Measurements of Mixtures of Asphaltene + Polystyrene + Toluene.....	130
A.1. Measurements of mixtures of asphaltene + polystyrene (M _w =393,400 g/mol) + toluene.....	130
A.2. Measurements of mixtures of asphaltene + polystyrene (M _w =700,000 g/mol) + toluene.....	144
Appendix B. Calculation of Asphaltene and Polystyrene Volume Fractions in The Separated Phases.....	158
Appendix C. Linear Fit Plots of Speed of Sound vs Concentration in the Binary Mixtures of Asphaltene + Toluene and Polystyrene + Toluene.....	160
Appendix D. Scaling Geometric Transformation of Dilution Lines p, q and r and the Tie Line $[\alpha \beta]$.....	162

Appendix E. Matlab Code for the Calculation of Speed of Sound and Attenuation Spectra Profiles from Recorded Waveforms.....	166
Appendix F. Matlab Code for the Calculation of the Composition and the Speeds of Sound in the Separated Phases.....	178
Appendix G. Matlab Code for the Calculation of the Phase Diagram of Colloidal Particles + non-adsorbing Polymer.....	210

List of Tables

Table 2.1. Comparison between experimental and theoretical critical points performed by Fleer et al.....	21
Table 4.1. Coefficients A_i and standard deviation σ of equation (4.3).....	62
Table 4.2. Effect of adding polystyrene in toluene to asphaltene in toluene Experimental data for mixtures (a-e) of asphaltene + polystyrene ($M_w=393,400$ g/mol) + toluene. Composition, speed of sound per phase, liquid-liquid interface elevation and volume fraction of the upper phase.....	65
Table 4.3. Experimental repeatability measurements of phase separation for mixture (d) for four successive mixings. Composition, speed of sound per phase, liquid-liquid interface elevation and volume fraction of the upper phase.....	65
Table 4.4. Experimental data for a mixture of asphaltene + polystyrene ($M_w=393,400$ g/mol) + toluene. Composition, speed of sound per phase, liquid-liquid interface elevation and volume fraction of the upper phase.....	66
Table 4.5. Experimental data for a mixture of asphaltene + polystyrene ($M_w=700,000$ g/mol) + toluene. Composition, speed of sound per phase, liquid-liquid interface elevation and volume fraction of the upper phase.....	67
Table 5.1. Values of the parameters B_i in equation (5.1) and the standard deviation σ	99
Table 5.2. Numerically calculated critical points using Fleer et al. model with two versions: polymers in good solvent and polymer in theta solvent.....	116

List of Figures

Figure 2.1. Schematic of a microgel particle in good solvent.....	10
Figure 2.2. Depletion flocculation mechanism.....	11
Figure 2.3. Diagram of a mixture of colloid + non-adsorbing polymer separating into colloid rich (phase I, L) and colloid poor (phase II, G) phases.....	13
Figure 2.4. Phase diagram of a colloid-polymer mixture for $q_R=1$ and $y_i=\Phi/\varphi_{ov}$	18
Figure 2.5.a. Numerical results of Fleer et al model extracted numerically for normalized colloidal particle volume fractions at the critical point and the triple points as a function of \tilde{q}_R^{-1}	19
Figure 2.5.b. Normalized polymer volume fractions $\tilde{\phi}_c$ and $\tilde{\phi}_t$, as a function of $\tilde{q}_R = q_R/0.388$ for a polymer in a good solvent, on a double-logarithmic scale.....	20
Figure 2.6. Binodal points for the ternary γ S+PEG1450+water system.....	23
Figure 2.7.a. Schematic representation of the binodal, dilution lines p, q and r and the intersections P, Q and R with a tie line in a phase diagram where the polymer volume fraction Φ is plotted against the colloid volume fraction η	24
Figure 2.7.b. Schematic representation of two tie lines $[\alpha \beta]$ and $[\alpha' \beta']$ with different slopes and lengths in a phase diagram where the polymer volume fraction Φ is plotted against the colloid volume fraction η	25
Figure 2.8. (a) Experimental variations of the upper phase volume fraction along the dilution lines, (b) binodal points extracted numerically from Bodnar et al.....	29
Figure 2.9. (a) Variations of the upper phase volume fraction along the dilution lines (b) Experimental phase diagram (extracted numerically) from Hennequin et al[33] for a mixture of silica nanoparticles ($a=42.4$ nm) + polystyrene ($M_w=8.5 \cdot 10^6$ g/mol):.....	31
Figure 3.1. Schematic views of the acoustic cell.....	37

Figure 3.2. Volume vs elevation calibration. Solid line: apparent elevation measured acoustically. Dotted line: elevation from the bottom of cell.....	39
Figure 3.3. Reflected waveform in toluene at 25 C and $z=18.5$ mm.....	39
Figure 3.4. Truncated reflected waveforms of the first and second reflected waveforms measured in toluene at 25 C: (---) $p_1(t)$, (—) $p_2(t)$	41
Figure 3.5. Autocorrelation function of an acoustic waveform in toluene at $T=25$ C and $z=18.5$ mm.....	41
Figure 3.6. Acoustic path length vs elevation based on speed of sound measurements in toluene at 25 C.....	42
Figure 3.7. Frequency spectra for the first and second reflection waveforms in toluene at 25 C and $z=18.5$ mm: (---) $\tilde{p}_1(f)$, (—) $\tilde{p}_2(f)$	42
Figure 3.8. (a) Preparation of a synthetic porous block partially saturated with bitumen. (b) Porous block immersed in heptane inside the cell during acoustic measurements.....	44
Figure 3.9.a. Speed of sound in methanol+ heptane mixtures at 25 C and 1.0 atm.....	45
Figure 3.9.b. Speed of sound in methanol+ mixed hexanes at 25 C and 1.0 atm.....	45
Figure 3.10. Evolution of speed of sound and attenuation profiles for 38.7 vol.% methanol in mixed hexanes during phase separation at 25 C and 1.0 atm.....	48
Figure 3.11. Equilibrium speed of sound and attenuation profiles for methanol in mixed hexanes: (a) 26.3% vol. methanol, (b) 38.7% vol. methanol (c) 49.7% vol. methanol.....	49
Figure 3.12. Travel time difference profiles at 22.5 C and 1 atm.....	51
Figure 4.1. Experimental variation of mixture composition in the phase diagram.....	58
Figure 4.2. Speed of sound profiles in asphaltene + toluene mixtures at 20 C and 1.0 atm. Asphaltene volume fraction is a parameter.....	59
Figure 4.3. Speed of sound profiles in toluene + polystyrene mixtures at 20 C and 1.0 atm. Polymer volume fraction is a parameter. (a) $M_w=393,400$ g/mol, (b) $M_w=700,000$ g/mol.....	60

Figure 4.4. Experimental speed of sound data and fitting equation (4.3) at 20 C and 1.0 atm in the binary mixtures: (a) asphaltene + toluene, (b) polystyrene ($M_w=393,400$ g/mol) + toluene, (c) polystyrene ($M_w=700,000$ g/mol) + toluene.....	63
Figure 4.5.a. Phase diagram and dilution lines p, q and r for mixtures of asphaltenes + polystyrene ($M_w=393,400$ g/mol) + toluene.....	68
Figure 4.5.b. Phase diagram and dilution lines p, q and r for mixtures of asphaltenes + polystyrene ($M_w=700,000$ g/mol) + toluene.....	68
Figure 4.6. Speed of sound profiles (i) acoustic wave attenuation spectra difference and (ii) attenuation difference at 7.9 MHz, at final times given in Table 4.1, and for global compositions (a-e) shown in Figure 4.5.a	69
Figure 4.7. (i) Evolution of the liquid-liquid, liquid-air interfaces and (ii) speed of sound per phase, (iii) speed of sound difference between the separated phases with time for global compositions (b-e) shown in Figure 4.5.a.....	70
Figure 4.8. Liquid-liquid interface elevation (i), volume fraction of the upper phase (ii), speed of sound difference between the coexisting phases (iii) for global compositions (b-e) shown in Figure 4.5.a	72
Figure 4.9. Reproducibility of phase separation at final time for a mixture (d) with composition: $\eta=10.7$ vol%, $\Phi=4.2$ vol%.....	73
Figure 4.10. (i) Variation with time of the liquid-liquid and liquid-air interfaces (ii) speed of sound per phase, (iii) speed of sound difference between the separated phases for mixture (d) after successive mixings	74
Figure 4.11. Effect of dilution on the phase separation for mixtures of asphaltenes + polystyrene ($M_w =393,400$ g/mol) + toluene.....	76
Figure 4.12. Effect of dilution on the phase separation for mixtures of asphaltenes+polystyrene($M_w =700,000$ g/mol)+toluene.....	78
Figure 4.13. Measurement of phase separation kinetics for a mixture of asphaltene + polystyrene ($M_w=393,400$ g/mol) + toluene ($\eta=14.78$ vol%, $\Phi=2.84$ vol%).....	81
Figure 4.14. (i) Variation with time of the liquid-liquid and liquid-air Interfaces, (ii) the speed of sound per phase, (iii) the speed of sound difference between the separated phases after phase separation for a mixture of asphaltene + polystyrene ($M_w=393,400$ g/mol) + toluene ($\eta=14.78$ vol%, $\Phi=2.84$ vol%)	83

Figure 4.15. Experimental phase separation results for a mixture with global composition ($\eta=14.72$ vol%, $\phi=2.88$ vol%).....	84
Figure 4.16. (a) Absorbance spectra in pure toluene, polystyrene in toluene solution and different asphaltene in toluene solutions, (b) absorbance spectra in diluted lower and upper phases.....	86
Figure 4.17. Absorbance difference between asphaltene in toluene solutions and pure toluene at a wavelength of 700 nm vs asphaltene concentration.....	87
Figure 4.18. Phase diagram for mixtures of asphaltenes + polystyrene + toluene with estimated phase boundaries and critical point : (a) $M_w=393,400$ g/mol, (b) $M_w=700,000$ g/mol.....	89
Figure 5.1. Variations of the upper phase volume fraction along dilution lines p,q and r for mixtures of asphaltene + polystyrene + toluene: (a) polystyrene molecular weight $M_w=393,400$ g/mol, (b) polystyrene molecular weight $M_w=700,000$ g/mol.	95
Figure 5.2. Experimental phase diagram for mixtures of asphaltene + polystyrene + toluene: (a) polystyrene molecular weight of 393,400 g/mol (b) polystyrene molecular weight of 700,000 g/mol.....	96
Figure 5.3. Parity plot for calculated speed of sound from equation 5.4 vs measured speed of sound.....	100
Figure 5.4. Comparison between calculated and experimental speeds of sound, after phase separation for mixtures of asphaltenes + polystyrene ($M_w=393,400$ g/mol) + toluene.....	101
Figure 5.5. Comparison between calculated and experimental speeds of sound after phase separation for mixtures of asphaltenes + polystyrene ($M_w=700,000$ g/mol) + toluene.....	102
Figure 5.6. Schematic presentation of the effect of γ on the tie line [I II] and dilution lines p, q and r.....	105
Figure 5.7. (a) Calculated and experimental speed of sound difference values vs asphaltene global composition. (x): Calculated speed of sound difference using experimental phase composition for a mixture with global composition composition ($\eta=14.7$ vol%, $\phi=2.9$ vol%), (b) calculated volume fraction difference of asphaltenes between phases vs global asphaltene composition. γ is a parameter. Polystyrene molecular weight $M_w=393,400$ g/mol.....	107
Figure 5.8. (a) Calculated and experimental speed of sound difference values vs asphaltene global composition, (b) calculated volume fraction difference of asphaltenes between phases vs global asphaltene composition. γ is a parameter. Polystyrene molecular weight $M_w=700,000$ g/mol.....	108

Figure 5.9. Comparison between calculated and experimental speeds of sound for $\gamma=0.63$, after phase separation along: (a) dilution lines p, (b) dilution line q, (c) dilution line r for mixtures of asphaltenes + polystyrene ($M_w=393,400$ g/mol) + toluene.....	110
Figure 5.10. Comparison between calculated and experimental speeds of sound for $\gamma=0.49$, after phase separation along: (a) dilution lines p, (b) dilution line q, (c) dilution line r for mixtures of asphaltenes + polystyrene ($M_w=700,000$ g/mol) + toluene.....	111
Figure 5.11. Composition of the separated phases in equilibrium (η_I, ϕ_I), (η_{II}, ϕ_{II}) for a mixture of asphaltenes + polystyrene ($M_w=393,400$ g/mol) + toluene and $\gamma=0.63$ with global composition (η, ϕ) moving along: (a) dilution line p, (b) dilution line q, (c) dilution line r.....	112
Figure 5.12. Composition of the separated phases in equilibrium (η_I, ϕ_I), (η_{II}, ϕ_{II}) for a mixture of asphaltenes + polystyrene ($M_w=700,000$ g/mol) + toluene and $\gamma=0.49$ with global composition (η, ϕ) moving along: (a) dilution line p, (b) dilution line q, (c) dilution line r.....	113
Figure 5.13. Experimental phase diagram for mixtures of asphaltene + polystyrene + toluene presented on the coordinates (η^*, ϕ): (a) for: $\gamma=0.63$ and a polystyrene molecular weight of 393,400 g/mol (b) for: $\gamma=0.49$ and a polystyrene molecular weight of 700,000 g/mol.....	115
Figure 5.14. Variations of the calculated critical point with decreasing particle radius. Values are given in Table 5.2. (a) mixtures with a polystyrene molecular weight of 393,400 g/mol. (b) mixtures with a polystyrene molecular weight of 700,000 g/mol. (c) comparison between mixtures with polystyrene molecular weight of 393,400 g/mol, and 700,000 g/mol. Calculations were performed for polymers in good solvent	117
Figure 5.15. Calculated phase diagram vs experimental phase diagram for mixtures of asphaltene colloidal particles+polystyrene ($M_w=393,400$ g/mol) + toluene and for two radii of asphaltene colloidal particles: (a) $a=6.4$ nm, (b) $a=23.5$ nm.....	120
Figure 5.16. Calculated phase diagram vs experimental phase diagram for mixtures of asphaltene colloidal particles + polystyrene ($M_w=700,000$ g/mol) + toluene and for two radii of asphaltene colloidal particles: (a) $a=7.0$ nm, (b) $a=26.0$ nm.....	121

Nomenclature

Symbols

ΔG_m	Gibbs free energy of mixing (J)
R	constant of perfect gas ($J/mol.K$)
T	Temperature (K) or the duration of the reflected pulse (μs)
n_i	number of moles of component i
m_i	the ratio of molar volume of component i to the molar volume of a reference component i to the molar volume of a reference component.
χ_{ij}	Flory-Huggins interaction parameter between component i and j
Φ_i	volume fraction of component i
Φ	volume fraction of the polymer
α	free volume fraction, or symbol for upper phase
β	function defined in equation (2.4), or symbol for lower phase
φ	volume fraction of the polymer in the free volume
φ_{ov}	overlap volume fraction of the polymer in the free volume
η	colloid, or asphaltene, volume fraction
a	colloidal particle radius (nm)
δ	depletion layer (nm)
q	ratio of depletion thickness over particle radius ($q=\delta/a$)
R_g	polymer radius of gyration (nm)
M_w	polymer molecular weight (g/mol)
N_A	Avogadro number
ρ_{polyst}	polystyrene density (g/ml)
(pv)	product of pressure \times particle volume, the product (pv) is in units of kT , where k is the Boltzmann constant
μ	colloid chemical potential ($kT/particle$)

n	slope of the tie line
l	length of the tie line
z	position along the elevation of the cell (mm)
t	time (μs)
$p(z,t)$	reflected waveform at elevation z
$p_1^{Echo}(z,t)$	first reflected pulse at elevation z
$p_2^{Echo}(z,t)$	second reflected pulse at elevation z
Δt	time difference between the first and second reflected waveform (μs)
C_p	autocorrelation function
$l(z)$	acoustic path distance at elevation z
$u(z)$	speed of sound (m/s) at elevation z
$\tilde{p}_1^{Echo}(z,t)$	Fourier transform of the first reflected waveform $p_1^{Echo}(z,t)$
$\tilde{p}_2^{Echo}(z,t)$	Fourier transform of the second reflected waveform $p_2^{Echo}(z,t)$
f	$f = \eta / (1 - \eta)$ defined in equation (2.6) and frequency (MHz) in Chapter 3
$A(z,f)$	attenuation at elevation z and frequency f
σ	standard deviation defined in equation (4.2)
A_i	correlation coefficients used in the speed of sound equation (4.3) and defined in Table 4.1.
$H_{interface}$	liquid-liquid interface elevation (mm)
R	volume fraction of the upper phase
Δu	speed of sound difference between the separated phases (m/s)
B_i	parameters used in equation (5.4) and defined in Table 5.1
η^*	volume fraction of asphaltene colloidal particles in Chapter 5 participating in the phase separation mechanism
η^0	volume fraction of asphaltenes that are too small to participate in the phase separation

γ exponent used in equations (2.8.a-b) and (2.17) and the fraction of asphaltene colloidal particles causing phase separation defined in equation (5.6)

Subscripts and superscripts

* value at the critical endpoint in Chapter 2 and asphaltene colloidal particles participating in the phase separation in Chapter 5

0 hard sphere contribution to the chemical potential and (pv) in Chapter 2 and the fraction of asphaltene that are too small to participate in the phase separation mechanism in Chapter 5

p polymer contribution to the chemical potential and (pv)

f colloidal fluid phase

s colloidal solid phase

g colloidal gas phase

l colloidal liquid phase

c critical point

t triple point

1 first derivative with respect to $f = \eta / (1 - \eta)$

2 second derivative with respect to $f = \eta / (1 - \eta)$

ov overlap

I, II lower and upper phases

exp experimental

cal calculated

$asph$ asphaltene

$polyst$ polystyrene

tol toluene

CHAPTER 1. Introduction

1.1. Background

1.1.1. Mixtures of colloids + non-adsorbing polymers

Colloids and polymers coexist in many biological and industrial mixtures. Examples can be found in living cells [1] [2], food products [3] and paint and ink [4]. The phase behavior of these mixtures depends on the concentration and interactions between the colloidal particles and the polymer. In mixtures of colloids + non-adsorbing polymers, an attractive force is induced between the colloidal particles. The attraction is caused by an unbalanced osmotic pressure [5] [6]. The range and strength of the attractive forces can be tuned by varying the molecular weight and the volume fraction of the polymer. When the attraction is strong enough, the mixture can separate into coexisting colloid rich and colloid poor liquid phases. The colloid rich phase can be either liquid-like or solid-like [7]. The mechanism causing phase separation in such mixtures is called “depletion flocculation”.

A large number of experimental investigations for the phase behavior of colloids + non-adsorbing polymer mixtures can be found in the literature. These include, water-in-oil microemulsion + polyisoprene [8], F actin (cylindrical protein) + polyethylene glycol (PEG) [9] and spherical protein (nanoparticle) + polyethylene glycol (PEG) [10]. Phase separation by depletion flocculation was also measured in mixtures of cross-linked swollen polystyrene–microgel-particles + linear polystyrene in toluene [11] and ethybenzene [12] and in mixtures of silica particles sterically stabilized with C₁₈ alcohol + polystyrene in toluene [13] [14].

1.1.2. Colloidal nature of asphaltene and the effect of polymer addition

Asphaltenes are another example of colloidal particles that are sterically stabilized in toluene [15]. More broadly, variations of pressure, temperature and composition in crude oil can result in asphaltene deposition [18] and can cause significant problems in oil production, transport and refining [19]. The colloidal nature of asphaltenes has been investigated by several authors. Their size and shape have been studied using a variety of experimental techniques [16] [17].

Polymers have been used extensively in the oil industry as additives to solve problems affecting oil production [20]. For example, they are used for viscosification, drag reduction in turbulent flows in pipelines, prevention of wax deposition at temperatures below the WAT (wax appearance temperature), breaking water in oil emulsions and stabilization of asphaltenes. Recent investigations focused on the effect of adding adsorbing polymers to asphaltene + toluene mixtures to cause flocculation [21], or to delay sedimentation [22].

The effect of adding a non-adsorbing polymer to asphaltene + toluene mixtures has not been investigated systematically in the past. Potential applications of depletion flocculation induced phenomena in the hydrocarbon production transport and refining sectors appear to have been overlooked. As asphaltenes form sterically stabilized colloidal particles, the addition of a non-adsorbing polymer should induce liquid-liquid phase behavior. The investigation of such phase behavior can provide new insights and new opportunities for using polymers in hydrocarbon production, transport and refining. The challenges in this investigation are both experimental and conceptual because detection of liquid-liquid phase behavior, experimentally, for such mixtures is not certain, and because asphaltenes themselves are so poorly defined.

1.2. Thesis outline

Following this introduction, the colloidal nature of asphaltenes, and phase behavior investigations of mixtures of colloids + non-adsorbing polymers are reviewed in Chapter 2. The experimental approach and apparatus, together with examples of acoustic measurements in liquid mixtures and porous media, are presented in Chapter 3. Results and data analysis related to the phase behavior of asphaltene + polystyrene + toluene mixtures are presented in Chapters 4-5. Modeled vs experimental phase compositions are compared in Chapter 5. Finally, conclusions and recommendations are presented in Chapter 6.

References

1. Zimmerman, S. & Minton, A. (1993) Macromolecular Crowding - Biochemical, Biophysical, and Physiological Consequences. *Annual Review of Biophysics and Biomolecular Structures* 22, 27-65.
2. Neu, B., Wenby, R., & Meiselman, H. J. (2008) Effects of dextran molecular weight on red blood cell aggregation. *Biophysical Journal* 95, 3059-3065.
3. Doublier, J., Garnier, C., Renard, D., & Sanchez, C. (2000) Protein-polysaccharide interactions. *Current Opinion in Colloid & Interface Science* 5, 202-214.
4. Hughes, D., Robb, I., & Dowding, P. (1999) Stability of copper phthalocyanine dispersions in organic media. *Langmuir* 15, 5227-5231.
5. Asakura, S. & Oosawa, F. (1954) On Interaction between 2 Bodies Immersed in a Solution of Macromolecules. *Journal of Chemical Physics* 22, 1255-1256.
6. Asakura, S. & Oosawa, F. (1958) Interaction Between Particles Suspended in Solutions of Macromolecules. *Journal of Polymer Science* 33, 183-192.
7. Fler, G. J. & Tuinier, R. (2008) Analytical phase diagrams for colloids and non-adsorbing polymer. *Advances in Colloid and Interface Science* 143, 1-47.

8. Mutch, K. J., van Duijneveldt, J. S., Eastoe, J., Grillo, I., & Heenan, R. K. (2008) Small-angle neutron scattering study of microemulsion-polymer mixtures in the protein limit. *Langmuir* 24, 3053-3060.
9. Hosek, M. & Tang, J. (2004) Polymer-induced bundling of F actin and the depletion force. *Physical Review E* 69.
10. Tanaka, S. & Ataka, M. (2002) Protein crystallization induced by polyethylene glycol: A model study using apoferritin. *Journal of Chemical Physics* 117, 3504-3510.
11. Sieglaff, C. (1959) Phase Separation in Mixed Polymer Solutions. *Journal of Polymer Science* 41, 319-326.
12. Clarke, J. & Vincent, B. (1981) Stability of non-aqueous microgel dispersions in the presence of free polymer. *Journal of the Chemical Society - Faraday Transactions I* 77, 1831-1843.
13. Ramakrishnan, S., Fuchs, M., Schweizer, K. S., & Zukoski, C. F. (2002) Entropy driven phase transitions in colloid-polymer suspensions: Tests of depletion theories. *Journal of Chemical Physics* 116, 2201-2212.
14. Hennequin, Y., Evens, M., Angulo, C., & van Duijneveldt, J. (2005) Miscibility of small colloidal spheres with large polymers in good solvent. *Journal of Chemical Physics* 123.
15. Mullins, O. C. (2010) The Modified Yen Model. *Energy & Fuels* 24, 2179-2207.
16. Mostowfi, F., Indo, K., Mullins, O. C., & McFarlane, R. (2009) Asphaltene Nanoaggregates Studied by Centrifugation. *Energy & Fuels* 23, 1194-1200.
17. Barre, L., Simon, S., & Palermo, T. (2008) Solution properties of asphaltenes. *langmuir* 24, 3709-3717.
18. Branco, V., Mansoori, G., Xavier, L., Park, S., & Manafi, H. (2001) Asphaltene flocculation and collapse from petroleum fluids. *Journal of Petroleum Science and Engineering* 32, 217-230.
19. Mullins, O. C. (2007) Asphaltenes, heavy oils, and petroleomics.
20. Lucas, E. F., Mansur, C. R. E., Spinelli, L., & Queiros, Y. G. C. (2009)

Polymer science applied to petroleum production. *Pure and Applied Chemistry* 81, 473-494.

21. Lima, A. F., Mansur, C. R. E., Lucas, E. F., & Gonzalez, G. (2010) Polycardanol or Sulfonated Polystyrene as Flocculants for Asphaltene Dispersions. *Energy & Fuels* 24, 2369-2375.

22. Hashmi, S. M., Quintiliano, L. A., & Firoozabadi, A. (2010) Polymeric Dispersants Delay Sedimentation in Colloidal Asphaltene Suspensions. *langmuir* 26, 8021-8029.

CHAPTER 2. Literature Review

2.1. Asphaltenes as Colloids

Asphaltenes are a fraction of oil deemed as insoluble in alkanes and soluble in benzene and toluene on the basis of filtration measurements (ASTM D4055). In toluene, asphaltenes aggregate and are thought to form colloidal particles similar to hairy tennis balls. The concentration at which the nanoaggregates stop growing is called “the critical nanoaggregate concentration” (CNAC). The CNAC was measured using different experimental techniques: high-Q ultrasonics [1] [2], DC-conductivity [3], centrifugation [4] and NMR hydrogen index measurements [5]. Reported values range from 50 to 200 mg/L. In toluene mixtures, the interactions between asphaltene colloidal particles are dominated by steric repulsive forces [6].

The colloidal state of asphaltenes in toluene has been the subject of several investigations. Rheological, centrifugation and SAXS measurements have been performed to characterize the size and shape of asphaltene aggregates in toluene [4] [7] [8] [9]. Mostowfi et al. [4] performed a centrifugation investigation of a solution of asphaltene in toluene with a concentration of 250 mg/l. They found that the diameter of asphaltenes ranged from less than 1.5 nm up to 10 nm. They attributed the lower bound to molecules and the upper bound to the largest aggregates present. At concentrations of several grams per liter, asphaltenes form larger aggregates. For example, at 3 % vol asphaltenes in toluene, the radius of gyration of the aggregates was found to fall in the range 6-16 nm [8]. Espinat et

al. [7] measured the size of asphaltenes in toluene using small-angle X-ray scattering (SAXS), small-angle neutron scattering (SANS) and dynamic light scattering to investigate the effect of temperature and pressure on the size of asphaltene aggregates in toluene. They found that their size decreased with temperature while pressure did not appear to have a significant effect. Zhao et al. [10] performed ultrafiltration studies of Maya crude oil (16 %w asphaltenes) at 473 K. They found that the amount of asphaltene retained depended on the filter pore size. 50 wt % of the asphaltenes passed through a 20 nm ceramic filter and 10 wt % passed through a 5 nm ceramic filter. None of the aggregates appeared to be greater than 100 nm. Ching et al. [11] performed nanofiltration experiments using Gore-Tex Teflon filters with a nominal pore size of 30 nm. Conventional crude oils containing up to 7.6 w% asphaltenes were filtered at 80 C, and toluene mixtures containing up to 15 g/L asphaltenes were filtered at room temperature. No retentates were observed for any of these cases. The viscosities of the crude oils before and after filtration were found to be the same. It was concluded that the size of asphaltene colloidal particles was below the 30 nm nominal pore size of the filter for the concentration range investigated. It was also suggested that the size of asphaltene colloidal particles could be larger in heavy oils and concentrated solutions of asphaltene in toluene. These prior results suggest that the size distribution of asphaltene colloidal particles in both crude oils and concentrated toluene solutions is bounded with nominal sizes ranging from ~ 1.5 to ~ 100 nm.

Phase separation methods for asphaltenes include: ultracentrifugation, variation of pressure, temperature, solvent evaporation and addition of antisolvent (alkane) [12] [13]. Phase separation in colloidal mixtures could also be achieved by adding a polymer[13]. In the following sections, the effect of adding polymers to asphaltene and colloidal solutions is discussed.

2.2. Chemical and polymeric additions to asphaltene solutions

Polymers are used in asphaltene solutions to prevent deposition and delay asphaltene sedimentation. Hashemi et al. [14] investigated the effect of adding alkylated phenol (4F) and polyolefin amide alkeneamine (AG) polymeric dispersants on asphaltene sedimentation in mixtures of oil + heptane. The delay in sedimentation was attributed to a decrease in asphaltene particle size and a change in asphaltene interparticle interactions. Chang et al. [15] investigated the effect of adding alkylbenzene-derived amphiphiles on asphaltene stability in alkane solvents. It was found that increasing the polarity of the amphiphile head group strengthens the attraction of amphiphiles to asphaltenes and therefore improves asphaltene stabilization. An amphiphile without a polar group (nonylbenzene) did not have any effect on asphaltene stability because the benzene group could not associate with it.

Recently, Lima et al [16] studied the flocculation of asphaltenes in organic solvents induced by polymeric compounds. It was suggested that the most suitable polymers contain polar groups that can associate with asphaltenes. Two sets of polymers were investigated: Polycardanol with different molar masses and sulfonated polystyrene with various degrees of sulfonation. It was shown that both sets of polymers behave as flocculants at low concentrations and as dispersants at higher concentrations. This was attributed to the relative amount of polymer polar groups available for association with asphaltene polar groups. Increasing polymer concentration increased the number of asphaltene-polymer interactions which initially increased the number of asphaltene aggregates associated to the polymer but a large number of asphaltene – polymer association was thought to cause less asphaltene-asphaltene association and therefore less aggregates were susceptible to flocculate. It was reported that polystyrene without polar groups did not modify asphaltene behaviour in dilute solutions [16]. This result from the literature is different from the anticipated behavior for the impact of a non-adsorbing polymer (polystyrene) in a good solvent (toluene) [17][18] on concentrated sterically

stabilized colloidal particles (asphaltenes) [6]. The result may reflect the dilute composition range investigated.

2.3. Phase behaviour of polymer + polystyrene mixtures and phase separation by depletion flocculation

Mixtures of polymer + polystyrene + toluene, where toluene is a good solvent for both polymers, can be fully miscible or can exhibit phase separation. Examples of fully miscible and partially miscible mixtures are poly(vinyl methyl ether) + polystyrene + toluene [19] and polybutadiene + polystyrene + toluene [20] respectively. The phase behavior of polymer + polystyrene + toluene depends both on the thermodynamic compatibility between the polymers and the solvent affinity for them [21]. According to Flory Huggins theory, the Gibbs free energy of mixing in a ternary mixture of two unlike polymers and a solvent is given by [20]:

$$\frac{\Delta G_m}{RT} = n_1 \ln \phi_1 + n_2 \ln \phi_2 + n_3 \ln \phi_3 + (\chi_{12} \phi_1 \phi_2 + \chi_{13} \phi_1 \phi_3 + \chi_{23} \phi_2 \phi_3) (m_1 n_1 + m_2 n_2 + m_3 n_3) \quad (2.1)$$

where: n_i is the number of moles of component i , m_i is the ratio of molar volume of component i to the molar volume of a reference component, χ_{ij} is the Flory-Huggins interaction parameter.

The above equation was derived for cases where polymer molecules overlap one another extensively [22] [24]. The first three terms in the right hand side of equation (2.1) represent the entropic contribution to the free energy of mixing and the remaining terms represent the enthalpy of mixing. For the case where the solvent is equally good for both polymers, ($\chi_{12} \approx \chi_{13} < 0.5$), the mixture separates when the binary interaction parameter exceeds a critical value: $\chi_{23} > \chi_{crit}$ [22]. In this case, phase separation is caused by the repulsion between unlike polymers. The enthalpy of mixing is positive and the mixture separates to reduce the free energy.



Figure 2.1. Schematic of a microgel particle in good solvent [23]

Phase separation in mixtures of polymer + polystyrene + toluene can be driven by entropic effects. For example, Seiglaflaff et al. [24] found that when the polymer added to polystyrene in toluene is a cross-linked polystyrene swollen particle, microgel particle [23] (Fig.2.1), the mixture separates into two phases. In this case, phase separation is attributed to entropy effects and not to the repulsion between unlike polymers. A mixture of polystyrene microgel swollen particle + polystyrene + ethyl-benzene behaves similarly [25] [26].

The mechanism driving phase separation for these mixtures is depletion flocculation, a mechanism first described by Asakura and Oosawa [27] [28]. The microgel polystyrene particles are assumed to be sufficiently cross-linked to prevent penetration by the linear polymer chains. In this case, the configurations for which the polymer penetrates the microgel particle are excluded. Effectively, the linear polymer is excluded from a depletion layer around each particle (Fig.2.2.a.i-ii). This layer generates a uniform osmotic pressure as shown in Figure 2.2.b.i. When two depletion layers overlap, the osmotic pressure around the particles becomes unbalanced giving rise to a net attractive force (Fig.2.2.b.ii). The resulting interaction potential between two colloidal particles is shown in Figure 2.2.c.i. The range of the attraction potential is proportional to the depletion thickness where its depth is proportional to the osmotic pressure and the overlap volume. At a sufficiently high polymer concentration, the mixture separates into colloid-poor and colloid-rich stable phases (Fig.2.2.c.ii).

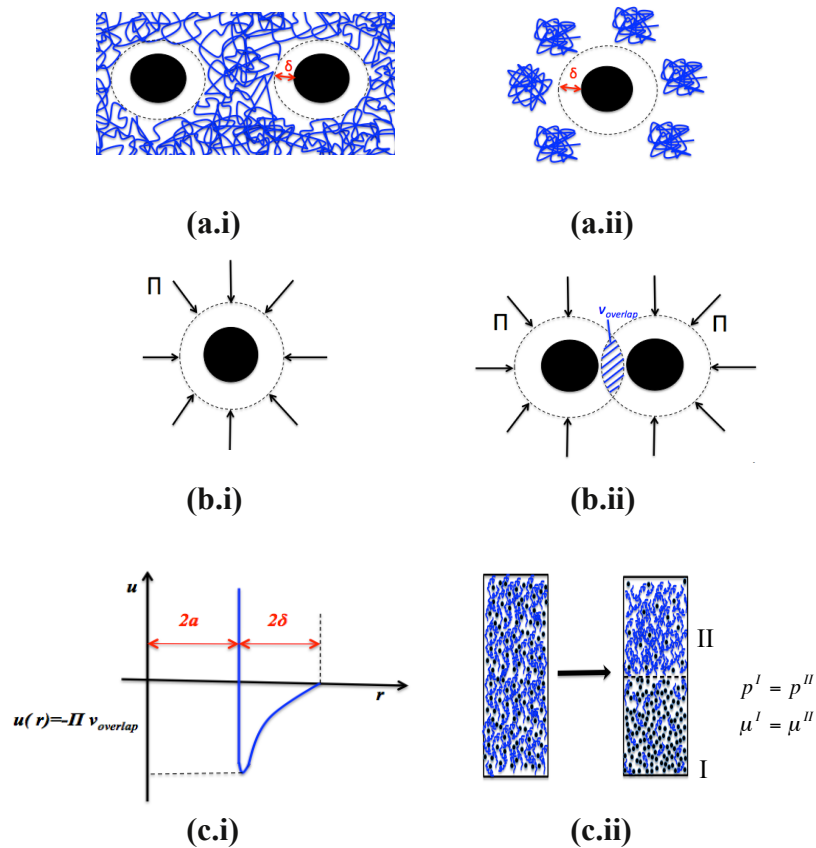


Figure 2.2. Depletion flocculation mechanism: (a.i) depletion layer for the case of $\varphi/\varphi_{ov} > 1$, (a.ii) depletion layer for the case of $\varphi/\varphi_{ov} < 1$, (b.i) osmotic pressure Π applied around each nanoparticle, (b.ii) overlap of two depletion layers and generation of a net attractive potential, (c.i) attractive potential between two colloidal particles, (c.ii) phase separation of a mixture of colloidal particles and a non-adsorbing polymer.

The colloid rich phase can be either liquid-like or solid-like. Thus, the addition of a non-adsorbing polymer can be considered as a way to control the attractive forces between the colloidal particles and to manipulate their phase behavior.

Microgel particles in good solvent are swollen particles sterically stabilized without a hardcore [23]. The same mechanism driving phase separation in mixtures of microgel-particles + non-adsorbing polymer applies to mixtures of colloidal particles with hardcore + non-adsorbing polymer.

2.4. Mixtures of colloidal particles + non-adsorbing polymers

Non-adsorbing polymers in colloidal solutions can induce phase separation by the mechanism of depletion flocculation [29]. The phase behavior of such mixtures depends on the volume fraction and the size of both the colloidal particles and the polymer. The prediction of the behavior of mixtures of colloids + non-adsorbing polymer was performed using computer simulations of hard spheres plus self avoiding polymer chains [30], thermodynamic perturbation theories [31], polymer-colloid liquid state theory [32] and density functional theory [33]. The calculation of the binodal line using these methods is computationally expensive [34]. A simpler theory, the osmotic equilibrium or the free volume theory, was developed by Lekkerkerker et al [35] for the prediction of the phase behavior of such mixtures. In this theory, polymer partitioning between the separated phases is taken into account. The depletion thickness δ is considered to be proportional to the radius of gyration R_g of the polymer. Lekkerkerker's model is valid when $R_g/a < 1$ (colloid limit) and where polymer concentration is below the overlap concentration ($\varphi/\varphi_{ov} < 1$). The model fails when the concentration of the polymer at the binodal points exceeds the overlap concentration ($\varphi/\varphi_{ov} > 1$). This situation occurs in the so-called protein limit where the polymer radius of gyration is larger than the colloidal particle radius ($R_g/a > 1$). In this limit, the depletion thickness δ is independent of the polymer chain length and is only function of the concentration of the polymer. Recently, Fler et al developed a model based on the free volume theory and valid for both the colloid ($R_g/a < 1$) and the protein ($R_g/a > 1$) limits and in the crossover between the two limits. According to this model, the depletion thickness is function of both (R_g/a) and the polymer volume fraction in the mixture. In this work, the recent thermodynamic model of Fler et al [34] for the depletion flocculation mechanism, with the predicted effects of colloidal particle size and polymer radius of gyration on the phase diagram, is outlined. The model was developed to predict the phase behavior of mixtures with polymers (excluded volume - ev - chains version) in good solvents and in theta solvents (mean field chains in theta solvent - mf - version). Experimental

techniques for the determination of the composition of coexisting phases are discussed. Examples from the literature of mixtures of colloidal particles + polystyrene in toluene are also presented.

2.4.1 Phase separation by depletion flocculation and the free volume fraction

Figure 2.3 shows a mixture of colloidal particles + non-adsorbing polymer where two phases coexist. The lower phase is colloid rich; it can be solid (S) or liquid-like (L). The upper phase is colloid poor and can be gas-like (G) or liquid-like (L). In a colloidal phase X, the overall polymer volume fraction Φ is given by:

$$\phi_X = \alpha_X \varphi, \quad (2.2)$$

where: X= G, L or S and φ : is the polymer volume fraction in the free volume not occupied by the particles and the depletion layer surrounding them. It is the same in both phases. α : is the free volume fraction. It is a function of the colloid volume fraction η and $q=\delta/a$, the ratio of the depletion thickness δ to the particle radius a . The free volume fraction, α , is given by the following equation:

$$\alpha = (1-\eta)\beta \quad (2.3)$$

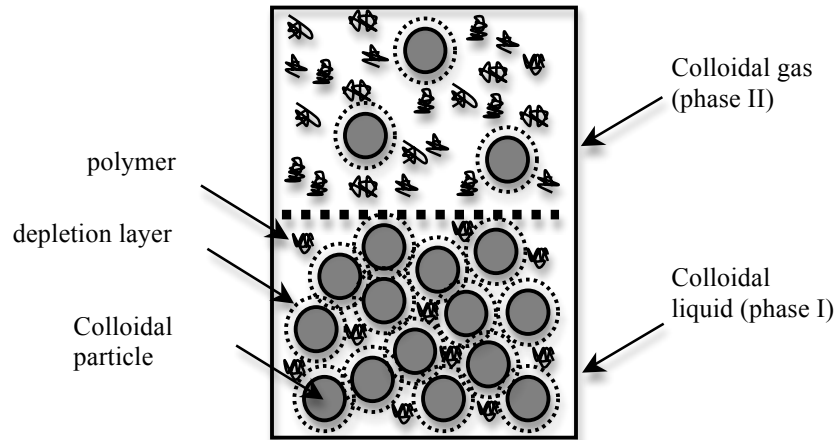


Figure 2.3. Diagram of a mixture of colloid + non-adsorbing polymer separating into colloid rich (phase I, L) and colloid poor (phase II, G) phases.

where:

$$\beta = e^{-Q} \quad (2.4)$$

$$Q = A f + B f^2 + C f^3, \quad (2.5)$$

$$f = \frac{\eta}{1-\eta}, \quad (2.6)$$

$$A=(1+q)^3-1 \quad B=3q^2(q+3/2) \quad C=3q^3 \quad (2.7)$$

The depletion thickness is a function of both (R_g/a) and the volume fraction of the polymer in the mixture. Thus, the ratio of the depletion thickness to the particle radius, for polymers in a good solvent (ev), is given by:

$$q = \frac{\delta}{a} = 0.865 \left\{ q_R^{-2} + c_1 Y^{2\gamma} \right\}^{-0.44}, \quad (2.8.a)$$

with $c_1=3.95$, $\gamma=0.77$. For polymers in theta solvent (mf), the ratio of the depletion thickness to the particle radius is given by:

$$q = \frac{\delta}{a} = 0.938 \left\{ q_R^{-2} + c_1 Y^{2\gamma} \right\}^{-0.45}, \quad (2.8.b)$$

with $c_1=6.02$, $\gamma=1.0$, where:

$$Y = \left(\frac{\varphi}{\varphi_{ov}} \right) q_R^{-1/\gamma}, \quad (2.9)$$

and:

$$q_R = R_g/a \quad (2.10)$$

The radius of gyration of polystyrene in toluene is given by [36]:

$$R_g = 0.012 M_w^{0.595}, \quad (2.11)$$

The volume fraction for which the polymer goes from dilute to semi-dilute solution, known as the overlap volume fraction, is given by [37]:

$$\varphi_{ov} = \frac{3M_w}{4\pi R_g^3 N_A \rho_{polyst}} \quad (2.12)$$

2.4.2. Thermodynamic model for a mixture of mono-dispersed colloidal particles + non-adsorbing polymer

2.4.2.1. Phase diagram calculation

In this thesis, experimental data are compared to the model developed by Fler et al [34]. Details for the calculation of the phase diagram can be found in their paper. Only a summary of the equations is presented here.

The chemical potential and the pressure are given as a sum of hard sphere and polymer contributions, as follows:

$$\mu = \mu^0 + \mu^P, \quad (pv) = (pv)^0 + (pv)^P, \quad (2.13)$$

where: v is the volume of one colloidal particle.

The hard sphere parts of the chemical potential and the pressure are given by:

$$\mu^0 = \begin{cases} \ln \eta + 8f + 7f^2 + 2f^3 & \text{fluid} \\ 2.1306 + \frac{3}{\left(1 - \frac{\eta}{\eta_{cp}}\right)} - 3\ln(\eta^{-1} - \eta_{cp}^{-1}) & \text{solid} \end{cases}, \quad (2.14)$$

$$(pv)^0 = \begin{cases} \eta + 4f^2 + 2f^3 & \text{fluid} \\ \frac{3}{f^{-1} - f_{cp}^{-1}} & \text{solid} \end{cases}, \quad (2.15)$$

where:

$$f = \frac{\eta}{1 - \eta}, \quad (2.16)$$

η is the volume fraction of the colloidal particles and $\eta_{cp}=0.741$ is the close packing volume fraction.

The polymer contribution to the chemical potential and (pv) are given by the following equation:

$$\left\{ \begin{array}{l} \mu^P = \int_0^Y [\beta - (1+f)\beta_1] [q_R^{-1/\gamma} + 3\gamma c_2 Y^{3\gamma-1}] dY \\ (pv)^P = \int_0^Y [\beta - f\beta_1] [q_R^{-1/\gamma} + 3\gamma c_2 Y^{3\gamma-1}] dY \end{array} \right. , \quad (2.17)$$

where: $c_2=1.62$ and $\gamma=0.77$ for excluded volume (ev) chains in good solvent ($\chi=0$) and $c_2=4.2$ and $\gamma=1.0$ for mean field chains (mf) in a theta solvent. β_1 is the first derivative of β with respect to f .

Binodal points are obtained from equal chemical potential and pressure in the two coexisting phases:

$$\text{Colloidal fluid-solid:} \quad \mu_f = \mu_s, \quad (pv)_f = (pv)_s \quad (2.18)$$

$$\text{Colloidal gas-liquid:} \quad \mu_g = \mu_l, \quad (pv)_g = (pv)_l \quad (2.19)$$

At the colloidal gas-liquid critical point, the first and second derivatives of the pressure with respect to f are zero:

$$(pv)_1 = (pv)_2 = 0, \quad (2.20)$$

Finally, at the triple point, the chemical potentials and the pressures in the colloidal gas, liquid and solid phases are equal:

$$\mu_g = \mu_l = \mu_s, \quad (pv)_g = (pv)_l = (pv)_s, \quad (2.21)$$

When q_R is above $q_R^*=0.388$, the critical end point value for excluded volume chains in good solvent, a colloidal liquid-gas region is predicted in the phase diagram. For the case of $q_R=R_g/a=1$, Fler et al [34] compared calculated phase diagram for mixtures of colloidal particles + non-adsorbing polymer in good solvent with experimental observations. This comparison is shown in Figure 2.4. This Figure shows that at fixed colloid volume fraction and with increasing polymer concentration, a mixture of colloids + non-adsorbing polymer moves from a stable single-phase region to a two-phase region where two stable colloidal liquid-colloidal gas phases coexist. The binodal curves meet at the colloidal gas-liquid critical point. With a further increase in the polymer volume fraction, the mixture moves to a three-phase coexistence region (gas-liquid-solid) and then to a two-phase region where colloidal gas and solid phases coexist. The last two regions are not observed in mixtures with polydispersed colloidal particles [38]. The vertices of the triangular three-phase region represent the three triple points (colloidal gas, colloidal liquid and crystal solid).

In the two-phase region, the volume fraction of each phase can be obtained by the lever rule. In mixtures with polydispersed colloidal particles, the formation of the colloidal solid phase is less favorable when compared to the colloidal liquid phase [34]. At relatively high polymer concentrations, these mixtures form a gel phase instead of a crystal solid phase [38].

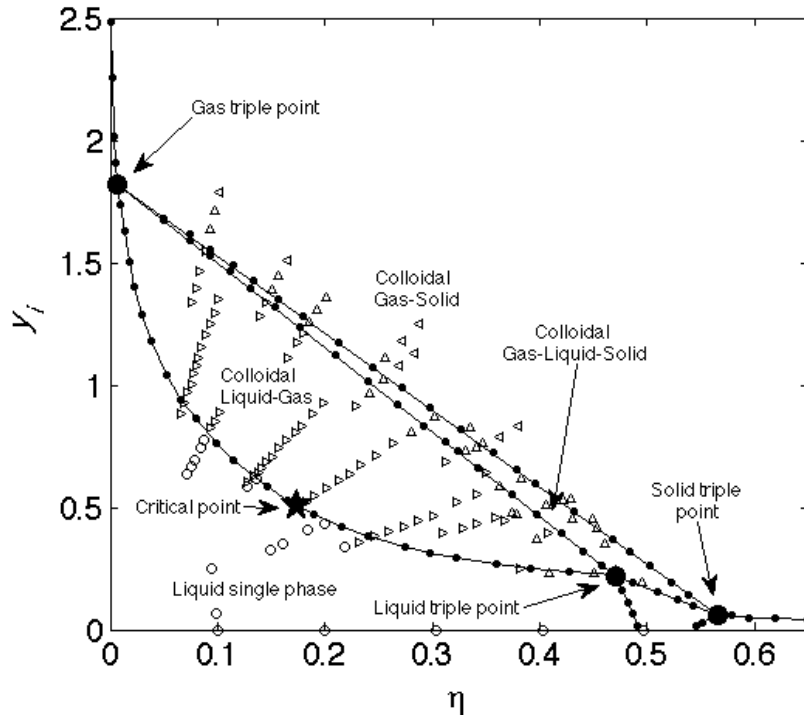


Figure 2.4. Phase diagram of a colloid + non-adsorbing polymer mixture for $q_R=1$ and $y_i=\Phi/\phi_{ov}$. (Filled circles): Phase boundaries calculations from Fler [34]. Experimental data for a mixture of PMMA colloidal particles ($a=130$ nm) + Polystyrene ($M_w=15.4 \times 10^6$ g/mol)+(cis-decalin+tetralin): [39] (open circle): stable single phase, (>): colloidal gas-liquid coexistence region, (^): colloidal gas-liquid-solid coexistence region, (<): colloidal gas-solid region.

2.4.2.2. Effect of polymer radius of gyration and colloidal particle size on the predicted phase diagram

The effects of varying $q_R=R_g/a$ from 0.4 to 5.0 on the volume fractions of the colloidal particles and the polymer at the critical and triple points were investigated by Fler et al[34]. They are shown in Figures 2.5.a-b. Figure 2.5.a shows that when q_R is increased, the volume fraction of the colloidal particles at the critical point decreases and converges to 0.10-0.11 and 0.06 for the cases of polymers in good solvent (ev) and polymers in theta solvent (mf) respectively. When q_R is increased, the volume fractions of the colloids at the gas, liquid and solid triple points converge to 0.0, 0.47 and 0.56 for the case of polymers in good solvent (ev) and to 0.0, 0.48 and 0.55 for the case of polymers in theta solvent

(mf). Figure 2.5.b shows that when q_R is increased at constant polymer radius of gyration – decreasing particle radius a -, the volume fraction of the polymer at the critical point increases monotonically with q_R . Similar variations of the volume fraction of the polymer at the triple points with q_R can be observed except for the initial decrease in the liquid triple point when $0.4 < q_R < 0.5$. When q_R is increased at constant particle radius a (increasing polymer radius of gyration), the volume fractions of the polymer at the critical and triple points are weakly dependent on q_R , particularly when q_R is increased above 0.6.

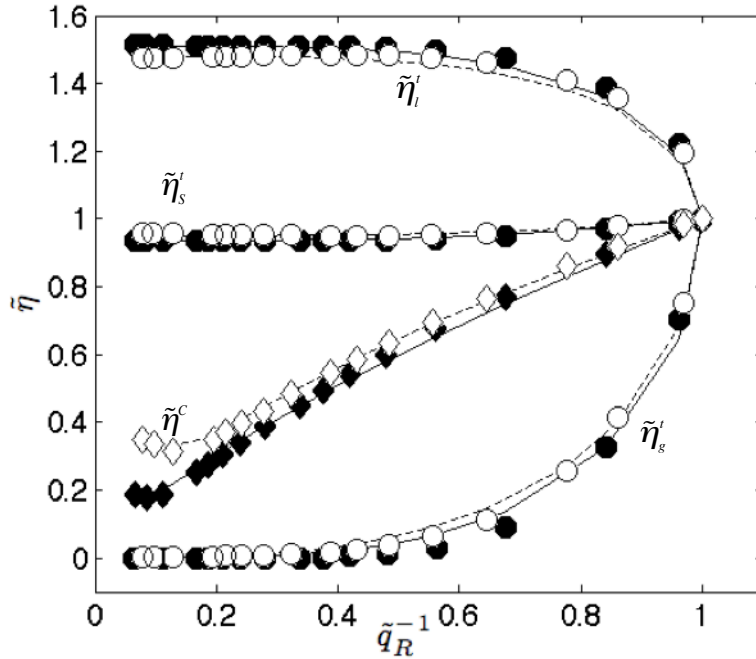


Figure 2.5.a. Numerical results of Fleer et al model extracted numerically for normalized colloidal particle volume fractions at the critical point $\tilde{\eta}^c = \eta^c / \eta^{c*}$ (diamonds) and the triple points $\tilde{\eta}_g^t = \eta_g^t / \eta_g^{t*}$, $\tilde{\eta}_l^t = \eta_l^t / \eta_l^{t*}$, and $\tilde{\eta}_s^t = \eta_s^t / \eta_s^{t*}$ (circles) as a function of \tilde{q}_R^{-1} where $\tilde{q}_R = q_R / q_R^*$ [34]. For excluded chains in good solvent (ev: open symbols) q_R^*, η^*, η_s^* are 0.388, 0.317 and 0.594. For mean-field chains in theta solvent (mf: closed symbols), these values are 0.337, 0.318 and 0.593.

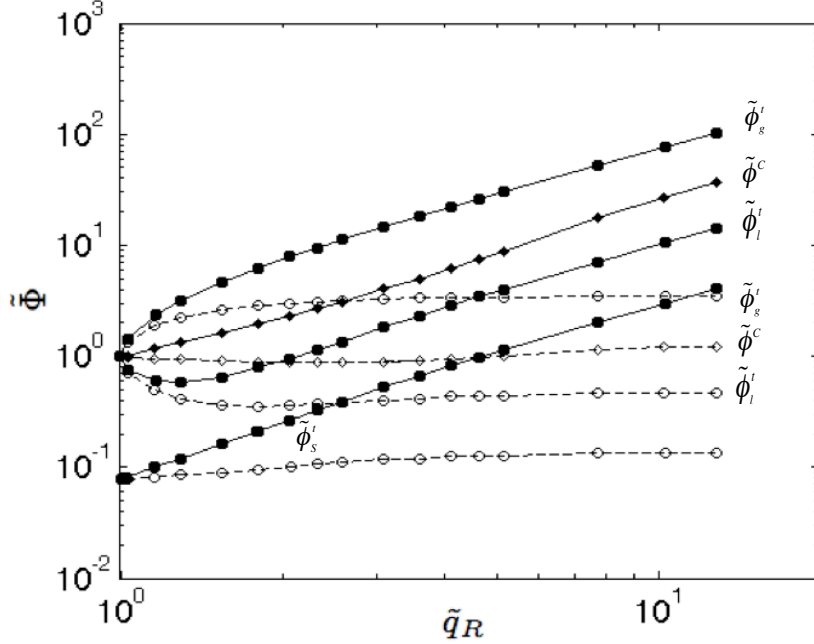


Figure 2.5.b. Normalized polymer volume fractions $\tilde{\phi}_c$ (critical points, diamonds) and $\tilde{\phi}_t$ (triple points, circles) as a function of $\tilde{q}_R = q_R/0.388$ for a polymer in a good solvent, on a double-logarithmic scale. Closed symbols and solid curves are for constant radius of gyration R_g , open symbols with dashed curves are for constant particle radius a ; the symbols correspond to the same set of q_R 's given in Figure 2.5.a. The normalized $\tilde{\phi}$ values may be converted to real volume fractions ϕ by multiplying with $\phi^* = \alpha^* \phi^*$, where $\phi^* = y^* \phi_{ov}^*$, $y^* = 0.428$ and $\alpha^* = 0.381$, where $*$ refers to values at the critical end point [34].

For large values of q_R , the normalized volume fractions of the polymer at the critical point $\tilde{\phi}^c$ and at the gas, liquid and solid triple points $\tilde{\phi}_s', \tilde{\phi}_l', \tilde{\phi}_s'$ reach the constant levels of 1.19, 2.62, 0.44 and 0.16 respectively. Figure 2.5.b was obtained for the case of polymers in good solvent, in the excluded volume limit. Similar variations can be obtained for the case of a theta solvent[34].

2.4.2.3. Comparison between predicted and experimental critical points

Fleer et al. [34] compared experimental critical points with modeling results for different mixtures of colloidal particles + non-adsorbing polymer. The comparison is shown in Table 2.1 for different values of $q_R = R_g/a$. The excluded volume (ev) chains version- used for polymers in good solvent - of the model

corresponds to polymers with an effective Flory-Huggins parameter of $\chi=0$ [40]. Polymers in good solvent, with a scaling behavior $R_g \propto M_w^{3/5}$, can be obtained for mixtures with Flory-Huggins parameter χ slightly below 0.5. An example of this is polystyrene in toluene where $\chi \approx 0.48$ [40]. In these cases where the solvent is slightly better than a theta solvent, calculations were performed using both versions: the excluded volume chains in a good solvent and the mean field chains in a theta solvent. Calculations using both versions provided upper and lower limits for the volume fractions of the colloidal particles and the polymer at the critical points[34].

The predicted trend of increasing polymer volume fraction at the critical point

$$y_c^i = \frac{\phi}{\varphi_{ov}} \text{ with increasing } q_R \text{ was globally supported by experimental results in}$$

Table 2.1. Model calculations predicted that, with increasing q_R , the volume fraction of the colloid at the critical point η^c decreased down to 0.11 for excluded

Table 2.1. Comparison between experimental and theoretical critical points performed by Fleer et al[34].

Mixture	q_R	Experiments		Theory			
				Excluded volume chains in good solvent (ev)		Mean field chains in theta solvent (mf)	
		η^c	$y_i^c = \phi / \varphi_{ov}$	η^c	$y_i^c = \phi / \varphi_{ov}$	η^c	$y_i^c = \phi / \varphi_{ov}$
sil/PDMS/chx	0.49	0.21	1.00	0.27	0.21	-	-
sil/PS/tol	0.67	-	0.35	0.22	0.30	-	-
cas/psc/w	0.86	-	0.45	0.19	0.41	-	-
γ Sprot/PEO/w	0.87	0.18	0.34	0.19	0.42	-	-
sil/PDMS/chx	1.08	-	1.6	0.17	0.58	-	-
sil/PS/tol	1.40	-	0.65	0.14	0.87	-	-
wp/psc/w	3.2	-	3.5	0.11	3.0	-	-
PMMA/PS/dec	0.56	0.1	0.36	0.25	0.24	0.22	0.18
PMMA/PS/dec	0.57	-	0.25	0.25	0.25	0.22	0.19
sil/PS/tol	4.2	0.13	2.2	0.11	4.2	0.06	1.52
sil/PiP/chx	4.8	0.13	1.6	0.11	5.0	0.06	1.74
sil/PS/to	5.2	0.09	2.6	0.11	5.6	0.06	1.89

Abbreviations:

sil: (stearily)silica, cas = caseine micelles, wp = whey proteins, γ Sprot = eye lens protein, PDMS: polydimethyl siloxane, PS = polystyrene, psc = polysaccharide, chx = cyclohexane, tol = toluene. w = water, PMMA = polymethylacrylate, PiP = polyisoprene, dec=decalin.

volume chains in good solvent and to 0.06 for mean field chains in theta solvent. It was reported that there were no direct experimental measurements to support this prediction but the data available in Table 2.1 suggested that at high q_R , the colloid volume fraction at the critical point η^c approached 0.1.

For mixtures of silica particles sterically stabilized + polystyrene in toluene, predicted polystyrene volume fractions at the critical points $(\phi^c/\varphi_{ov})_{theo}=0.30$, $(\phi^c/\varphi_{ov})_{theo}=0.87$ compared well with experimental data $(\phi^c/\varphi_{ov})_{exp}=0.35$, $(\phi^c/\varphi_{ov})_{exp}=0.65$ for $q_R=0.67$ and 1.4, respectively. Calculations have been performed using the polymer in good solvent version (excluded volume chains – ev-). When $q_R=4.2$ and 5.2, the experimental critical points $(\eta^c=0.13, \phi^c/\varphi_{ov}=2.2)_{exp}$, $(\eta^c=0.09, \phi^c/\varphi_{ov}=2.6)_{exp}$ appeared to be in the range between the critical points predicted for the cases of excluded volume chains in good solvent $(\eta^c=0.11, \phi^c/\varphi_{ov}=4.2)_{theo}$, $(\eta^c=0.11, \phi^c/\varphi_{ov}=5.6)_{theo}$ and mean field chains in theta solvent $(\eta^c=0.06, \phi^c/\varphi_{ov}=1.52)_{theo}$, $(\eta^c=0.06, \phi^c/\varphi_{ov}=1.89)_{theo}$.

In this work, calculated phase boundaries and critical points are compared with experimental results for mixtures of asphaltene + polystyrene + toluene. By varying the size of the particles, the monodispered model for polymers in good solvent, is used to estimate an interval for the radii of asphaltene colloidal particles participating in the phase separation mechanism.

2.4.3. Experimental determination of phase composition

The binodal points of the phase diagram of colloids + non-adsorbing polymer mixtures can be determined experimentally by direct sampling and measurement of the composition of the separated phases. Figure 2.6 shows the composition of the separated phases determined experimentally for a mixture of nanoparticles (γ_S spherical protein, $M_w=20,800$ g/mol, $a=1.8$ nm) + non-adsorbing polymer (polyethylene glycol, $M_w=1450$ g/mol, $R_g=1.56$ nm) + water [41]. The concentration of protein (nanoparticle) in each phase was obtained by UV

absorption, where the concentration of the non-adsorbing polymer PEG was determined by taking an aliquot of known weight from each phase. The polymer was separated from the protein by ultra filtration and its concentration in the filtrate was measured using a refractive index detector.

In opaque fluids, Erne et al. [42] used an infrared technique to measure the phase behavior and the composition of the phases for a mixture of nanoparticles ($a=4.5$ nm, magnetite Fe_3O_4 sterically stabilized with oleic acid) + poly(dimethyl siloxane) ($M_w=41500$ g/mol, $R_g=8.5$ nm) + toluene. Infrared spectra were measured at different positions along the height of the cell to obtain the composition profile of the mixture in the cell. This technique analyzes only a thin layer near the wall (~ 1 μm), it is therefore limited to cases where adsorption at the wall is negligible. The IR absorption spectra of the polymer and the nanoparticles should be sufficiently distinct to allow for the determination of the composition of the separated phases.

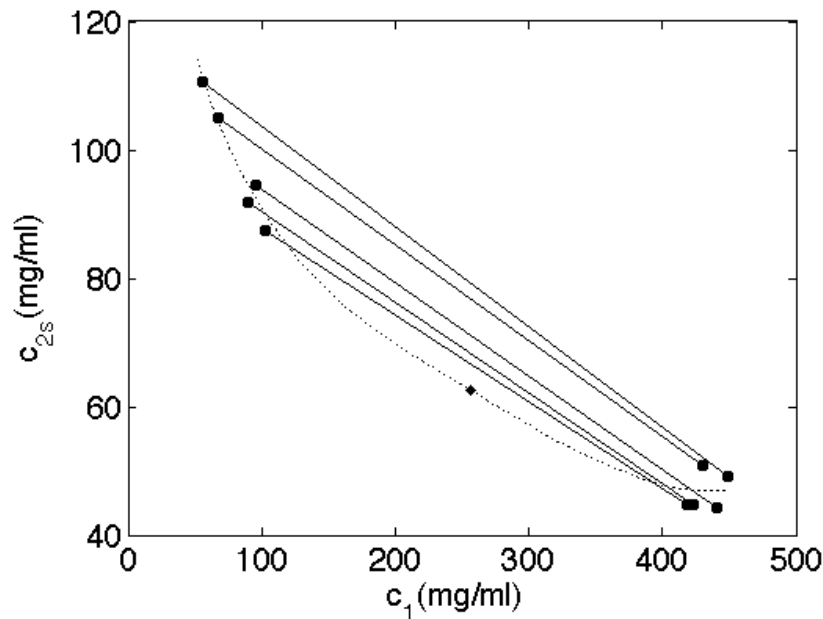


Figure 2.6. Binodal points for the ternary $\gamma\text{S}+\text{PEG1450}+\text{water}$ system. The critical point at $c_{1c}=260$ mg/ml. For PEG1450, $R_g=1.56$ nm, whereas $a=1.80$ nm is estimated from the molecular weight and specific volume of γS [41].

Bodnar et al[43] proposed an indirect method to estimate the composition of the separated phases for a mixture of colloidal silica particles ($a=47$ nm) + non-adsorbing polymer (polydimethylsiloxane, $R_g=23$ nm) + cyclohexane. This method is based on measuring the variations of the volume fractions along at least three dilution lines. The binodal points are obtained using the lever rule by varying the length and the slope of the tie lines to fit the experimental volume fractions of the separated phases. This is illustrated in Figures 2.7.a-b. For example, a mixture in state P in the phase diagram separates into a colloid poor phase (α) and a colloid rich phase (β). The volume fraction of the colloid poor phase (upper phase) is given by:

$$R^P = \frac{V_\alpha}{V_\alpha + V_\beta} = \frac{\eta^\beta - \eta^P}{\eta^\beta - \eta^\alpha} = \frac{\phi^P - \phi^\beta}{\phi^\alpha - \phi^\beta}, \quad (2.22)$$

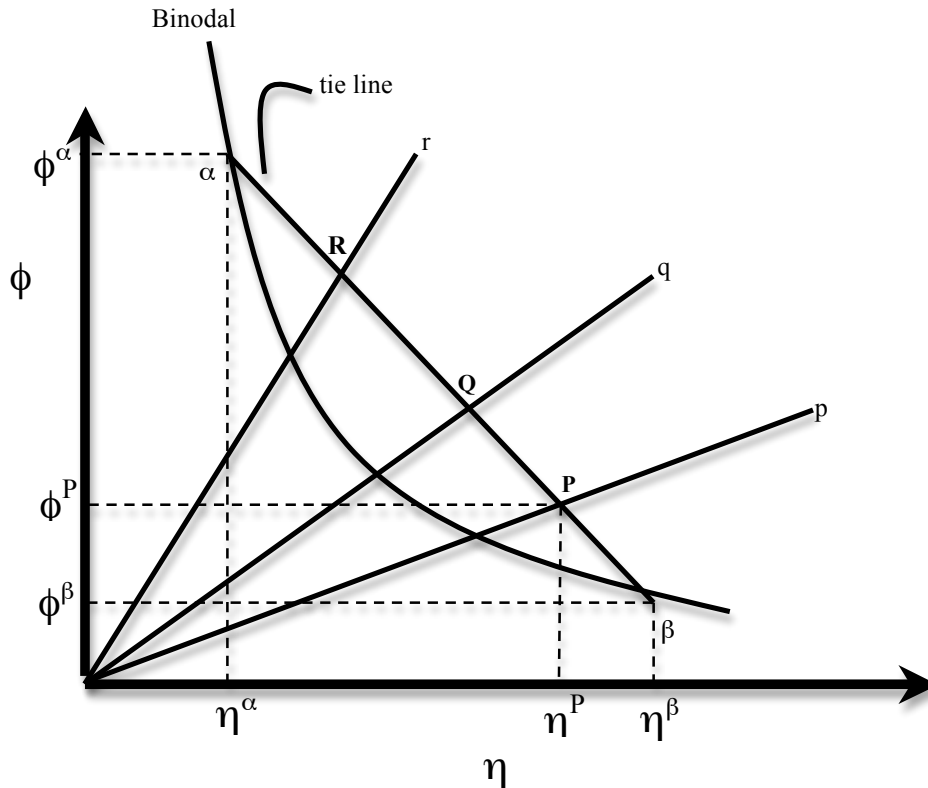


Figure 2.7.a. Schematic representation of the binodal, dilution lines p, q and r and the intersections P, Q and R with a tie line in a phase diagram where the polymer volume fraction Φ is plotted against the colloid volume fraction η [43].

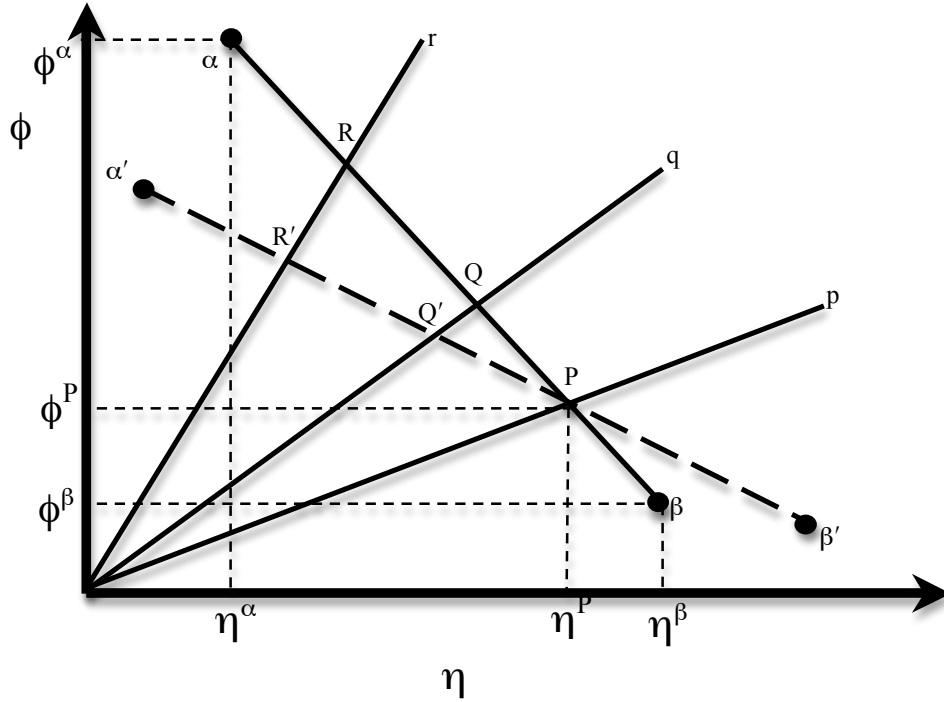


Figure 2.7.b. Schematic representation of two tie lines $[\alpha \beta]$ and $[\alpha' \beta']$ with different slopes and lengths in a phase diagram where the polymer volume fraction Φ is plotted against the colloid volume fraction η .

The volume fraction of the polymer in point P can be given by:

$$\phi^P = \left(\frac{\eta^\beta \phi^\alpha - \eta^\alpha \phi^\beta}{\eta^\beta - \eta^\alpha} \right) + \left(\frac{\phi^\beta - \phi^\alpha}{\eta^\beta - \eta^\alpha} \right) \eta^P = d + n \eta^P, \quad (2.23)$$

where d , n are the intercept and the slope of the tie line $[\alpha \beta]$.

Similarly:

$$\phi^\beta = d + n \eta^\beta \quad (2.24)$$

The volume fraction of the upper phase can also be given by:

$$R^P = \frac{\sqrt{(\eta^\beta - \eta^P)^2 + (\phi^\beta - \phi^P)^2}}{\sqrt{(\eta^\beta - \eta^\alpha)^2 + (\phi^\alpha - \phi^\beta)^2}} \quad (2.25)$$

After substitution of equations (2.23) and (2.24) in equation (2.25), the following equation is obtained:

$$\sqrt{n^2 + 1} (\eta^\beta - \eta^p) = R^p \cdot l \quad (2.26)$$

$$\eta^\beta = \eta^p + \frac{R^p \cdot l}{\sqrt{n^2 + 1}} \quad (2.27)$$

For any point P along dilution line p with volume fraction f_p^P , the volume fractions of the colloid at the binodal points are given by:

$$\begin{cases} \eta^\beta = \eta^p + \frac{f_p^P \cdot l}{\sqrt{n^2 + 1}} \\ \eta^\alpha = \eta^p - \frac{(1 - f_p^P) \cdot l}{\sqrt{n^2 + 1}} \end{cases} \quad (2.28)$$

Similarly, using points Q and R in dilution lines q and r, the colloid volume fractions at the binodal points are given by:

$$\begin{cases} \eta^\beta = \eta^q + \frac{f_q^Q \cdot l}{\sqrt{n^2 + 1}} \\ \eta^\alpha = \eta^q - \frac{(1 - f_q^Q) \cdot l}{\sqrt{n^2 + 1}} \end{cases} \quad (2.29)$$

$$\begin{cases} \eta^\beta = \eta^r + \frac{f_r^R \cdot l}{\sqrt{n^2 + 1}} \\ \eta^\alpha = \eta^r - \frac{(1 - f_r^R) \cdot l}{\sqrt{n^2 + 1}} \end{cases} \quad (2.30)$$

The slopes of dilution lines p, q and r are given by:

$$c_p = \frac{\phi^P}{\eta^p}, c_q = \frac{\phi^Q}{\eta^q}, c_r = \frac{\phi^R}{\eta^r}, \quad (2.31)$$

After substitution in equation (2.22):

$$c_p \eta^P = d + n \eta^P, \quad (2.32)$$

similarly:

$$c_q \eta^Q = d + n \eta^Q, \quad (2.33)$$

$$c_r \eta^R = d + n \eta^R, \quad (2.34)$$

By combining equation (2.33) with (2.32) and (2.34) with (2.32), the following equations are obtained:

$$\eta^Q = \eta^P \frac{c_p - n}{c_q - n}, \quad (2.35)$$

$$\eta^R = \eta^P \frac{c_p - n}{c_r - n}, \quad (2.36)$$

After substitution of equations (2.35) and (2.36) in equations (2.29) and (2.30) for η^Q and η^R , The colloid volume fraction in the binodal points belonging to a tie line passing through state P can be determined from the following equations:

$$\begin{cases} \eta^\beta = \eta^P + \frac{f_p^P \cdot l}{\sqrt{n^2 + 1}} \\ \eta^\alpha = \eta^P - \frac{(1 - f_p^P) \cdot l}{\sqrt{n^2 + 1}} \end{cases}, \quad (2.28)$$

$$\begin{cases} \eta^\beta = \eta^P \frac{c_p - n}{c_q - n} + \frac{f_q^Q \cdot l}{\sqrt{n^2 + 1}} \\ \eta^\alpha = \eta^P \frac{c_p - n}{c_q - n} - \frac{(1 - f_q^Q) \cdot l}{\sqrt{n^2 + 1}} \end{cases}, \quad (2.37)$$

$$\begin{cases} \eta^\beta = \eta^P \frac{c_p - n}{c_r - n} + \frac{f_r^R \cdot l}{\sqrt{n^2 + 1}} \\ \eta^\alpha = \eta^P \frac{c_p - n}{c_r - n} - \frac{(1 - f_r^R) \cdot l}{\sqrt{n^2 + 1}} \end{cases}, \quad (2.38)$$

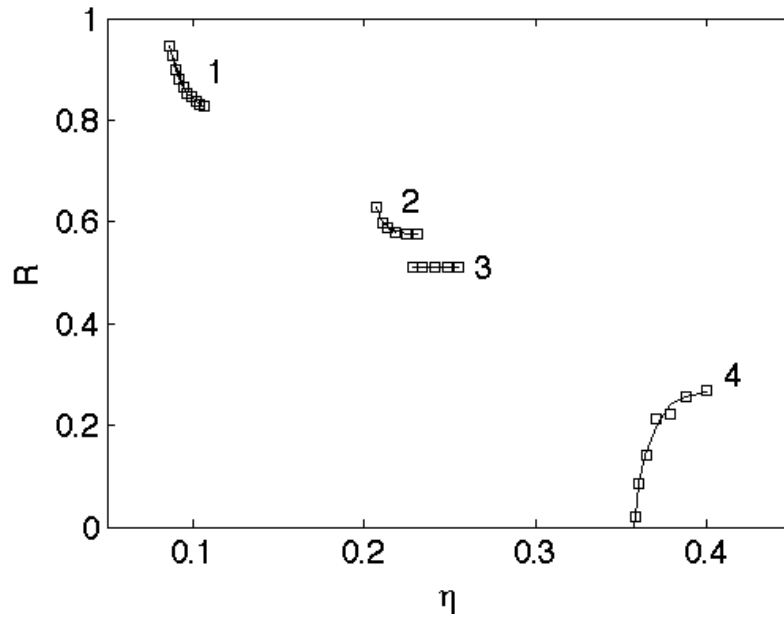
In theory, three dilution lines (p, q and r) can be used to determine the composition of the coexisting phases. More dilution lines can be used to reduce the effect of the experimental error. For a tie line passing through point P with slope n and length l , the colloid volume fraction in the coexisting phases can be estimated using equations (2.28), (2.37) and (2.38). Three values can be obtained for the colloid volume fraction at the binodal points $\eta_{(x=p,q,r)}^\alpha, \eta_{(x=p,q,r)}^\beta$. The composition is then averaged to obtain $\bar{\eta}^\alpha, \bar{\eta}^\beta$. Values of the slope n and the length l of the tie line are varied (Fig.2.7.b) to minimize the following objective function:

$$Obj(n, l) = \sum_{x=p,q,r} \left[(n^2 + 1) \left(\eta_{(x)}^\alpha - \bar{\eta}^\alpha \right) \right]^2 + \sum_{x=p,q,r} \left[(n^2 + 1) \left(\eta_{(x)}^\beta - \bar{\eta}^\beta \right) \right]^2, \quad (2.39)$$

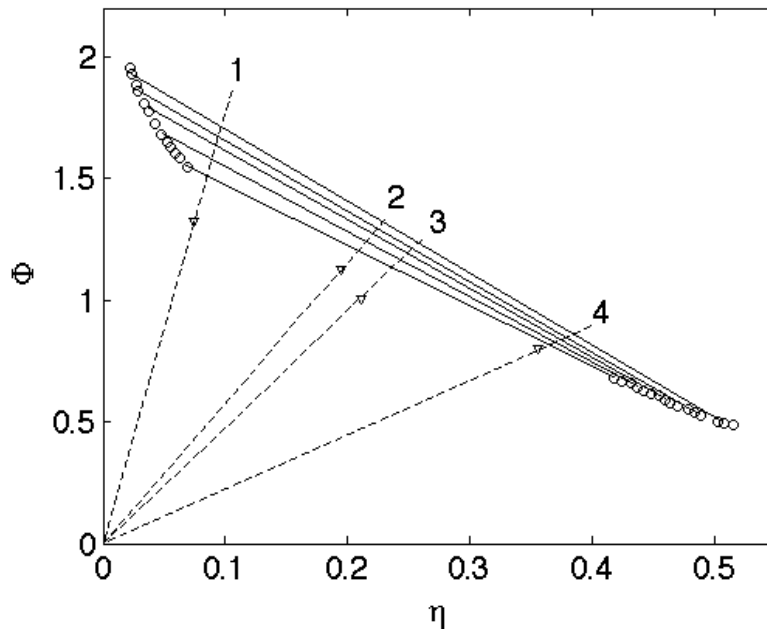
The numerical procedure described above was applied by Bondar et al[43] to a mixture of colloidal silica particles $a=43$ nm and polydimethylsiloxane ($M_w=204$ 000 g/mol, $R_g=23$ nm) in cyclohexane. The variations of the volume fraction of the upper phase along the four dilution lines and the calculated binodal points are shown in Figures 2.8.a-b [43]. It was suggested that a good estimate of the critical point could be obtained by extrapolating the centers of the tie lines towards the experimental phase boundary [43].

2.4.4. Experimental measurements of phase separation for mixtures of colloidal particles + polystyrene + toluene

Ramkrishnan et al [44] [45] measured the phase behavior of silica particles ($a=50$ nm) sterically stabilized with stearly alcohol + polystyrene in toluene. Different polystyrene molecular weights were investigated: $M_w=2.43 \times 10^3, 2.93 \times 10^4, 2.214 \times 10^5, 5.5 \times 10^5, 1.88 \times 10^6$ g/mol. They found that homogenous gel formation, dense (solid)-dilute phase separation and liquid-liquid separation were observed as the ratio R_g/a increased from 0.026 to 1.395. Hennequin et al [37] measured the



(a)



(b)

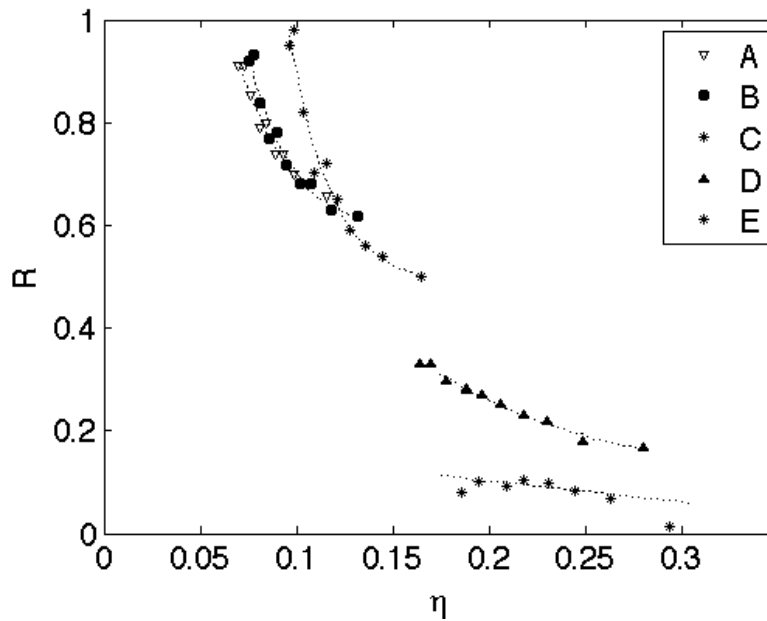
Figure 2.8. (a) Experimental variations of the upper phase volume fraction along the dilution lines, (b) binodal points extracted numerically, from Bondar et al[43]. (triangle): observed binodal points. Data are obtained for the case of a mixture of colloidal silica particles $a=43$ nm and polydimethylsiloxane, $R_g=23$ nm.

phase behavior of silica particles, sterically stabilized with stearly alcohol in toluene + polystyrene ($M_w=8.5 \times 10^6$ g/mol) for $R_g/a=4.1$ ($a=42.5$ nm) and $R_g/a=5.2$ ($a=33$ nm). They found that for both cases and above a certain polymer concentration, the mixtures separated into two stable liquid phases, one colloid rich and one colloid poor. An interface was first observed to form at the bottom of the cuvette, moving upwards and becoming sharper. Phase separation was complete and equilibrium reached nearly 1 hour after of homogenization.

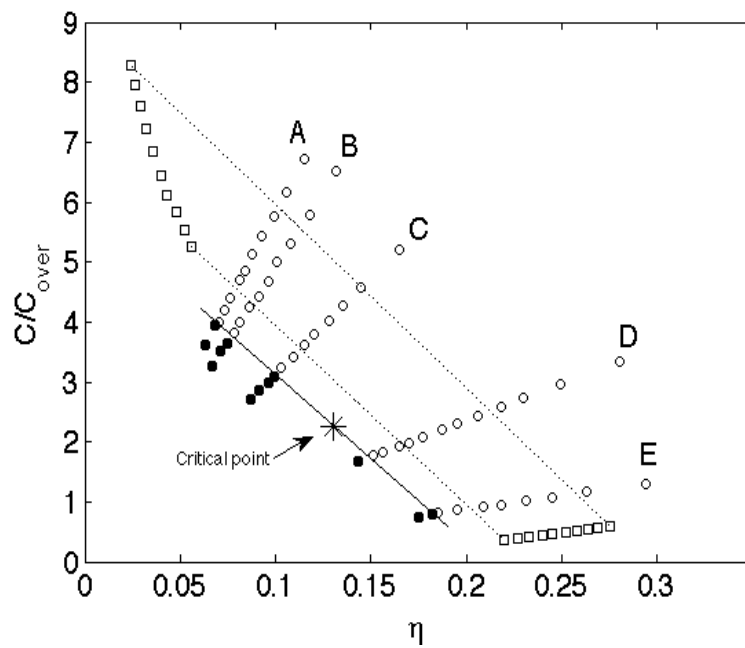
Figure 2.9.a shows the variations of the upper phase volume fraction along dilution lines A-E. The upper phase volume fraction appears to increase significantly along dilution lines A, B and C, where it increases slightly along dilution lines D and E. This behavior could be attributed to the movement of the liquid-liquid interface with dilution. Figure 2.9.b shows the experimental phase diagram with calculated binodal points and estimated critical point.

2.5. Objective

In this work, the phase behavior of asphaltene + polystyrene + toluene mixtures is investigated. Speed of sound and attenuation profile measurements along the cell are measured for different mixtures of asphaltene + polystyrene + toluene. The composition of the separated phases is calculated from experimental phase volume fraction and speed of sound data. For a mixture with fixed global composition, calculated phase compositions are compared with compositions obtained from UV-Visible spectrophotometry measurements and mass balance equations. The fraction and the size of asphaltene colloidal particles participating in the phase separation mechanism are estimated. Finally, the possibility of improving asphaltene separation by adding non-adsorbing polymers is discussed.



(a)



(b)

Figure 2.9. (a) Variations of the upper phase volume fraction along the dilution lines (b) Experimental phase diagram (extracted numerically) from Hennequin et al[37] for a mixture of silica nanoparticles ($a=42.4$ nm) + polystyrene ($M_w=8.5 \cdot 10^6$ g/mol): (open circle) liquid-liquid phase behavior, (filled circle): single phase behavior, (open square): estimated binodal points, (star): estimated critical point.

References

1. Andreatta, G., Bostrom, N., & Mullins, O. (2005) High-Q ultrasonic determination of the critical nanoaggregate concentration of asphaltenes and the critical micelle concentration of standard surfactants. *Langmuir* 21, 2728-2736.
2. Andreatta, G., Goncalves, C., Buffin, G., Bostrom, N., Quintella, C., Arteaga-Larios, F., Perez, E., & Mullins, O. (2005) Nanoaggregates and structure-function relations in asphaltenes. *Energy & Fuels* 19, 1282-1289.
3. Zeng, H., Song, Y.-Q., Johnson, D. L., & Mullins, O. C. (2009) Critical Nanoaggregate Concentration of Asphaltenes by Direct-Current (DC) Electrical Conductivity. *Energy & Fuels* 23, 1201-1208.
4. Mostowfi, F., Indo, K., Mullins, O. C., & McFarlane, R. (2009) Asphaltene Nanoaggregates Studied by Centrifugation. *Energy & Fuels* 23, 1194-1200.
5. Lisitza, N. V., Freed, D. E., Sen, P. N., & Song, Y.-Q. (2009) Study of Asphaltene Nanoaggregation by Nuclear Magnetic Resonance (NMR). *Energy & Fuels* 23, 1189-1193.
6. Wang, S., Liu, J., Zhang, L., Xu, Z., & Masliyah, J. (2009) Colloidal Interactions between Asphaltene Surfaces in Toluene. *Energy & Fuels* 23, 862-869.
7. Espinat, D., Fenistein, D., Barre, L., Frot, D., & Briolant, Y. (2004) Effects of temperature and pressure on asphaltenes agglomeration in toluene. A light, X-ray, and neutron scattering investigation. *Energy & Fuels* 18, 1243-1249.
8. Barre, L., Simon, S., & Palermo, T. (2008) Solution properties of asphaltenes. *langmuir* 24, 3709-3717.
9. Sheu, E. Y. (2006) Small angle scattering and asphaltenes. *Journal of Physics-Condensed Matter* 18, S2485-S2498.
10. Zhao, B. & Shaw, J. M. (2007) Composition and size distribution of coherent nanostructures in Athabasca bitumen and Maya crude oil. *Energy & Fuels* 21, 2795-2804.
11. Ching, M. J. T. M., Pomerantz, A. E., Andrews, A. B., Dryden, P., Schroeder, R., Mullins, O. C., & Harrison, C. (2010) On the Nanofiltration of Asphaltene Solutions, Crude Oils, and Emulsions. *Energy & Fuels* 24, 5028-5037.
12. Branco, V., Mansoori, G., Xavier, L., Park, S., & Manafi, H. (2001) Asphaltene flocculation and collapse from petroleum fluids. *Journal of Petroleum Science and Engineering* 32, 217-230.
13. Myakonkaya, O. & Eastoe, J. (2009) Low energy methods of phase separation in colloidal dispersions and microemulsions. *Advances in Colloid and Interface Science* 149, 39-46.
14. Hashmi, S. M., Quintiliano, L. A., & Firoozabadi, A. (2010) Polymeric Dispersants Delay Sedimentation in Colloidal Asphaltene Suspensions. *langmuir* 26, 8021-8029.
15. Chang, C. L. & Fogler, H. S. (1994) Stabilization of Asphaltenes in Aliphatic Solvents Using Alkylbenzene - Derived Amphiphiles 1. Effect of the Chemical - Structure of Amphiphiles on Asphaltene Stabilization. *Langmuir* 10,

1749-1757.

16. Lima, A. F., Mansur, C. R. E., Lucas, E. F., & Gonzalez, G. (2010) Polycardanol or Sulfonated Polystyrene as Flocculants for Asphaltene Dispersions. *Energy & Fuels* 24, 2369-2375.
17. Noda, I., Higo, Y., Ueno, N., & Fujimoto, T. (1984) Semidilute Region for Linear-Polymers in Good Solvents. *Macromolecules* 17, 1055-1059.
18. Luckham, P. (1991) Measurement of the Interaction Between Adsorbed Polymer Layers - The Steric Effect. *Advances in Colloid and Interface Science* 34, 191-215.
19. Bank, M., J, L., & Thies, C. (1971) Influence of Solvent Upon Compatibility of Polystyrene and Poly(Vinyl Ether). *Macromolecules* 4, 43.
20. Narasimhan, V, H. R. B. C. (1983) Polymer Polymer Interaction Parameters of Polystyrene and Polybutadiene from Studies in Solutions of Toluene or Tetrahydrofuran. *Journal of Polymer Science Part B - Polymer Physics* 21, 1993-2001.
21. Hsu, C. & Prausnitz, J. (1974) Thermodynamics of Polymer Compatibility in Ternary Systems. *Macromolecules* 7, 320-324.
22. J., P. Flory (1953) Principles of Polymer Chemistry. *Cornell University Press*.
23. Saunders, B. & Vincent, B. (1999) Microgel particles as model colloids: theory, properties and applications. *Advances in Colloid and Interface Science* 80, 1-25.
24. Sieglaff, C. (1959) Phase Separation in Mixed Polymer Solutions. *Journal of Polymer Science* 41, 319-326.
25. Clarke, J. & Vincent, B. (1981) Stability of non-aqueous microgel dispersions in the presence of free polymer. *Journal of the Chemical Society - Faraday Transactions I* 77, 1831-1843.
26. Vincent, B. (2008) A Journey Through Colloid Science. *New Frontiers in Colloid Science - A celebration of the career of Brian Vincent* , 1-40.
27. Asakura, S. & Oosawa, F. (1954) On Interaction between 2 Bodies Immersed in a Solution of Macromolecules. *Journal of Chemical Physics* 22, 1255-1256.
28. Asakura, S. & Oosawa, F. (1958) Interaction Between Particles Suspended in Solutions of Macromolecules. *Journal of Polymer Science* 33, 183-192.
29. Poon, W. C. K. (2002) The physics of a model colloid-polymer mixture. *Journal of Physics-Condensed Matter* 14, R859-R880.
30. Bolhuis, P., Meijer, E., & Louis, A. (2003) Colloid-polymer mixtures in the protein limit. *Physical Review Letters* 90.
31. Pelissetto, A. & Hansen, J.-P. (2006) An effective two-component description of colloid-polymer phase separation. *Macromolecules* 39, 9571-9580.
32. Fuchs, M. & Schweizer, K. (2002) Structure of colloid-polymer suspensions. *Journal of Physics-Condensed Matter* 14, R239-R269.
33. Schmidt, M. & Fuchs, M. (2002) Penetrability in model colloid-polymer mixtures. *Journal of Chemical Physics* 117, 6308-6312.
34. Fleer, G. J. & Tuinier, R. (2008) Analytical phase diagrams for colloids and non-adsorbing polymer. *Advances in Colloid and Interface Science* 143, 1-47.

35. Lekkerkerker, H. N. W., Poon, W. C. K., Pusey, P. N., A., S., & Warren, P. B. (1992) Phase Behavior of Colloid Plus Polymer Mixtures. *Europhysics Letters* 20, 559-564.
36. Fetters, L., Hadjichristidis, N., Lindner, J., & Mays, J. (1994) Molecular Weight Dependence of Hydrodynamic and Thermodynamic Properties for Well-Defined Linear Polymer in Solution. *Journal of Physical and Chemical Reference Data* 23, 619-640.
37. Hennequin, Y., Evens, M., Angulo, C., & van Duijneveldt, J. (2005) Miscibility of small colloidal spheres with large polymers in good solvent. *Journal of Chemical Physics* 123.
38. Aarts, D. & Lekkerkerker, H. (2004) Confocal scanning laser microscopy on fluid-fluid demixing colloid-polymer mixtures. *Journal of Physics-Condensed Matter* 16, S4231-S4242.
39. Tuinier, R., Smith, P. A., Poon, W. C. K., Egelhaaf, S. U., Aarts, D. G. A. L., Lekkerkerker, H. N. W., & Fleer, G. J. (2008) Phase diagram for a mixture of colloids and polymers with equal size. *A letters Journal Exploring the Frontier of Physics* 82.
40. Zhang, Z. & van Duijneveldt, J. (2006) Experimental phase diagram of a model colloid-polymer mixture in the protein limit. *Langmuir* 22, 63-66.
41. Annunziata, O., Ogun, O., & Benedek, G. (2003) Observation of liquid-liquid phase separation for eye lens gamma S-crystallin. *Proceedings of the National Academy of Sciences of the United States of America* 100, 970-974.
42. Erne, B., van der Maas, J., Kuipers, B., Visser, T., & Philipse, A. (2003) Vertical concentration profiles in colloidal fluids measured by FTIR-ATR spectroscopy. *Langmuir* 19, 3081-3083.
43. Bodnar, I. & Oosterbaan, W. (1997) Indirect determination of the composition of the coexisting phases in a demixed colloid polymer mixture. *Journal of Chemical Physics* 106, 7777-7780.
44. Ramakrishnan, S., Fuchs, M., Schweizer, K. S., & Zukoski, C. F. (2002) Concentration fluctuations in a model colloid-polymer suspension: Experimental tests of depletion theories. *Langmuir* 18, 1082-1090.
45. Ramakrishnan, S., Fuchs, M., Schweizer, K. S., & Zukoski, C. F. (2002) Entropy driven phase transitions in colloid-polymer suspensions: Tests of depletion theories. *Journal of Chemical Physics* 116, 2201-2212.

Chapter 3. Phase Behaviour and Phase Separation Kinetics Measurement Using Acoustic Arrays

3.1. Introduction

Online measurements of thermodynamic property profiles in opaque materials are needed in many industrial applications. Examples include the phase behaviour of heavy oil, water in oil emulsions, colloidal phase separation, natural gas hydrate formation and dissociation, and liquid diffusion in porous media. The focus here is on hydrocarbon energy sector applications where unresolved and significant issues related to phase equilibrium, process kinetics and transport properties arise. A variety of experimental methods have been applied to make such measurements. Each has limitations linked to cost or range of application. For example, X-ray transmission tomography has been used to measure the phase behaviour of opaque heavy oil + solvent mixtures [1], to make mutual diffusion mass transfer measurements [2] and to measure local compositions in oil + water emulsions and dispersions [3]. Infrared spectroscopy has been used to measure the phase behaviour and the composition of phases in opaque mixtures comprising a colloidal dispersion and a non-adsorbing polymer [4]. This latter technique analyzes only a thin layer near the wall and is limited to cases where adsorption at the wall is negligible. The same infrared technique was used to characterize hydrate formation in porous media [5]. Proton magnetic resonance spectroscopy has been applied to measure phase separation of opaque oil in water emulsions [6]. In solvent based oil recovery processes, diffusion measurements are challenging because of the difficulty of measuring local compositions in bitumen, particularly in porous media. Afsahi et al [7] used an NMR technique to measure solvent mass transfer in bitumen in the presence and absence of sand. An MRI

technique has also been used to measure composition profiles and asphaltene deposition in porous media [8] [9] with a resolution of 0.86 mm/pixel.

Acoustic speed and wave attenuation measurements, with a single emitter and receiver, have been used to determine liquid mixture composition [10], thermodynamic properties [11] and phase behaviour [12] [13]. They have also been used in porous media where acoustic speed and attenuation depend on the properties of the fluids contained in the pores [14]. Acoustic measurements are accurate, non-intrusive and are sensitive to the composition of liquid mixtures and to the presence of interfaces. Therefore, measurements of acoustic property profiles, at fine length scales using an array of emitters and receivers, has potential as a sensor for the characterization of the behaviour of fluids in divers applications. Energy sector applications are illustrated here.

3.2. Experimental methodology

3.2.1. Experimental apparatus

A Schematic of the acoustic cell apparatus is shown in Figure 3.1. The cell is made from PBI (PolyBenzImidazole), it was purchased as a rod from Goodfellow Cambridge Limited. It contains a cavity where the sample is introduced as shown in the front view of Figure 3.1. The cell is held in place using a cylindrical aluminium frame. The frame is milled on two sides so that the emitting and receiving probes can be located and positioned accurately. The cell is sealed with a stainless steel cap that fits into the cavity. The temperature is controlled by circulating water from a thermostatted reservoir (Fisher Scientific Isotemp 3006D) through two copper blocks located on both sides of the sample as shown on the side view and the top view of Figure 3.1. Temperature is controlled to within ± 0.1 C. The acoustic phased array probes, 10L64-A2 [15], comprise an array of 64 elements with a nominal frequency of 10 MHz. The 7 mm wide elements are 0.6 mm high. The probes are positioned parallel to each other and

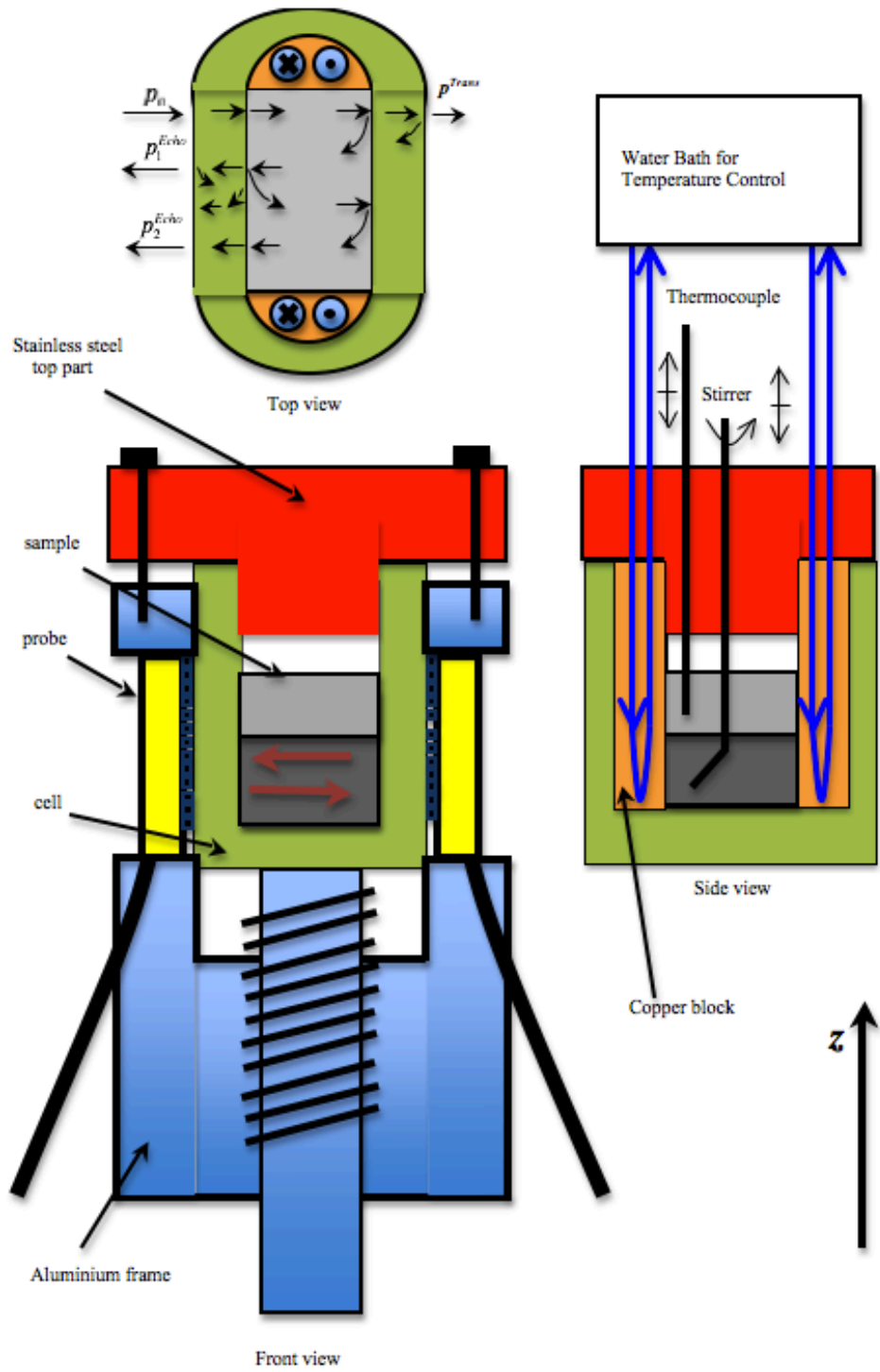


Figure 3.1. Schematic views of the acoustic cell

can operate in both pulse/echo and transmission modes. The acoustic waves emitted travel through the wall for a distance of 6.7 mm and through the sample for a distance of 16 mm. A fraction of the waves are reflected and travel back to the emitter (pulse/echo mode), the other fraction is transmitted to the receiver (transmission mode). The acoustic paths are shown on the top view of the cell in Figure 3.1. The reflected waveform is recorded at a sampling rate of 100 MHz, it contains the first and second echoes of the pulses (p_1^{Echo}, p_2^{Echo}) that travel through the sample and echoes from the reflection at the wall-sample interface. In this work the pulse/echo mode was used for measurements in liquids and for monitoring liquid-liquid phase separation, while the transmission mode was used for measurements in porous media. The latter mode permitted measurements through the highly attenuating porous medium that were not possible in the pulse/echo mode.

Single and multiphase liquid mixtures were prepared within the cell prior to measurement by introducing the constituents separately with a syringe. The contents were then stirred for 4-5 minutes before the stirrer was removed. The acoustic measurements were started just before removing the stirrer, to capture the acoustic properties just after mixing (time $t=0$ s), at a rate of 1 Hz for the first 20 seconds. Five acoustic measurements were then performed for up to 10 minutes after mixing.

3.2.2. Measurement methodology and calibration

Data acquisition hardware (TomoScan Focus LT™) and software (TomoView™ Software) from Olympus NDT were used for data acquisition. For local speed of sound measurements, the acoustic cell operates in pulse-echo mode where 113 acoustic beams are sent and then received by the same probe. Each beam is formed by pulses sent by 8 acoustic elements: the first beam is formed by the 1st to 8th elements, the second by the 1st to 9th elements, the third by the 2nd to 9th elements, the fourth by the 2nd to 10th elements, and so on.... The vertical

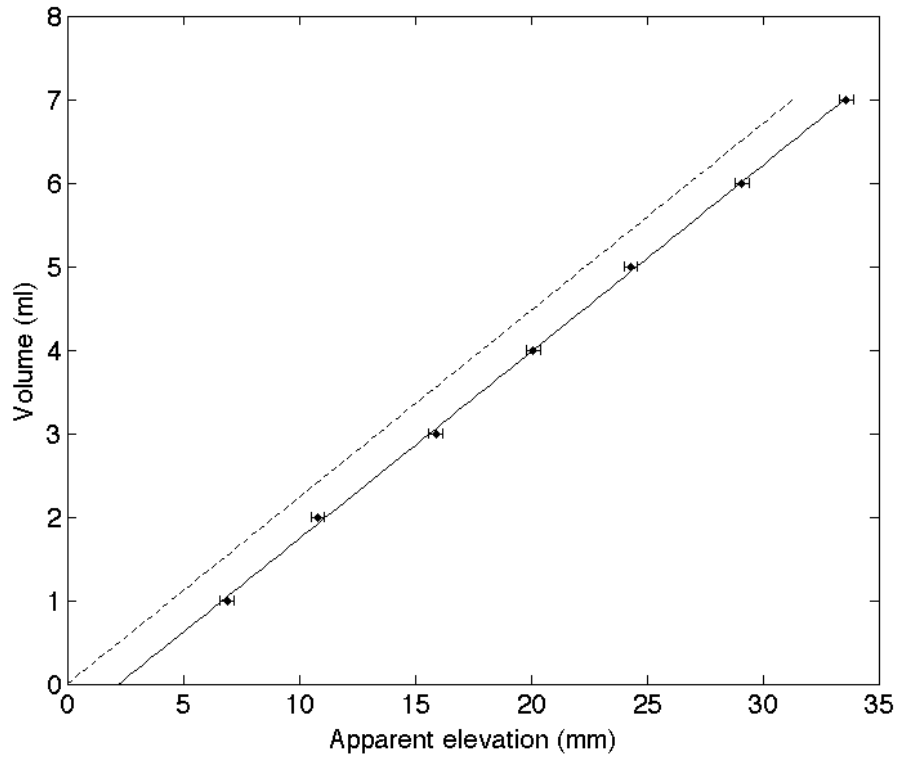


Figure 3.2. Volume vs elevation calibration. Solid line: apparent elevation measured acoustically. Dotted line: elevation from the bottom of cell.

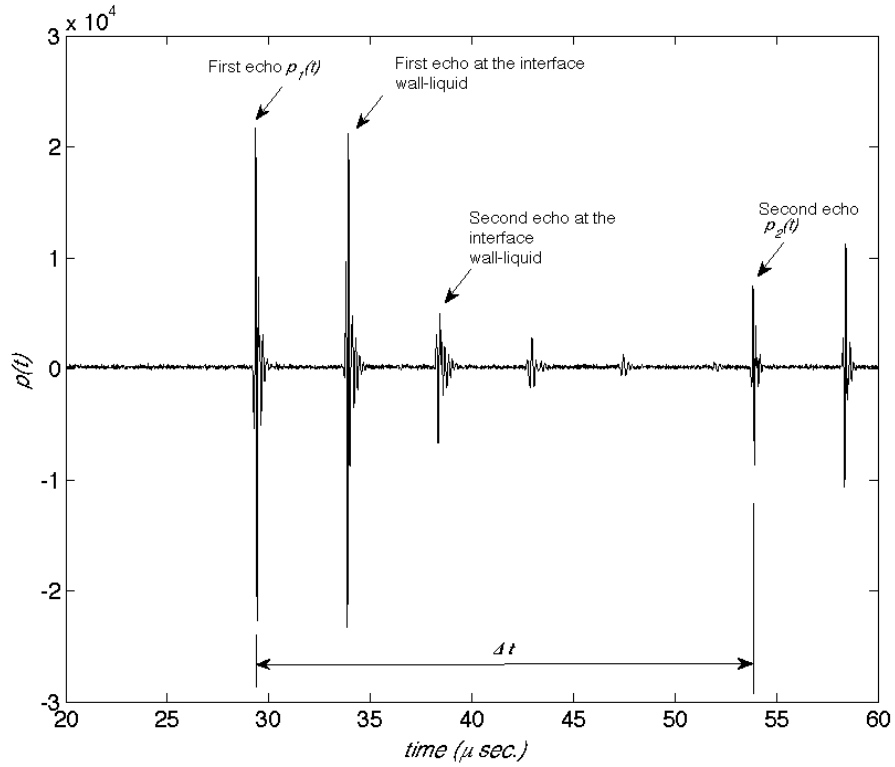


Figure 3.3. Reflected waveform in toluene at 25 C and $z=18.5$ mm.

resolution is half the height of an element - 0.3 mm. Relative elevation is measured from the first acoustic beam. From volume calibration measurements based on liquid-air interface elevation, Figure 3.2, the first acoustic beam is measured at 2.2 mm below the base of the cell. An example of a reflected waveform $p(z,t)$ in pure toluene at an elevation $z = 18.5$ mm is shown in Figure 3.3. It is recorded from time $t = 20 \mu\text{s}$ to $t = 60 \mu\text{s}$ after firing the pulse. It contains two reflections of the initial pulse $p_1^{Echo}(z,t)$ and $p_2^{Echo}(z,t)$ as shown in Figs 3.3 and 3.4:

$$\begin{cases} p_1^{Echo}(z,t) = p(z, t_i < t < t_i + T) \\ p_2^{Echo}(z,t) = p(z, t_i + \Delta t(z) < t < t_i + T + \Delta t(z)) \end{cases}, \quad (3.1)$$

where t_i is the start time of the first echo and T is the duration of the reflection waveform. $\Delta t(z)$ is the travel time between the first and the second echoes $p_1^{Echo}(z,t)$, $p_2^{Echo}(z,t)$ at elevation z .

The autocorrelation function of the waveform $p(z,t)$, shown in Figure 3.5, is given by:

$$C_p(z,\tau) = \int_0^{t_{\max}} p(z,t) p(z,t+\tau) dt. \quad (3.2)$$

The local speed of sound is calculated using the following equation:

$$u(z) = \frac{2l(z)}{\Delta t(z)}, \quad (3.3)$$

where $l(z)$ is the acoustic path length and $\Delta t(z)$ is the time delay between the first and the second echoes $p_1^{Echo}(z,t)$ and $p_2^{Echo}(z,t)$ at elevation z . $\Delta t(z)$ corresponds to the time delay of the second maximum in the autocorrelation function. The first maximum corresponds to the reflection at the wall-liquid interface.

Acoustic path length, Figure 3.6, was calibrated at each elevation based on literature data for the speed of sound in toluene at 25 C (1302.9 m/s) [16], and it varies systematically with elevation from 15.85 mm to 15.99 mm. These acoustic path lengths were used for local speed of sound evaluation, equation (3.3).

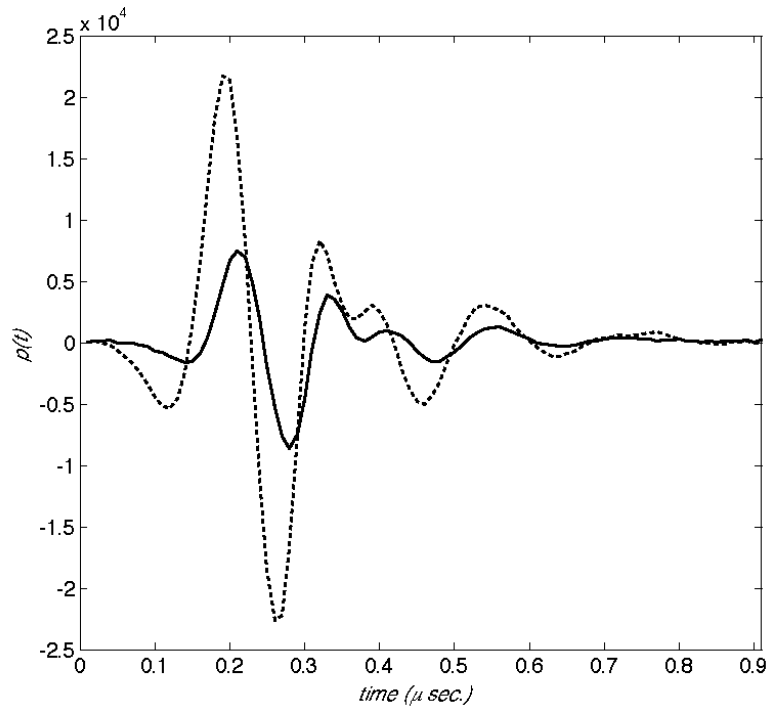


Figure 3.4. Truncated reflected waveforms of the first and second reflected waveforms measured in toluene at 25 C: (---) $p_1(t)$, (—) $p_2(t)$.

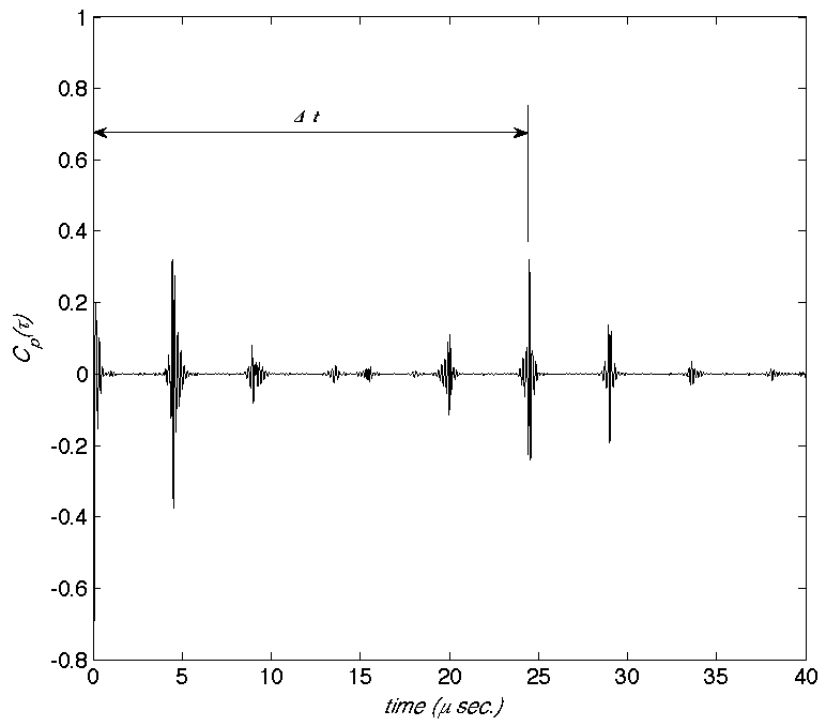


Figure 3.5. Autocorrelation function of an acoustic waveform in toluene at $T=25$ C and $z=18.5$ mm.

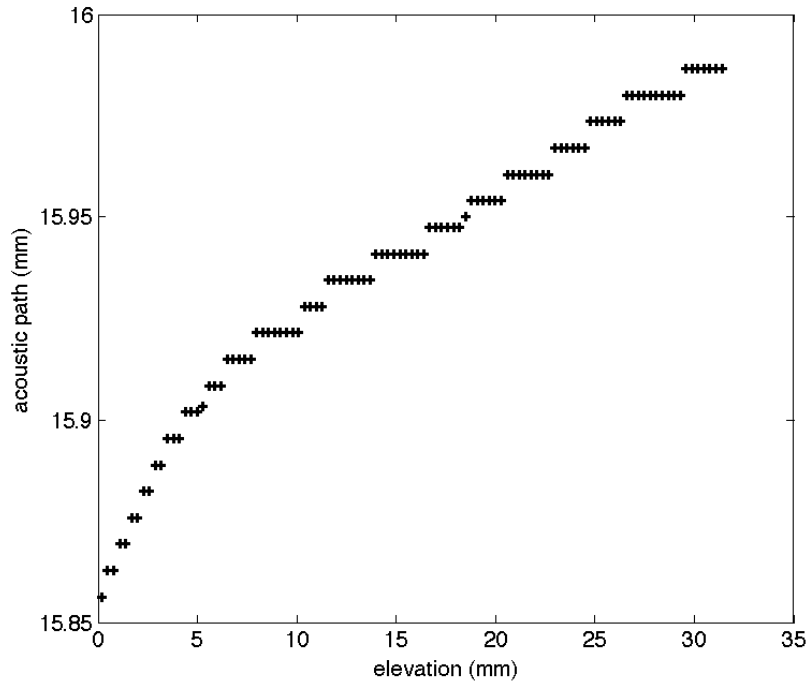


Figure 3.6. Acoustic path length vs elevation based on speed of sound measurements in toluene at 25 C.

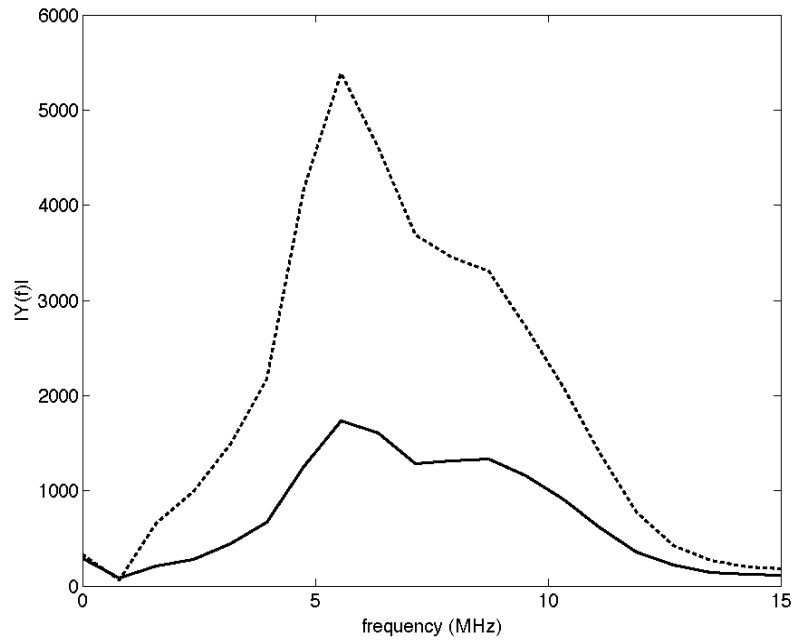


Figure 3.7. Frequency spectra for the first and second reflection waveforms in toluene at 25 C and $z=18.5$ mm: (---) $\tilde{p}_1(f)$, (—) $\tilde{p}_2(f)$.

Attenuation spectra are calculated using the following equation:

$$A(z,f) = -10 \log_{10} \left(\frac{\tilde{p}_2^{Echo}(z,f)}{\tilde{p}_1^{Echo}(z,f)} \right), \quad (3.4)$$

where $\tilde{p}_1^{Echo}(z,t)$, $\tilde{p}_2^{Echo}(z,t)$ are the Fourier transforms of $p_1^{Echo}(z,t)$, $p_2^{Echo}(z,t)$ respectively. Example Fourier transforms, for first and second echos for toluene at 25 C, at elevation $z = 18.5 \text{ mm}$ are presented in Figure 3.7. The spectra of the waveforms possess maxima between 4 MHz and 9 MHz. Consequently, the evolution of the attenuation spectra were monitored in this frequency range. The attached matlab code was developed to analyze the data and produce speed of sound and attenuation results and videos of the phase separation kinetics from the recorded waveforms.

3.2.3. Materials

Toluene (99%), n-heptane (99%), mixed hexanes (65% n-hexane) were purchased from Fisher scientific. Methanol (99%) was purchased from Aldrich. All were used without further purification.

The synthetic porous medium comprised a block (16 mm x 12 mm x 38 mm) cut from a ChemGlass filter disk ($\varnothing 190 \text{ mm} \times 15 \text{ mm}$). After cleaning with concentrated hydrochloric acid, the block was washed and then soaked for 24 hours in distilled water. It was then dried under vacuum at 80 C for 12 hours. Mercury porosity measurement showed that the block had an average pore diameter of 13 μm and a porosity of 23.7 % vol. The porous block was partially filled with Athabasca bitumen by immersing it in bitumen at 60 C for 80 minutes as shown in Figure 3.8.a. Bitumen penetrated the pores and was imbibed by capillary pressure to approximately half the height of the block [17]. The block was then immersed in heptane within the cell, at 22.5 C and 1 atm (Fig.3.8.b).

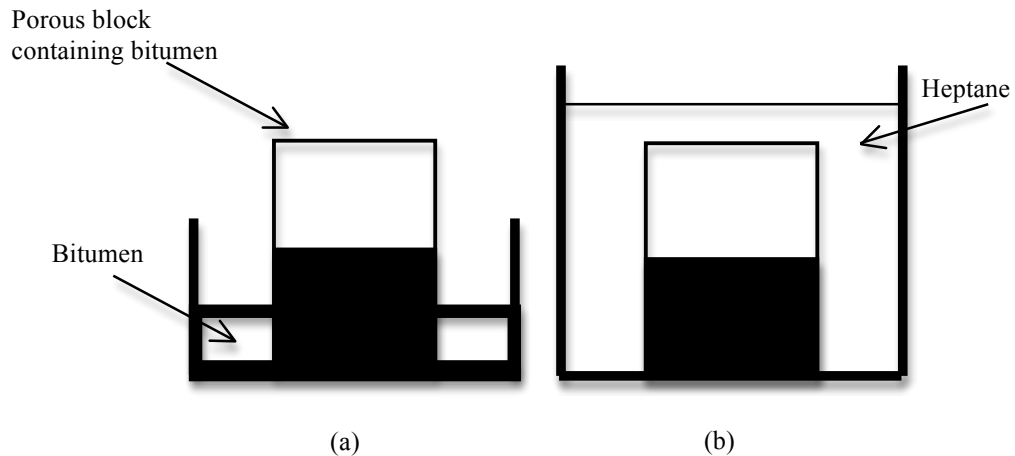


Figure 3.8. (a) Preparation of a synthetic porous block partially saturated with bitumen. (b) Porous block immersed in heptane inside the cell during acoustic measurements.

3.3. Results and discussion

3.3.1. Acoustic measurements of liquid-liquid separation in organic mixtures

3.3.1.1. Speed of sound vs composition

The speed of sound was measured in mixtures of methanol + heptane and methanol + mixed hexanes. Values are reported in Figures 3.9 a and b. The speed of sound decreases with increasing methanol volume fraction for both cases until the mixtures separate into alkane-rich and methanol-rich liquid phases. At high methanol volume fractions, the mixtures pass from the liquid-liquid region to the single-phase methanol-rich liquid region. The speed of sound then increases with methanol volume fraction, in the single phase region, rising to the speed of sound in pure methanol. For mixtures of methanol + heptane, the average speeds of sound in the, fixed-composition, heptane-rich and methanol-rich phases are 1115.0 m/s and 1080.4 m/s respectively as indicated by the two horizontal dotted lines in Figure 3.9.a. The saturated compositions of methanol in the two liquid phases are 6.5 vol% and 71.9 vol%. These values are in good agreement with ones reported in the literature 4.7 vol % and 72.1 vol% for the same mixture [18]. For the mixed hexanes + methanol case, the transition from liquid to liquid-liquid phase behavior is marked by cusps in the speed of sound-composition

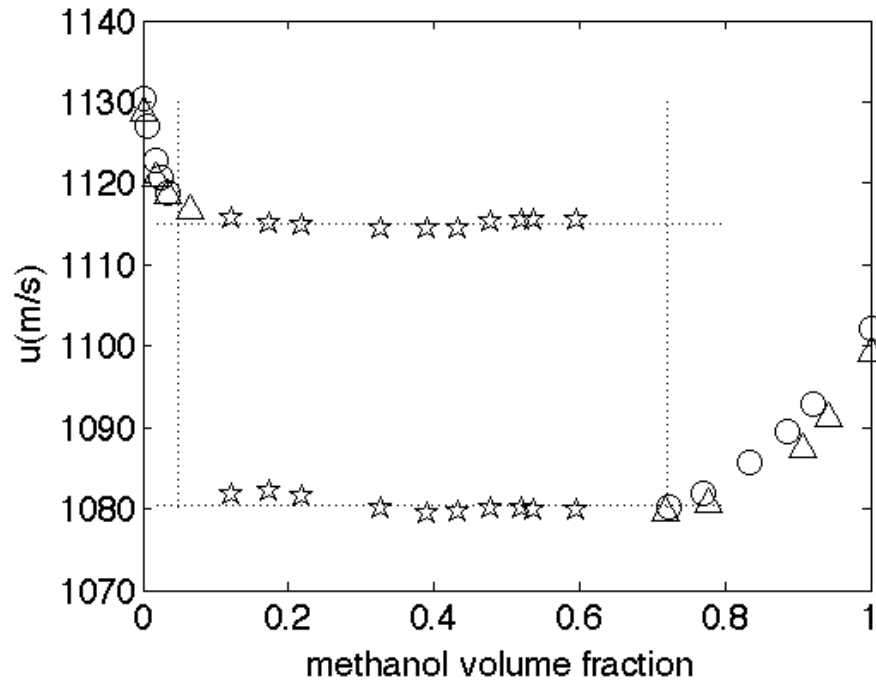


Figure 3.9.a. Speed of sound in methanol + heptane mixtures at 25 C and 1 atm: (circle): experimental data [18] (triangle): single-phase region, (star): two-phase region. Dotted vertical lines: binodals reported in the literature.

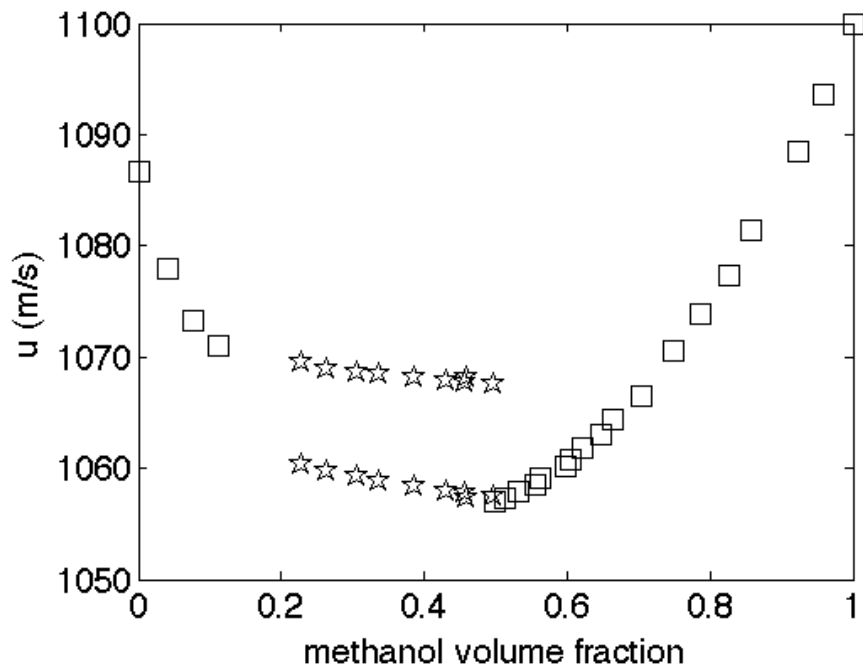
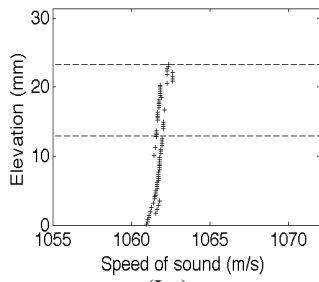


Figure 3.9.b. Speed of sound in methanol + mixed hexanes at 25 C and 1 atm: (square): single-phase region, (star): two-phase region.

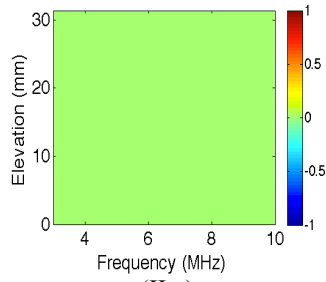
dependence. As there are multiple components present, the speeds of sound in the two phase region vary with global composition, as seen in Figure 3.9b.

3.3.1.2. Acoustic property profiles and the kinetics of phase separation in liquid mixtures

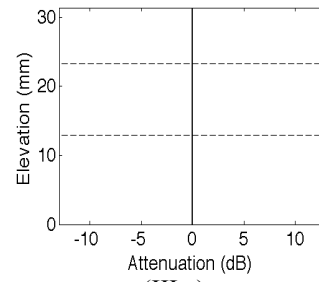
Figure 3.10 shows the time dependent evolution of the speed of sound, column I, the attenuation difference spectra map, column II, and the value of the attenuation difference at 7.94 MHz, column III, from time $t=0$ s (just after mixing) to time t_f (after completion of phase separation) for mixed hexanes + methanol (38.7 % vol). Values were measured at 113 elevations simultaneously. The attenuation difference is the difference between the attenuation at time t ($A(z,f)|_t$) and time $t=0$ s ($A(z,f)|_{t=0}$) just after mixing. The evolution of the speed of sound and attenuation difference measurements as functions of elevation provide insights into the phase separation process. The phases begin to separate within one second, and within 9 seconds, the hexane-rich and methanol-rich phases are largely separated as shown in Figure 3.10 I.a – I.j. The speed of sound increases with time in the upper part of the cell and decreases in the lower part. Only slight systematic variations of speed of sound with elevation remain in each phase after 9 seconds. The attenuation spectra profiles, presented in Figure 3.10 II.b-II.d, show that large attenuation difference regions are formed from the top and the bottom of the cell. These attenuation regions are likely caused by losses in the acoustic energy at the liquid-liquid interface between the nucleating phase and the continuous phase. The high attenuation regions appear to coalesce to form an attenuation peak/spike at the horizontal liquid-liquid interface (Fig 3.10 II.e-II.j). Large random fluctuations persist at and above the liquid-air interface. Ultrasonic attenuation and speed of sound profiles both provide independent measures of interface location and the dynamics of the phase separation. The evolution of local compositions, and the scale and devolution of the interfacial region are readily traced using either local speed of sound or attenuation measurements.



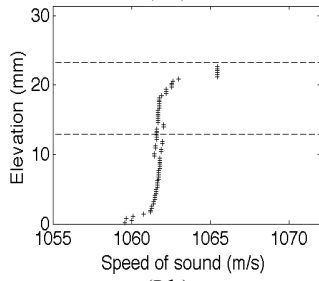
(I.a)



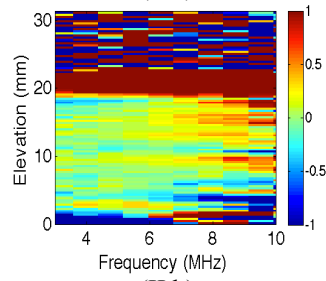
(II.a)



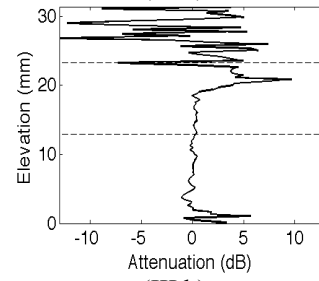
(III.a)



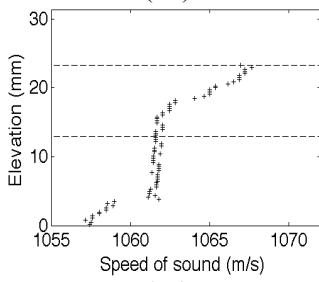
(I.b)



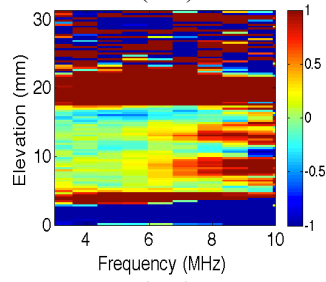
(II.b)



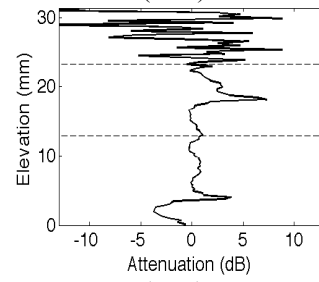
(III.b)



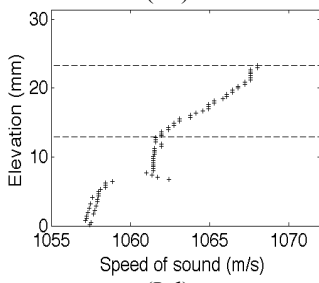
(I.c)



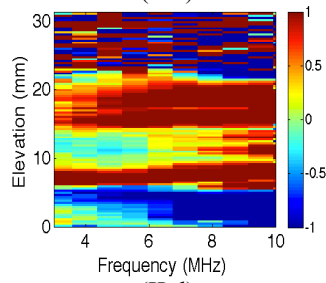
(II.c)



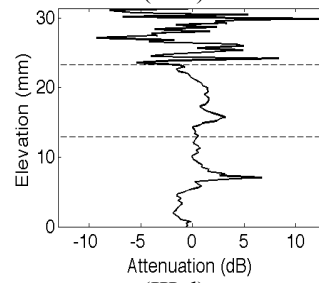
(III.c)



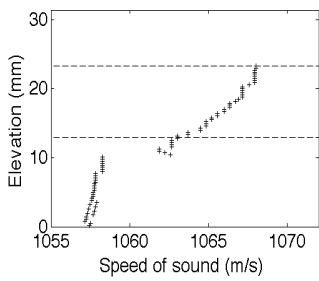
(I.d)



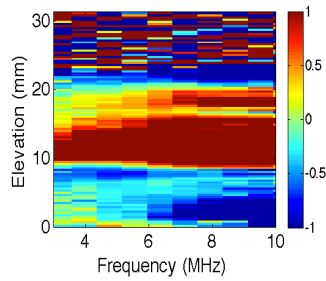
(II.d)



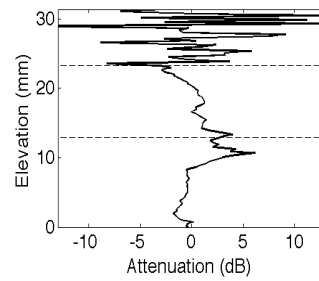
(III.d)



(I.e)



(II.e)



(III.e)

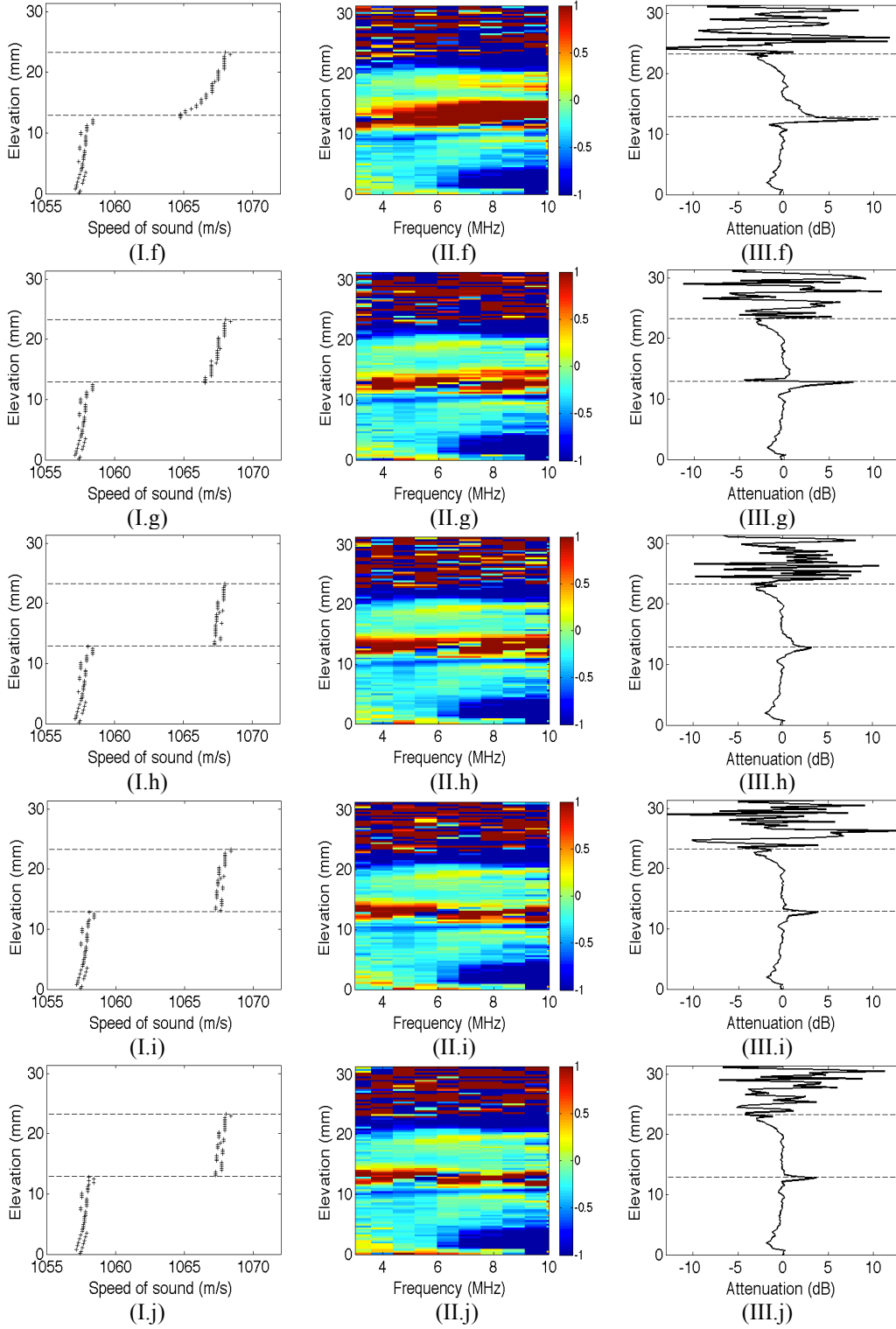


Figure 3.10. Evolution of speed of sound and attenuation profiles for 38.7 vol.% methanol in mixed hexanes during phase separation at 25 C and 1 bar: (a) $t=0$ s, (b) $t=1$ s, (c) $t=2$ s, (d) $t=3$ s, (e) $t=4$ s, (f) $t=5$ s, (g) $t=6$ s, (h) $t=7$ s, (i) $t=8$ s, (j) $t=9$ s. Column (I): speed of sound, column (II) attenuation difference spectra $\Delta A(f,z)$, column (III) attenuation difference at $f = 7.94$ MHz ($\Delta A(f=7.94 \text{ MHz}, z)$).

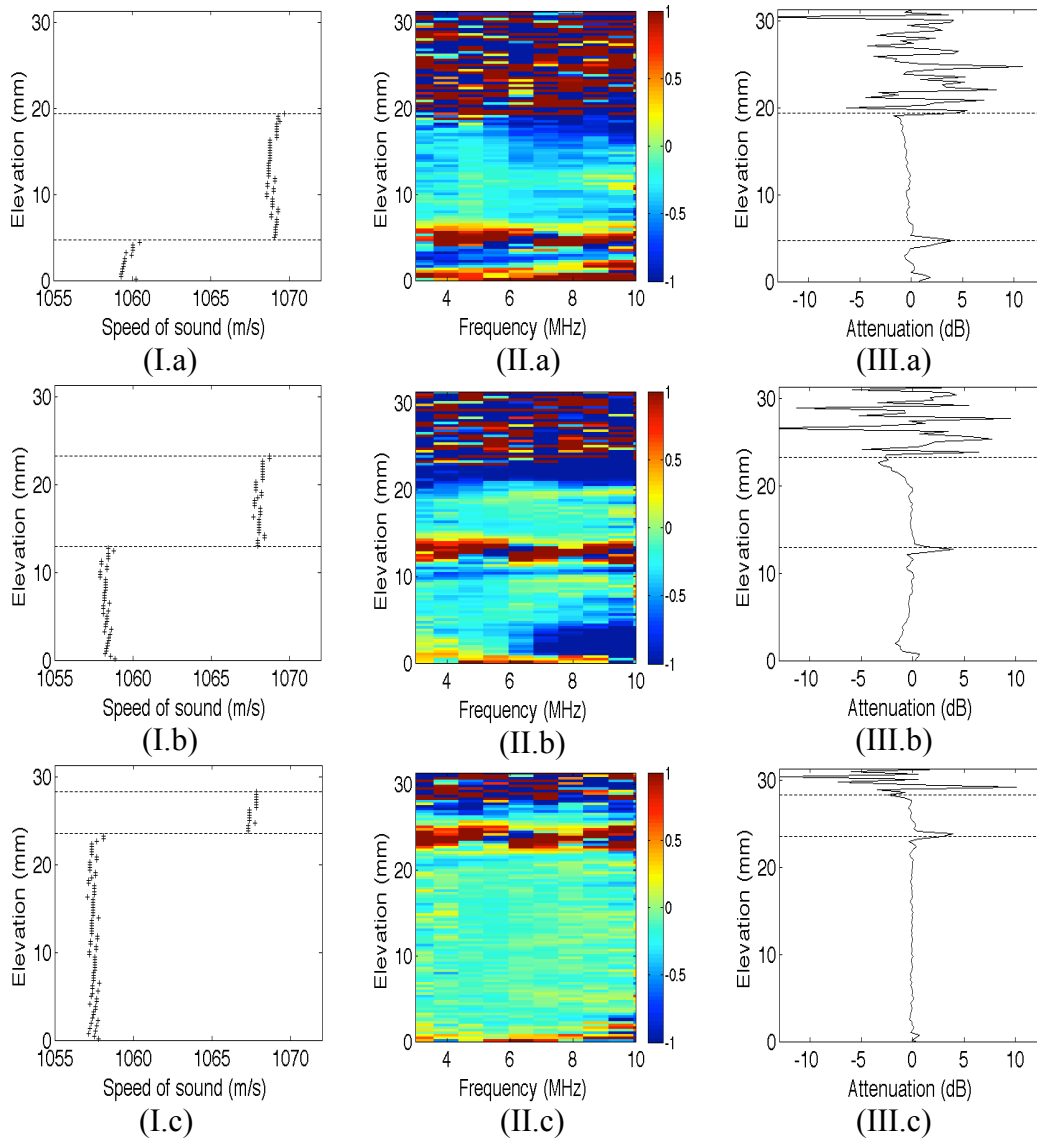


Figure 3.11. Equilibrium speed of sound and attenuation profiles for methanol in hexane: (a) 26.3% vol. methanol, (b) 38.7% vol. methanol (c) 49.7% vol. methanol. Along the columns: (I): speed of sound, (II) attenuation difference spectra $\Delta A(f,z)$, (III) attenuation difference at $f = 7.94$ MHz ($\Delta A(f=7.94 \text{ MHz}, z)$). Horizontal lines indicate liquid-liquid and liquid-air interfaces.

Figure 3.11 shows the speed of sound and acoustic attenuation profiles 10 minutes after phase separation for three different methanol + mixed hexane compositions. For these cases, the liquid-liquid and liquid-air interfaces are well defined by

discontinuities in the speed of sound and spikes in the attenuation profiles and the relative volume fractions are consistent with expectations.

3.3.2. Acoustic measurements in porous media

For these experiments, the acoustic cell was operated in transmission mode. Acoustic wave transmission time measurements performed 2 hours after immersing a porous block in heptane were used as a baseline for transmission time differences for a porous block partially filled with bitumen that was subsequently immersed in heptane, where heptane filled the upper part and the free space on both sides of the block as shown in Figure 3.8 b. Transmission time difference profiles are shown in Figure 3.12, for immersion times: 2 hours, 23 hours and 53 hours. Ultrasonic waves travel faster in the bitumen filled porous medium because the speed of the acoustic waves increases with the viscosity of the fluid [14]. Bitumen is orders of magnitude more viscous [19] than heptane. The transmission time difference in the lower part of the block decreases with time as a consequence of heptane penetration and counter diffusion of bitumen. In the upper part of the block, transmission times change little with time, indicating that bitumen moves upward only slowly through the porous medium – less than 4 mm in 53 hrs. This can be attributed to the fact that bitumen also diffuses to heptane in the free space on the sides of the block. In the absence of a porous medium, bitumen is detected more than 20 mm vertically upward from a pentane-bitumen interface within 24 hours [20] [2]. Clearly, imbibition, diffusion and other processes are readily monitored in porous media using differences in local speed of sound or transmission time values. Numerous applications with standard industrial cores and synthetic cores are envisioned.

3.3.3. Two Dimensional acoustic mapping

The results above are promising. Organic phases, composition gradients and fluid movement/diffusion are readily measured as averages at specific elevations even

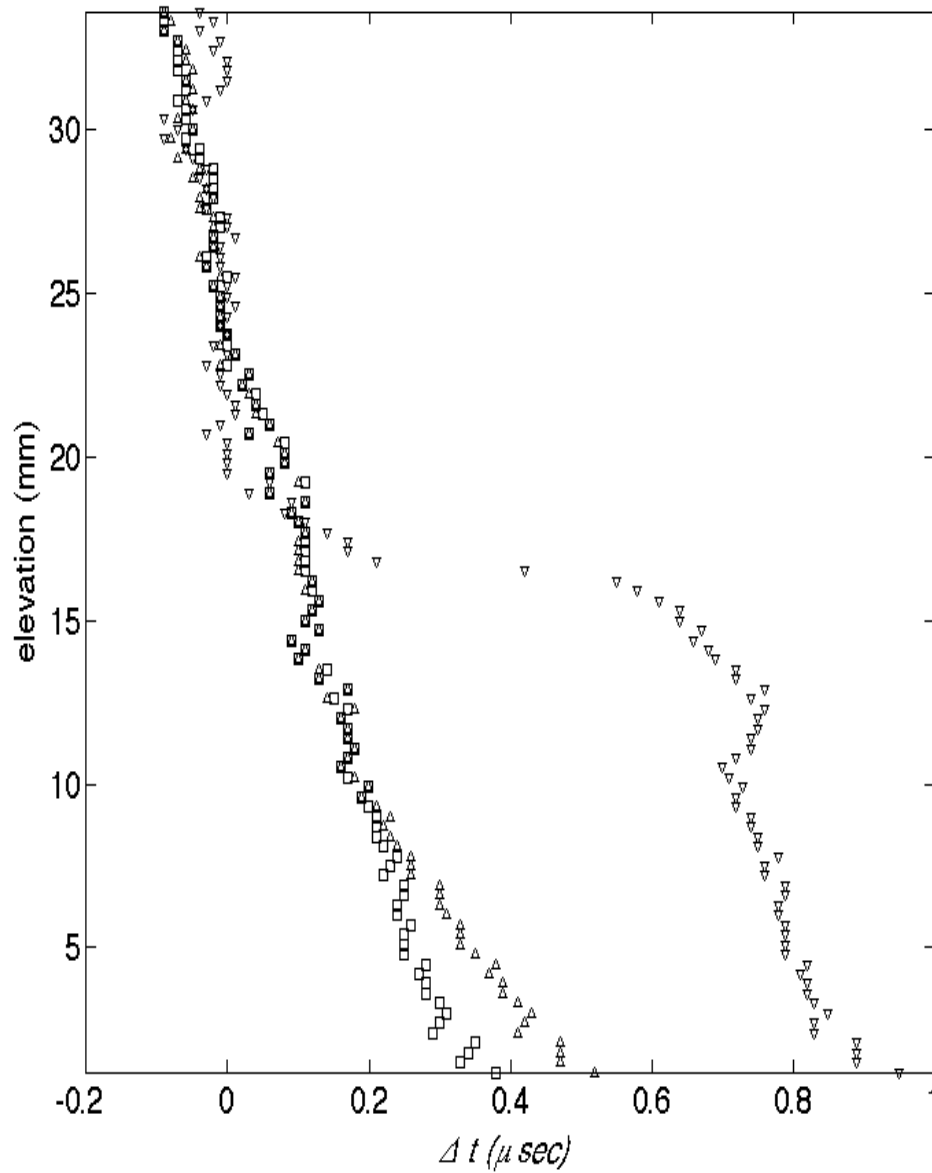


Figure 3.12. Travel time difference profiles, at 22.5 C and 1 atm in: (∇) a porous block partially saturated with bitumen in its lower part immersed in heptane for 2 hours, (Δ) a porous block after 23 hours, (sq) porous block after 53 hours.

in porous media. These results set the stage for the creation of two dimensional speed of sound and acoustic attenuation maps where spatial variation at fixed elevation is evaluated. In principal, this can be realized using acoustic arrays but it is computationally complex from both a data acquisition and processing perspective. However, such images would provide rich understanding of processes dynamics at fine length and time scales with industrial fluids.

References

1. Abedi, S., Cai, H., Seyfaie, S., & Shaw, J. (1999) Simultaneous phase behaviour, elemental composition and density measurement using X-ray imaging. *Fluid Phase Equilibria* 158, 775-781.
2. Zhang, X., Fulem, M., & Shaw, J. M. (2007) Liquid-phase mutual diffusion coefficients for Athabasca bitumen plus pentane mixtures. *Journal of Chemical and Engineering Data* 52, 691-694.
3. Zhang, X., Chodakowski, M., & Shaw, J. (2004) Dynamic interfacial zone and local phase concentration measurements in emulsions, dispersions, and slurries. *Journal of Dispersion Science and Technology* 25, 277-285.
4. Erne, B., van der Maas, J., Kuipers, B., Visser, T., & Philipse, A. (2003) Vertical concentration profiles in colloidal fluids measured by FTIR-ATR spectroscopy. *Langmuir* 19, 3081-3083.
5. Kumar, R., Lang, S., Englezos, P., & Ripmeester, J. (2009) Application of the ATR-IR Spectroscopic Technique to the Characterization of Hydrates Formed by CO₂, CO₂/H₂ and CO₂/H₂/C₃H₈. *Journal of Physical Chemistry A* 113, 6308-6313.
6. Pilhofer, G., Mccarthy, M., Kauten, R., & German, J. (1993) Phase Separation in Optically Opaque Emulsions. *Journal of Food Engineering* 20, 369-380.
7. Afsahi, L. & Kantzas, A. (2007) Advances in diffusivity measurement of solvents in oil sands. *Journal of Canadian Petroleum Technology* 46, 56-61.
8. D.B. Fisher, (2000) Use of Magnetic Resonance Imaging and Advanced Image Analysis as a Tool to Extract Mass Transfer Information from a 2D Physical Model of The Vapex Process. *SPE/DOE Improved Oil Recovery Symposium, Tulsa, Oklahoma, 2000: p. SPE 59330*.
9. K. Karmaker, B. B. M. (2003) A Stochastic Approach to Extract Vapex Related Dispersion Coefficients from Magnetic Resonance Images.. *SPE Annual Technical Conference and Exhibition, Denver, Colorado, 2003: p. SPE 84198*.
10. Machefer, S. & Schnitzlein, K. (2007) Inline concentration monitoring of binary liquid mixtures in the presence of a dispersed gas phase with a modified speed of sound immersion probe. *Chemical Engineering & Technology* 30, 1381-1390.
11. Khasanshin, T., Shchamialiou, A., & Poddubskij, O. (2003)

Thermodynamic properties of heavy n-alkanes in the liquid state: n-dodecane. *International Journal of Thermophysics* 24, 1277-1289.

12. Takagi, T., Fujita, K., Furuta, D., & Tsuji, T. (2003) Bubble point pressure for binary mixtures of propane and pentafluoroethane. *Fluid Phase Equilibria* 212, 279-283.

13. Lu, Z., Daridon, J., Lagourette, B., & Ye, S. (1999) Phase comparison technique for measuring liquid-liquid phase equilibrium. *Review of Scientific Instruments* 70, 2065-2068.

14. Gurevich, B., Osypov, K., Ciz, R., & Makarynska, D. (2008) Modeling elastic wave velocities and attenuation in rocks saturated with heavy oil. *Geophysics* 73, E115-E122.

15. NDT, O. (2007) Introduction to Phased Array Ultrasonic Technology Applications.

16. webbook.nist.gov

17. Siddique, J. I., Anderson, D. M., & Bondarev, A. (2009) Capillary rise of a liquid into a deformable porous material. *Physics of Fluids* 21.

18. Orge, B., Iglesias, M., Rodriguez, A., Canosa, J., & Tojo, J. (1997) Mixing properties of (methanol, ethanol, or 1-propanol) with (n-pentane, n-hexane, n-heptane and n-octane) at 298.15 K. *Fluid Phase Equilibria* 133, 213-227.

19. Bazyleva, A. B., Hasan, A., Fulem, M., Becerra, M., & Shaw, J. M. (2010) Bitumen and Heavy Oil Rheological Properties: Reconciliation with Viscosity Measurements. *Journal of Chemical and Engineering Data* 55, 1389-1397.

20. Zhang, X. & Shaw, J. M. (2007) Liquid-phase mutual diffusion coefficients for heavy oil plus light hydrocarbon mixtures. *Petroleum Science and Technology* 25, 773-790.

Chapter 4. Phase Behavior of Asphaltenes + Polystyrene + Toluene Mixtures at 293 K, Part One: Experimental Results and Discussion

4.1. Introduction

Asphaltenes are defined as the fraction of oil insoluble in alkanes and soluble in benzene and toluene on the basis of filtration experiments (ASTM D4055). In toluene, asphaltenes aggregate to form sterically stabilized colloidal particles. The size of these particles has been the subject of several investigations. For example, Barre et al [1] measured the radius of gyration of asphaltene colloidal particles in a 3 vol% toluene solution using small-angle X-ray scattering (SAXS). They found that the size of asphaltene aggregates fall in the range 6.3 to 16 nm. In heavy oils (15 to 20 w% asphaltenes [2]) nanofiltration experiments showed that asphaltene nanoaggregates form large aggregates up to 50 to 100 nm in both Athabasca bitumen and Maya crude oil [3]. Espinat et al [4] measured the size of asphaltenes in toluene using small-angle X-ray scattering (SAXS), small-angle neutron scattering (SANS) and dynamic light scattering to investigate the effect of temperature and pressure on the size of asphaltene aggregates in toluene. They found that the size of asphaltene aggregates decreased with temperature, while pressure did not appear to have a significant effect on size. The interaction forces between asphaltene colloidal particles in toluene are dominated by repulsion. Steric repulsive forces between asphaltene coated surfaces in toluene were measured by Wang et al [5].

If asphaltene containing mixtures are treated as colloidal solutions, energy intensive phase separation methods include: ultracentrifugation, variation of pressure, temperature, solvent evaporation and addition of antisolvent [6] [7]. Alternatives include polymer addition[7]. In a recent work, Lima et al [8] focused on the impact of adsorbing polymers, polycardanol and sulfonated polystyrene, on asphaltene solutions. Polycardanol polymers were added to asphaltene in toluene solutions (60 mg/L) and sulfonated polystyrene was added to asphaltene in toluene + acetone solution. Asphaltene + polymer solutions were left for 24 hours and then centrifuged at 3000 rpm for 30 min. The effect of polymer addition was estimated by measuring the concentration of asphaltenes left in the solutions with a UV-Visible spectrophotometer. The authors found that at low polymer concentrations (0 to 0.4-0.7 w/vol% for polycardanol and 0 to 0.2 w/vol% for sulfonated polystyrene) both sets of polymers act as flocculants. In this case, polymer molecules adsorb to more than one nanoaggregate. The nanoaggregates become attached to one another and form flocs. At higher polymer concentrations, the polymers behave as a dispersant. It was reported that polystyrene without polar groups did not modify asphaltene behavior in dilute solution. This result from the literature is different from the anticipated behavior for the impact of a non-adsorbing polymer (polystyrene) in a good solvent (toluene) [9][10] on concentrated sterically stabilized colloidal particles (asphaltenes) [5]. The result may reflect the dilute composition range investigated.

Sieglaff et al [11] found that when linear polystyrene is added to a cross-linked polystyrene swollen particle – microgel particle- sterically stabilized in toluene, the mixture separates into two stable liquid phases. A similar result was obtained by Clarke et al [12] for a mixture of polystyrene microgel particle + linear polystyrene + ethylbenzene. Phase separation was attributed to entropy effects. The mechanism driving phase separation for these mixtures is depletion flocculation, it was first described by Asakura and Oosawa [13] [14]. The microgel polystyrene particles are assumed to be sufficiently cross-linked to prevent penetration by linear polymer chains. In this case, the configurations for

which the polymer penetrates the microgel particle are excluded. Effectively, a polymer free depletion layer forms around the dispersed particles. When two depletion layers overlap, the osmotic pressure around the particles becomes unbalanced giving rise to a net attractive force. For a sufficiently high polymer concentration, mixtures can separate into colloid-poor and colloid-rich stable phases of uniform composition. The colloid rich phase can be either liquid-like or solid-like. The addition of non-adsorbing polymers can therefore be used to control the attractive forces between the colloidal particles and to manipulate their phase behavior. The phase behavior of mixtures of colloids and non-adsorbing polymers has been the subject of a substantial number of experimental and theoretical investigations[15]. For example, Ramkrishnan et al [16] measured the phase behavior of silica particles ($a=50$ nm) coated with 1-octadecanol + polystyrene in toluene. They observed fluid-gel, fluid-crystal and fluid-fluid transitions as the ratio of polymer radius of gyration to colloidal particle radius (R_g/a) increased from 0.026 to 1.395. Hennequin et al [17] measured the phase behavior of silica particles sterically stabilized with 1-octadecanol in toluene + polystyrene for $R_g/a=4.1$ and 5.2. They found that, after nearly one hour of homogenization and over a range of compositions, the mixtures separated into two stable liquid phases: one colloid rich and one colloid poor. The method developed by Bodnar et al [18] was then used to estimate the composition of the phases in equilibrium.

In this work, asphaltenes in toluene solutions are investigated at concentrations greater than 5.0 vol%. At these concentrations, asphaltenes form sterically stabilized colloidal particles. Thus, the phase behavior of concentrated asphaltene + polystyrene + toluene solutions is expected to be analogous to that of silica colloidal particles sterically stabilized with C_{18} alcohol + polystyrene + toluene. In this work, the ultrasonic phase array acoustic cell, described in the previous Chapter, is used to investigate the phase behavior of mixtures of asphaltene + polystyrene + toluene at 293 K.

4.2. Experimental methodology

4.2.1. Chemicals and solution preparation

Toluene 99% was purchased from Fisher Scientific and pentane asphaltenes were prepared from Maya crude oil according to ASTM standard D4055 and to the titration method [19] [20]. Asphaltene in toluene mixtures were prepared by adding toluene to vials containing asphaltenes. They were mixed with a vortex mixer and hand shaking for at least 45 min until they appeared homogeneous and liquid like. They were then stirred to make sure that there were no macroscopic solid aggregates in the solution. Polystyrene with two different average molecular weights: $M_w = 393,400$ g/mol and $M_w = 700,000$ g/mol were purchased from Aldrich.

The volume fractions of asphaltenes and polystyrene were calculated assuming an asphaltene density of 1.17 g/cm³ [21] and by using the density of polystyrene specified by the supplier, 1.047 g/cm³.

4.2.2 Experimental apparatus and measurements

A detailed description of the experimental apparatus and the measurement methodology is available in the previous chapter. Key points are summarized here. Phase boundaries are detected on the basis of two independent measurements namely: speed of sound differences between phases, and spikes in acoustic wave attenuation, that arise at liquid-liquid interfaces. Uniformity of compositions within phases is evaluated from speed of sound profiles. Composition gradients are readily detected as are composition differences between phases. Both sets of measurements are obtained from reflected waveforms measured with a phased array acoustic probe attached to the walls of a PolyBenzImidazole cell. Measurements were performed at 113 elevations simultaneously with the first waveform being measured at an elevation of 1.2 mm

from the bottom of the cell. Acoustic wave attenuation is less accurate than speed of sound for interface detection but plays an important supporting role in cases where the volume of a phase is too small to obtain a speed of sound measurement.

Asphaltene + polystyrene + toluene mixtures were prepared in the cell by introducing mixtures of asphaltene in toluene and polystyrene in toluene separately with a syringe. The final composition of the mixture depended on the relative amounts of the added mixtures as shown in Figure 4.1. The contents were stirred for 5 minutes before the stirrer was removed. The acoustic measurements were started after removing the stirrer to capture the acoustic properties just after mixing (time $t=0$ min), and then at a rate of about 5 min for at least the first hour after homogenization. The rate of the measurements was then decreased.

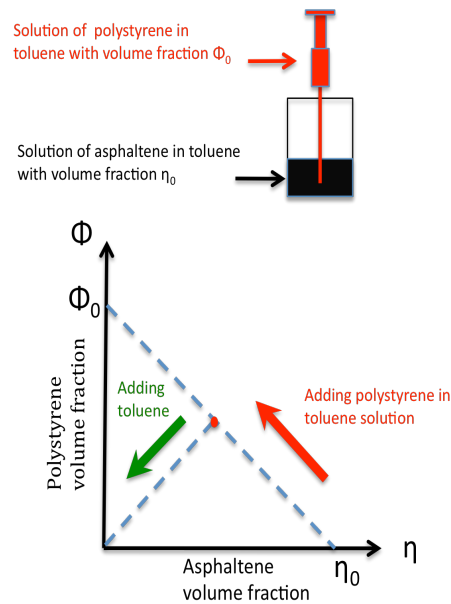


Figure 4.1. Experimental variation of mixture composition in the phase diagram

The temperature of the mixture just after mixing can be still affected by the temperature of the added solution and the surrounding air. It may not have reached its stable equilibrium temperature. This could have an impact on the speed of sound measurement at $t=0$ min. Temperature shifts of ± 0.1 C can

change speed of sound values in both phases. Changes in the temperature of the environment can also have an impact on the measured speed of sound.

4.3. Dependence of the speed of sound and acoustic wave attenuation on the volume fraction of asphaltenes and polystyrene in toluene

Figure 4.2 shows the variations of the speed of sound with elevation for five asphaltene volume fractions in toluene. Each measurement was performed at least 1 hour after introducing the mixtures into the cell. For the case of 23.4 vol% asphaltene in toluene, the measurement is performed 17 hours later. For each asphaltene volume fraction, five speed of sound profiles are superimposed. They are calculated from five different waveforms. The profiles of the speed of sound appear nearly vertical lines. This suggests that asphaltenes are stable and the mixtures are homogenous.

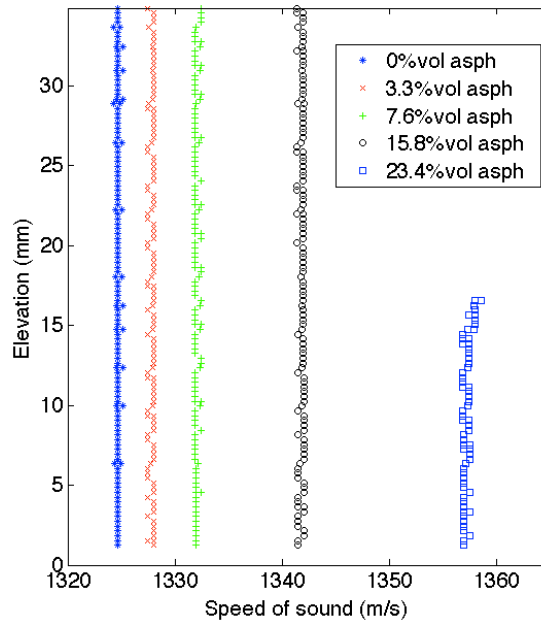
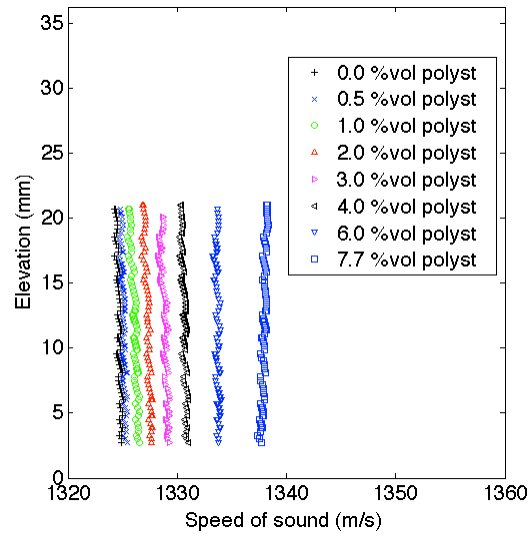
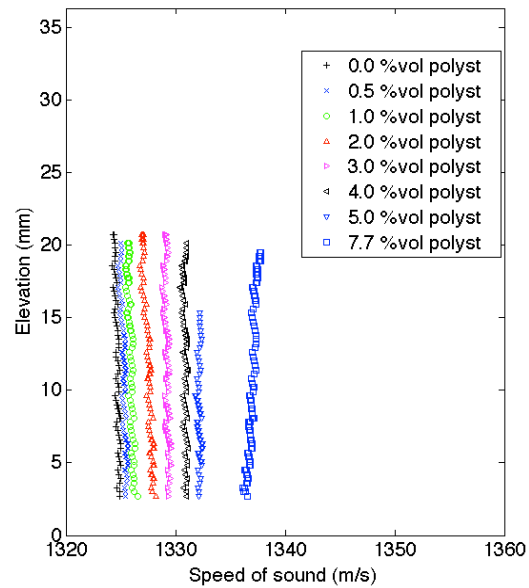


Figure 4.2. Speed of sound profiles in asphaltene + toluene mixtures at 20 C and 1.0 atm. Asphaltene volume fraction is a parameter.

Figures 4.3.a-b show the variations of the profiles of the speed of sound with elevation for seven polystyrene volume fractions and for two polystyrene molecular weights ($M_w=393,400$ g/mol, $M_w=700,000$ g/mol). Measurements were



(a)



(b)

Figure 4.3. Speed of sound profiles in toluene + polystyrene mixtures at 20 C and 1.0 atm. Polymer volume fraction is a parameter. (a) $M_w=393,400$ g/mol, (b) $M_w=700,000$ g/mol.

performed 22-24 hours after introducing the solutions in the cell. Phase separation was not observed. The gradient in the speed of sound values with elevation, evident for mixtures of 7.7 vol% polystyrene in toluene, may reflect small thermal or composition gradients.

The apparent speeds of sound in asphaltene and polystyrene were estimated by assuming that the speeds of sound in the binary mixtures asphaltene + toluene and polystyrene + toluene vary linearly with volume fraction, over the composition range where experimental speed of sound data are available. The estimated values of the speeds of sound are 1457.7 m/s, 1490.65 m/s and 1483.7 m/s for asphaltene, and polystyrenes ($M_w=393,400$ g/mol, $M_w=700,000$ g/mol) respectively (Figures C.1-3).

A model based on the Redlich-Kister correlation is used to describe the deviation of the experimental speed of sound from the average volume fraction values [22] in the binary mixtures of asphaltenes + toluene and polystyrene + toluene:

$$\begin{aligned}\Delta u &= u_{\text{exp}} - (\Phi_j u_j + (1 - \Phi_j) u_{\text{tol}}) \\ &= \Phi_j (1 - \Phi_j) \sum_{k=0}^3 A_k [\Phi_k - (1 - \Phi_k)]^k\end{aligned}\quad (4.1)$$

where Φ_j and u_j are the volume fractions and speeds of sound of asphaltenes (η , u_{asph}) or polystyrene (ϕ , u_{polyst}). The coefficients A_k are obtained by minimizing the standard deviation σ , defined by:

$$\sigma = \sqrt{\frac{\sum_{i=1}^N (u_{\text{exp}} - u_{\text{cal}})^2}{N}}\quad (4.2)$$

where N is the number of data points and u_{cal} is the calculated speed of sound, given by the following equation [22]:

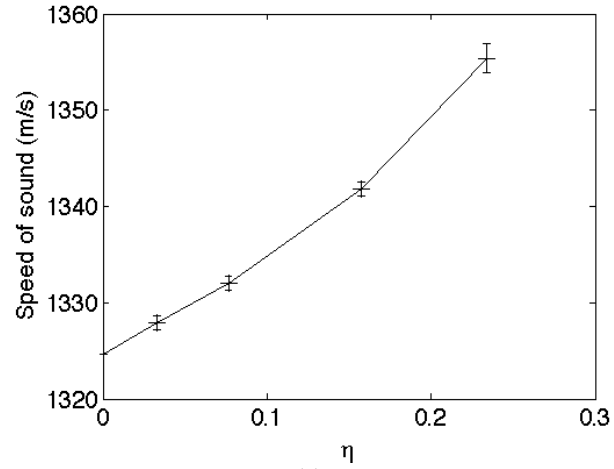
$$u_{cal} = (\Phi_j u_j + (1 - \Phi_j) u_{tol}) + \Phi_j (1 - \Phi_j) \sum_{k=0}^3 A_k [\Phi_k - (1 - \Phi_k)]^k \quad (4.3)$$

The coefficients A_k and the standard deviations are given in Table 4.1 for the binary mixtures: asphaltenes + toluene, polystyrene ($M_w=393,400$ g/mol) + toluene and polystyrene ($M_w=700,000$ g/mol) + toluene. For these binary mixtures, experimental vs calculated speeds of sound using the fitting equation (4.3) are presented in Figures 4.4. The average experimental speed of sound for a mixture of 23.4 vol% asphaltenes in toluene was obtained by averaging the speed of sound profiles of six mixtures prepared separately.

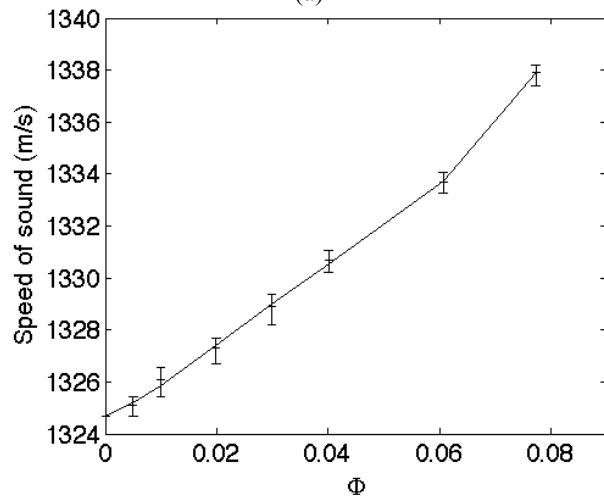
Table 4.1. Coefficients A_i and standard deviation σ of equation (4.3)

	A_0	A_1	A_2	A_3	σ
Asphaltenes + toluene	126.81	163.95	-283.22	-296.11	6.32×10^{-13}
Polystyrene ($M_w=393\,400$ g/mol) + toluene $\times 10^{-5}$	0.6945	2.2858	2.5069	0.9164	0.12
polystyrene ($M_w=700\,000$ g/mol) + toluene $\times 10^{-5}$	0.7285	2.4216	2.6807	0.9884	0.06

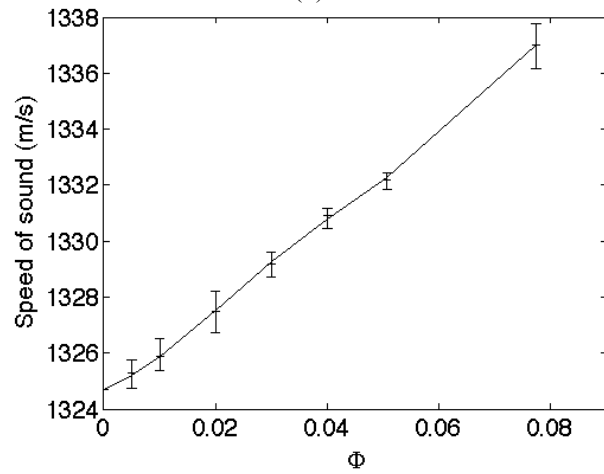
In this work, the attenuation difference between mixtures at time t after mixing and time $t = 0$ min just after mixing: $\Delta A = A(z,f)|_t - A(z,f)|_{t=0 \text{ min}}$ is monitored to detect phase separation and the elevation of the liquid-liquid interface.



(a)



(b)



(c)

Figure 4.4. Experimental speed of sound data and fitting equation (4.3) at 20 C and 1.0 atm in the binary mixtures: (a) asphaltene + toluene, (b) polystyrene ($M_w=393,400$ g/mol) + toluene, (c) polystyrene ($M_w=700,000$ g/mol) + toluene.

4.4. Results and discussion:

In this section, the effect of adding a mixture of polystyrene in toluene to a mixture of asphaltene in toluene is examined. This permits movement in the phase diagram roughly parallel to the tie lines within the liquid liquid region. The effect of dilution with toluene on the volume fractions of the phases in the two-phase region is also examined. This permits movements in the phase diagram that are nominally orthogonal to the tie lines. The repeatability of the phase boundaries and relative volumes of phases at fixed global composition is also evaluated. Acoustic measurements of phase separation kinetics in mixtures of asphaltene + polystyrene + toluene are presented. Finally, UV-Visible spectrophotometry measurements are performed to measure the concentration of asphaltenes in two equilibrium phases for a mixture with a defined global composition. The concentration of polystyrene in the separated phases is estimated using mass balance equations.

Phase behavior of mixtures with global composition (η , ϕ), upper phase volume fraction R , and experimental speed of sound before and after phase separation for Maya asphaltenes + toluene + polystyrene ($M_w = 393,400$ g/mol and $700,000$ g/mol) are presented in Tables 4.2-5.

4.4.1. Effect of adding a solution of polystyrene in toluene to a mixture of asphaltene in toluene

In an initial experiment, aliquots of polystyrene ($M_w = 393,400$), $\Phi = 7.7$ vol%, in toluene were added to an asphaltene, $\eta = 23.4$ vol%, in toluene mixture. The trajectory follows the segment line a-e in the phase diagram, shown in Figure 4.5.a. Experimental data for these mixtures at equilibrium are summarized in Table 4.2. Speeds of sound and attenuation profile measurements are shown in Figure 4.6.

Table 4.2. Effect of adding polystyrene in toluene to asphaltene in toluene. Experimental data for mixtures (a-e) of asphaltene + polystyrene ($M_w=393,400$ g/mol) + toluene. Composition, speed of sound per phase, liquid-liquid interface elevation and volume fraction of the upper phase.

	Global Composition		Average Speed of Sound (m/s)				Elevation (mm)	Vol. fraction of upper phase	Time for phase separation (min)	Final time (min)
	η	ϕ	Phase1	Phase2	Diff	Mix	$H_{interface}$	R		
Mix a	0.217	0.0058	1352.7	1352.7	-	1352.4	-	-	-	1129
Mix b	0.142	0.0305	1348.5	1345.2	3.3	1347.4	11.0	0.55	38	1413
Mix c	0.119	0.0383	1347.1	1343.8	3.3	1345.8	9.2	0.68	24	156
Mix d	0.107	0.0419	1346.2	1343.0	3.2	1345.0	8.6	0.73	33	427
Mix e	0.102	0.0438	1344.7	1341.8	2.9	1344.1	8.0	0.76	40	1614

Abbreviations. Diff: speed of sound difference between the separated phases, Mix: speed of sound before phase separation, H_{int} : Elevation of the liquid-liquid interface (mm).

Table 4.3. Experimental repeatability measurements of phase separation for mixture (d) for four successive mixings. Composition, speed of sound per phase, liquid-liquid interface elevation and volume fraction of the upper phase.

	Global Composition		Average Speed of Sound (m/s)				Elevation (mm)	Vol. fraction of upper phase	Time for phase separation (min)	Final time (min)
	η	ϕ	Phase1	Phase2	Diff	Mix	H_{int}	R		
Mixing 1	0.107	0.042	1346.2	1343.0	3.2	1345.0	8.6	0.73	33	427
Mixing 2	0.107	0.042	1346.3	1343.1	3.2	1344.7	8.3	0.74	35	142
Mixing 3	0.107	0.042	1346.9	1343.5	3.4	1344.9	8.3	0.74	34	685
Mixing 4	0.107	0.042	1345.6	1342.5	3.1	1345.1	8.3	0.74	30	345

Abbreviations. Diff: speed of sound difference between the separated phases, Mix: speed of sound before phase separation, H_{int} : Elevation of the liquid-liquid interface (mm).

Table 4.4. Experimental data for a mixture of asphaltene + polystyrene ($M_w=393,400$ g/mol) + toluene. Composition, speed of sound per phase, liquid-liquid interface elevation and volume fraction of the upper phase.

		Global Composition		Average Speed of Sound (m/s)				Elevation (mm)	Vol. frac. of upper phase	Time for phase sep. (min)	Final time (min)	Phase Behavior
		η	ϕ	Phase 1	Phase 2	Diff	Mix					
	Mix p ₁	0.069	0.0544	-	1342.4	-	1342.3	<1.2	>0.94	46	904	tp
Dilution line p	Mix 1	0.098	0.0450	1346.0	1342.7	3.3	1345.0	4.1	0.83	37	374	tp
	Mix 2	0.093	0.0429	1344.7	1341.6	3.1	1343.5	3.8	0.85	32	136	tp
	Mix 3	0.089	0.0410	1343.4	1340.6	2.8	1342.3	3.2	0.88	35	129	tp
	Mix 4	0.085	0.0392	1342.6	1339.7	2.9	1341.3	2.6	0.91	36	126	tp
	Mix 5	0.078	0.0361	1342.0	1339.0	3.0	1340.7	2.0	0.93	41	222	tp
	Mix 6	0.077	0.0354	1342.6	1338.7	3.9	1339.7	1.7	0.95	37	144	tp
	Mix 7	0.073	0.0335	1338.0	1338.0	-	1339.0	<1.2	>0.96	47	1082	tp
	Mix 8	0.070	0.0323	1338.5	1338.5	-	1338.6	<1.2	>0.96	48	1182	tp
Dilution line r	Mix 1	0.196	0.0123	1353.6	1349.4	4.2	1354.2	14.3	0.25	50	306	tp
	Mix 2	0.185	0.0115	1351.3	1348.4	2.9	1351.5	15.2	0.25	43	144	tp
	Mix 3	0.167	0.01045	1348.6	1345.9	2.7	1348.8	16.1	0.28	41	120	tp
	Mix 4	0.153	0.0095	1346.8	1344.6	2.2	1346.6	17.0	0.30	41	187	tp
	Mix 5	0.146	0.0091	1344.9	1342.8	2.1	1345.2	17.6	0.31	46	127	tp
	Mix 6	0.128	0.0080	1342.3	1342.3	-	1342.4	-	-	-	688	sp
	Mix 7	0.118	0.0074	1341.2	1341.2	-	1341.1	-	-	-	1334	sp
	Mix 8	0.109	0.0068	1339.7	1339.7	-	1340.1	-	-	-	1705	sp
Dilution line q	Mix 1	0.148	0.0284	1349.7	1346.1	3.6	1348.6	11.6	0.43	39	785	tp
	Mix 2	0.142	0.0272	1347.9	1345.0	2.9	1347.5	12.2	0.43	41	133	tp
	Mix 3	0.134	0.0258	1346.1	1343.5	2.6	1345.9	12.2	0.46	39	170	tp
	Mix 4	0.127	0.0245	1345.0	1342.7	2.3	1344.6	12.2	0.49	37	203	tp
	Mix 5	0.118	0.0227	1343.9	1342.0	1.9	1343.5	12.0	0.53	32	126	tp
	Mix 6	0.113	0.0217	1342.5	1341.2	1.3	1342.3	10.5	0.61	49	125	tp
	Mix 7	0.108	0.0208	1341.4	1341.4	-	1341.6	-	-	-	1211	sp
	Mix 8	0.098	0.0188	1339.9	1339.9	-	1339.9	-	-	-	1643	sp
Line V	Mix 1	0.168	0.0204	1349.8	1346.9	2.9	1350.3	14.6	0.33	41	677	tp
	Mix 2	0.139	0.0169	1344.7	1342.9	1.8	1345.6	17.0	0.35	36	108	tp
	Mix 3	0.118	0.0142	1341.4	1340.9	0.5	1342.4	18.8	0.39	37	1400	tp
Line W	Mix 1	0.172	0.0254	1352.7	1348.6	4.1	1351.3	17.9	0.36	62	2030	tp
	Mix 2	0.154	0.0340	1353.1	1349.0	4.1	1350.8	17.3	0.45	75	1104	tp
	Mix 3	0.142	0.0398	1353.8	1349.6	4.2	1351.3	16.4	0.52	89	8918	tp

Abbreviations. Diff: speed of sound difference between the separated phases, Mix: speed of sound before phase separation, H_{int} : Elevation of the liquid-liquid interface (mm).

Table 4.5. Experimental data for a mixture of asphaltene + polystyrene ($M_w=700,000$ g/mol) + toluene. Composition, speed of sound per phase, liquid-liquid interface elevation and volume fraction of the upper phase.

		Global Composition		Average Speed of Sound (m/s)				Elevation (mm)	Vol. frac. of upper phase	Time for phase sep. (min)	Final time (min)	Phase Behavior
		η	ϕ	Phase 1	Phase 2	Diff	Mix					
	Mix p ₁	0.075	0.0528	-	1339.0	-	1340.6	-	0	-	1440	sp
	Mix p ₂	0.095	0.0462	1342.0	1339.4	2.6	1341.9	2.3	0.90	59	394	tp
Dilution line p	Mix 1	0.108	0.0419	1343.2	1340.7	2.5	1342.2	4.4	0.83	50	169	tp
	Mix 2	0.104	0.0405	1343.4	1340.6	2.8	1341.6	4.1	0.85	45	688	tp
	Mix 3	0.098	0.0384	1341.1	1338.8	2.3	1341.2	3.5	0.88	49	182	tp
	Mix 4	0.094	0.0368	1339.9	1337.9	2.0	1339.8	3.2	0.89	45	404	tp
	Mix 5	0.090	0.0351	1338.6	1337.1	1.5	1338.8	2.6	0.92	44	133	tp
	Mix 6	0.087	0.0341	1338.6	1336.7	1.9	1338.1	2.0	0.94	43	137	tp
	Mix 7	0.089	0.0323	1339.8	1336.7	3.1	1337.6	1.4	0.96	41	604	tp
	Mix 8	0.081	0.0315	1338.0	1338.0	-	1337.6	<1.2	>0.96	53	1571	tp
Dilution line r	Mix 1	0.199	0.0115	1353.7	1350.3	3.4	1353.1	15.2	0.25	61	124	tp
	Mix 2	0.188	0.0109	1351.3	1348.2	3.1	1351.0	15.8	0.26	60	309	tp
	Mix 3	0.181	0.0105	1349.7	1347.0	2.7	1349.3	16.4	0.26	50	127	tp
	Mix 4	0.171	0.0099	1348.3	1345.9	2.4	1347.9	17.0	0.28	50	128	tp
	Mix 5	0.163	0.0094	1346.8	1344.7	2.1	1346.5	17.6	0.29	52	128	tp
	Mix 6	0.154	0.0089	1345.7	1343.8	1.9	1345.3	17.9	0.32	53	129	tp
	Mix 7	0.148	0.0086	1344.8	1343.1	1.7	1344.4	18.3	0.32	55	127	tp
	Mix 8	0.141	0.0081	1344.0	1342.5	1.5	1343.6	18.8	0.34	59	123	tp
	Mix 9	0.135	0.0078	1342.7	1341.7	1.0	1342.6	19.5	0.34	72	845	tp
	Mix10	0.127	0.0074	1340.0	1340.0	-	1341.3	-	-	-	3053	sp
	Mix11	0.119	0.0069	1338.3	1338.3	-	1339.4	-	-	-	2695	sp
Dilution line q	Mix 1	0.156	0.0258	1346.8	1343.6	3.2	1347.4	11.3	0.46	50	425	tp
	Mix1 (rep)	0.156	0.0258	1347.2	1344.0	3.2	1346.9	11.3	0.45	50	942	tp
	Mix 2	0.152	0.0250	1345.0	1342.1	2.9	1345.8	11.6	0.46	50	204	tp
	Mix 3	0.135	0.0222	1342.4	1340.0	2.4	1342.9	12.2	0.49	40	334	tp
	Mix 4	0.130	0.0214	1341.5	1339.3	2.2	1341.7	12.0	0.52	27	167	tp
	Mix 5	0.121	0.0200	1341.0	1339.1	1.9	1340.7	11.7	0.56	24	740	tp
	Mix 6	0.112	0.0185	1339.8	1338.2	1.6	1340.0	10.4	0.64	19	158	tp
	Mix 7	0.107	0.0176	1338.6	1337.6	1.0	1338.9	8.3	0.73	33	127	tp
	Mix 8	0.104	0.0171	1338.4	1337.7	0.7	1338.3	5.3	0.83	95	1069	tp
	Mix 9	0.099	0.0163	1337.4	1337.4	-	1338.0	-	-	-	1331	sp
Mix10	0.094	0.0155	1336.6	1336.6	-	1337.6	-	-	-	727	sp	

Abbreviations. Diff: speed of sound difference between the separated phases, Mix: speed of sound before phase separation, H_{int} : Elevation of the liquid-liquid interface (mm).

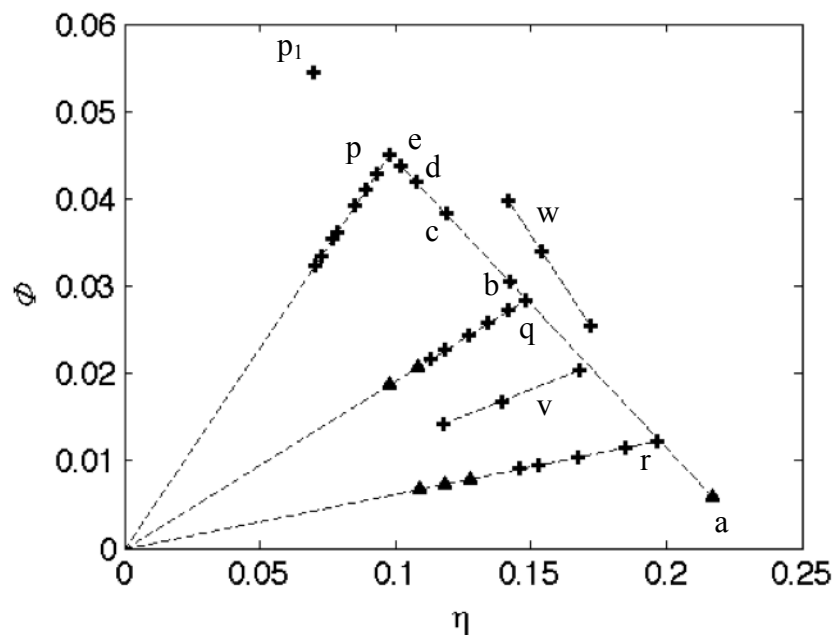


Figure 4.5.a. Phase diagram and dilution lines p, q and r for mixtures of asphaltenes + polystyrene ($M_w=393,400$ g/mol) + toluene. (cross): Two-phase region, (triangle): single-phase region.

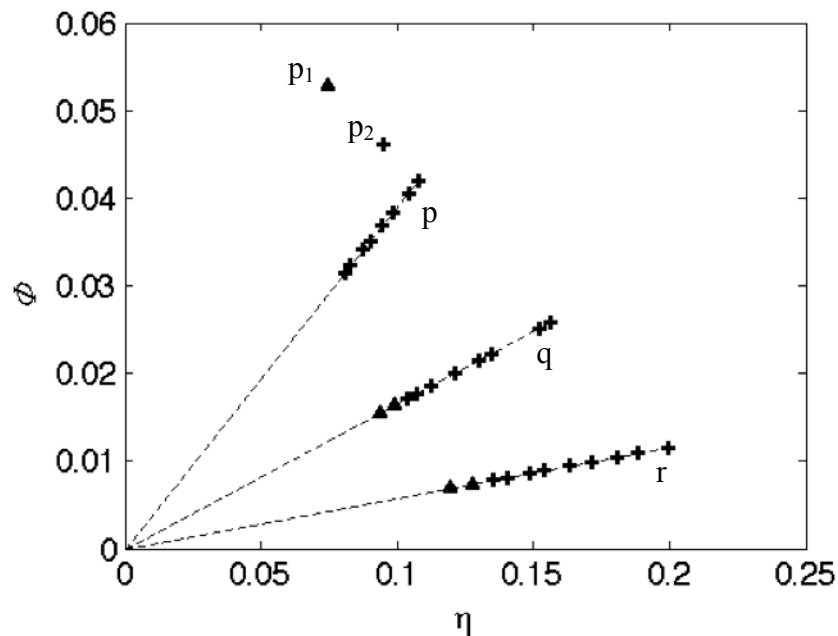


Figure 4.5.b. Phase diagram and dilution lines p, q and r for mixtures of asphaltenes + polystyrene ($M_w=700,000$ g/mol) + toluene. (cross): Two-phase region, (triangle): single-phase region.

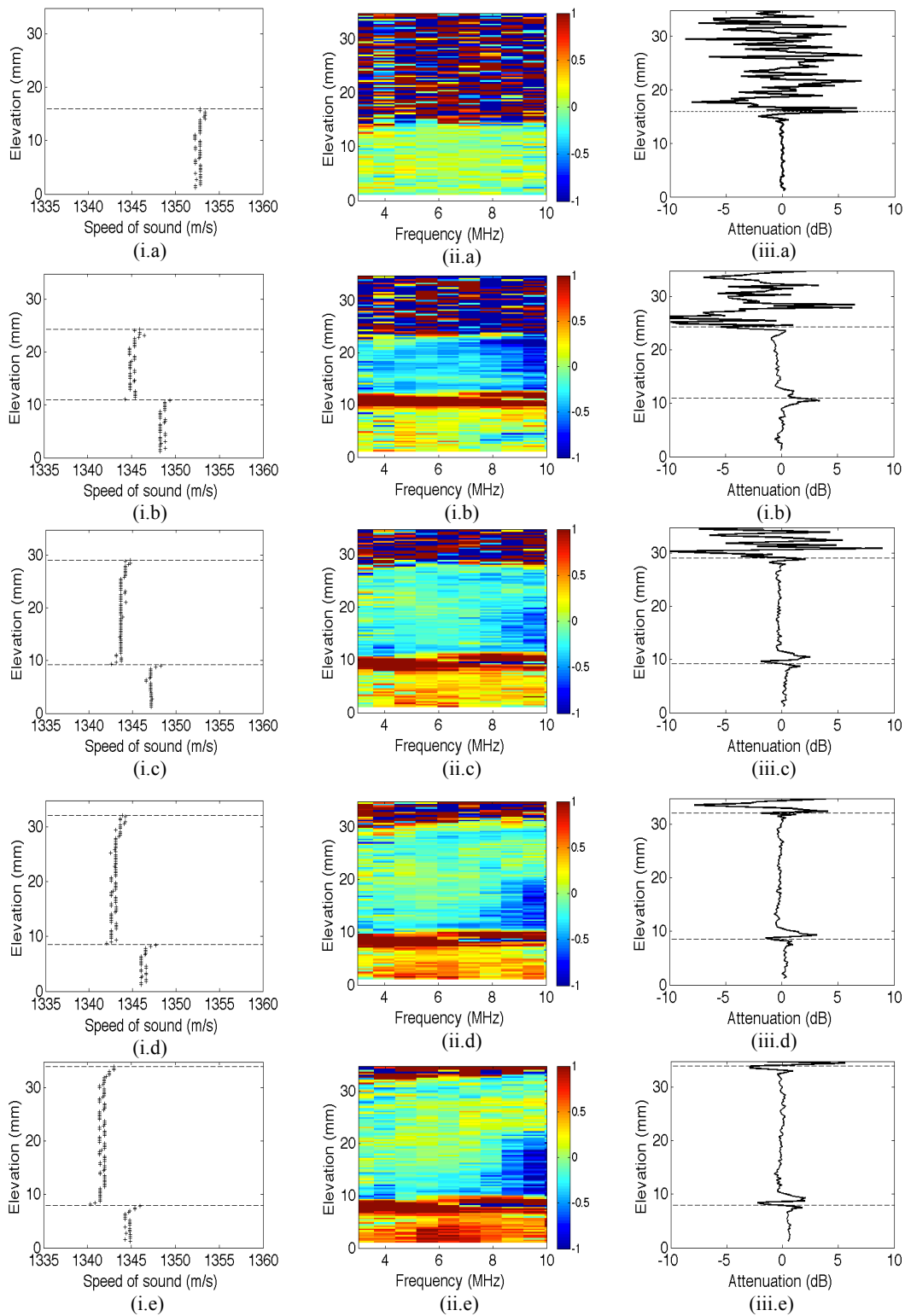


Figure 4.6. Speed of sound profiles (i) acoustic wave attenuation spectra difference and (ii) attenuation difference at 7.9 MHz, at final times given in Table 4.1, and for global compositions (a-e) shown in Figure 4.5.a.

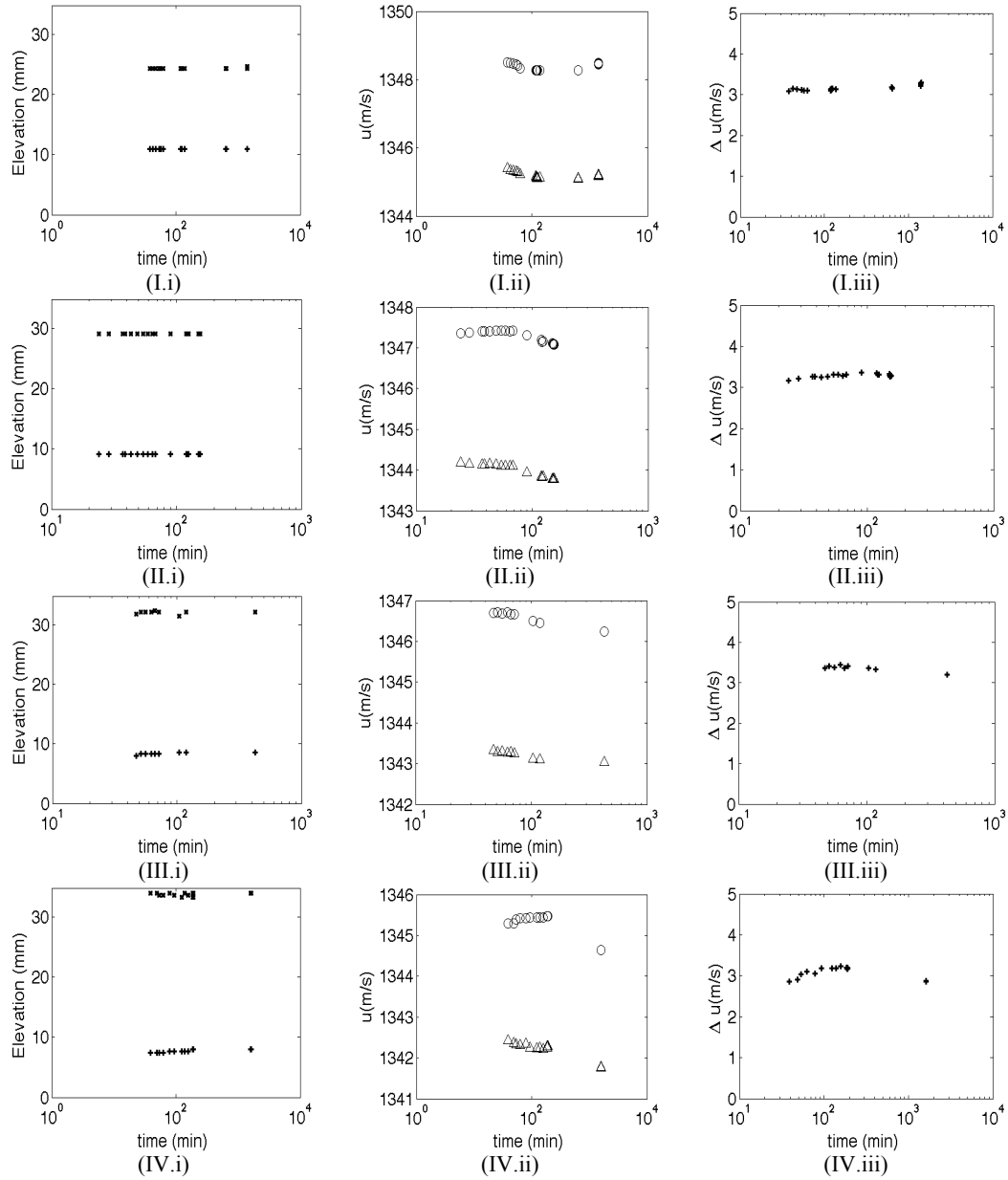


Figure 4.7. (i) Evolution of the liquid-liquid, liquid-air interfaces, (ii) speed of sound: (triangle) upper phase, (circle) lower phase, (iii) speed of sound difference between the phases with time for global compositions (b-e) shown in Figure 4.5.a: (I) composition (b), (II) composition (c), (III) composition (d), (IV) composition (e).

Mixture (a) remained homogenous and there was no evidence of phase separation even after 19 hours. As more of the polystyrene + toluene mixture was added, distinct upper and lower phases with uniform compositions, separated by an interface, emerged. Figure 4.7 shows the variations with time, from phase separation to final time, of the liquid-liquid interface, the speed of sound in the

separated phases and the speed of sound difference between the separated phases for mixtures (b-e). This Figure shows that the elevation of the liquid-liquid interface and the speed of sound difference between the separated phases are stable with time within 0.3 mm and 0.4 m/s respectively, while the speed of sound in the separated phases can shift in both phases by up to 1 m/s. The variations of the speed of sound with time may be caused by small temperature variations of the circulating fluid (± 0.1 C) or changes in the temperature of surrounding air.

The variations of the elevation of the liquid-liquid interface, $H_{\text{interface}}$, the volume fraction of the upper phase, R , and the speed of sound difference between the separated phases from mixture (b) to (e) are shown in Figures 4.8.i-iii. These Figures show that when the amount of polystyrene in toluene is increased from mixture (b) to (e), the liquid-liquid interface decreases (Fig.4.8.i), the volume fraction, R , of the upper phase increases (Fig.4.8.ii) and the speed of sound difference between the separated phases did not appear to change significantly (Fig.4.8.iii).

4.4.2. Reproducibility of phase separation

For mixture (d) with composition: $\eta=10.7$ vol%, $\Phi=4.2$ vol%, the reproducibility of the phase separation measurement was examined. Four successive trials were performed. Results are summarized in Figure 4.9 and Table 4.2. After each separation, the mixture was remixed for 5 minutes. In all four cases, phase separation was complete within 30-35 minutes. The speeds of sound in the separated phases were repeatable within 1.5 m/s. Measured speeds of sound variations in liquid phases are likely caused by temperature variations. Volume fractions of the upper phase, R , and speed of sound difference values appear to be repeatable within 0.01 and 0.3 m/s respectively. These measurements are obtained at the final time of the phase separation measurement: 7 hours after homogenization for mixing 1, 3 hours for mixing 2, 11 hours for mixing 3 and 6 hours for mixing 4. Note that in all cases, local speed of sound values can be

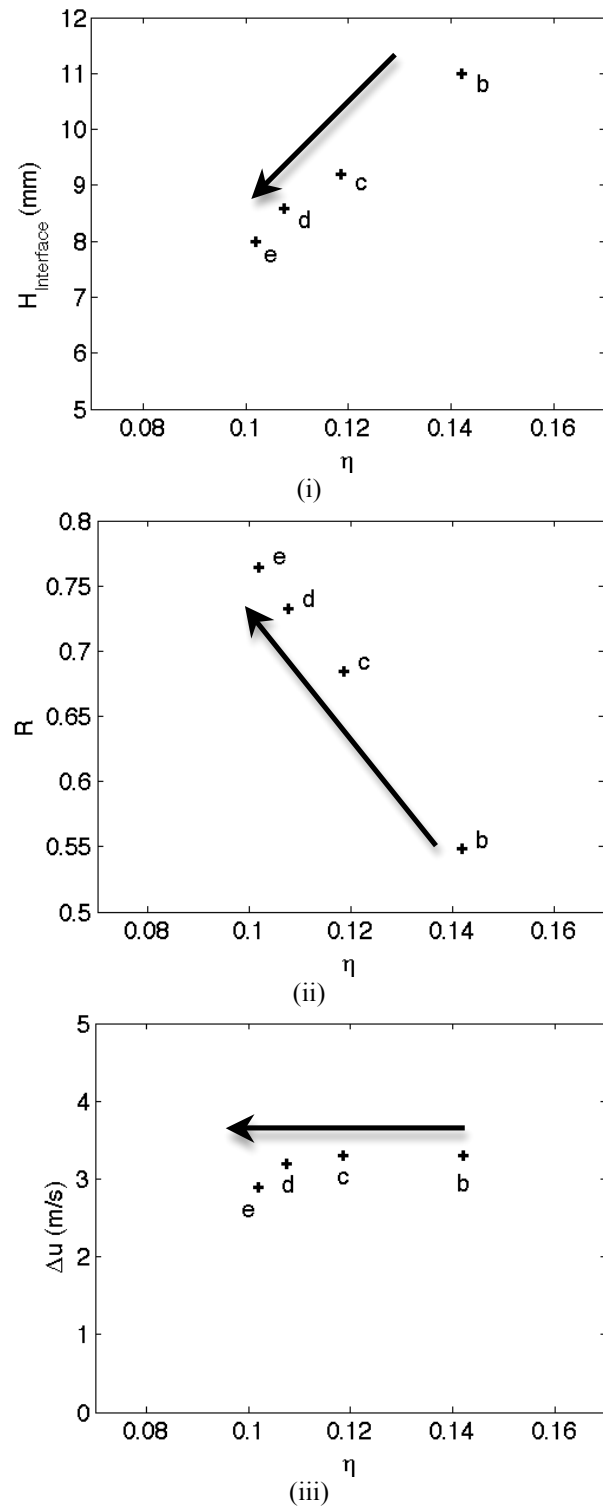


Figure 4.8. Liquid-liquid interface elevation (i), volume fraction of the upper phase (ii), speed of sound difference between the coexisting phases (iii) for global compositions (b-e) shown in Figure 4.5.a.

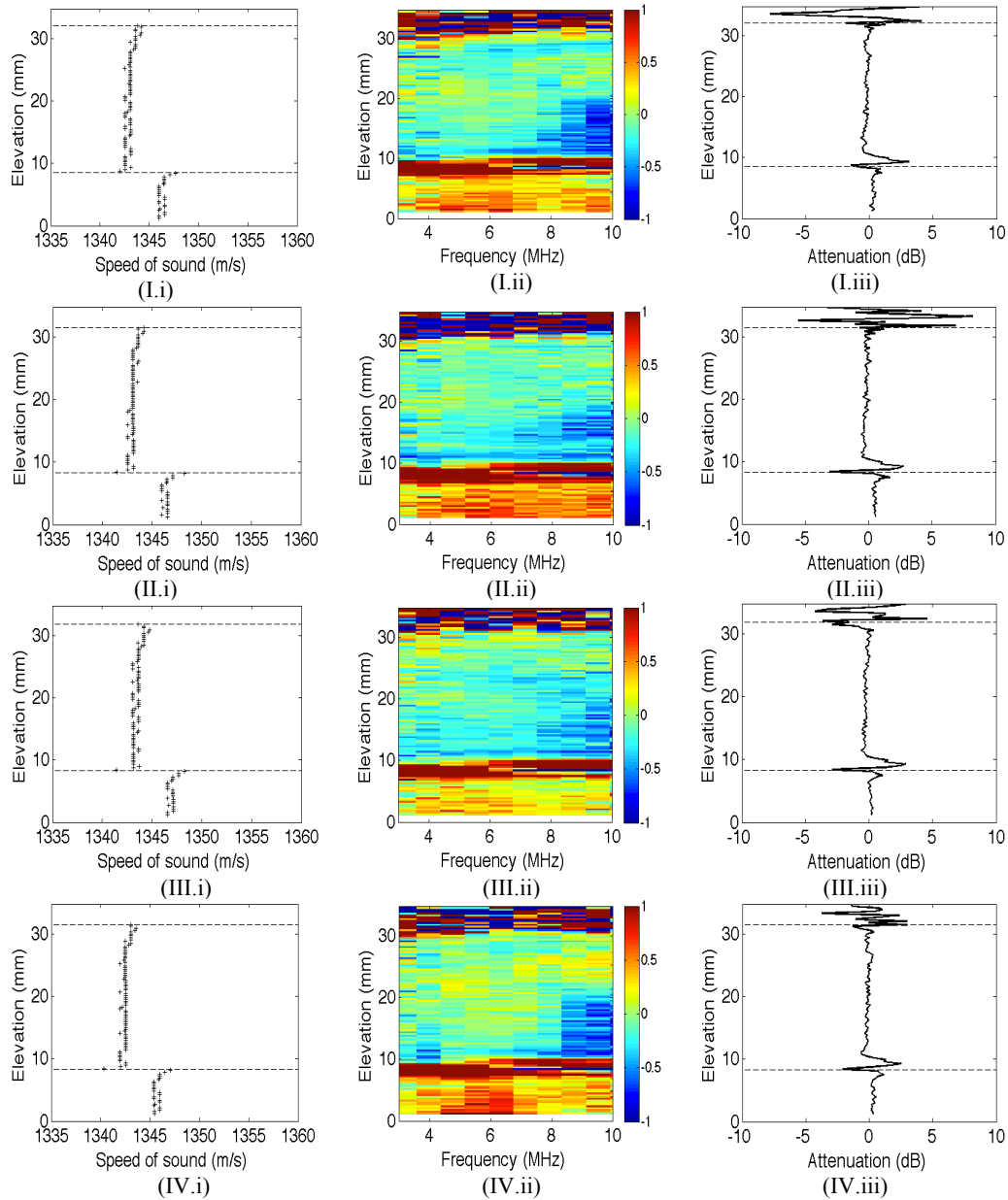


Figure 4.9. Reproducibility of phase separation at final time for mixture (d) with composition: $\eta=10.7$ vol%, $\Phi=4.2$ vol%. (i) Speed of sound profile, (ii) acoustic wave attenuation spectra difference and (iii) attenuation difference at 7.9 MHz. (I): mixing 1, upper phase volume fraction $R=0.73$, $\Delta u=3.2$ m/s, (II) mixing 2, $R=0.74$, $\Delta u=3.2$ m/s, (III) mixing 3, $R=0.74$, $\Delta u=3.4$ m/s, (IV) mixing 4, $R=0.74$, $\Delta u=3.1$ m/s.

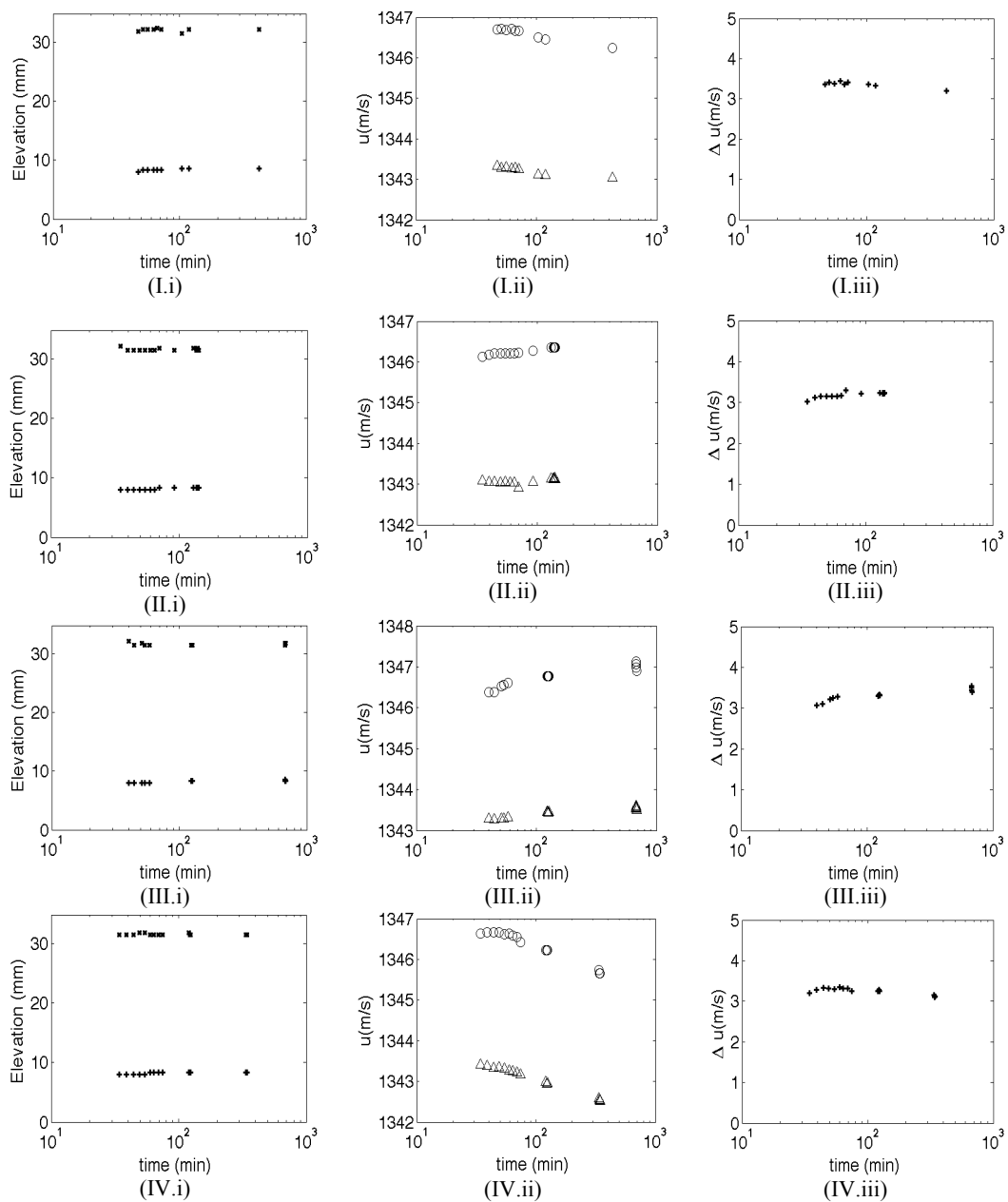


Figure 4.10. (i) Variation with time of the liquid-liquid and liquid-air interfaces (ii) speed of sound per phase: (triangle): upper phase, (circle): lower phase. (iii) speed of sound difference between the separated phases for mixture (d) after successive mixings: mixing 1 (I), mixing 2 (II), mixing 3 (III), mixing 4 (IV).

significantly affected by the discontinuity at the liquid-liquid interface. The stability with time of the elevation of the liquid-liquid interface, the speed of sound in the separated phases and the speed of sound difference between the separated phases are shown in Figure 4.10. This Figure shows that the liquid-liquid interface and the speed of sound difference between the separated phases are stable with time within 0.3 mm and 0.5 m/s respectively. The speed of sound in the separated phases shift with time in a similar way by up to 1 m/s.

The results presented above show that phase separations of mixtures of asphaltenes + toluene + polystyrene are reproducible. Therefore, the mechanism causing the phase separation has a consistent effect.

4.4.3. Effect of adding toluene to a mixture of asphaltene + polystyrene + toluene

Phase behavior measurements were subsequently made along dilution lines p, q and r shown in Figure 4.5.a for $M_w=393,400$ g/mol. These measurements were performed by adding small aliquots of toluene to three mixtures of asphaltene + polystyrene + toluene with different ratios of polystyrene/asphaltene volume fractions. When the volume of toluene added was large enough, the mixtures moved from a two-phase region to a single-phase region. The effects of dilution on the elevation of the liquid-liquid interface, the volume fraction of the upper phase and the speed of sound difference between the separated phases are shown in Figure 4.11. The ratios of polystyrene/asphaltene volume fractions are 0.46, 0.19 and 0.06 along dilution lines p, q and r respectively. Large volume fractions of the upper phase are obtained along dilution line p and smaller fractions are obtained along dilution lines q and r. This suggests that the upper phase is polystyrene rich and the lower phase is asphaltene rich.

The position of the liquid-liquid interface along dilution line p decreases from 4.1 mm to 1.7 mm, as the volume fraction of the upper phase increases from 83% to

95%vol. When the phase boundary approaches the base of the cell ($H_{\text{interface}} < 1.2$ mm), acoustic wave attenuation is used to detect the presence of the interface. The speed of sound difference between the two coexisting phases decreases initially. The abrupt increase that follows is caused by the fact that only few speed of sound values are available in the lower phase and they are affected by their proximity to the liquid-liquid interface. Along dilution line r, the liquid-liquid interface increases from elevation 14.3 mm to 17.6 mm, the volume fraction of the upper phase increases slightly from 25 % vol to 31 % vol and the speed of sound difference decreases from 4.2 m/s to 2.1 m/s.

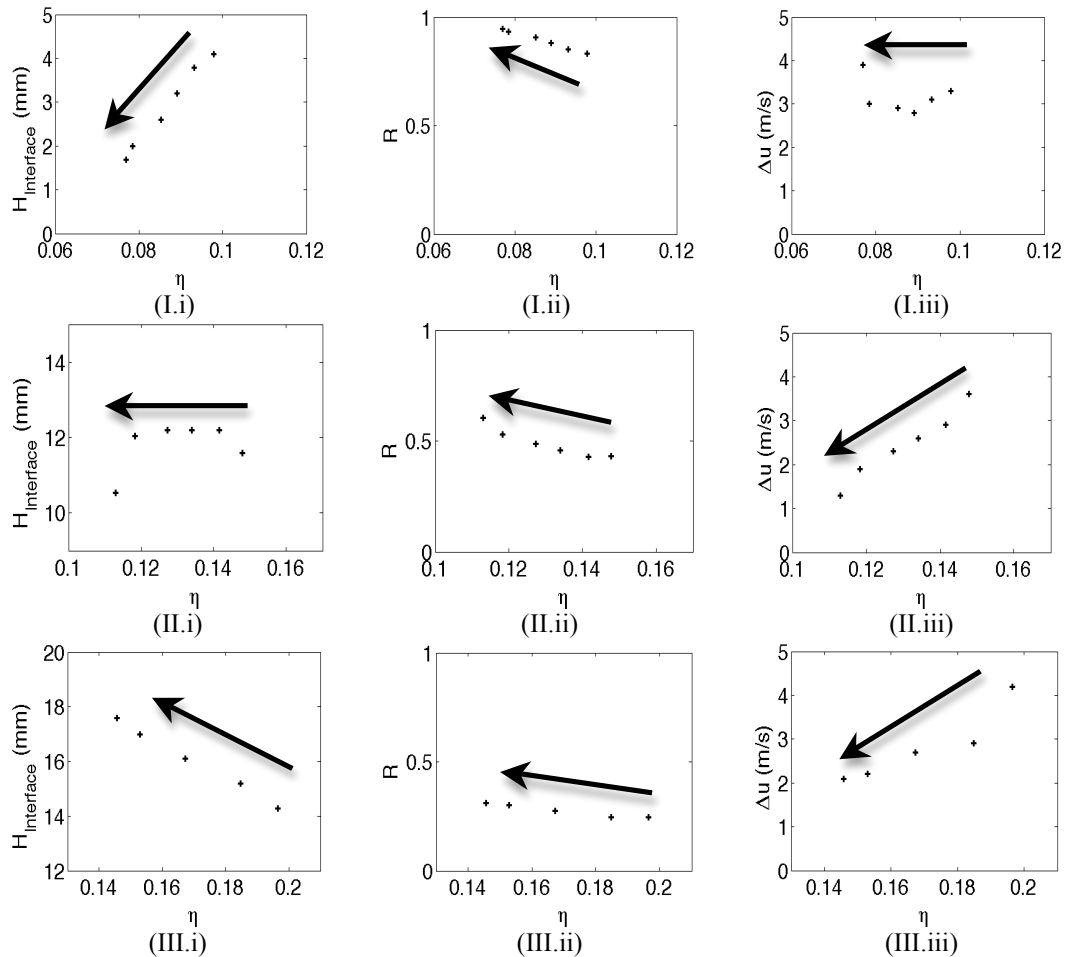


Figure 4.11. Effect of dilution on the phase separation for mixtures of asphaltenes + polystyrene ($M_w = 393,400$ g/mol) + toluene. (I) Dilution line p, (II) dilution line q, (III) dilution line r. (i) Elevation of the liquid-liquid interface, (ii) volume fraction of the upper phase, (iii) speed of sound difference between the coexisting phases.

The elevation of the liquid-liquid interface along dilution line q appears to present a maximum. The volume fraction of the upper phase increases from 43% to 61 % and the speed of sound difference between the separated phases decreases from 3.6 m/s to 1.3 m/s.

At a critical point the compositions and phase volumes of the two phases become identical. In this context, the speed of sound difference goes to zero (identical phase composition) and the volume fraction of the phases is 0.5. If the global composition is marginally rich in one component, the phase volumes diverge from 0.5 as the boundary is approached. The gradient and direction of the divergence provide directional and proximity information related to the location of the critical point. On the basis of these criteria, the critical point is located between dilution lines q and r on the phase boundary (Fig.4.5.a).

Similar results were obtained for mixtures of asphaltene + polystyrene + toluene with a polystyrene molecular weight of 700,000 g/mol. Dilution lines r, q and p are presented in Figure 4.5.b. The effects of dilution on the elevation of the liquid-liquid interface, the volume fraction of the upper phase and the speed of sound difference are shown in Figure 4.12. In this case, the ratios of polystyrene/asphaltene volume fractions are 0.39, 0.16 and 0.06 along dilution lines p, q and r respectively. Again, large volume fractions of the upper phase are obtained along dilution line p and smaller fractions are obtained along dilution lines q and r. The position of the liquid-liquid interface along dilution line p decreases from 4.4 mm to 1.4 mm, as the volume fraction of the upper phase increases from 83% to 96%vol. When the phase boundary approaches the base of the cell ($H_{\text{interface}} < 1.2$ mm), acoustic wave attenuation is used to detect the presence of the interface. Along dilution line r, the liquid-liquid interface increases from elevation 15.2 mm to 19.5 mm, the volume fraction of the upper phase increases slightly from 25 %vol to 34 %vol and the speed of sound difference decreases from 3.4 m/s to 1.0 m/s.

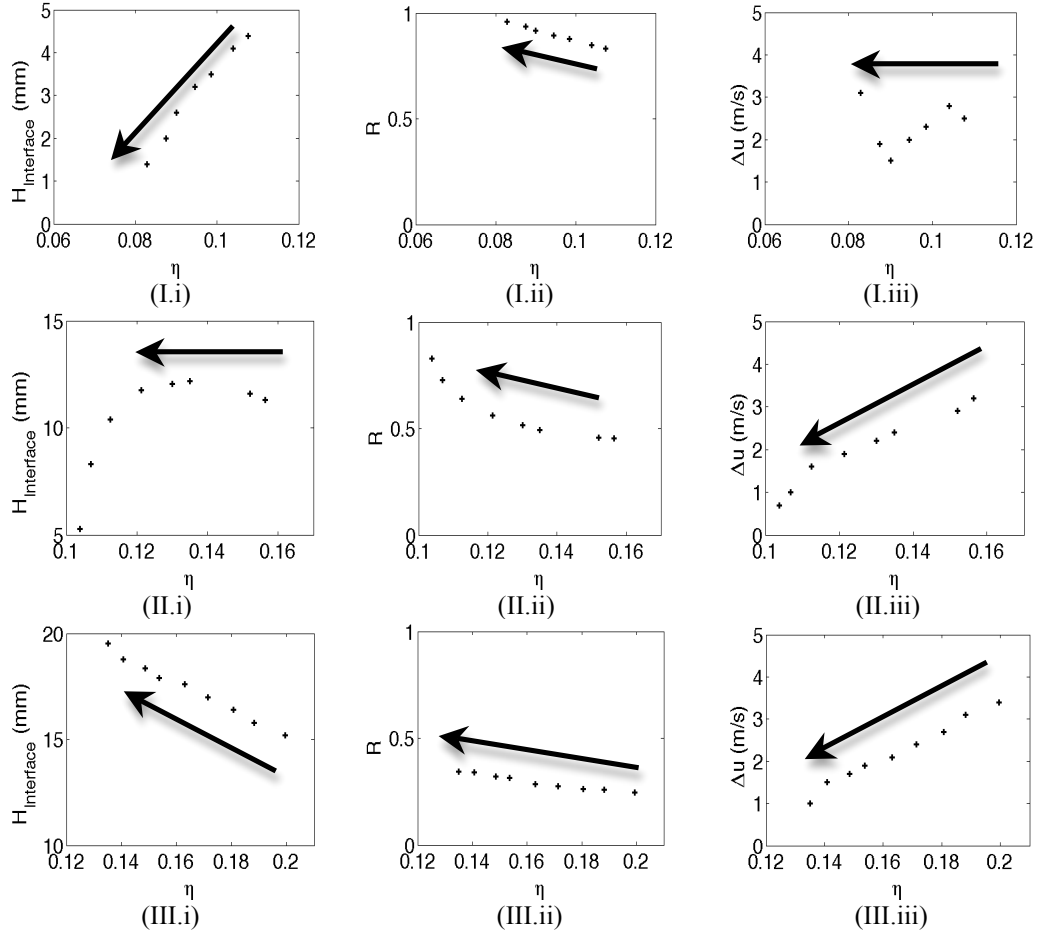


Figure 4.12. Effect of dilution on the phase separation for mixtures of asphaltenes + polystyrene ($M_w = 700,000$ g/mol) + toluene. (I) Dilution line p, (II) dilution line q, (III) dilution line r. (i) Elevation of the liquid-liquid interface, (ii) volume fraction of the upper phase, (iii) speed of sound difference between the coexisting phases.

The elevation of the liquid-liquid interface along dilution line q appears to present a maximum. The volume fraction of the upper phase increases from 46% to 83 % and the speed of sound difference between the separated phases decreases from 3.2 m/s to 0.7 m/s. Again, the critical point in this case is suggested to be located between dilution lines r and q on the phase boundary (Fig.4.5.b).

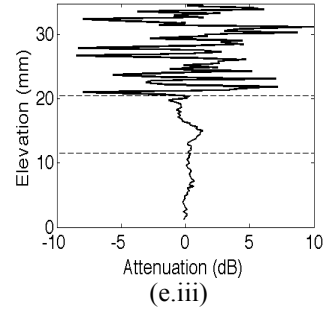
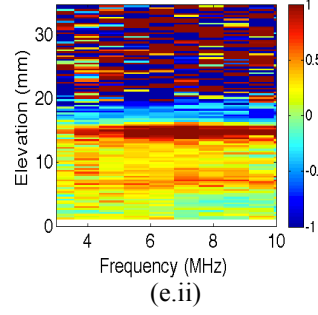
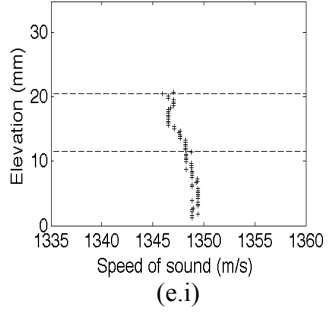
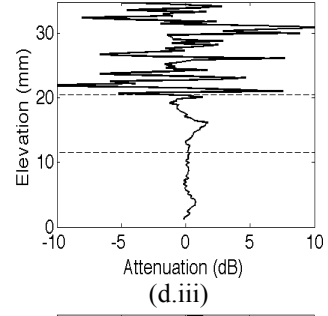
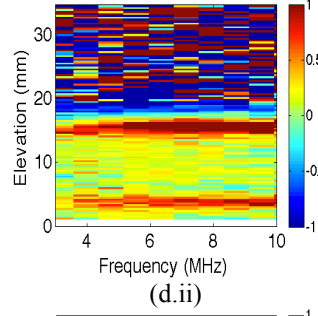
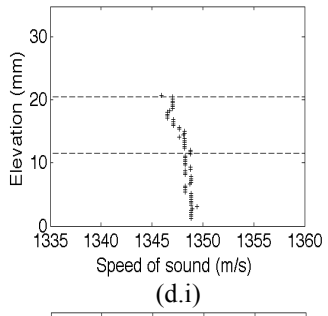
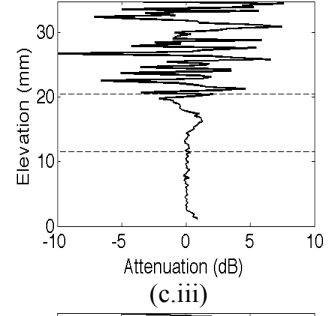
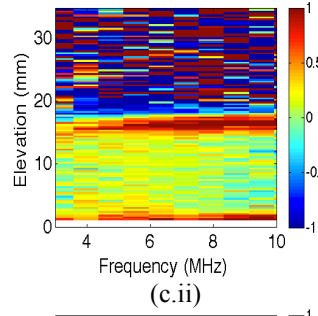
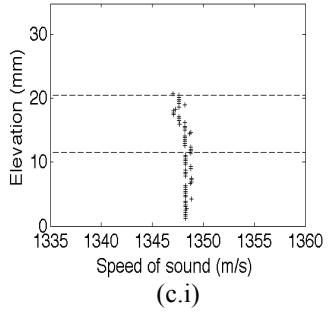
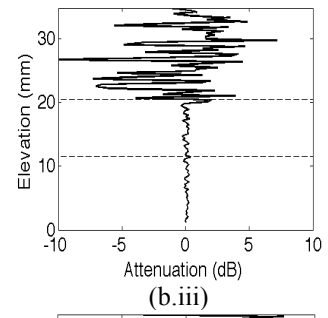
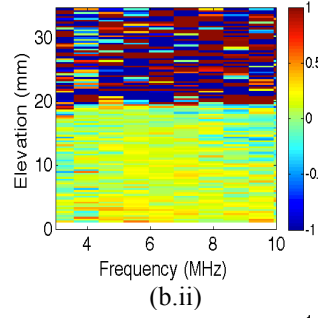
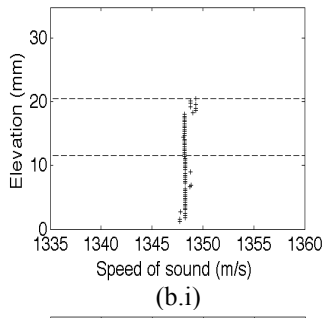
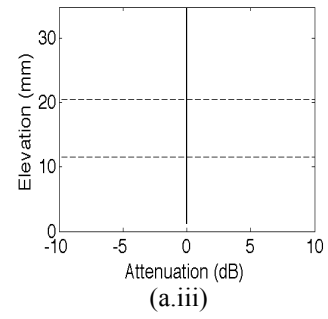
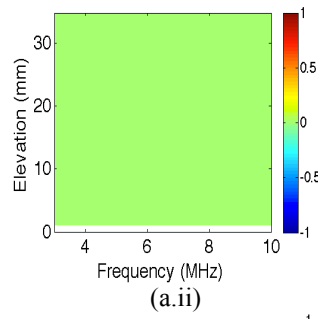
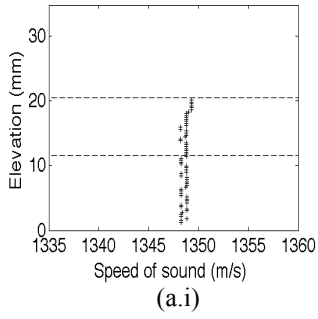
Concentrated asphaltene in toluene solutions form colloidal particles sterically stabilized. Polystyrene was reported not to modify asphaltene behavior in dilute solutions[8]. It does not possess polar groups that can associate to asphaltenes. Thus, the mixture asphaltene + polystyrene + toluene can be considered to be

analogous to that of colloidal particles sterically stabilized + polystyrene + toluene. Therefore, it can be suggested that the mechanism driving phase separation is depletion flocculation. Indeed, the variations of the upper phase volume fractions, shown in Figures 4.11-12, along the dilution lines are similar to those observed in mixtures of colloidal particles sterically stabilized + a non-adsorbing polymer [18][17]. Unlike these mixtures, however, asphaltene colloidal particles are not monodispersed and their size can depend on concentration.

4.4.4. Phase separation kinetics

An example of an acoustic measurement of phase separation kinetics for a mixture of asphaltene + polystyrene ($M_w=393,400$ g/mol) + toluene ($\eta=14.78$ vol%, $\Phi=2.84$ vol%) is shown in Figure 4.13. This mixture corresponds to the first composition in dilution line q shown in Figure 4.5.a. It shows the evolution of the speed of sound and acoustic wave attenuation difference profiles from time $t = 0$ min just after mixing to time $t = 784$ min. The attenuation difference is the difference between the attenuation at time t and that at time $t = 0$ min just after mixing.

At $t = 0$ min, the profile of the speed of sound is a continuous vertical line. With increasing time, the speed of sound decreases in the upper part of the cell and increases slightly in the lower part. Large attenuation difference regions are evident at the top and bottom of the cell. These attenuation regions are similar to those observed in methanol + hexanes liquid-liquid phase separation and reported in Chapter 3. They are attributed to losses in the acoustic energy at the liquid-liquid interface. Phase separation is complete when the speed of sound profiles separate into two parallel vertical lines (39 minutes after mixing) each corresponding to the speed of sound in the separated phases. The position of the liquid-liquid interface corresponds to a high attenuation region with a thickness of few millimetres. In cases where the speed of sound difference between phases is small, or a phase volume is too small to permit speed of sound measurements,



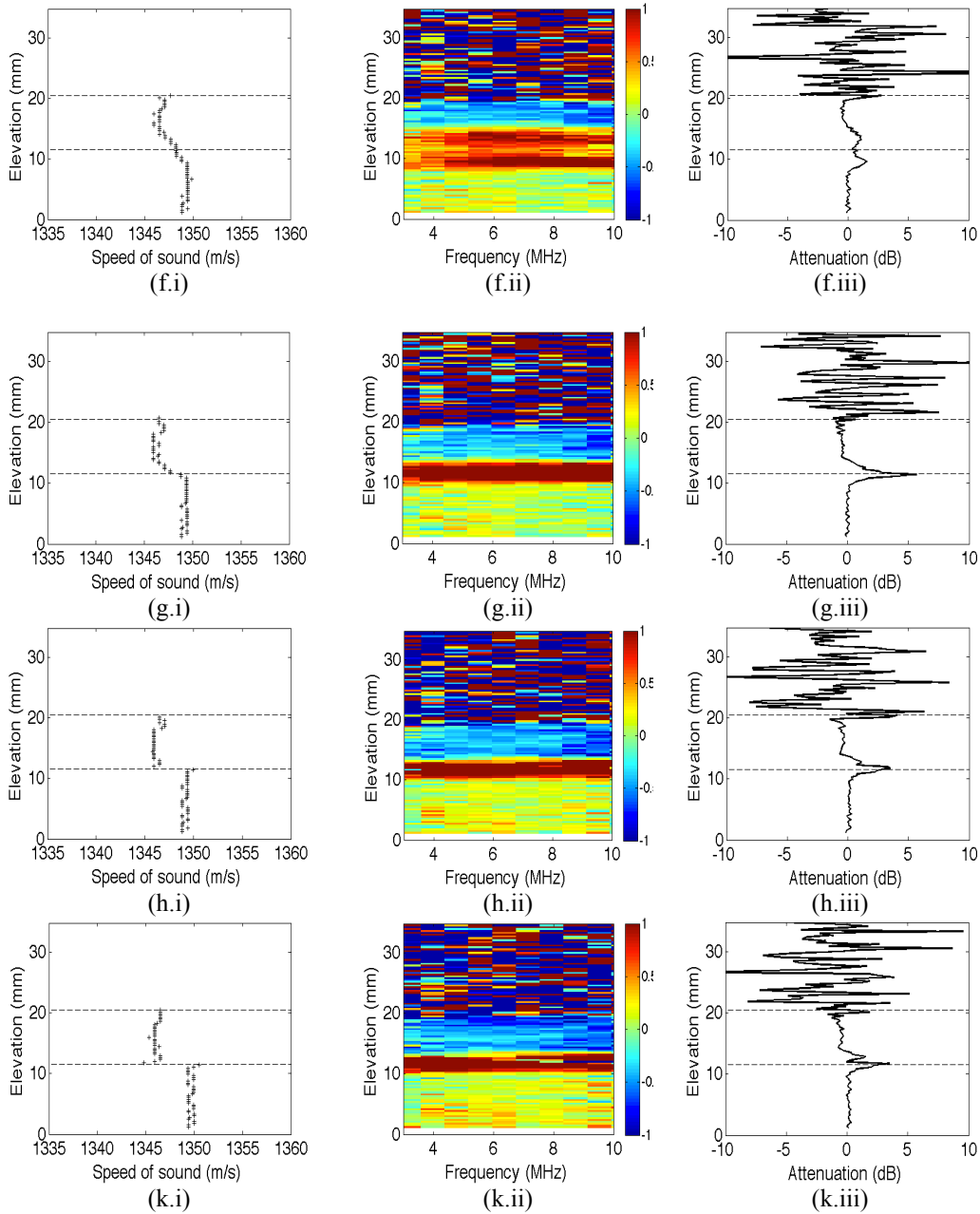


Figure 4.13. Measurement of phase separation kinetics for a mixture of asphaltene + polystyrene ($M_w=393,400$ g/mol) + toluene ($\eta=14.78$ vol%, $\Phi=2.84$ vol%) – first composition along dilution line q-. (i) Speed of sound profile (ii) acoustic wave attenuation spectra difference and (iii) attenuation difference at 7.9 MHz. Time elapsed after mixing: (a) 0 min , (b) 4 min, (c) 14 min, (d) 19 min, (e) 24 min, (f) 29 min, (g) 35 min, (h) 39 min , (k) 13 hours and 5 min (784 min).

attenuation profile measurements can be used for the detection of the liquid-liquid interface. The stability of the liquid-liquid interface, the speed of sound per phase and the speed of sound difference between the separated phases over 785 minutes after phase separation are presented in Figure 4.14. Elevation of the liquid-liquid interface and the speed of sound difference between the separated phases are stable within 0.3 mm and 0.5 m/s respectively.

Although, the phase separation presented above is qualitatively similar to that reported for a mixture of methanol + hexanes. The time required for completing phase separation (~39 min) is significantly larger than the few seconds required for the separation of methanol + hexanes mixtures.

Tables 4.2-5 summarize the times required for the phase separation of different asphaltene + polystyrene + toluene mixtures. In average, phase separation took 30 - 40 min after mixing to be completed. This is in agreement with the time reported for completion of phase separation for mixtures of colloidal particles + non-adsorbing polymers. For example, Hennequin et al [17] reported that after homogenizing mixtures of silica colloidal particles + polystyrene + toluene, a fuzzy interface first formed at the bottom of the cuvette, moving upwards and becoming sharper as phase separation proceeded. All samples investigated reached equilibrium nearly 1 hour after homogenization. They reported that the separated phases were clearly visible with a sharp and flat mirrorlike interface. Ramakrishnan et al. [16] reported that for mixtures of silica colloidal particles + polystyrene + toluene, a meniscus separating two fluid phases appeared few minutes after mixing. The bottom phase was more concentrated in colloidal particles than the upper phase and both phases could flow easily. Aarts et al [23] reported that for mixtures of fluorescent PMMA nanoparticles + polystyrene in *cis/trans* decalin, phase separation was complete within 15 min at intermediate polymer concentrations and up to few hours at high polymer concentration.

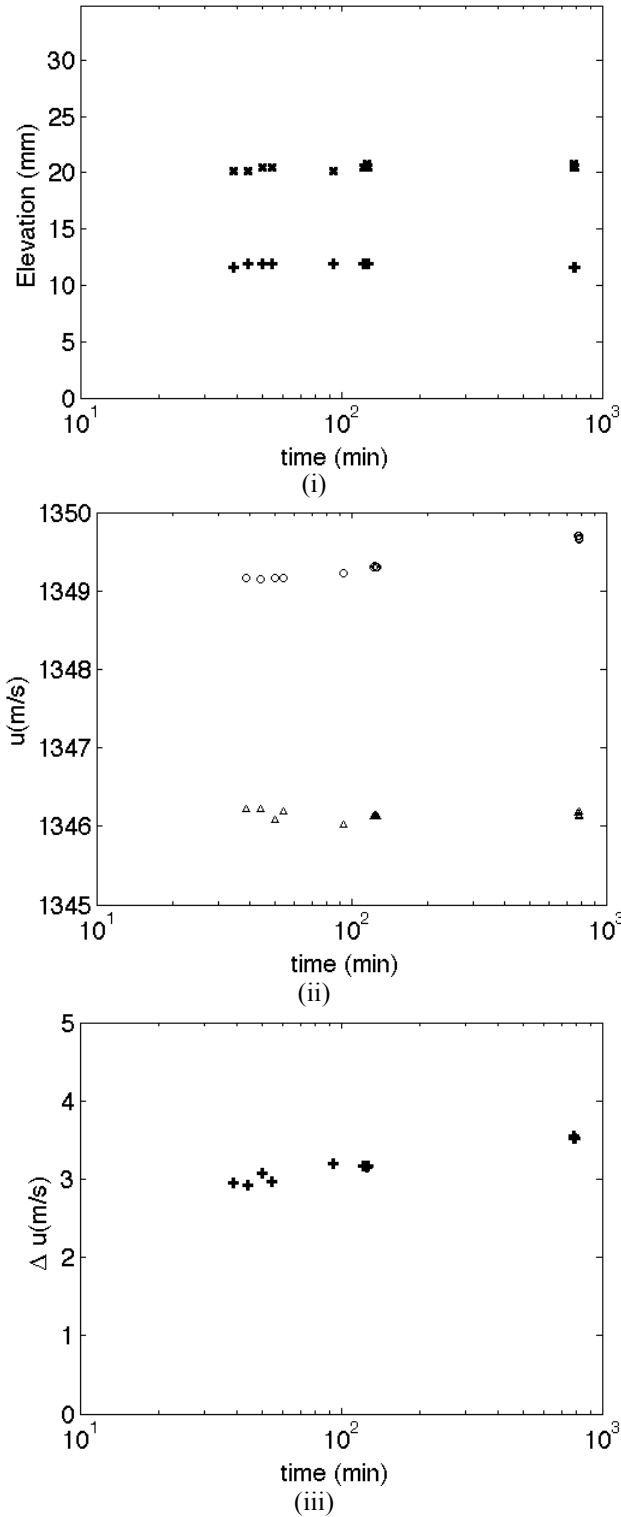


Figure. 4.14. (i) Variation with time of the liquid-liquid and liquid-air interfaces (ii) the speed of sound per phase: (triangle) upper phase, (circle): lower phase, (iii) speed of sound difference between the separated phases after phase separation for a mixture of asphaltene + polystyrene ($M_w=393,400$ g/mol) + toluene ($\eta=14.78$ vol%, $\Phi=2.84$ vol%) – first composition along dilution line q-.

4.5. UV-Visible spectrophotometry measurements of asphaltene composition in the separated phases

A mixture of asphaltene + polystyrene ($M_w=393,400$ g/mol) + toluene ($\eta=14.72$ vol%, $\phi=2.88$ vol%) with a composition close to that of mixture 1 in dilution line q ($\eta=14.78$ vol%, $\phi=2.84$ vol%) was prepared. Phase separation was completed 52 min after mixing. The profiles of speed of sound and the attenuation spectra are shown in Figure 4.15. Measured volume fraction of the upper phase R is 0.42, this value compares well with that measured for mixture 1 in dilution line q, $R=0.43$. Upper and lower phases were extracted successively from the cell and aliquots of 0.4 ml of each phase were diluted in 100 ml of toluene.

A Variant Carry 50 Scan UV-Visible spectrophotometer was used to measure the concentration of asphaltene in the separated phases. The specified instrument tolerance for absorbance measurement is ± 0.005 Abs at 1 Abs. Samples were introduced in a 10 mm path quartz cell. Absorbance spectra in pure toluene, and polystyrene 7.8 vol% in toluene, and for nine asphaltene + toluene mixtures are presented in Figure 4.16.a. Neither toluene nor polystyrene + toluene mixtures absorb significantly in the wavelength range 500-800 nm. Their absorbance is ~ 0.03 Abs.

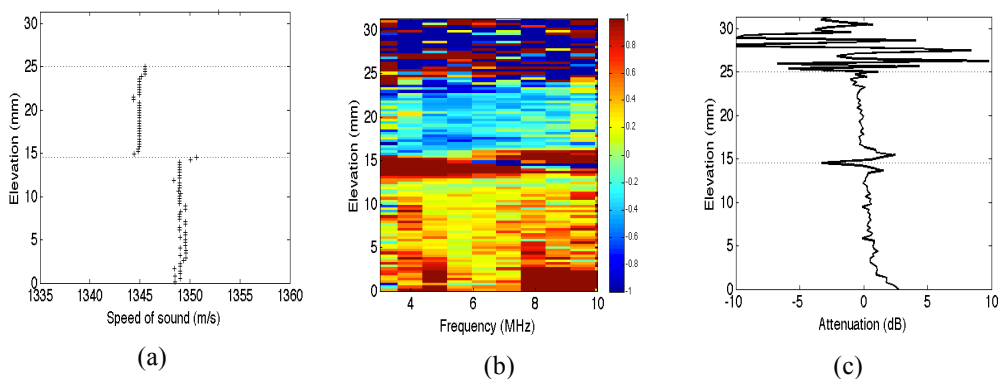


Figure 4.15. Experimental phase separation results for a mixture with global composition ($\eta=14.72$ vol%, $\phi=2.88$ vol%), 167 min after mixing: (i) Speed of sound profile, (ii) Acoustic wave attenuation spectra difference and (ii) ultrasound attenuation difference at 7.9 MHz.

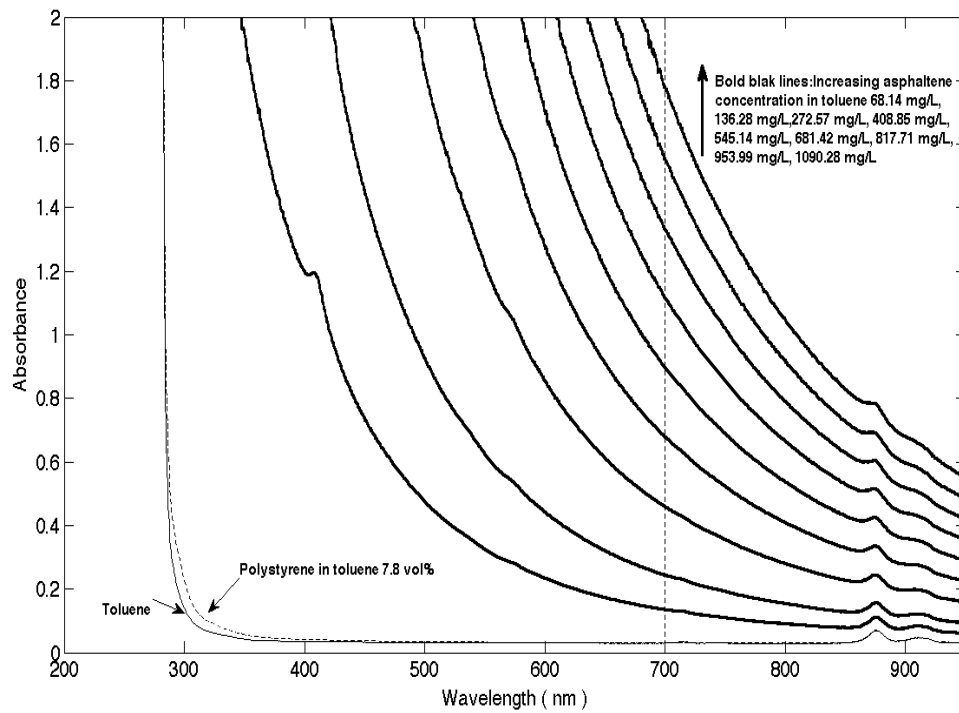
Absorbance spectra measured in diluted samples extracted from upper and lower phases are shown in Figure 4.16.b. Maya asphaltene molecules contains no significant chromophore in the range 500 – 900 nm [24]. Absorbance in this range is attributed to scattering effects by asphaltene colloidal particles. The concentration of asphaltenes in the diluted upper and lower phase samples is obtained using the calibration curve of absorbance at a wavelength of 700 nm vs asphaltene concentration in toluene (Figures 4.17). Figure 4.17 shows that the calibration curve is a straight line with a correlation coefficient R^2 of 0.9999904. The straight line has a non-zero intercept that is within the instrument tolerance (± 0.005). The absorbance of pure toluene is subtracted from the absorbance measured in the lower phase and the absorbance of polystyrene in toluene solution 7.8 vol% is subtracted from the absorbance measured in the upper phase.

The concentration of asphaltene in the diluted solutions of the samples extracted from the lower and upper phases are 938.7 mg/L and 346.4 mg/L respectively. This corresponds to asphaltene volume fractions of $\eta_I = 20.06 \pm 0.58$ vol% and $\eta_{II} = 7.40 \pm 0.26$ vol% in the original lower and upper phases respectively. Using the mass balance equation, the overall volume fraction of asphaltene can be calculated as follows:

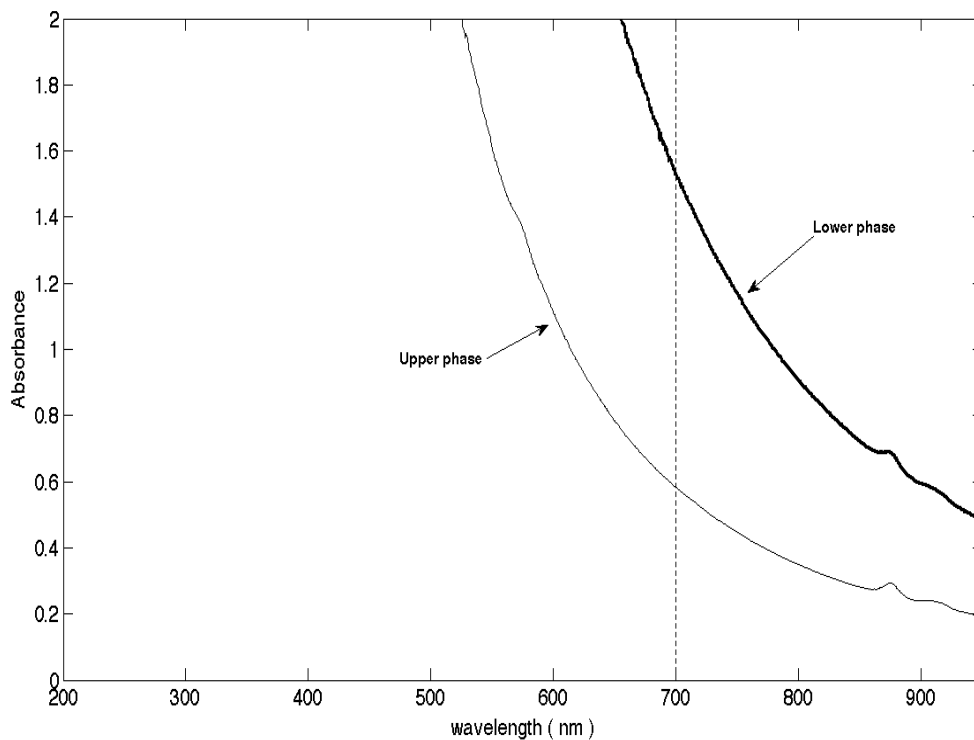
$$\eta = R \eta_{II} + (1-R) \eta_I = 14.74 \pm 0.73 \text{ vol\%} \quad (4.5)$$

This value is in agreement with the global volume fraction of asphaltene in the original solution (14.72 ± 0.58 vol%).

The volume fraction of polystyrene in the two phases can be estimated by evaporating toluene from two vials containing liquid samples from the upper and lower phases. The vials were left in the oven for 10 hours at 90 C and in a vacuum oven for 6 hours at 80 C.



(a)



(b)

Figure 4.16. (a) Absorbance spectra in pure toluene, polystyrene in toluene solution and different asphaltene in toluene solutions, (b) absorbance spectra in diluted lower and upper phases.

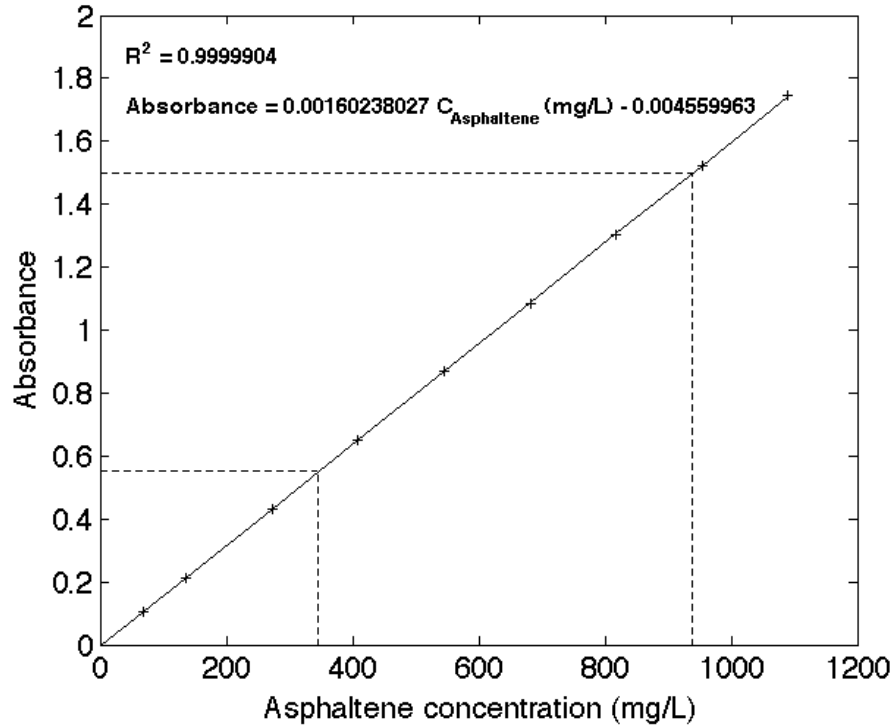


Figure 4.17. Absorbance difference between asphaltene in toluene solutions and pure toluene at a wavelength of 700 nm vs asphaltene concentration. Dashed lines indicate the absorbance and the concentration of asphaltene in the diluted samples extracted from the upper and the lower phases.

From the mass differences (Appendix B), the volume fraction of polystyrene in the lower and upper phases are: $\phi_I = -0.18 \pm 0.67 \text{ vol}\% \approx 0.00 \pm 0.67 \text{ vol}\%$ and $\phi_{II} = 6.0 \pm 0.32 \text{ vol}\%$ respectively. The overall polystyrene volume fraction in the mixture can be estimated from the following mass balance equation:

$$\phi = R \phi_{II} + (1-R) \phi_I = 2.52 \pm 0.50 \text{ vol}\% \quad (4.6)$$

The deviation between this value and the global volume fraction of polystyrene ($2.88 \pm 0.25 \text{ vol}\%$) is $0.36 \text{ vol}\%$. This deviation falls into the estimated error range of equation (4.6).

Figures 4.18.a-b show the experimental phase diagrams for mixtures of asphaltene + polystyrene + toluene for the two case of polystyrene molecular weights. These figures show the estimated phase boundaries and critical points. The critical

points fall, on the liquid-liquid to liquid boundary, between lines r and q for the cases of polystyrene with molecular weights of 393,400 g/mol and 700,000 g/mol. The critical point was found to be in the range: ($10.8 < \eta^c < 14.5$ vol%, $0.8 < \phi^c < 2.2$ vol%) for the case of polystyrene with a molecular weight of 393,400 g/mol and in the range: ($9.9 < \eta^c < 13.5$ vol%, $0.8 < \phi^c < 1.7$ vol%) for the case of polystyrene with a molecular weight of 700,000 g/mol. Figure 4.18.a also shows phase compositions obtained experimentally with error bars for a mixture with global composition $\eta=14.7$ vol%, $\phi=2.9$ vol%. For this mixture, the asphaltene volume fraction in the asphaltene poor phase is 7.4 vol% and it is 20.1 vol% in the asphaltene rich phase.

4.6. Conclusions

Reproducible liquid-liquid phase behavior was observed for mixtures of asphaltene + polystyrene + toluene over a broad range of composition at 293 K and atmospheric pressure. The speed of sound in the lower phase was larger than in the upper phase. The upper phase volume fraction was found to increase with the volume fraction ratio of polystyrene/asphaltene. Acoustic measurements of the phase separation kinetics were found to be similar to those measured in a mixture of methanol + hexanes and the time required for the completion of the phase separation was in the same range as that reported for mixtures of colloidal particles + non-adsorbing polymer. Phase boundaries and critical phenomena were identified for two polystyrene molecular weights.

UV-Visible spectrophotometry measurements and mass balance equations were used to determine the concentration of asphaltenes and polystyrene in the separated phases for a mixture with an overall composition of $\eta=14.7$ vol% and $\phi=2.9$ vol%. The lower phase is asphaltene rich and polystyrene poor ($\eta_I=20.1$ vol%, $\phi_I \sim 0$ vol%). The upper phase is asphaltene poor and polystyrene rich ($\eta_{II}=7.4$ vol%, $\phi_{II}=6.0$ vol%) relative to the feed.

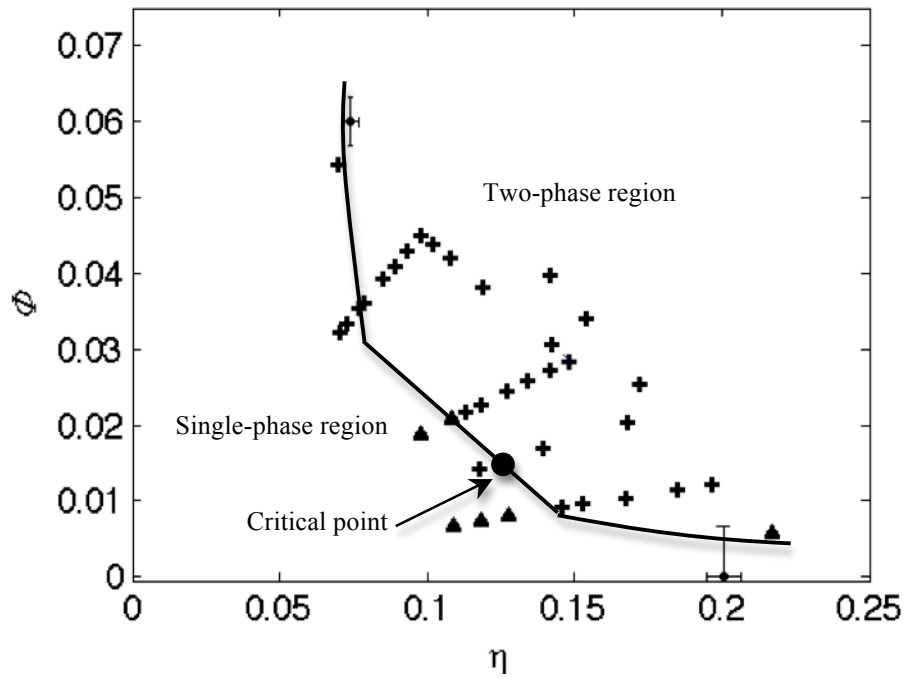


Figure 4.18.a. Phase diagram for mixtures of asphaltenes + polystyrene ($M_w=393,400$ g/mol) + toluene with estimated phase boundaries and critical point: (cross) two-phase region, (triangle): single-phase region, (dot): with error bars, experimental phase compositions for a mixture with global composition: $\eta=14.7$ vol%, $\phi=2.9$ vol%.

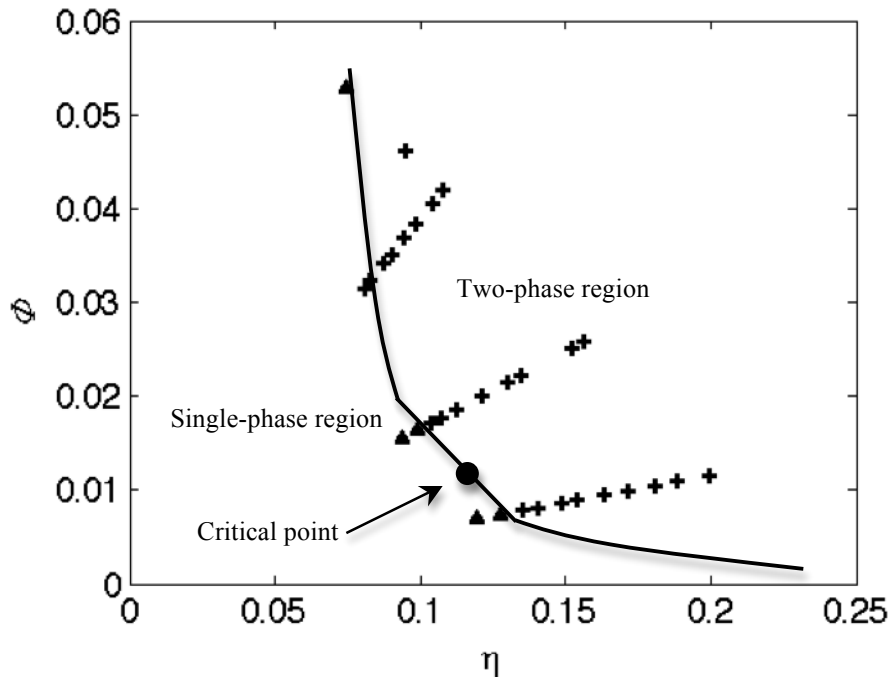


Figure 4.18.b. Phase diagram for mixtures of asphaltenes + polystyrene ($M_w=700,000$ g/mol) + toluene with estimated phase boundaries and critical point: (cross) two-phase region, (triangle): single-phase region.

The phase behavior of mixtures of asphaltenes + polystyrene + toluene conforms with that of sterically stabilized colloidal particles (asphaltenes) + a non-adsorbing (polymer) in a good solvent (toluene). The mechanism proposed for the phase separation is depletion flocculation. As asphaltene colloidal particles in toluene are polydispersed, it is not clear what fraction of the asphaltenes participate in the depletion flocculation process.

References

1. Barre, L., Simon, S., & Palermo, T. (2008) Solution properties of asphaltenes. *langmuir* 24, 3709-3717.
2. Zhao, B., Becerra, M., & Shaw, J. M. (2009) On Asphaltene and Resin Association in Athabasca Bitumen and Maya Crude Oil. *Energy & Fuels* 23, 4431-4437.
3. Zhao, B. & Shaw, J. M. (2007) Composition and size distribution of coherent nanostructures in Athabasca bitumen and Maya crude oil. *Energy & Fuels* 21, 2795-2804.
4. Espinat, D., Fenistein, D., Barre, L., Frot, D., & Briolant, Y. (2004) Effects of temperature and pressure on asphaltenes agglomeration in toluene. A light, X-ray, and neutron scattering investigation. *Energy & Fuels* 18, 1243-1249.
5. Wang, S., Liu, J., Zhang, L., Xu, Z., & Masliyah, J. (2009) Colloidal Interactions between Asphaltene Surfaces in Toluene. *Energy & Fuels* 23, 862-869.
6. Branco, V., Mansoori, G., Xavier, L., Park, S., & Manafi, H. (2001) Asphaltene flocculation and collapse from petroleum fluids. *Journal of Petroleum Science and Engineering* 32, 217-230.
7. Myakonkaya, O. & Eastoe, J. (2009) Low energy methods of phase separation in colloidal dispersions and microemulsions. *Advances in Colloid and Interface Science* 149, 39-46.
8. Lima, A. F., Mansur, C. R. E., Lucas, E. F., & Gonzalez, G. (2010) Polycardanol or Sulfonated Polystyrene as Flocculants for Asphaltene Dispersions. *Energy & Fuels* 24, 2369-2375.
9. Noda, I., Higo, Y., Ueno, N., & Fujimoto, T. (1984) Semidilute Region for Linear-Polymers in Good Solvents. *Macromolecules* 17, 1055-1059.
10. Luckham, P. (1991) Measurement of the Interaction Between Adsorbed Polymer Layers - The Steric Effect. *Advances in Colloid and Interface Science* 34, 191-215.
11. Sieglaff, C. (1959) Phase Separation in Mixed Polymer Solutions. *Journal of Polymer Science* 41, 319-326.
12. Clarke, J. & Vincent, B. (1981) Stability of non-aqueous microgel dispersions in the presence of free polymer. *Journal of the Chemical Society - Faradat Transactions I* 77, 1831-1843.

13. Asakura, S. & Oosawa, F. (1954) On Interaction between 2 Bodies Immersed in a Solution of Macromolecules. *Journal of Chemical Physics* 22, 1255-1256.
14. Asakura, S. & Oosawa, F. (1958) Interaction Between Particles Suspended in Solutions of Macromolecules. *Journal of Polymer Science* 33, 183-192.
15. Tuinier, R., Rieger, J., & de Kruif, C. G. (2003) Depletion-induced phase separation in colloid-polymer mixtures. *Advances in Colloid and Interface Science* 103, 1-31.
16. Ramakrishnan, S., Fuchs, M., Schweizer, K. S., & Zukoski, C. F. (2002) Entropy driven phase transitions in colloid-polymer suspensions: Tests of depletion theories. *Journal of Chemical Physics* 116, 2201-2212.
17. Hennequin, Y., Evens, M., Angulo, C., & van Duijneveldt, J. (2005) Miscibility of small colloidal spheres with large polymers in good solvent. *Journal of Chemical Physics* 123.
18. Bodnar, I. & Oosterbaan, W. (1997) Indirect determination of the composition of the coexisting phases in a demixed colloid polymer mixture. *Journal of Chemical Physics* 106, 7777-7780.
19. Buenrostro-Gonzalez, E., Lira-Galeana, C., Gil-Villegas, A., & Wu, J. (2004) Asphaltene precipitation in crude oils: Theory and experiments. *AIChE Journal* 50, 2552-2570.
20. Fulem, M., Becerra, M., Hasan, M. D. A., Zhao, B., & Shaw, J. M. (2008) Phase behaviour of Maya crude oil based on calorimetry and rheometry. *Fluid Phase Equilibria* 272, 32-41.
21. Mostowfi, F., Indo, K., Mullins, O. C., & McFarlane, R. (2009) Asphaltene Nanoaggregates Studied by Centrifugation. *Energy & Fuels* 23, 1194-1200.
22. Beliajeva, O., Grebenkov, A., Zajatz, T., & Timofejev, B. (1999) Speed of sound in the liquid phase of the R134a/152a refrigerant blend. *International Journal of Thermophysics* 20, 1689-1697.
23. Aarts, D. & Lekkerkerker, H. (2004) Confocal scanning laser microscopy on fluid-fluid demixing colloid-polymer mixtures. *Journal of Physics-Condensed Matter* 16, S4231-S4242.
24. Dechaine, G. P. & Gray, M. R. (2011) Membrane Diffusion Measurements Do Not Detect Exchange between Asphaltene Aggregates and Solution Phase. *Energy & Fuels* 25, 509-523.

Chapter 5. Phase Behavior of Asphaltenes + Polystyrene + Toluene Mixtures at 293 K, Part Two: Data Analysis

5.1. Introduction

From Chapter 4, mixtures of asphaltene + polystyrene + toluene separate into asphaltene rich and asphaltene poor liquid phases. This behavior is analogous to the behavior of colloidal particles + non-adsorbing polymer in a good solvent where separation into colloid-poor and colloid-rich stable phases occurs by depletion flocculation (Figure 2.2). The prediction of the phase behavior of mixtures of colloids + non-adsorbing polymer was performed using computer simulations of hard spheres plus self avoiding polymer chains [1], thermodynamic perturbation theories [2], polymer-colloid liquid state theory [3] and density functional theory [4]. The calculation of the binodal line using these methods is computationally expensive [5]. A simpler approach, the osmotic equilibrium theory or the free volume theory, was developed by Lekkerkerker et al [6] for the prediction of the phase behavior of such mixtures. In this theory, polymer partitioning between the separated phases is taken into account. The depletion thickness δ is considered to be proportional to the radius of gyration R_g of the polymer. Lekkerkerker's model is valid when $R_g/a < 1$ (colloid limit) and where polymer concentration is below the overlap concentration ($\varphi/\varphi_{ov} < 1$). The model fails when the concentration of the polymer at the binodal points exceeds the overlap concentration ($\varphi/\varphi_{ov} > 1$). This situation occurs in the so-called protein limit where the polymer radius of gyration is larger than the colloidal particle radius ($R_g/a > 1$). In this limit, the depletion thickness δ is independent of the polymer chain length and is only function of the concentration of the polymer. Recently, Fler et al developed a model based on the free volume theory and valid for both the colloid ($R_g/a < 1$) and the protein ($R_g/a > 1$) limits and in the crossover between the two limits. According to this theory, the depletion thickness is

function of both (R_g/a) and the polymer volume fraction in the mixture. The agreement between this model and experimental data was discussed in Chapter 2 [5].

The binodal compositions can be determined experimentally by direct measurement/sampling of the phases [7], or indirectly, by measuring the variations of volume fractions of the two phases along at least three dilution lines [8]. The binodal points are obtained by varying the length and the slope of the tie lines to fit the experimental volume fractions of the phases. In opaque liquids, Erne et al [9] used an infrared technique to measure the phase behavior and the concentration of the colloidal particles and the non-adsorbing polymer. This technique is limited to cases where adsorption at the wall is negligible and where the IR spectra of the polymer and the colloidal particles are sufficiently distinct to allow for the estimation of the volume fractions of the particles and the polymer separately.

In this work, the composition of the phases in mixtures of asphaltene + polystyrene + toluene are first calculated from the variations of the volume fraction of the separated phases along the dilution lines using the procedure described by Bodnar et al[8]. It is initially assumed that all asphaltene colloidal particles are participating in the phase separation mechanism. Calculated binodal points are then used for the calculation of the speeds of sound in the separated phases, results are compared with measured speed of sound values. A fraction γ of asphaltene colloidal particles participating in the phase separation mechanism is introduced to improve the agreement between calculated and experimental speeds of sound in the separated phases by increasing the slope of the calculated tie lines. For a mixture with a specific global composition, calculated compositions of the separated phases are compared with the results obtained from UV-Visible spectrophotometry measurements. Finally, an interval for the radii of asphaltene colloidal particles participating in the phase separation is estimated by comparing

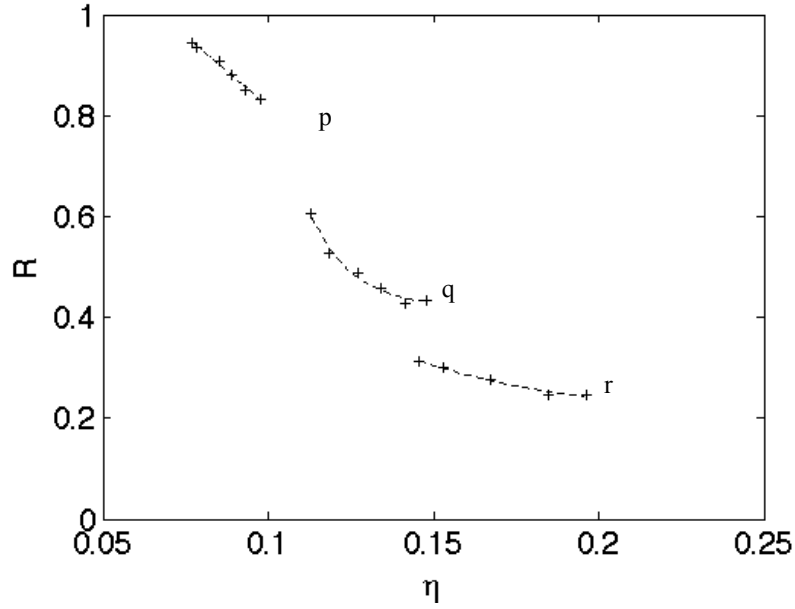
the experimental phase diagram with model calculation results for a mixture of monodispersed colloidal particles + non-adsorbing polymer [5].

5.2. Evaluation of binodal compositions

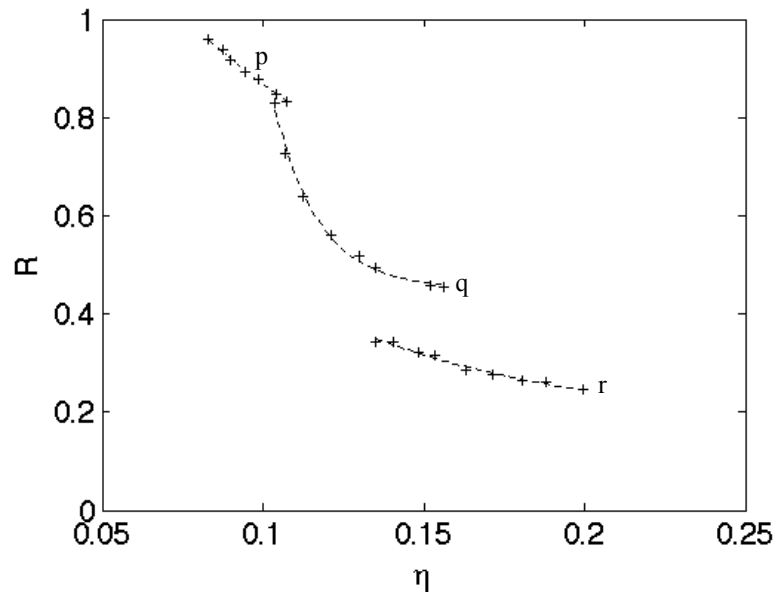
5.2.1 Phase volume, mass balance and UV spectrophotometry data

For a mixture of asphaltene + polystyrene + toluene moving along dilution line p, q or r with global composition (η, Φ) , the compositions of the phases (η_I, Φ_I) , (η_{II}, Φ_{II}) are estimated using the variations of the volume fraction of the upper phase along the three dilution lines p, q and r. These variations were fitted with a first order exponential function [10] as shown in Figure 5.1. The numerical algorithm of Bodnar et al [8], based on the lever rule and described in Chapter 2 is used in this work. In the mixtures investigated by Bodnar et al. [8] and Hennequin et al. [10], both the size and the volume fraction of the colloidal particles were known. The particles were monodispersed and dilution had no effect on their size.

In this work, it is initially assumed that all asphaltenes in the solution form colloidal particles participating in the depletion flocculation mechanism and causing phase separation. Binodal points, calculated by minimizing the objective function, equation (2.39), are presented in Figures 5.2.a-b for the two polystyrene molecular weights. The volume fractions of asphaltenes in the upper and lower phases vary from 7.0 vol% to 8.1 vol% and from 18.9 vol% to 22.4 vol% respectively. Polystyrene volume fraction varies from 0.2 to 0.3 vol% in the lower phase and from 3.9 vol% to 5.3 vol% in the upper phase. The effect of the molecular weight on the phase diagram is not apparent. Parts of the binodal are not constructed because the tie lines can be calculated only when they intersect three dilution lines [8]. The critical points are estimated by extrapolating the centres of the tie lines to the experimentally observed liquid-liquid phase boundary [8]. The critical points obtained, $(\eta^C=12.1 \text{ vol}\%, \phi^C=1.7 \text{ vol}\%)$ for mixtures with a polystyrene molecular weight of 393,400 g/mol and $(\eta^C=11.6 \text{ vol}\%, \phi^C=1.2 \text{ vol}\%)$ for mixtures with a polystyrene molecular weight of

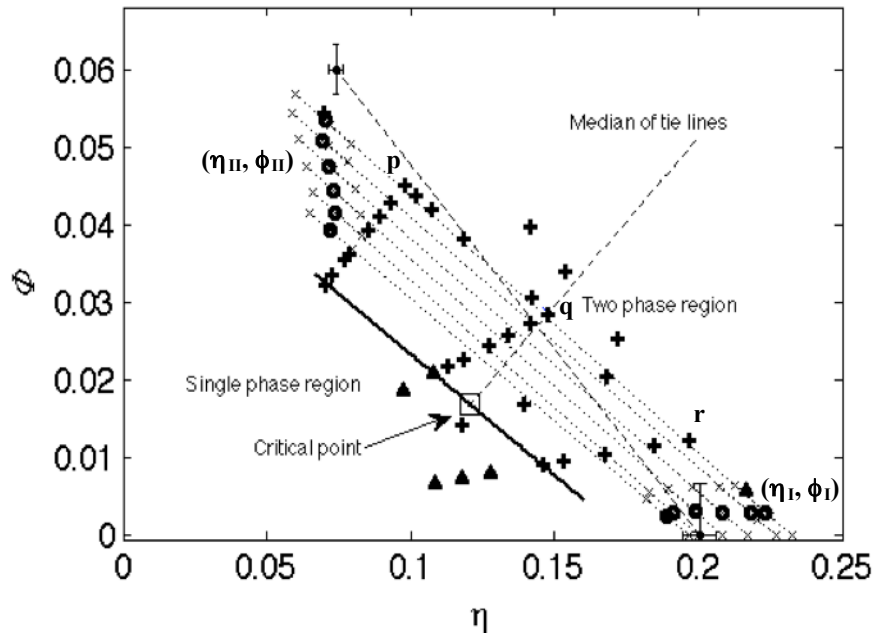


(a)

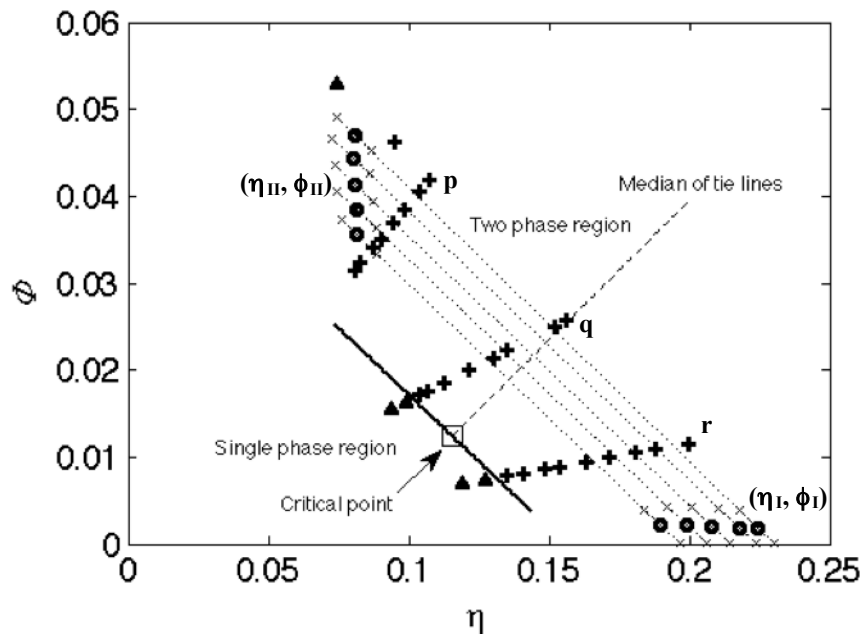


(b)

Figure 5.1. Variations of the upper phase volume fraction with asphaltene volume fraction along dilution lines p, q and r for mixtures of asphaltene + polystyrene + toluene: (a) polystyrene molecular weight $M_w=393,400$ g/mol, (b) polystyrene molecular weight $M_w=700,000$ g/mol. Dotted line: first order exponential function fit.



(a)



(b)

Figure 5.2. Experimental phase diagram for mixtures of asphaltene + polystyrene + toluene: (a) polystyrene molecular weight of 393,400 g/mol (b) polystyrene molecular weight of 700,000 g/mol. Symbols: (+) two-phase, (Δ) single-phase, (square): estimated critical point, (open circle): calculated binodal points. (dot): with error bars in (a) represents the experimental phase compositions for a mixture with global composition ($\eta=14.7$ vol%, $\phi=2.9$ vol%).

700,000 g/mol, fall within the estimated composition ranges for direct phase boundary measurements.

For a mixture of asphaltene + polystyrene ($M_w=393,400$ g/mol) + toluene with a global composition ($\eta=14.7$ vol%, $\phi=2.8$ vol%), calculated phase compositions ($\eta_I=22.4 \pm 1.0$ vol%, $\phi_I=0.30 \pm 0.3$ vol%)_{calculated} for the lower phase and ($\eta_{II}=7.0 \pm 1.0$ vol%, $\phi_{II}=5.3 \pm 0.3$ vol%)_{calculated} for the upper phase are obtained. Calculated error for binodal points varies on the extension of the tie line.

From a combination of spectrophotometry measurements + mass balance equations (Section 4.5), for a mixture with a similar global composition ($\eta=14.7 \pm 0.6$ vol%, $\phi=2.9 \pm 0.3$ vol%) –Fig.5.2 a-, phase compositions ($\eta_I=20.1 \pm 0.6$ vol%, $\phi_I=0.0 \pm 0.7$ vol%)_{experimental} lower phase and ($\eta_{II}=7.4 \pm 0.3$ vol%, $\phi_{II}=6.0 \pm 0.3$ vol%)_{experimental} upper phase are obtained. The slope of the calculated tie line appears to be smaller than the experimental line. The difference between the calculated and measured phase compositions may be attributed to shortcomings in the composition extrapolation procedure. The lever rule used for the calculation of the composition of the phases is only valid if asphaltenes may be considered as a single species. Polydispersity of asphaltene colloidal particles and their size dependence on concentration may have impacted the estimated phase compositions. Only a fraction of asphaltene may be large enough to participate in the depletion flocculation mechanism and cause phase separation. This potential shortcoming can account for the difference between the slopes of the calculated and the experimental tie lines in the two-phase region.

5.2.2 Speed of sound data and the fraction of asphaltenes participating in the phase separation mechanism

Another way to compare the estimated compositions of the phases with experimental data is to compare computed speed of sound values for estimated binodal compositions (shown in Figures 5.2.a-b) with experimental speed of

sound measurements. The deviations between experimental speeds of sound from average volume fraction values in the ternary mixtures of asphaltene + polystyrene + toluene are fitted with the following Cibulka equation [11]:

$$\begin{aligned}\Delta u &= u_{\text{exp}} - (\eta u_{\text{asph}} + \phi u_{\text{polyst}} + (1 - \eta - \phi) u_{\text{tol}}) \\ &= \Delta u_{\text{bin}} + \eta \phi (1 - \eta - \phi) (B_1 + B_2 \eta + B_3 \phi)\end{aligned}\quad (5.1)$$

where Δu_{bin} is the sum of the deviations of experimental speeds of sound from average volume fraction values in the three binaries: asphaltene + toluene, polystyrene + toluene and asphaltene + polystyrene. It is given by:

$$\Delta u_{\text{bin}} = \Delta u_{\text{asph-tol}} + \Delta u_{\text{polyst-tol}} + \Delta u_{\text{asph-polyst}}, \quad (5.2)$$

$\Delta u_{\text{asph-tol}}$ and $\Delta u_{\text{polyst-tol}}$ were calculated using equation (4.1). Since no experimental data are available for the binary system asphaltene + polystyrene, the speed of sound deviation for this binary is neglected ($\Delta u_{\text{asph-polyst}} = 0$).

Coefficients B_1 , B_2 and B_3 were obtained by minimizing the standard deviation σ between experimental and calculated speeds of sound, before phase separation, along dilution lines p, q and r. The standard deviation σ is given by the following equation:

$$\sigma = \sqrt{\frac{\sum_{i=1}^N (u_{\text{exp}} - u_{\text{cal}})^2}{N}} \quad (5.3)$$

where N is the number of data points and u_{cal} is the calculated speed of sound, given by the following equation:

$$u_{\text{cal}} = (\Phi_j u_j + (1 - \Phi_j) u_{\text{tol}}) + \Delta u_{\text{bin}} + \eta \phi (1 - \eta - \phi) (B_1 + B_2 \eta + B_3 \phi) \quad (5.4)$$

Values of the parameters B_i are reported in Table 5.1 for the ternary mixtures asphaltene + polystyrene ($M_w=393,400$ g/mol) + toluene and asphaltene + polystyrene ($M_w=700,000$ g/mol) + toluene.

Table 5.1. Values of the parameters B_i in equation (5.1) and the standard deviation σ .

	Asphaltene + polystyrene ($M_w=393,400$ g/mol) + toluene	Asphaltene + polystyrene ($M_w=700,000$ g/mol) + toluene
B_1	0.4934×10^4	0.2866×10^4
B_2	-1.6593×10^4	-0.8906×10^4
B_3	-7.8027×10^4	-6.3309×10^4
σ	0.7296	0.8639

Figure 5.3 shows a parity plot of calculated vs experimental speeds of sound in the single-phase region and in the separated phases where the composition was measured experimentally. The largest deviation between calculated and experimental speeds of sound in the single-phase region is found to be 2.3 m/s. The origin of the deviations could be attributed to the error in the experimental composition, small temperature variations, or to the speed of sound model given in equation (5.4). When the speed of sound is calculated using the compositions determined experimentally. The impact of the composition measurement error on the speed of sound is such that the deviation between experimental and calculated speed of sound varies in the range 0 m/s to 4.2 m/s.

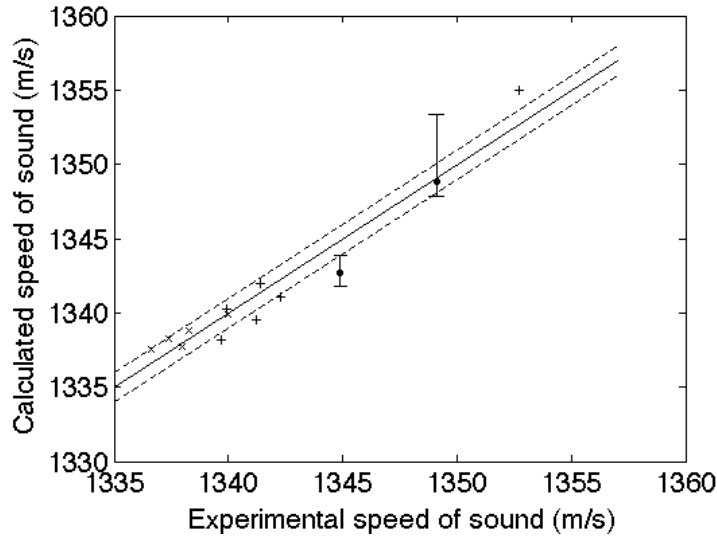


Figure 5.3. Parity plot for calculated speed of sound using equation 5.4 vs measured speed of sound in: (+) single phase region for the case of $M_w=393,400$ g/mol, (x) single phase region for the case of $M_w=700,000$ g/mol, (dot): with error bars, lower and upper phases calculated with measured compositions ($\eta_I=20.1 \pm 0.6$ vol%, $\phi_I=0.0 \pm 0.7$ vol%)_{experimental} and ($\eta_{II}=7.4 \pm 0.3$ vol%, $\phi_{II}=6.0 \pm 0.3$ vol%)_{experimental} respectively. (dashed lines): continuous line shifted by ± 1 m/s.

Figures 5.4.a-c and 5.5.a-c show a comparison between experimental speeds of sound in the mixtures after phase separation and calculated values along the three dilution lines (p, q and r) and for the two cases of polystyrene molecular weight. Also shown in Figure 5.4.b are calculated speeds of sound obtained from equation 5.4 and experimental phase compositions. When speeds of sound are calculated using the binodal compositions shown in Figures 5.2.a-b. Figures 5.4.a-c and 5.5.a-c show that for the case of polystyrene with an average molecular weight of 393,400 g/mol, the largest deviations between experimental and calculated speeds of sound in the separated phases are 8.8 m/s, 5.4 m/s and 7.8 m/s along dilution lines p, q and r respectively (Fig.5.4). These values are 11.6 m/s, 9.3 m/s and 10.0 m/s for the case of polystyrene with a molecular weight of 700,000 g/mol (Figs.5.5.a-c). Calculated speed of sound differences between the separated phases vary between 8.1 m/s and 15.9 m/s where experimental values vary between 1.2 m/s and 4.2 m/s. The deviations between calculated and experimental

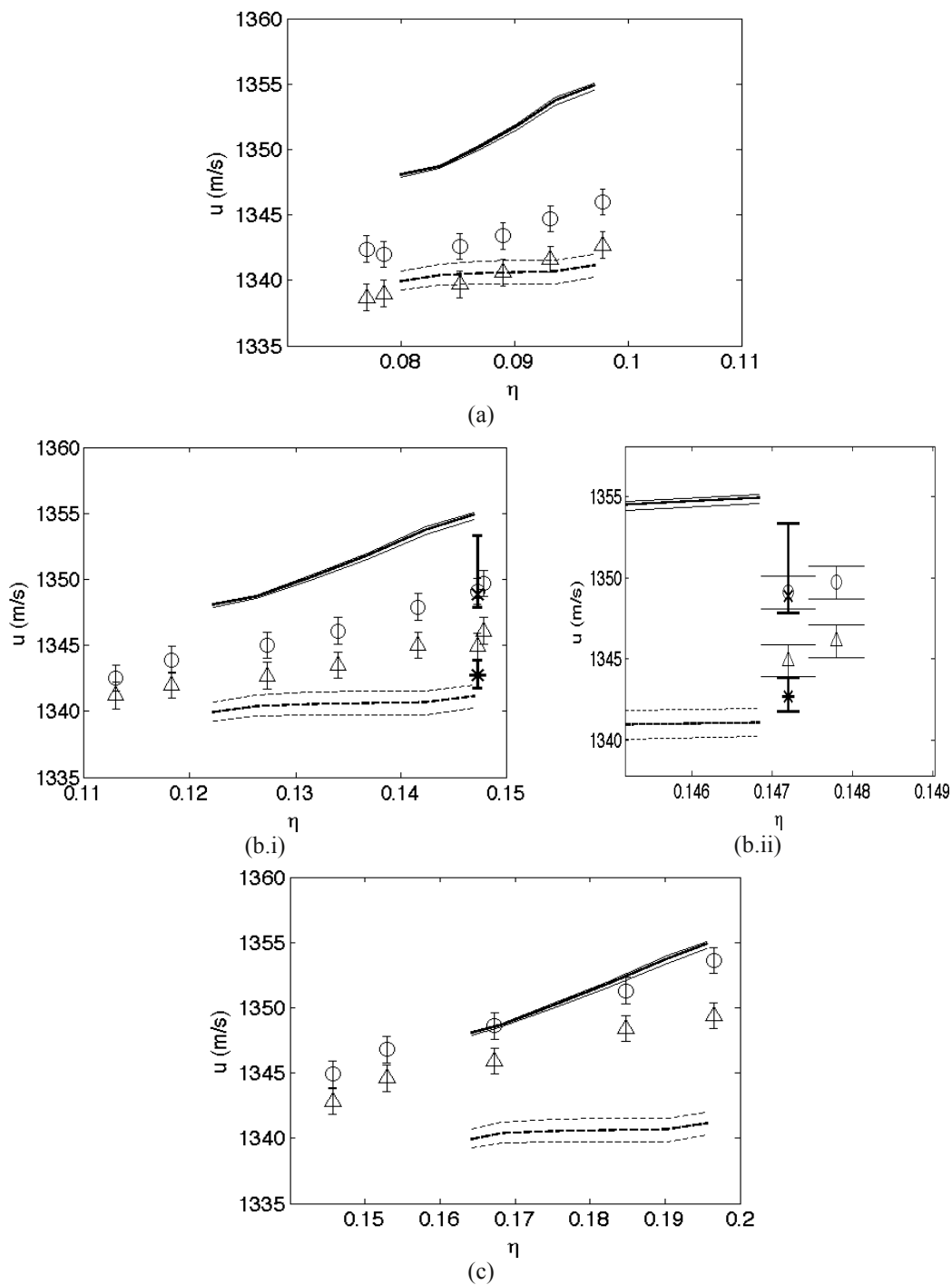
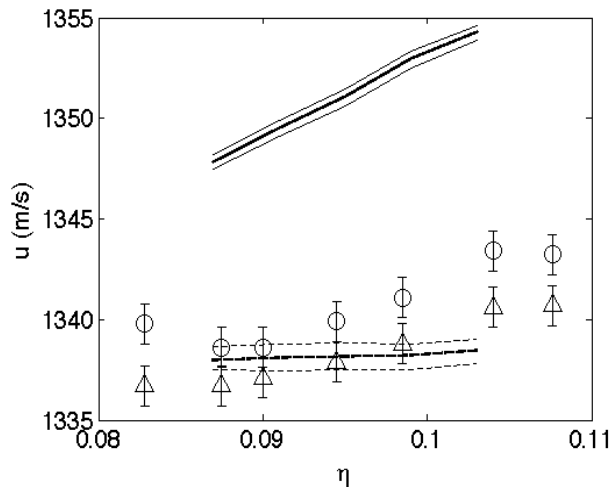
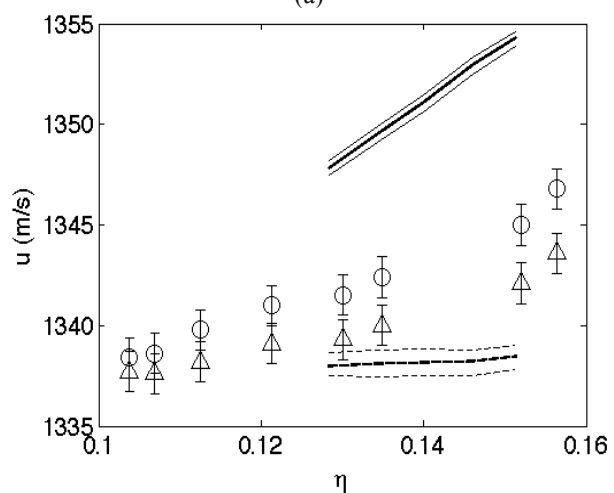


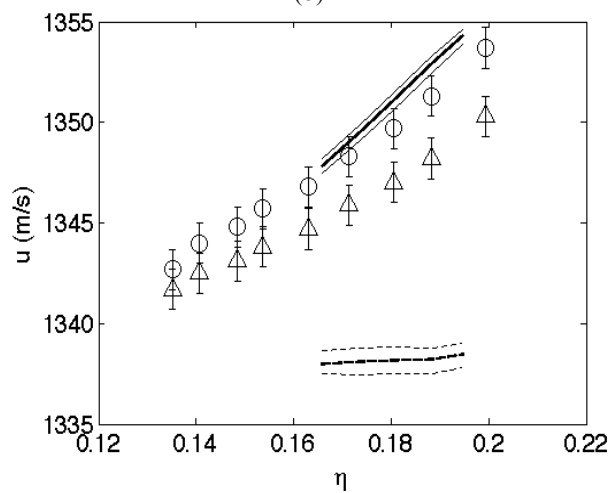
Figure 5.4. Comparison between calculated and experimental speeds of sound, after phase separation, along: (a) dilution line p, (b.i) dilution line q, (b.ii) computed speed of sound based on experimental phase compositions for a mixture with global composition ($\eta=14.7$ vol%, $\phi=2.9$ vol%): (x) lower phase, (*) upper phase. (c) dilution line r for mixtures of asphaltenes + polystyrene ($M_w=393,400$ g/mol) + toluene. Experimental speeds of sound: (o): lower phase, (Δ): upper phase. Calculated values: (continuous line): lower phase, (dashed line): upper phase.



(a)



(b)



(c)

Figure 5.5. Comparison between calculated and experimental speeds of sound after phase separation, along: (a) dilution line p, (b) dilution line q, (c) dilution line r for mixtures of asphaltenes + polystyrene ($M_w=700,000$ g/mol) + toluene. Experimental speeds of sound: (o): lower phase, (Δ): upper phase. Calculated values: (continuous line): lower phase, (dashed line): upper phase.

values can be attributed to the prediction accuracy of the binodal points shown in Figure 5.2. One way to reduce the calculated speed of sound difference between the separated phases and improve the agreement with experimental speed of sound data is to assume that only a fraction γ of asphaltene colloidal particles are large enough to cause phase separation. In this case, the predicted polystyrene volume fraction in the separated phases does not change, the slopes of dilution lines p^* , q^* and r^* increase and the slope and the length of the tie lines change such that the difference between the colloidal particle volume fractions in the separated phases decreases by a factor of γ (Fig.5.6). Additional details are provided in Appendix D. For this analysis, asphaltene colloidal particles participating in the phase separation mechanism are assumed to be invariant with global composition.

The total volume fraction of asphaltenes, η , in a mixture of asphaltene + polystyrene + toluene, is modeled as:

$$\eta = \eta^* + \eta^0, \quad (5.5)$$

where:

$$\eta^* = \gamma \eta \quad (5.6)$$

$$\eta^0 = (1-\gamma) \eta \quad (5.7)$$

η^* is the volume fraction of asphaltene colloidal particles that are large enough to cause phase separation, η^0 : the volume fraction of asphaltenes that are too small to participate in the phase separation and γ : the fraction of asphaltene colloidal particles causing phase separation.

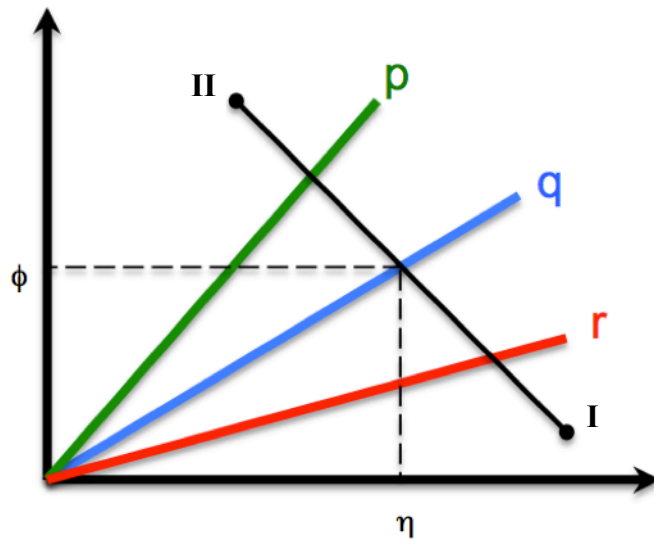
After phase separation, the volume fractions of asphaltenes in the coexisting phases (I), (II) are given by:

$$\begin{cases} \eta_I = \eta_I^* + \eta_I^0 \\ \eta_{II} = \eta_{II}^* + \eta_{II}^0 \end{cases} \quad (5.8)$$

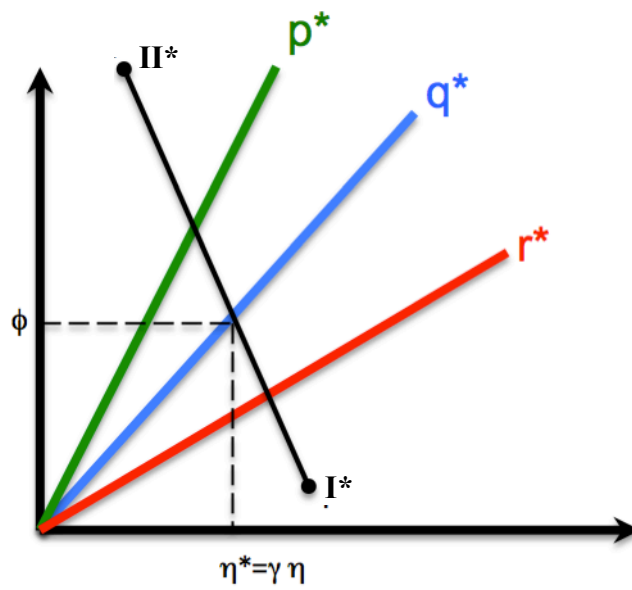
The volume fractions of asphaltenes that are too small to participate in the phase separation mechanism are assumed to be unaffected by separation:

$$\eta_I^0 = \eta_{II}^0 = \eta^0 = (1-\gamma)\eta \quad (5.9)$$

For a given value of the fraction γ , the geometrical transformation given in equation (5.6) is applied to dilution lines p, q and r and binodal points $(\eta_I, \phi_I), (\eta_{II}, \phi_{II})$ to obtain dilution lines p*, q* and r* and binodal points $(\eta_I^*, \phi_I^*), (\eta_{II}^*, \phi_{II}^*)$ of asphaltene colloidal particles participating in the phase separation mechanism. By incorporating this modification for the determination of phase compositions in the calculation of the speed of sound in the separated phases (Eq.5.4), it is possible to calculate the speed of sound difference between the upper and lower liquid phases as a function of γ and to compare computed values with measurements.



(a)



(b)

Figure 5.6. Schematic presentation of the effect of γ on the tie line [I II] and dilution lines p , q and r : (a) $\gamma=1$, (b) $\gamma<1$: $(\eta_{I^*}-\eta_{II^*})=\gamma(\eta_I-\eta_{II})$.

When the fraction γ is decreased, the slopes of the tie lines increase, the asphaltene volume fraction difference between the phases in equilibrium decreases and the speed of sound difference between coexisting phases decreases. The calculated speed of sound difference is sensitive to asphaltene and polystyrene composition variation. The ranges placed on the computed estimates reflect composition uncertainties in the upper and lower liquid phases ($\Delta\phi \approx \pm 0.3$ vol%, $\Delta\eta \approx \pm 1.0$ vol%) on the extension of the tie lines. Figures 5.7.a-8.a show a comparison between calculated and experimental speed of sound differences between the separated phases for different values of the fraction γ and for the two cases of polystyrene molecular weight. These figures suggest that $\gamma \approx 0.63$ and 0.49 for the cases of $M_w=393,400$ g/mol and $M_w=700,000$ g/mol respectively. The errors in the phase compositions obtained from the UV measurements are too large to contribute to the evaluation of γ on the basis of speed of sound value comparisons.

Figures 5.7.b-8.b show calculated asphaltene volume fraction difference between the phases for the two cases of polystyrene molecular weights. The experimental asphaltene volume fraction difference obtained from UV measurements ($\Delta\eta = 12.7 \pm 0.8$ vol%)_{exp} is larger than the calculated value for $\gamma \approx 0.63$ ($\Delta\eta = 9.7 \pm 1.1$ vol%)_{cal}, as shown in Fig.5.7.b. However, allowing for composition uncertainty in the calculation places the values close to quantitative agreement (within ≈ 1 vol%). The reason for the difference in the fraction γ between the two polystyrene molecular weight cases cannot be attributed at this time.

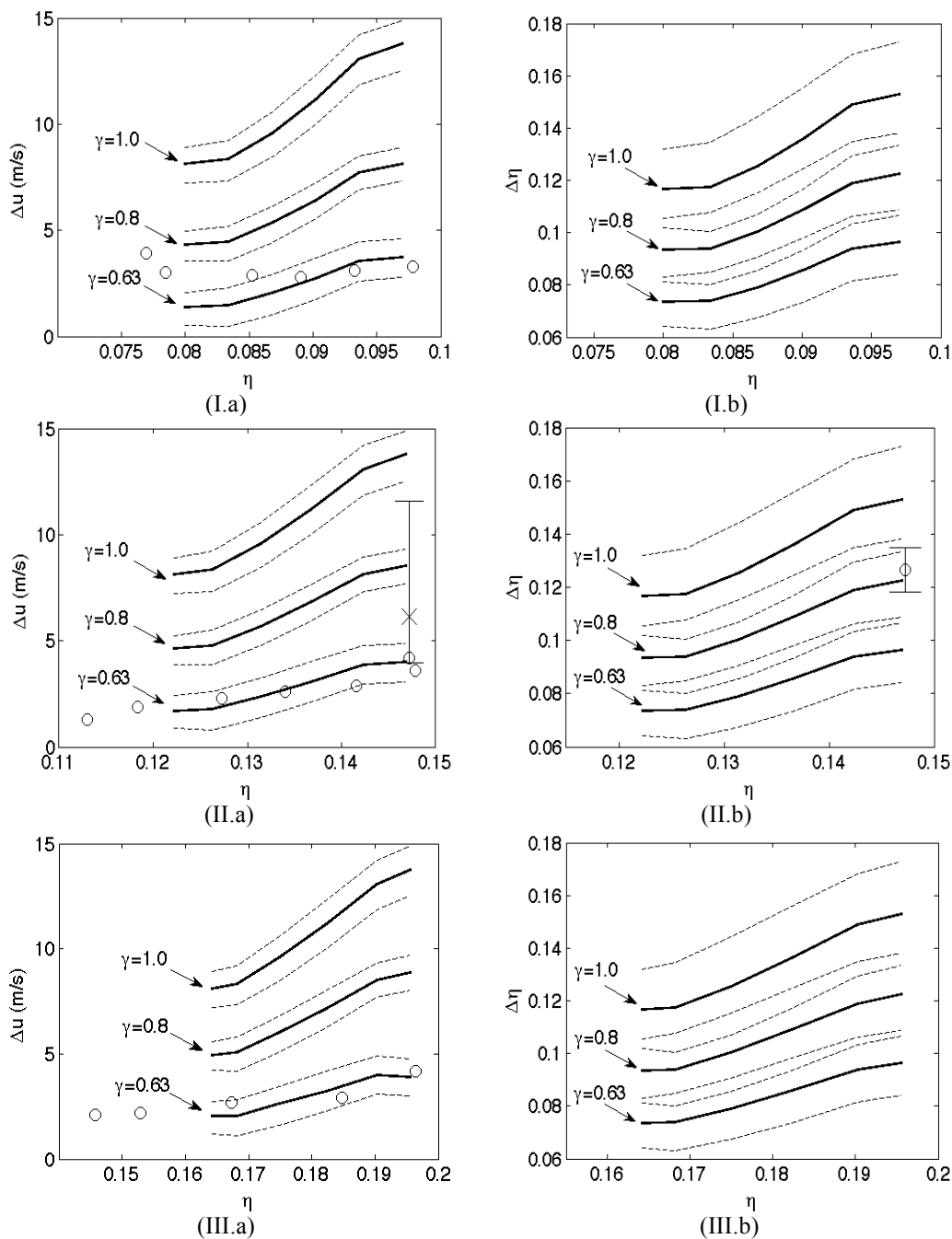


Figure 5.7. (a) Calculated (line) and experimental (circle) speed of sound difference values vs asphaltene global composition. (x): Calculated speed of sound difference using experimental phase composition for a mixture with global composition composition ($\eta=14.7$ vol%, $\phi=2.9$ vol%), (b) calculated (line) volume fraction difference of asphaltenes between phases vs global asphaltene composition. (I) Dilution line p, (II) dilution line q, (circle): experimental volume fraction difference of asphaltene between phases (III) dilution line r. γ is a parameter. Polystyrene molecular weight $M_w=393,400$ g/mol.

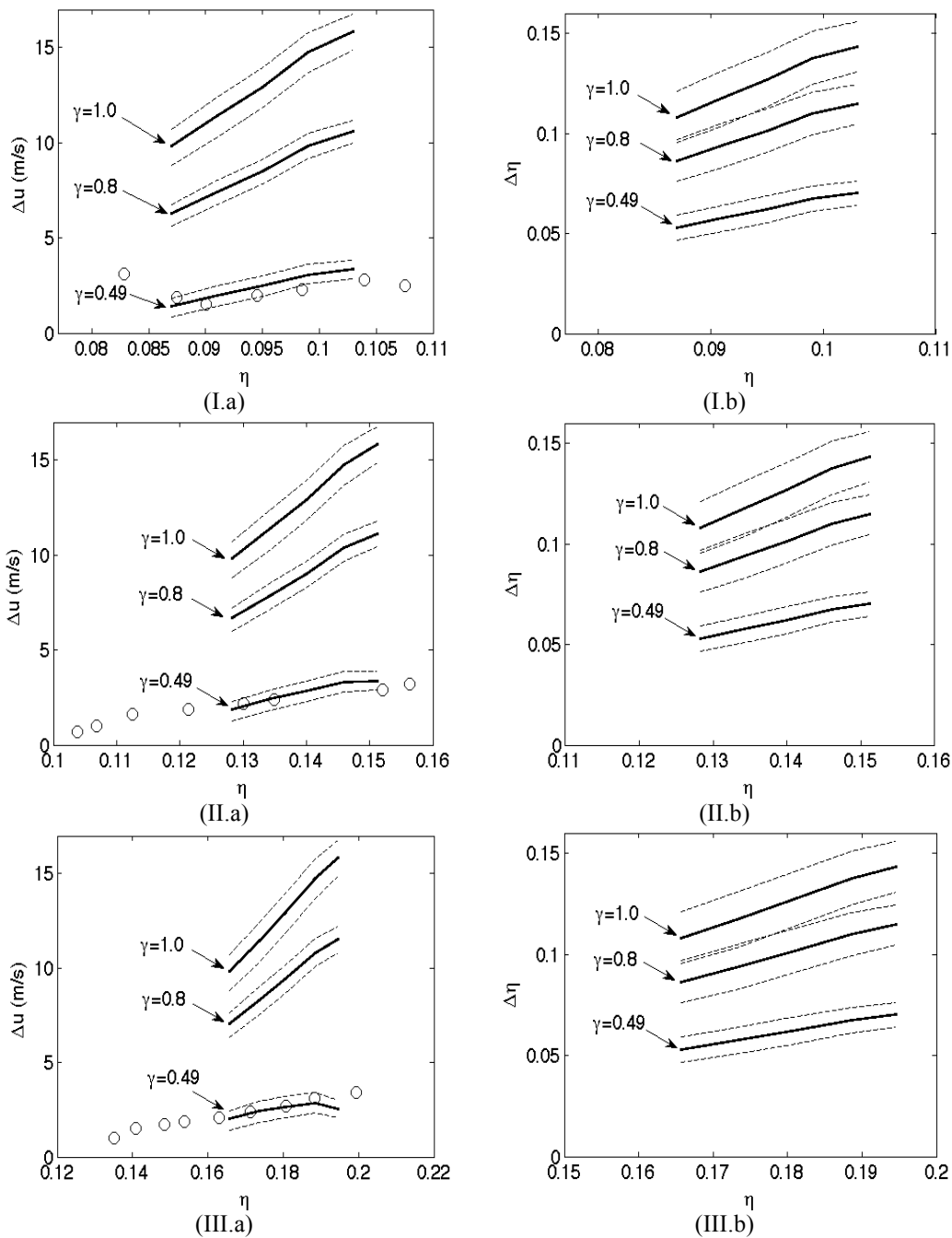
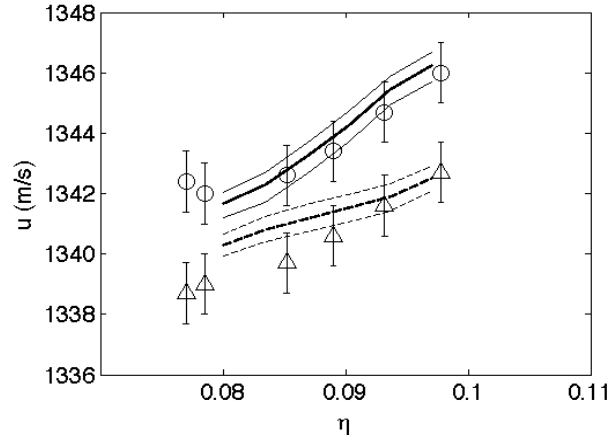


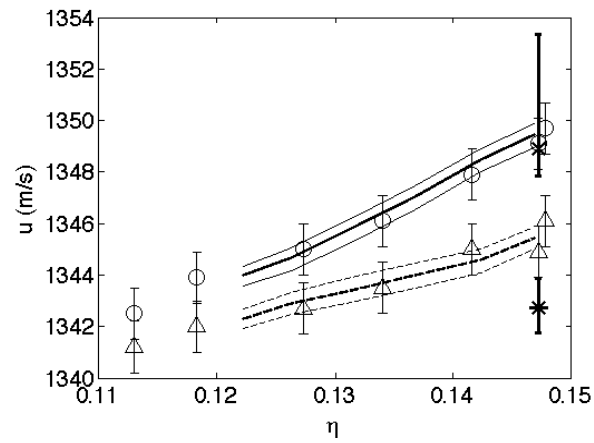
Figure 5.8. (a) Calculated (line) and experimental (circle) speed of sound difference values vs asphaltene global composition, (b) calculated volume fraction difference of asphaltenes between phases vs global asphaltene composition. (I) Dilution line p, (II) dilution line q, (III) dilution line r. γ is a parameter. Polystyrene molecular weight $M_w=700,000$ g/mol.

Figures 5.9-10 show calculated vs experimental speeds of sound for mixtures moving along dilution lines p, q and r. For the case of polystyrene with a molecular weight of 393,400 g/mol and $\gamma=0.63$ (Fig.5.9), the largest deviations between calculated and experimental speeds of sound in the separated phases are 1.3 m/s, 0.5 m/s and 1.5 m/s along dilution lines p, q and r respectively. A significant improvement compared with the case of $\gamma=1.0$, where the largest deviations are 8.8 m/s, 5.4 m/s, 7.8 m/s. For a polystyrene molecular weight of 700,000 g/mol, these values are 1.8 m/s, 1.7 m/s and 1.5 m/s for the case of $\gamma=0.49$ with (Fig.5.10) vs 11.6 m/s, 9.3 m/s, 10.0 m/s, for $\gamma = 1$. Thus, the agreement between experimental and calculated speeds of sound in the separated phases is significantly improved when γ is reduced.

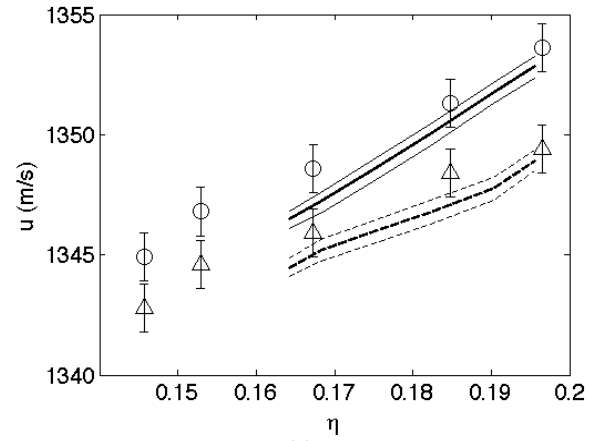
The volume fraction of asphaltene, η^0 , unaffected by the phase separation, is a fraction $(1-\gamma)$ of the global asphaltene composition (Eq.5.9). Therefore, overall phase compositions (η_I, ϕ_I) , (η_{II}, ϕ_{II}) , in the separated phases depend on the global composition of the mixture before separation (η, ϕ) . Phase compositions for mixtures moving along dilution line p, q and r for the two cases of polystyrene molecular weights ($M_w=393,400$ g/mol and $\gamma=0.63$) and ($M_w=700,000$ g/mol and $\gamma=0.49$) are illustrated in Figures 5.11.a-c and 5.12.a-c. These Figures show that overall phase compositions depend on the global composition of the mixtures in dilution lines p, q and r. Figure 5.11.b shows that the calculated composition in the lower phase agrees with that determined experimentally for a mixture with global composition ($\eta=14.7$ vol%, $\phi=2.9$ vol%). In the upper phase, the polymer and the colloidal particle volume fractions are underpredicted and overpredicted respectively. These deviations have compensating effects on the calculation of the speed of sound.



(a)



(b)



(c)

Figure 5.9. Comparison between calculated and experimental speeds of sound for $\gamma=0.63$, after phase separation, along: (a) dilution line p, (b) dilution line q, (c) dilution line r for mixtures of asphaltenes + polystyrene ($M_w=393,400$ g/mol) + toluene. Experimental speeds of sound: (o): lower phase, (Δ): upper phase. Calculated values: (continuous line): lower phase, (dashed line): upper phase. Additional data in (b): computed speed of sound based on experimental phase compositions for a mixture with global composition ($\eta=14.7$ vol%, $\phi=2.9$ vol%): (x) lower phase, (*) upper phase.

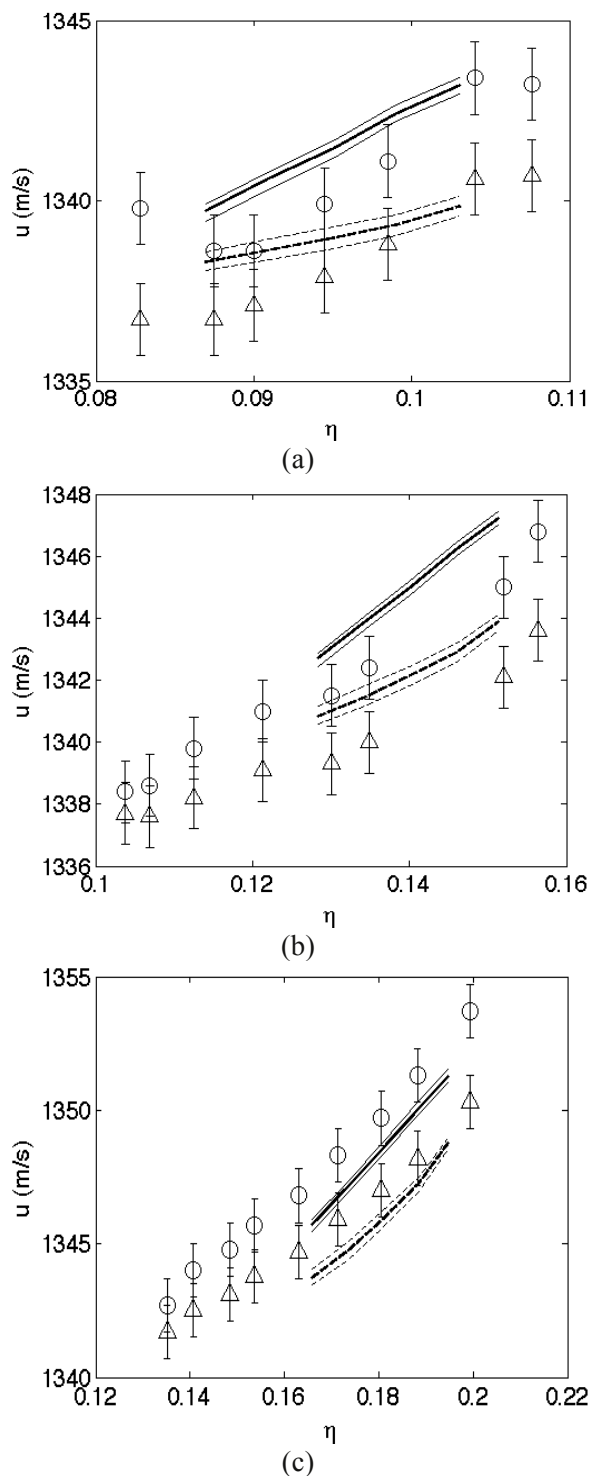
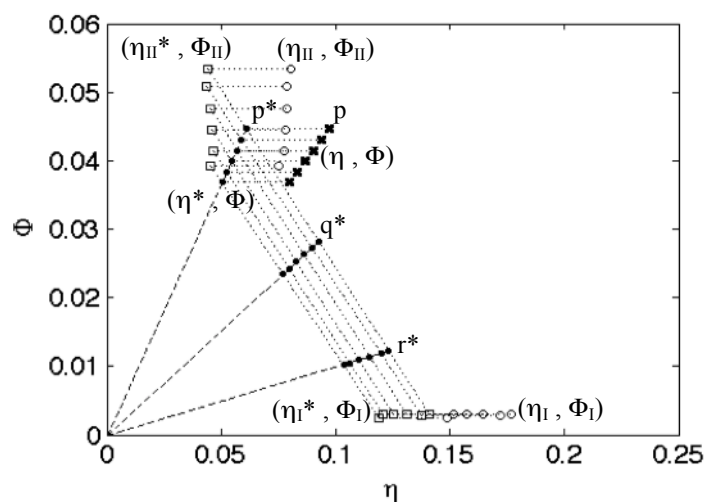
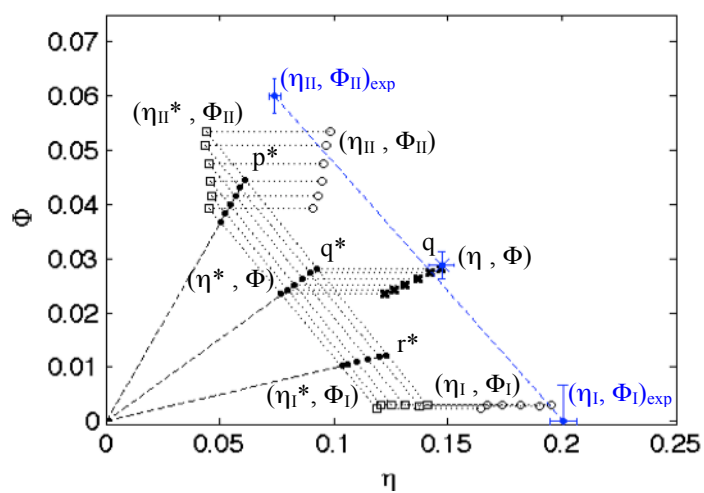


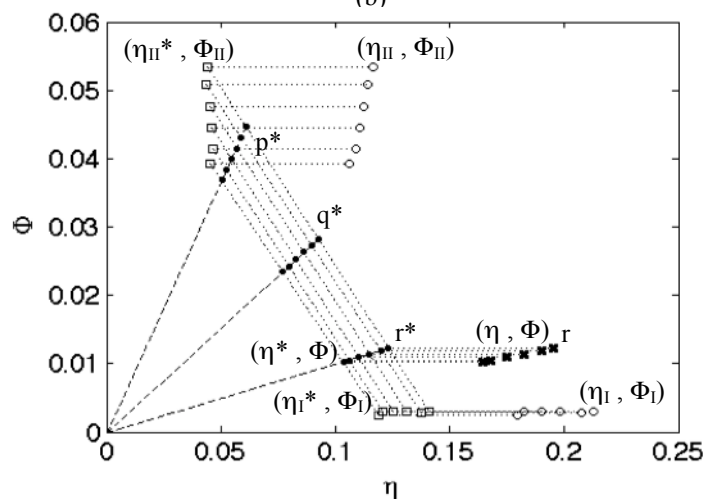
Figure 5.10. Comparison between calculated and experimental speeds of sound for $\gamma=0.49$, after phase separation, along: (a) dilution line p, (b) dilution line q, (c) dilution line r for mixtures of asphaltenes + polystyrene ($M_w=700,000$ g/mol) + toluene. Experimental speeds of sound: (o): lower phase, (Δ): upper phase. Calculated values: (continuous line): lower phase, (dashed line): upper phase.



(a)

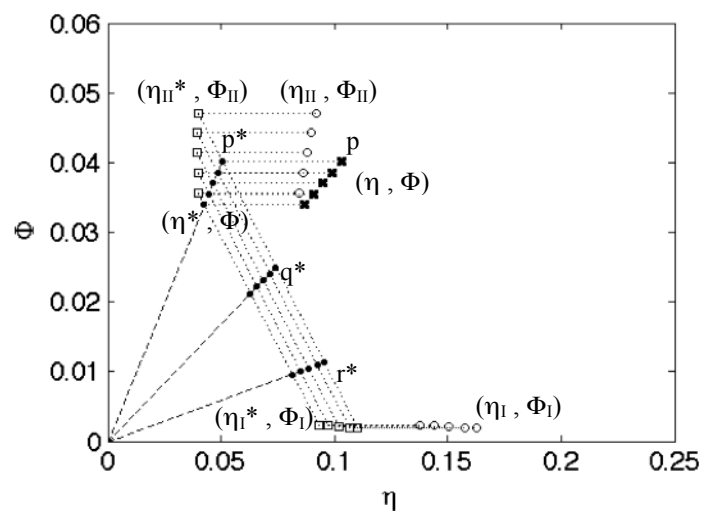


(b)

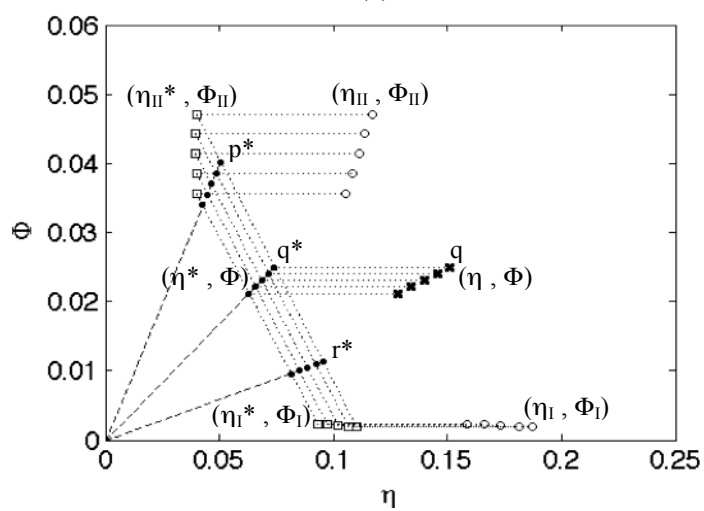


(c)

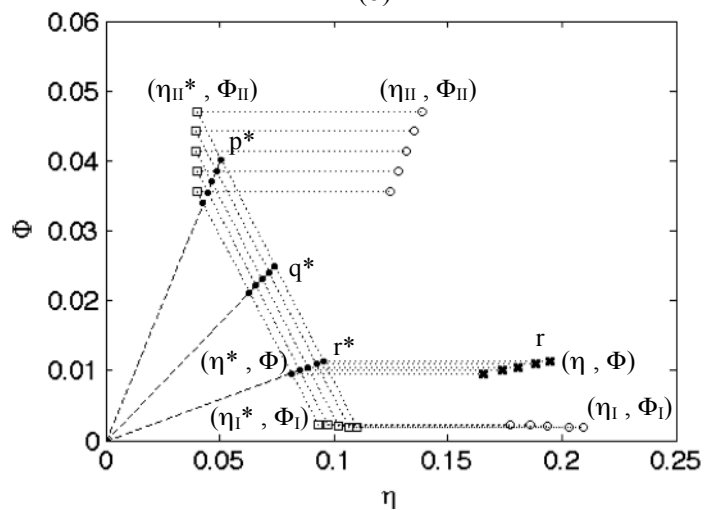
Figure 5.11. Composition of the separated phases in equilibrium (η_I, Φ_I) , (η_{II}, Φ_{II}) for a mixture of asphaltenes + polystyrene ($M_w=393,400$ g/mol) + toluene and $\gamma=0.63$ with global composition (η, Φ) moving along: (a) dilution line p, (b) dilution line q. Dots with error bars represent the composition of the separated phases determined experimentally for a mixture with global composition $(\eta=14.7$ vol%, $\Phi=2.9$ vol%). (c) dilution line r.



(a)



(b)



(c)

Figure 5.12. Composition of the separated phases in equilibrium (η_I, ϕ_I) , (η_{II}, ϕ_{II}) for a mixture of asphaltenes + polystyrene ($M_w=700,000$ g/mol) + toluene and $\gamma=0.49$ with global composition (η, ϕ) moving along: (a) dilution line p, (b) dilution line q, (c) dilution line r.

5.2.3. Comparison between experimental phase boundaries, critical points and the depletion flocculation theory

To compare with depletion flocculation theory, the experimental phase diagrams must be expressed in terms of η^* , the asphaltene fraction participating in the phase separation mechanism. The volume fractions of asphaltene colloidal particles, obtained from experimental phase compositions, are estimated by subtracting the fraction of asphaltene not participating in the phase separation mechanism from measured phase compositions:

$$\eta_{I}^* = \eta_{I \text{ exp}} - (1-\gamma) \eta_{\text{exp}} , \quad (5.10.a)$$

$$\eta_{II}^* = \eta_{II \text{ exp}} - (1-\gamma) \eta_{\text{exp}} , \quad (5.10.b)$$

The volume fraction of asphaltene colloidal particles participating in the phase separation mechanism in the lower and upper phases are respectively larger and lower than those in the original mixture before separation. This suggests that when the calibration curve (Fig. 4.17) – based on colloidal particle scattering effect - is used to estimate the composition of the phases, the concentration of asphaltene in the upper phase is underestimated where that in the lower phase is overestimated. The arrows in Figure 5.13.a indicate the likely directional change in composition of the colloidal binodal points.

Figures 5.13.a-b show modified experimental phase diagrams with phase boundaries and critical points for mixtures of asphaltene + polystyrene + toluene presented on the coordinates (η^* , ϕ). The estimated critical points become ($\eta^{c*}=7.6$ vol%, $\phi^c=1.7$ vol%) and ($\eta^{c*}=5.7$ vol%, $\phi^c=1.2$ vol%) for the mixtures with polystyrene molecular weights of 393,400 g/mol and 700,000 g/mol respectively.

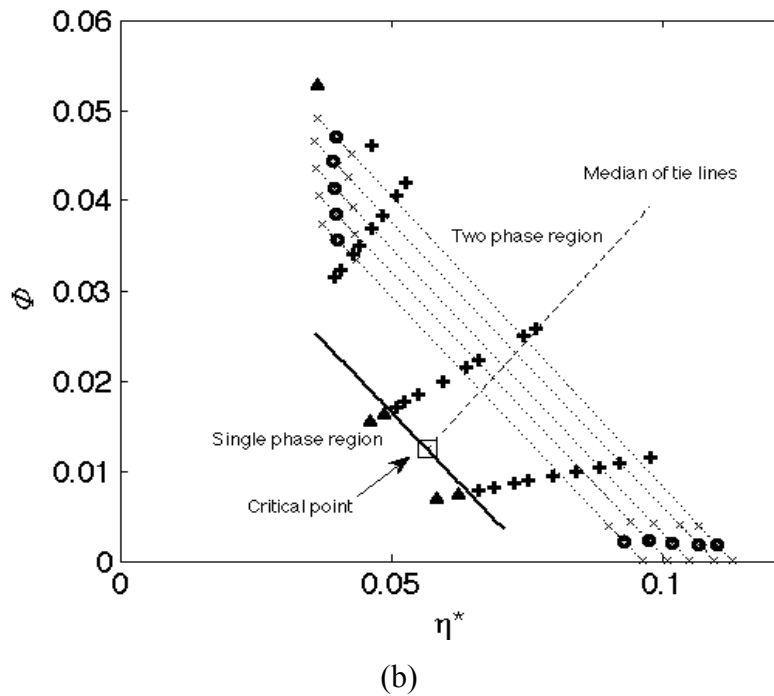
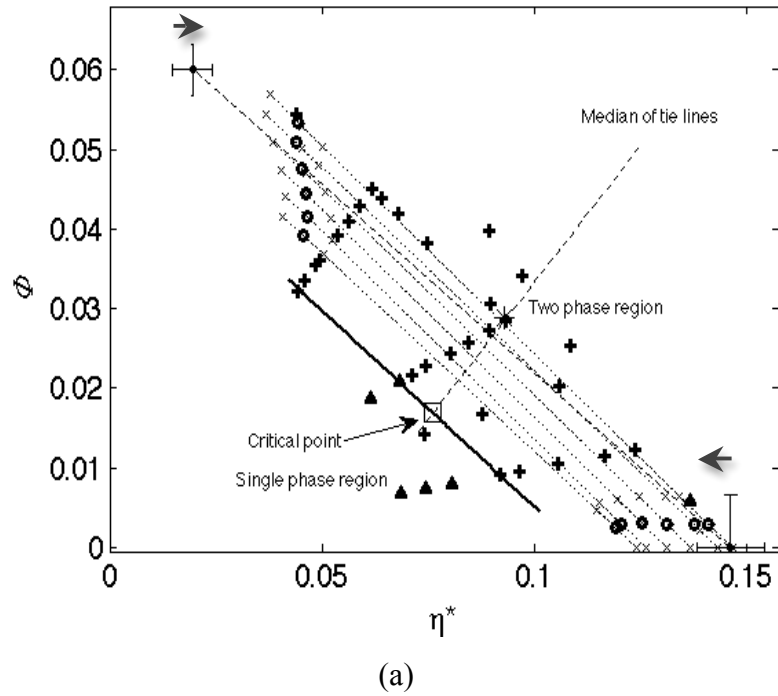


Figure 5.13. Experimental phase diagram for mixtures of asphaltene + polystyrene + toluene presented on the coordinates (η^*, ϕ) : (a) for: $\gamma=0.63$ and a polystyrene molecular weight of 393,400 g/mol (b) for: $\gamma=0.49$ and a polystyrene molecular weight of 700,000 g/mol. Symbols: (+) two-phase, (Δ) single-phase, (square): estimated critical point, (open circle): Calculated binodal points. (dot): with error bars in (a) represents the experimental phase compositions for a mixture with global composition ($\eta=14.7$ vol%, $\phi=2.9$ vol%).

According to the depletion flocculation theory of Fleer et al[5], the volume fraction of the polymer at the critical point ϕ^c increases with decreasing particle size and that of the colloidal particles η^c decreases asymptotically to a constant value $\sim 10 - 11$ vol% for mixtures with polymers in good solvent, and to ~ 6.0 vol% for mixtures with polymers in theta solvent, as shown in Figures 5.14.a-b. Numerical results are tabulated in Table 5.2. Calculations were performed using both versions of the depletion theory: polymers in good solvent (excluded volume chains in good solvent) and polymers in theta solvent (mean field-chains in theta solvent). Fleer et al [5] model for mixtures with polymers in good solvent is valid in the excluded volume (ev) limit. It corresponds to polymers in solvents with an effective Flory-Huggins parameter of $\chi=0$ [12]. Polymers in good solvent with a scaling behavior $R_g \propto M_w^{3/5}$, can be obtained for mixtures with Flory-Huggins parameter χ slightly below 0.5.

Table 5.2. Numerically calculated critical points using Fleer et al. model with two versions: polymers in good solvent (excluded volume chains in good solvent) and polymer in theta solvent (mean-field chains in theta solvent).

	Mixtures of asphaltene + polystyrene ($M_w=393,400$ g/mol) + toluene				Mixtures of asphaltene + polystyrene ($M_w=700,000$ g/mol) + toluene			
	Good solvent (ev)		Theta solvent (mf)		Good solvent (ev)		Theta solvent (mf)	
a (nm)	η^c (vol%)	ϕ^c (vol%)	η^c (vol%)	ϕ^c (vol%)	η^c (vol%)	ϕ^c (vol%)	η^c (vol%)	ϕ^c (vol%)
32.0	20.1	0.3	17.3	0.2	16.0	0.3	13.1	0.2
28.4	18.6	0.4	15.8	0.2	14.8	0.4	11.9	0.2
25.6	17.3	0.5	14.5	0.3	13.8	0.5	10.9	0.3
21.3	15.3	0.6	12.5	0.3	12.3	0.6	9.3	0.3
18.3	13.8	0.7	10.9	0.4	11.2	0.8	8.2	0.4
16.0	12.7	0.9	9.8	0.5	10.5	1.0	7.4	0.4
14.2	11.8	1.1	8.9	0.5	10.1	1.2	6.8	0.5
12.8	11.1	1.3	8.1	0.6	10.0	1.5	6.4	0.6
10.5	10.2	1.8	7.0	0.7	10.2	2.0	6.0	0.7
8.5	10.0	2.6	6.2	1.0	10.8	2.7	6.1	0.9
6.4	10.7	3.9	6.0	1.4	11.3	4.0	6.3	1.2
5.1	11.2	5.4	6.3	1.7	11.5	5.4	6.3	1.5
4.3	11.4	6.8	6.3	2.0	11.7	6.9	6.4	1.8

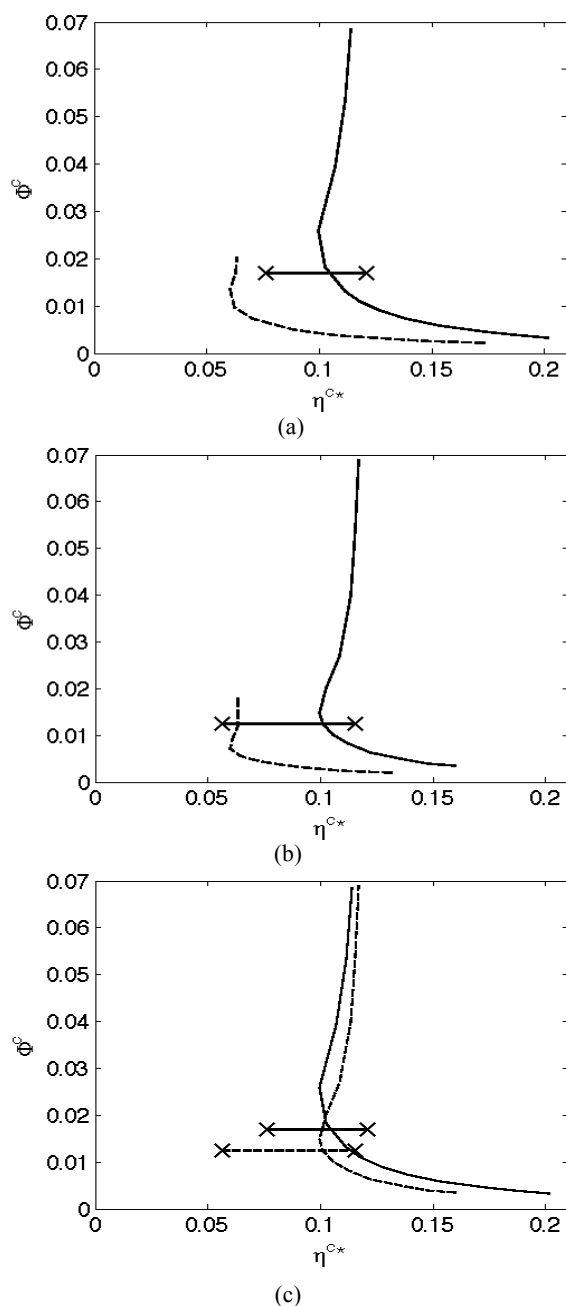


Figure 5.14. Variations of calculated critical points with varying particle radius. Values are given in Table 5.2. Horizontal line segments represent the variations of the experimental critical point with γ from 0.63 to 1.0 for 393,400 g/mol and from 0.49 to 1.0 for 700,000 g/mol. (a) mixtures with a polystyrene molecular weight of 393,400 g/mol: calculations performed for polymers in good solvent (continuous line), in theta solvent (dashed line). (b) mixtures with a polystyrene molecular weight of 700,000 g/mol. : calculations performed for polymers in good solvent (continuous line), in theta solvent (dashed line). (c) comparison between mixtures with polystyrene molecular weight of 393,400 g/mol (continious line), and 700,000 g/mol (dashed line). Calculations were performed for polymers in good solvent

An example of this is polystyrene in toluene where $\chi \approx 0.48$ [12]. In this case, toluene is a good solvent for polystyrene but is only slightly better than a theta solvent. Calculations using both versions of the model would be expected to provide lower and upper limits for the critical points, as suggested by Fleer et al[5].

Direct measurements of volume fraction data place the critical points at ($\eta^c = 12.1$ vol %, $\phi^c = 1.7$ vol%) and ($\eta^c = 11.6$ vol%, $\phi^c = 1.2$ vol%) for polystyrene molecular weights of $M_w = 393,400$ g/mol and $700,000$ g/mol respectively, above the minimum threshold from theory $\approx 10 - 11$ vol% for polymers in good solvent (Figs 5.14.a-c). The modified values, fit on the basis of speed of sound data, ($\eta^{c*} = 7.6$ vol %, $\phi^c = 1.7$ vol%) and ($\eta^{c*} = 5.7$ vol%, $\phi^c = 1.2$ vol%), fall roughly between the critical points predicted for mixtures with good solvent and theta solvent as shown in Figures 5.14.a-b. Figure 5.14.c shows that increasing polymer molecular weight from $393,400$ g/mol to $700,000$ g/mol does not have a significant effect on the predicted critical point, particularly for small colloidal particles ($a < 12.8$ nm).

As both the polystyrene and the asphaltenes are polydispersed, only qualitative comparison with the model of Fleer et al[5] for monodispersed colloidal particles and non-adsorbing polymer is feasible. From Figures 5.14.a-b and Table 5.2, it would appear that the experimental polymer volume fractions at the critical points correspond to those predicted theoretically for monodispersed particles falling in the range (5-14 nm). The upper bound of this range is obtained using the model with polymers in good solvent version (ev) where the lower bound is obtained using the model with polymers in theta solvent version (mf).

Figures 5.15.a-b and Fig. 5.16.a-b show a comparison between the experimental phase diagram presented in the coordinates (η^* , ϕ) and the theory of the depletion flocculation mechanism for mixtures with polymers in good solvent. For polystyrenes with a molecular weight of $M_w = 393,400$ g/mol, it is found that if the

particles have radii smaller than $a_{\min}=6.4$ nm, all mixtures are predicted to be in the single-phase region. For radii smaller than $a_{\max}=23.5$ nm, all mixtures that separated experimentally are predicted to be in the two-phase region. If the colloidal particles have larger radii, mixtures that were found experimentally to exhibit single-phase behavior are predicted to separate. In this manner, lower and upper limits for the radii of asphaltene colloidal particles causing phase separation are obtained ($6.4 < a < 23.5$ nm). For the case of polystyrene with a molecular weight of $M_w=700,000$ g/mol, a similar interval is obtained ($7.0 < a < 26.0$ nm). These intervals are in agreement with the range expected for asphaltenes in concentrated toluene mixtures in the absence of polymer. For example, Barre et al [13] performed Small Angle X-ray Scattering measurements on different liquid fractions separated by ultracentrifugation from a solution of 3 % vol asphaltene in toluene. They found that the radius of gyration of asphaltene fall in the range 6-16 nm [13]. High temperature filtration measurements of Maya crude oil (16 %w asphaltene) [14] have shown that 50 wt % of the asphaltenes passed through the 20 nm filter with none of the aggregates being greater than 100 nm.

5.3. Conclusion

The compositions of the liquid phases for mixtures of asphaltene + polystyrene + toluene were estimated by using the volume fraction of the upper phase along three dilution lines, experimental speed of sound data and a mass balance model.

The volume fractions of asphaltene in the lower and upper phases were overpredicted and underpredicted, respectively, when compared to experimental values for a mixture with a specific composition ($\eta=14.7$ vol%, $\phi=2.9$ vol%). The volume fraction of polystyrene in the upper phase was underpredicted.

Large deviations were obtained when speeds of sound in the phases were calculated using estimated binodal points. However, calculated speeds of sound with phase compositions measured experimentally showed that variations of

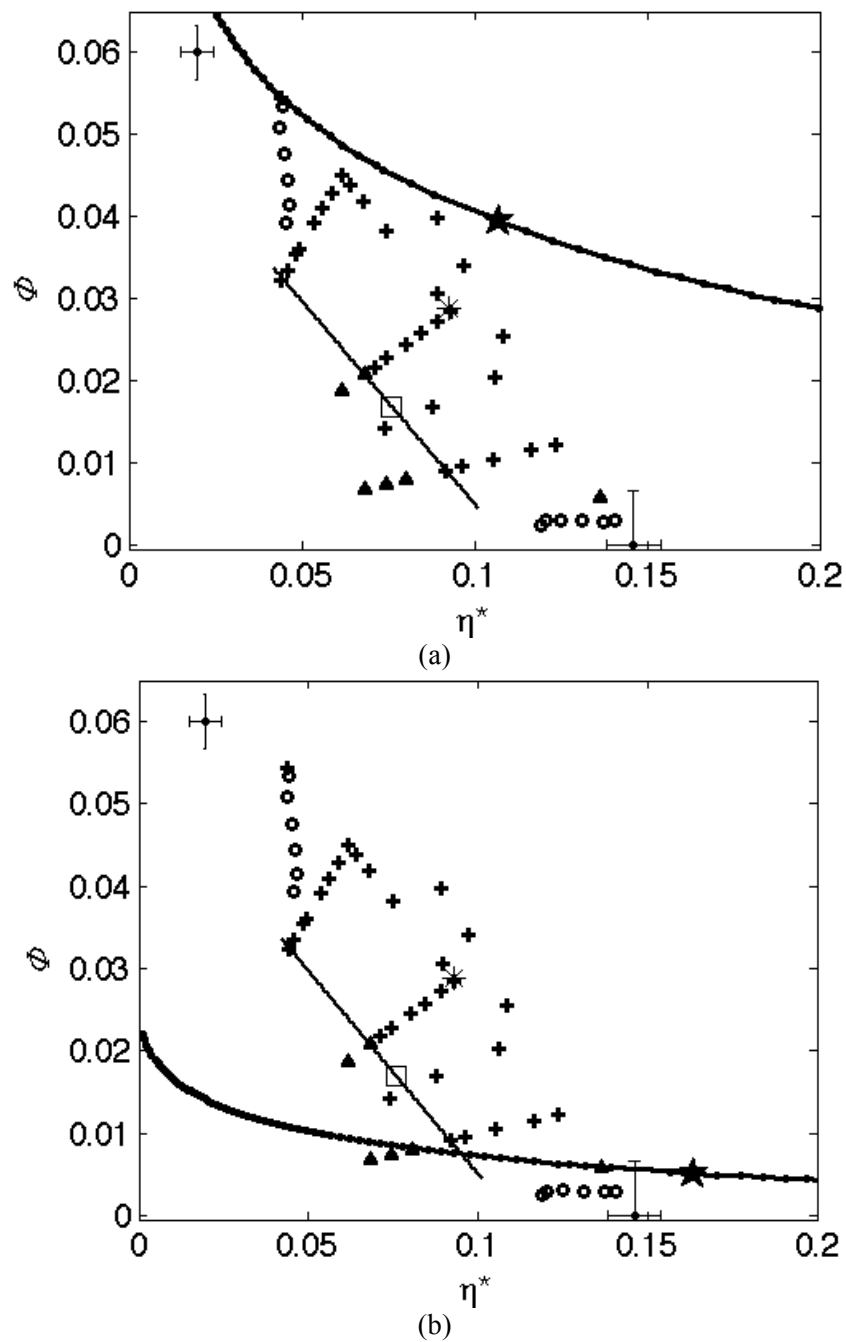


Figure 5.15. Calculated phase diagram vs experimental phase diagram for mixtures of asphaltene colloidal particles + polystyrene ($M_w=393,400$ g/mol) + toluene and for two radii of asphaltene nanoparticles: (a) $a=6.4$ nm, (b) $a=23.5$ nm. (star): calculated critical point. (cross): experimental two phase behavior. (triangle): single phase behavior. Calculations were performed for polymers in good solvent. (circle): binodal points calculated from experimental data. (square): experimental critical point.

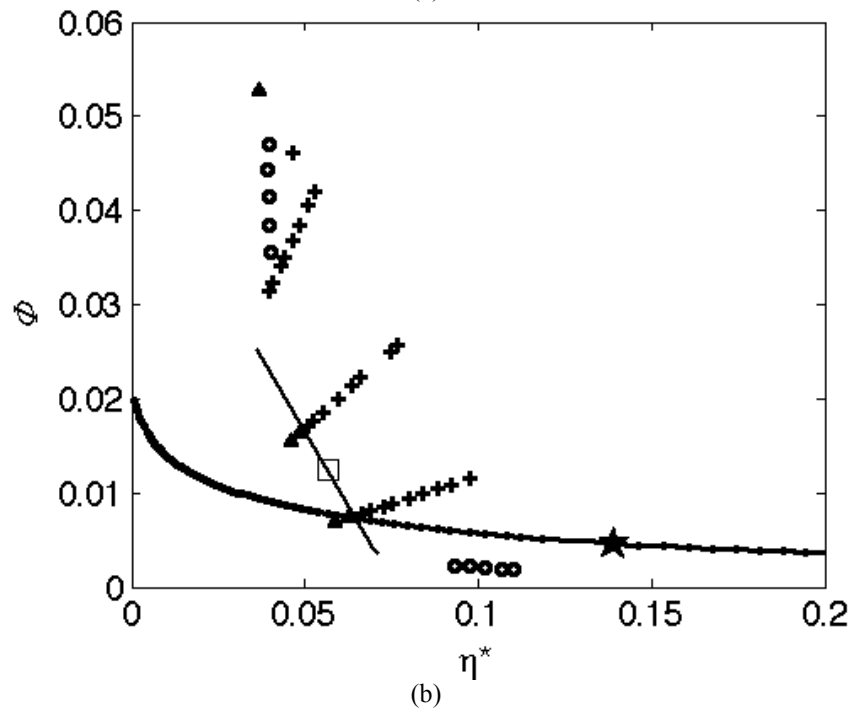
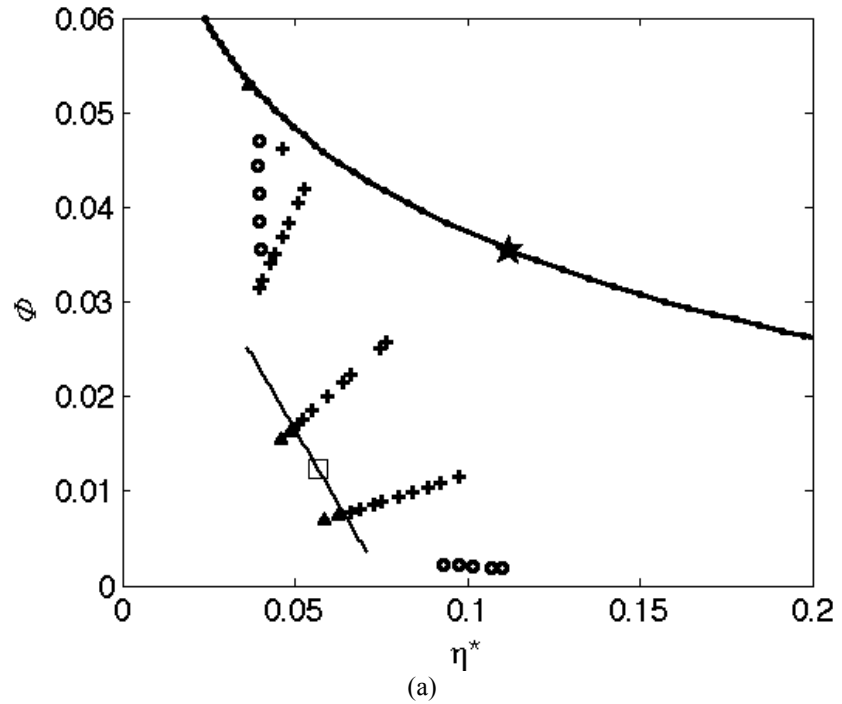


Figure 5.16. Calculated phase diagram vs experimental phase diagram for mixtures of asphaltenes colloidal particles + polystyrene ($M_w=700,000$ g/mol) + toluene and for two radii of asphaltene colloidal particles: (a) $a=7.0$ nm, (b) $a=26.0$ nm. (star): calculated critical point. Calculations were performed for polymers in good solvent. (cross): experimental two phase behavior. (triangle): single phase behavior. (circle): binodal points calculated from experimental data. (square): experimental critical point.

asphaltene and polystyrene volume fractions in the measurement error range can cause large deviations between calculated and experimental values. A parameter γ , interpreted as the fraction of asphaltene colloidal particles causing phase separation, was introduced to improve the agreement between experimental and calculated speeds of sound. The volume fractions of polystyrene in the upper and lower phases were not modified. The best agreement was obtained when the parameter γ was decreased from 1.0 to 0.63 for the case of $M_w=393,400$ g/mol and from 1.0 to 0.49 for the case of $M_w=700,000$ g/mol. Calculated phase compositions were compared with experimental results for a mixture with a specific global composition ($\eta=14.7$ vol%, $\phi=2.9$ vol%). It was found that in the upper phase, the volume fractions of polystyrene and asphaltene were underpredicted and overpredicted respectively. In the lower phase, an agreement within 0.5 vol% was obtained between calculated and experimental asphaltene and polystyrene volume fractions.

Experimental phase diagrams were compared with model predictions for phase boundaries for mixtures of monodispersed colloidal particles + non-adsorbing polymer. It was estimated that the radii of asphaltene colloidal particles causing phase separation fall in the range $6 < a < 26$ nm.

References

1. Bolhuis, P., Meijer, E., & Louis, A. (2003) Colloid-polymer mixtures in the protein limit. *Physical Review Letters* 90.
2. Pelissetto, A. & Hansen, J.-P. (2006) An effective two-component description of colloid-polymer phase separation. *Macromolecules* 39, 9571-9580.
3. Fuchs, M. & Schweizer, K. (2002) Structure of colloid-polymer suspensions. *Journal of Physics-Condensed Matter* 14, R239-R269.
4. Schmidt, M. & Fuchs, M. (2002) Penetrability in model colloid-polymer mixtures. *Journal of Chemical Physics* 117, 6308-6312.
5. Fler, G. J. & Tuinier, R. (2008) Analytical phase diagrams for colloids and non-adsorbing polymer. *Advances in Colloid and Interface Science* 143, 1-47.
6. Lekkerkerker, H. N. W., Poon, W. C. K., Pusey, P. N., A., S., & Warren, P. B. (1992) Phase Behavior of Colloid Plus Polymer Mixtures. *Europhysics Letters* 20, 559-564.

7. Annunziata, O., Ogun, O., & Benedek, G. (2003) Observation of liquid-liquid phase separation for eye lens gamma S-crystallin. *Proceedings of the National Academy of Sciences of the United States of America* 100, 970-974.
8. Bodnar, I. & Oosterbaan, W. (1997) Indirect determination of the composition of the coexisting phases in a demixed colloid polymer mixture. *Journal of Chemical Physics* 106, 7777-7780.
9. Erne, B., van der Maas, J., Kuipers, B., Visser, T., & Philipse, A. (2003) Vertical concentration profiles in colloidal fluids measured by FTIR-ATR spectroscopy. *Langmuir* 19, 3081-3083.
10. Hennequin, Y., Evens, M., Angulo, C., & van Duijneveldt, J. (2005) Miscibility of small colloidal spheres with large polymers in good solvent. *Journal of Chemical Physics* 123.
11. Savaroglu, G., Tasagal, D., & Aral, E. (2007) Excess molar isentropic compressibilities, excess molar volumes, and excess sound speeds of the 1-propanol plus diethyl ether plus 1-octanol ternary mixture and constituent binary mixtures at 298.15 K. *International Journal of Thermophysics* 28, 245-258.
12. Zhang, Z. & van Duijneveldt, J. (2006) Experimental phase diagram of a model colloid-polymer mixture in the protein limit. *Langmuir* 22, 63-66.
13. Barre, L., Simon, S., & Palermo, T. (2008) Solution properties of asphaltenes. *langmuir* 24, 3709-3717.
14. Zhao, B. & Shaw, J. M. (2007) Composition and size distribution of coherent nanostructures in Athabasca bitumen and Maya crude oil. *Energy & Fuels* 21, 2795-2804.

CHAPTER 6. Conclusions and Recommendations

6.1. Phased array acoustic cell

In this work, a cell was designed and constructed for online measurement of acoustic speed and attenuation profiles in opaque materials. The cell was operated in both pulse-echo and transmission modes. The pulse-echo mode was used to measure speed of sound and attenuation profiles in liquid mixtures where the transmission mode was used to measure the travel time profiles in porous media. The kinetics of phase separation were measured in mixtures of methanol + mixed hexanes. Phase separation was complete when the speed of sound profile split into two parallel lines. Each profile line corresponded to the speed of sound in one phase. The elevation of the interface was identified as a discontinuity in the profiles.

The elevation of the liquid-liquid interface was measured independently using spikes in the attenuation profiles caused by a significant loss in the acoustic energy at the liquid-liquid interface. This independent measurement was useful in cases where the speed of sound difference between the two phases approached the experimental error. Liquid-liquid equilibria can be detected even if the difference between the properties of the phases is small.

Acoustic transmission measurements were performed in a porous structure partially saturated with heptane and bitumen. It was found that the acoustic waves travel faster in the bitumen saturated regions than in the heptane saturated region. As heptane diffused in the bitumen saturated region, the profile of the travel time increased in the regions initially saturated with bitumen. This demonstrated that the experimental technique developed in this work may be used for the

measurement of diffusion in porous media. It can therefore present an alternative to other experimental techniques [1][2][3] or provide a technique where others are not applicable.

The acoustic cell designed and constructed in this work may be applied to investigate the phase behaviour of challenging opaque mixtures, from water in oil emulsions[4][5] and colloidal particles + non-adsorbing polymer mixtures[6] to natural gas hydrates.

6.2. Measurements of phase behaviour of mixtures of asphaltene + polystyrene + toluene

Speed of sound and attenuation profile measurements were performed in mixtures of asphaltene + polystyrene + toluene. Liquid-liquid phase behaviour was observed over broad ranges of composition. Phase separation was complete within 30-90 minutes. This time range is in agreement with the time reported for the phase separation of colloidal particles + non-adsorbing polymer mixtures [7] [8]. Acoustic phase separation measurements were found to be qualitatively similar to those of mixtures of methanol + hexanes.

The variation of phase volumes along dilution lines revealed the presence of critical points. It was proposed that the key mechanism causing phase separation is depletion flocculation where asphaltenes in toluene are colloidal particles sterically stabilized and polystyrene is the non-adsorbing polymer.

At fixed polymer molecular weight and volume fraction, the phase behavior of mixtures of colloidal particles + non-adsorbing polymer + toluene depends on the size and the volume fraction of the colloidal particles. Experimental variation of the upper phase volume fraction along the dilution lines were used to calculate phase compositions using an algorithm based on the lever rule, these compositions were then used to estimate the speeds of sound in the separated

phases. A fraction γ of asphaltene colloidal particles participating in the phase separation was introduced to improve the agreement between calculated and measured speeds of sound in the phases. It was estimated that $\sim 0.5 - 0.6$ of asphaltenes were participating in the phase separation by the mechanism of depletion flocculation.

For a mixture with global composition $\eta=14.7$ vol% and $\phi=2.9$ vol%, the compositions of the separated phases determined with UV-Visible spectrophotometry were compared with calculated values. It was found that when all asphaltene colloidal particles were assumed to participate in the phase separation mechanism, the volume fraction of asphaltenes were overpredicted and underpredicted in the lower and upper phases, respectively. The volume fraction of polystyrene in the upper phase was underestimated. When only a fraction 0.63 of asphaltenes was assumed to participate in the phase separation mechanism, the calculated composition in the lower phase agreed with experimental data. In the upper phase, the volume fraction of polystyrene and asphaltene were underestimated and overestimated respectively. The fraction $\gamma=0.63$ was obtained by fitting speed of sound data with an underestimated polymer volume fraction in the upper phase. This has caused an overestimation of the asphaltene volume fraction in the upper phase to improve the agreement with speed of sound per phase and speed of sound difference between the phases.

An interval for the radii of asphaltene colloidal particles was estimated by comparing the experimental phase diagrams with the phase boundaries predicted by Fler et al model [9]. It was estimated that the radii of asphaltene colloidal particles, participating in the phase separation, fall in the range 6 - 26 nm. This interval is in agreement with the range obtained from nanofiltration results for Maya heavy oil asphaltenes [10] and SAXS measurements in a solution of asphaltene in toluene 3 vol% [11].

6.3. Future work and recommendations

- In mixtures of colloidal particles + non-adsorbing polymers, the colloid volume fraction difference between the separated phases can be increased by increasing the concentration of the polymer. Another way to improve the separation is to increase the colloidal particle size. For mixtures of asphaltenes + polystyrene + toluene, this can be achieved by controlling asphaltene particle size in the solution. For example, by injecting colloidal particles (or water in oil emulsion) in the solution such that asphaltenes sorb to their surface. The size of the colloidal particles would be the size of the particles injected and the steric-repulsive forces between their asphaltene-covered surfaces would dominate the interaction forces. In this way, phase separation between asphaltene rich and asphaltene poor phases could be improved by controlling particle size without increasing polymer concentration.

- The effect of polydispersity of the colloidal dispersion on the phase separation by depletion flocculation was not included in this work [9]. This could be part of a future investigation.

- The comparison between calculated phase compositions and compositions obtained from UV-Visible spectrophotometry measurements can be extended to a wide range of global compositions for mixtures of asphaltene + polystyrene + toluene.

- The acoustic cell could be used in other applications for the investigation of opaque materials. Future work consists of finding new applications. Examples of future investigations would be: measurements of hydrate formation in porous media, solvent diffusion in bitumen saturated porous media, and phase behavior of colloidal dispersions in opaque mixtures.

- The acoustic cell permits simultaneous measurements of acoustic waveforms at different elevations along the height of the cell. These measurements could be used to obtain acoustic mappings of opaque materials (liquid or solid) [12]. A computer code for the deconvolution of measured waveforms and the calculation of the mapped acoustic properties needs to be developed.

References

1. Afsahi, L. & Kantzas, A. (2007) Advances in diffusivity measurement of solvents in oil sands. *Journal of Canadian Petroleum Technology* 46, 56-61.
2. K. Karmaker, B. B. M. (2003) A Stochastic Approach to Extract Vapex Related Dispersion Coefficients from Magnetic Resonance Images.. *SPE Annual Technical Conference and Exhibition, Denver, Colorado, 2003: p. SPE 84198*.
3. D.B. Fisher, A.K.S., S. K. D. J. G. C. J. (2000) Use of Magnetic Resonance Imaging and Advanced Image Analysis as a Tool to Extract Mass Transfer Information from a 2D Physical Model of The Vapex Process. *SPE/DOE Improved Oil Recovery Symposium, Tulsa, Oklahoma, 2000: p. SPE 59330*.
4. Silset, A., Hannisdal, A., Hemmingsen, P. V., & Sjoblom, J. (2010) Emulsions of Heavy Crude Oils. II. Viscous Responses and Their Influence on Emulsion Stability Measurements. *Journal of Dispersion Science and Technology* 31, 1432-1445.
5. Mutch, K. J., van Duijneveldt, J. S., Eastoe, J., Grillo, I., & Heenan, R. K. (2009) Testing the Scaling Behavior of Microemulsion-Polymer Mixtures. *Langmuir* 25, 3944-3952.
6. Erne, B., van der Maas, J., Kuipers, B., Visser, T., & Philipse, A. (2003) Vertical concentration profiles in colloidal fluids measured by FTIR-ATR spectroscopy. *Langmuir* 19, 3081-3083.
7. Hennequin, Y., Evens, M., Angulo, C., & van Duijneveldt, J. (2005) Miscibility of small colloidal spheres with large polymers in good solvent. *Journal of Chemical Physics* 123.
8. Aarts, D. & Lekkerkerker, H. (2004) Confocal scanning laser microscopy on fluid-fluid demixing colloid-polymer mixtures. *Journal of Physics-Condensed Matter* 16, S4231-S4242.
9. Fler, G. J. & Tuinier, R. (2008) Analytical phase diagrams for colloids and non-adsorbing polymer. *Advances in Colloid and Interface Science* 143, 1-47.
10. Zhao, B. & Shaw, J. M. (2007) Composition and size distribution of coherent nanostructures in Athabasca bitumen and Maya crude oil. *Energy & Fuels* 21, 2795-2804.
11. Barre, L., Simon, S., & Palermo, T. (2008) Solution properties of asphaltenes. *langmuir* 24, 3709-3717.
12. Shi, J.-Q., Xue, Z., & Durucan, S. (2007) Seismic monitoring and modelling of supercritical CO₂ injection into a water-saturated sandstone:

Interpretation of P-wave velocity data. *International Journal of Greenhouse Control* 1, 473-480.

Appendix A. Acoustic Measurements of Mixtures of Asphaltene + Polystyrene + Toluene

A.1. Measurements of mixtures of asphaltene + polystyrene ($M_w=393,400$ g/mol) + toluene (Figures for data in Table 4.4):

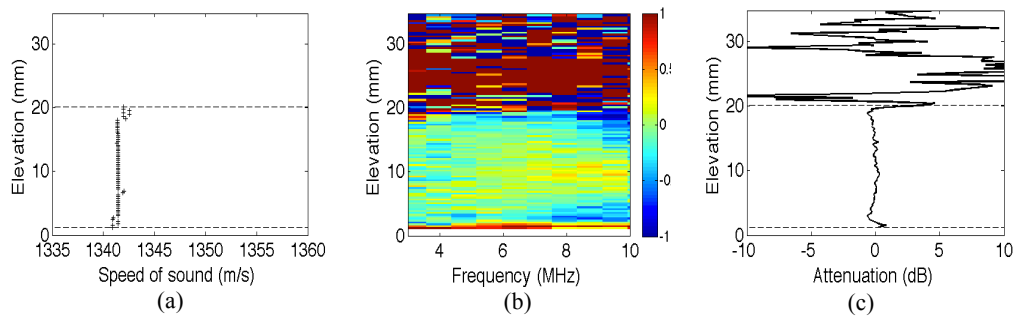
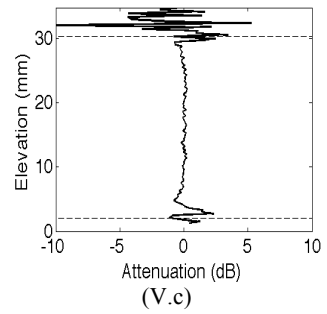
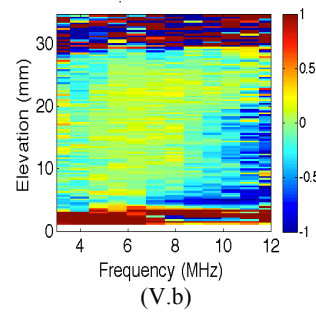
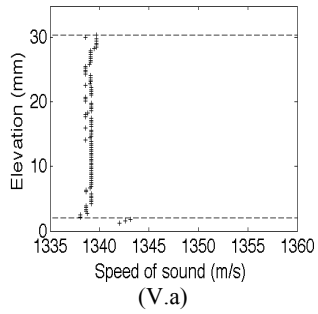
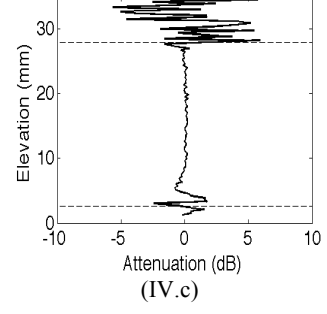
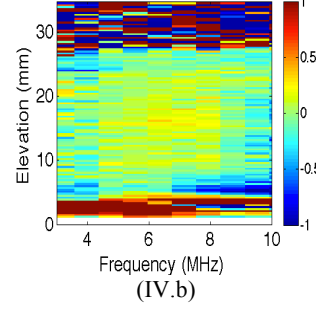
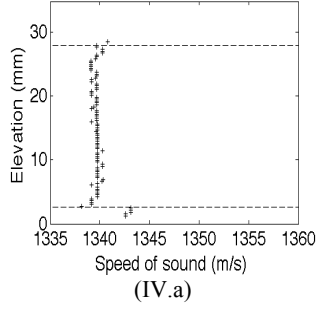
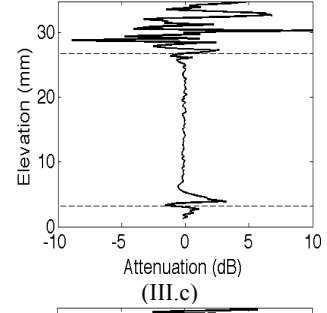
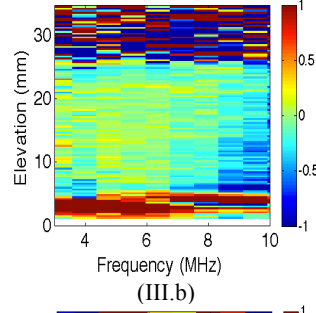
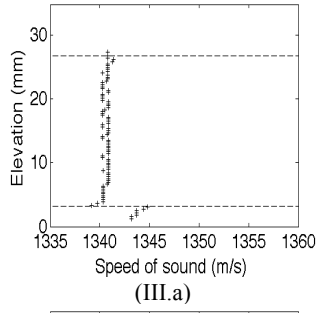
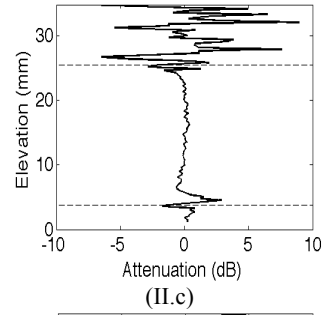
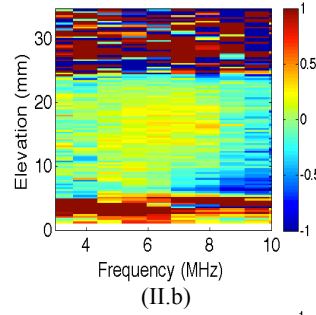
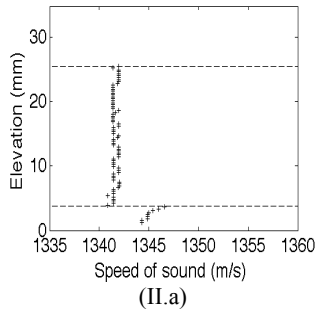
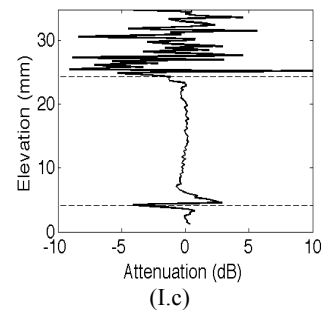
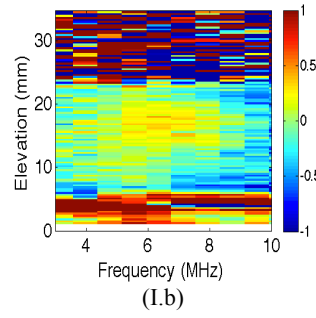
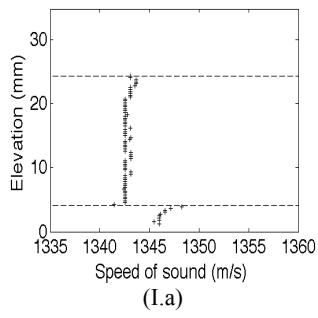


Figure A.1. (a) Speed of sound profile, (b) attenuation spectra profile, (c) attenuation at $f=7.9$ MHz for mixture P_1 in Table 4.4.



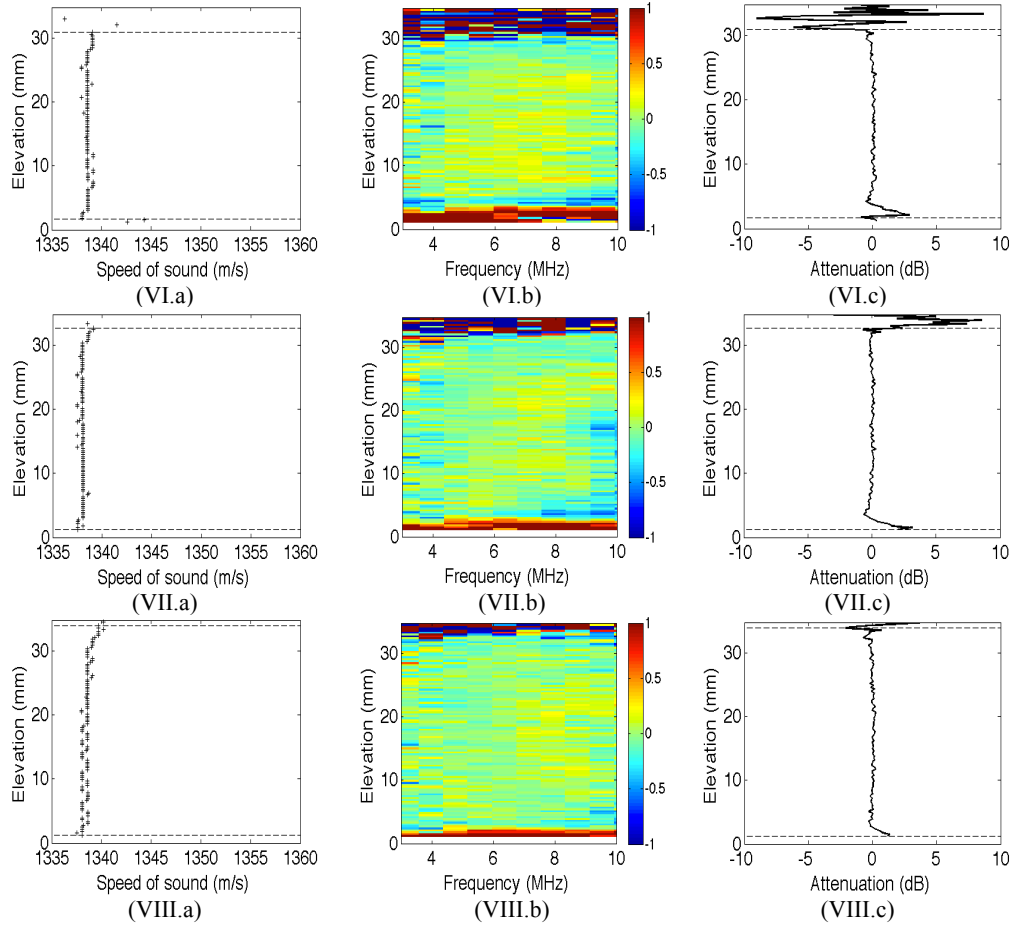


Figure A.2.1. (a) Speed of sound profile, (b) attenuation spectra profile, (c) attenuation at $f=7.9$ MHz for mixtures along dilution line p. Roman symbols refer to mixture numbers in Table 4.4.

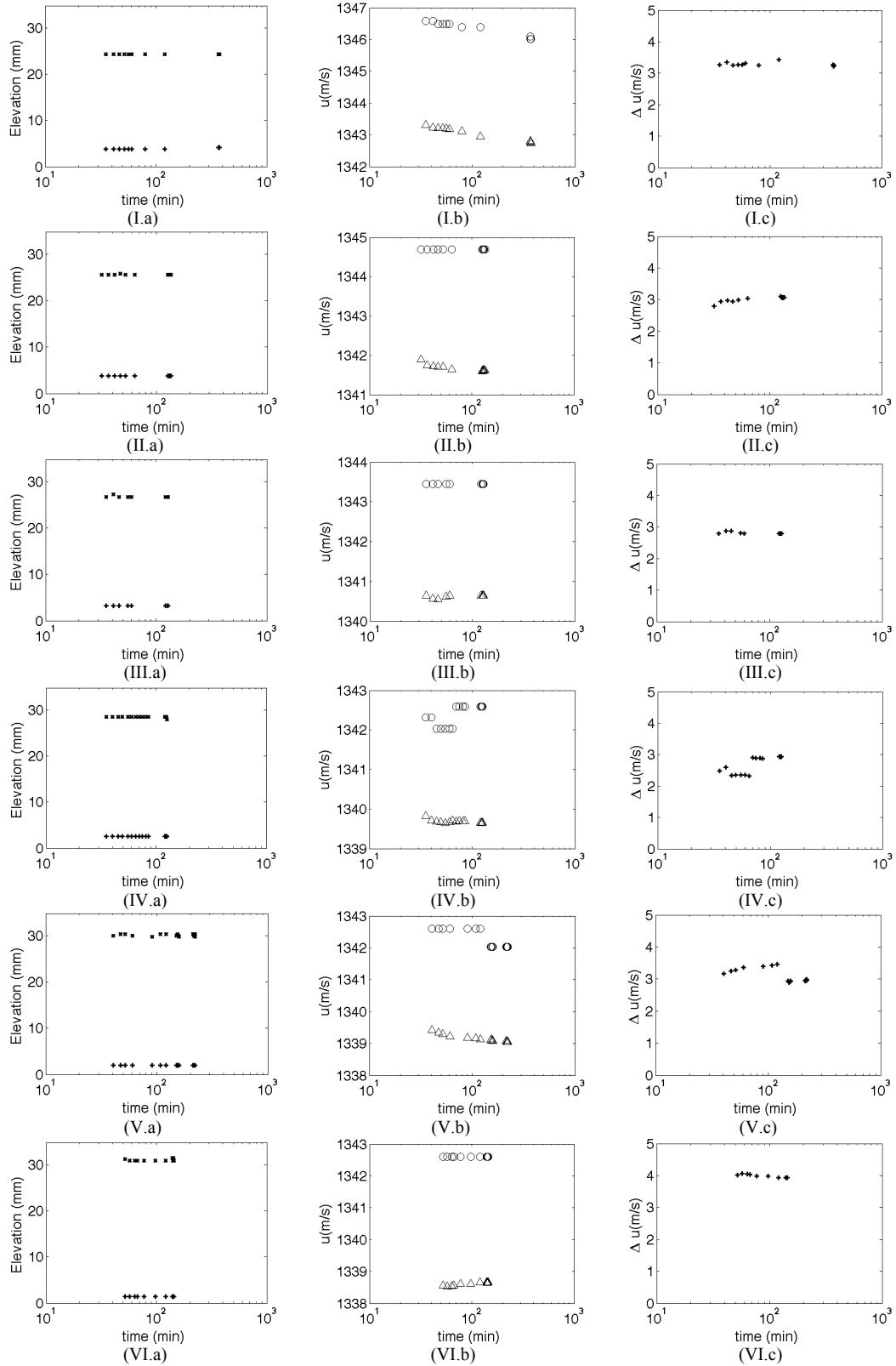
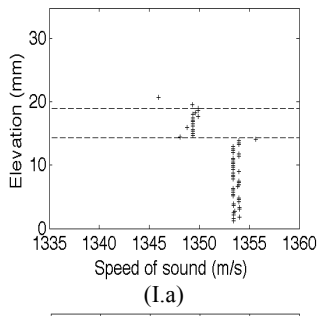
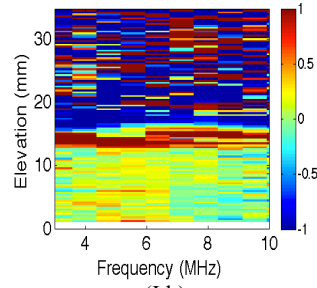


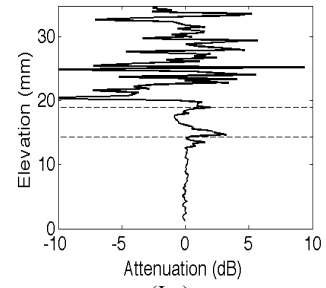
Figure A.2.2. (a) Variations of the liquid-liquid and liquid-air interfaces, (b) Speeds of sound in the separated phases: (triangle): upper phase, (circle): lower phase, (c) Speed of sound difference between the separated phases, for dilution line p. Roman symbols refer to mixture numbers in Table 4.4.



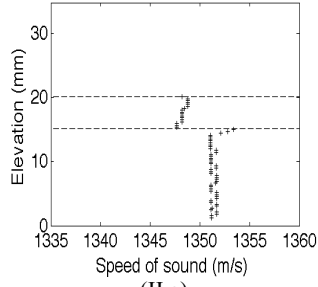
(I.a)



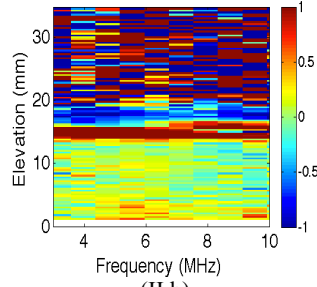
(I.b)



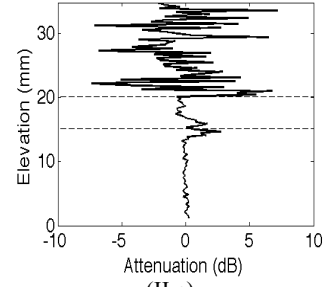
(I.c)



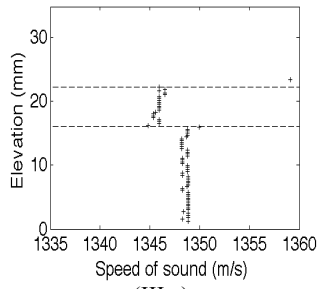
(II.a)



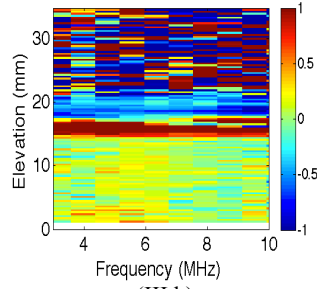
(II.b)



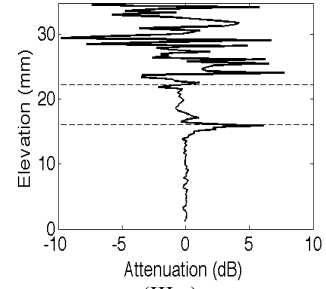
(II.c)



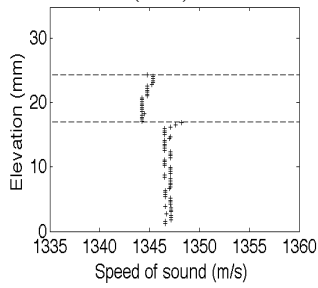
(III.a)



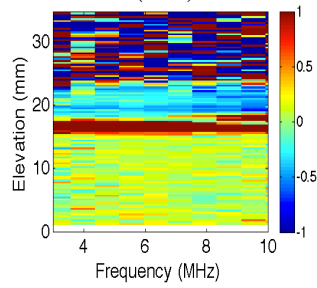
(III.b)



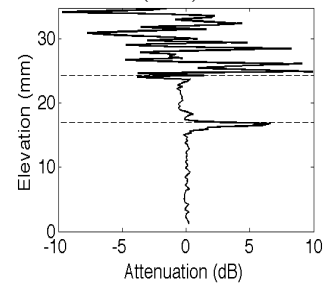
(III.c)



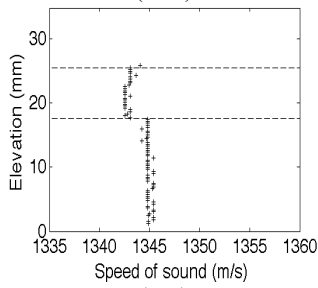
(IV.a)



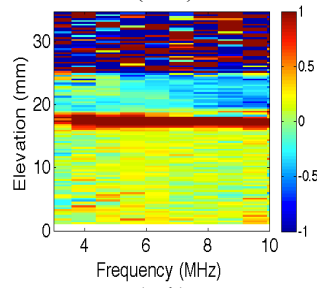
(IV.b)



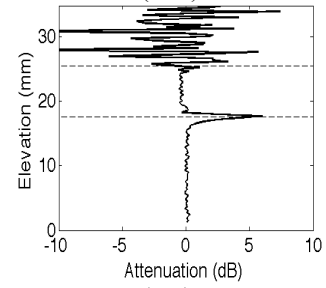
(IV.c)



(V.a)



(V.b)



(V.c)

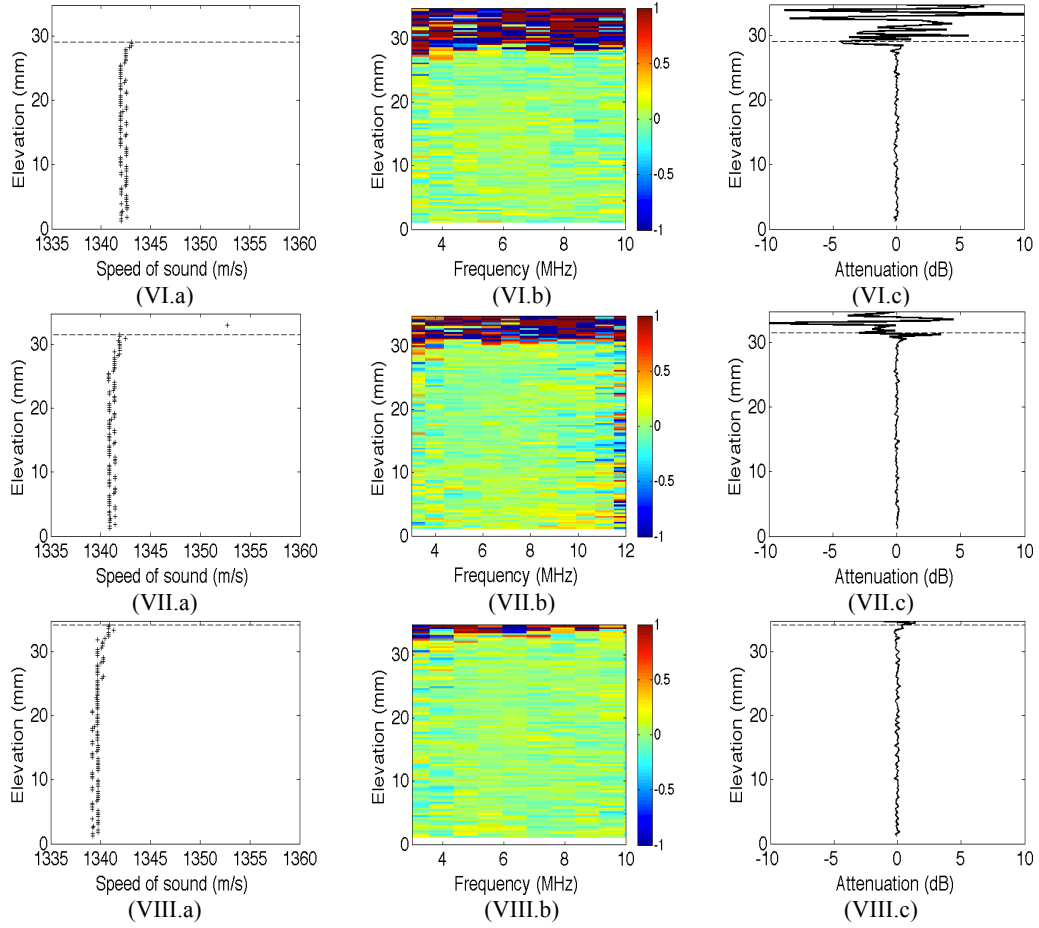


Figure A.3.1. (a) Speed of sound profile, (b) attenuation spectra profile, (c) attenuation at $f=7.9$ MHz for mixtures along dilution line r. Roman symbols refer to mixture numbers in Table 4.4.

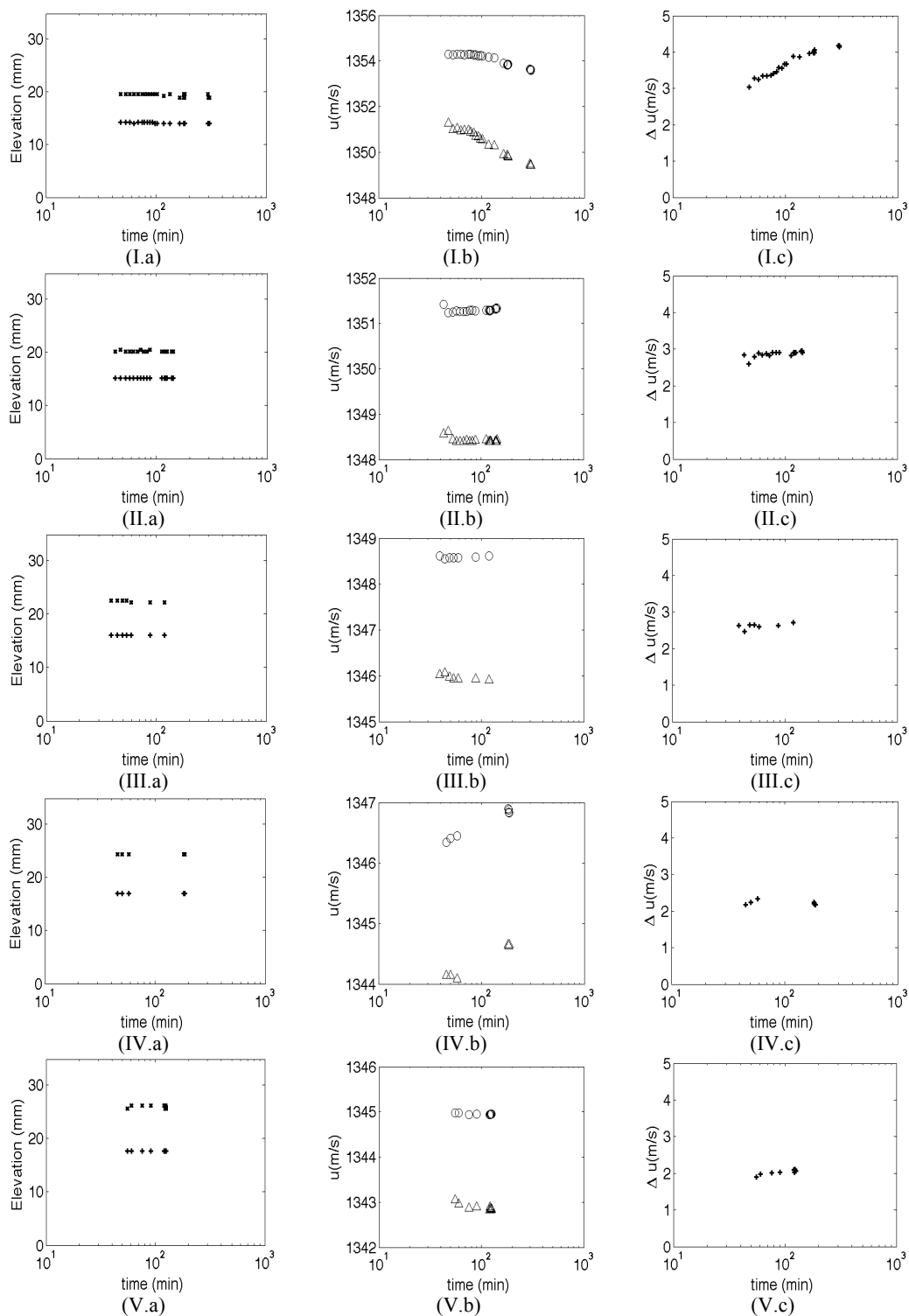
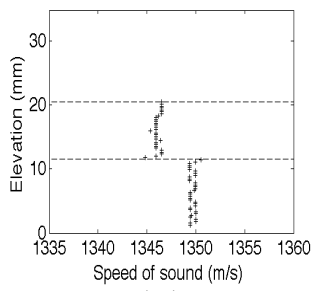
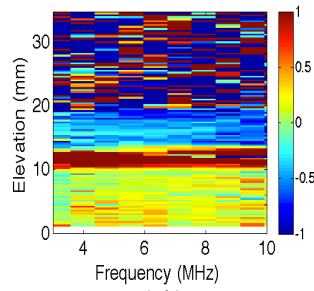


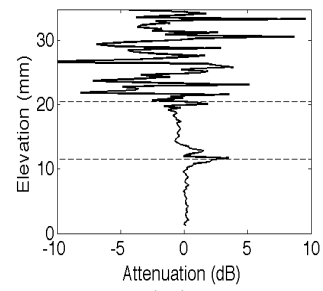
Figure A.3.2. (a) Variations of the liquid-liquid and liquid-air interfaces, (b) Speeds of sound in the separated phases: (triangle): upper phase, (circle): lower phase, (c) Speed of sound difference between the separated phases, for dilution line r. Roman symbols refer to mixture numbers in Table 4.4.



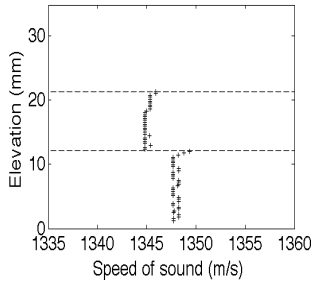
(I.a)



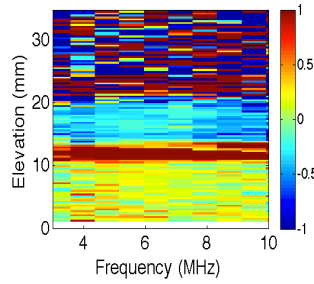
(I.b)



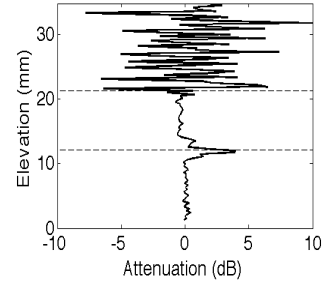
(I.c)



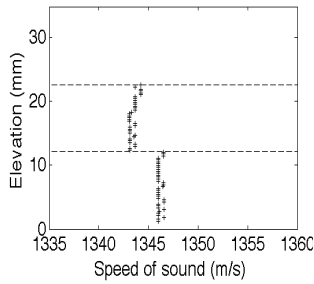
(II.a)



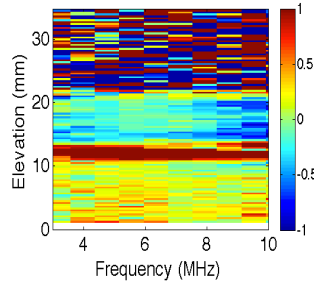
(II.b)



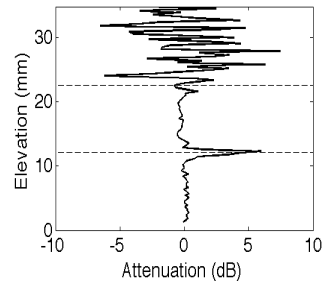
(II.c)



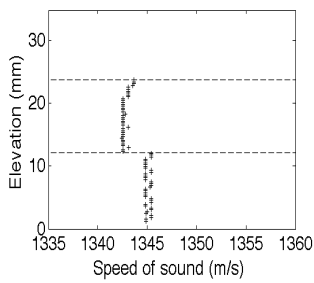
(III.a)



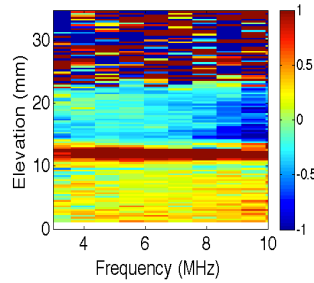
(III.b)



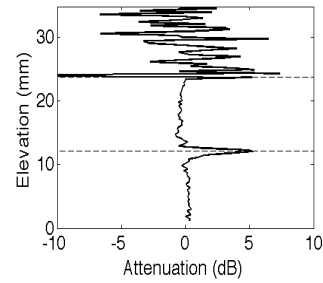
(III.c)



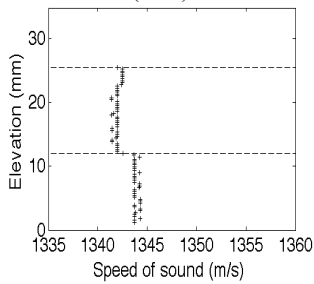
(IV.a)



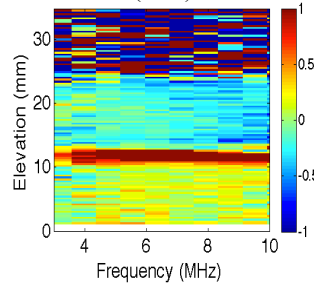
(IV.b)



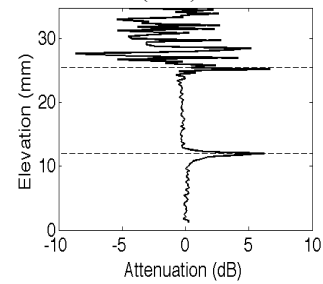
(IV.c)



(V.a)



(V.b)



(V.c)

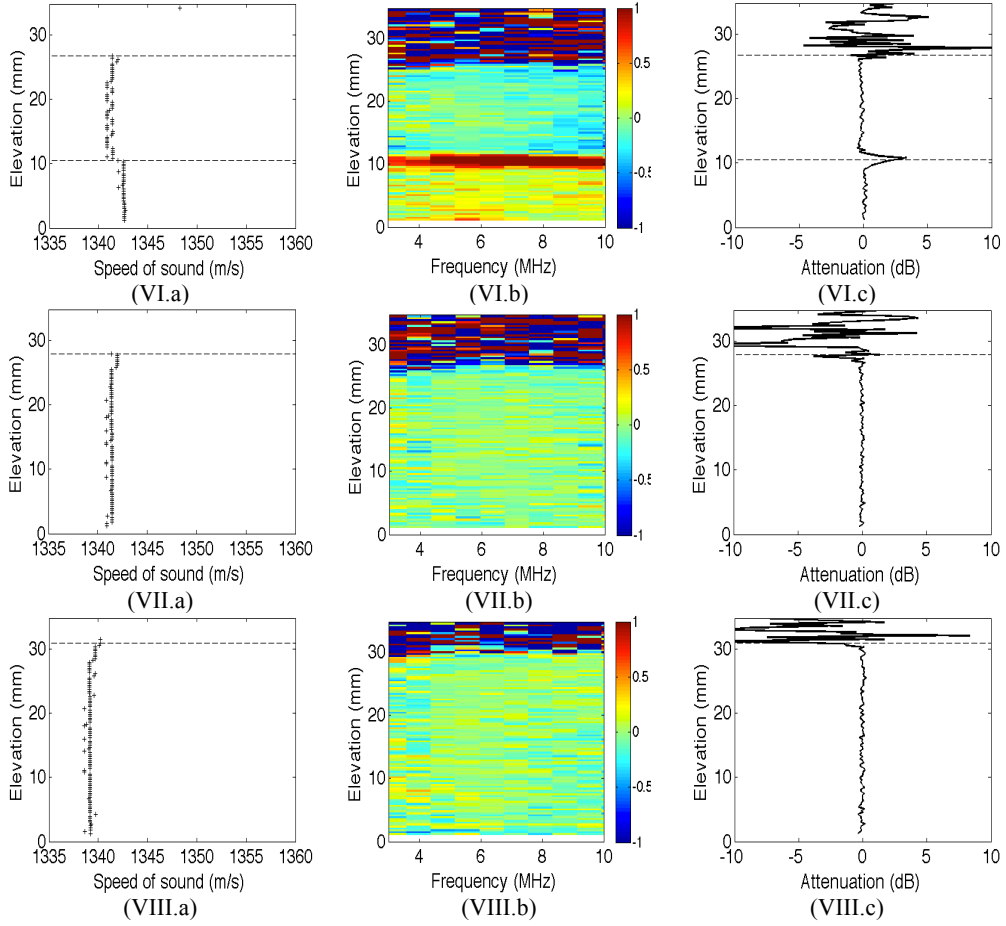
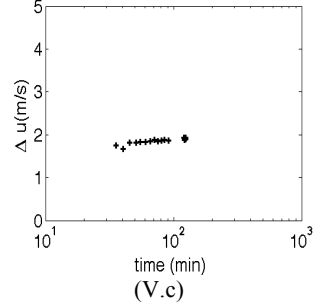
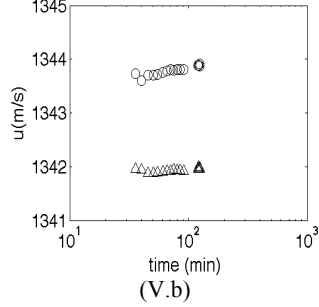
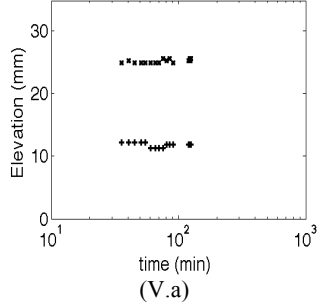
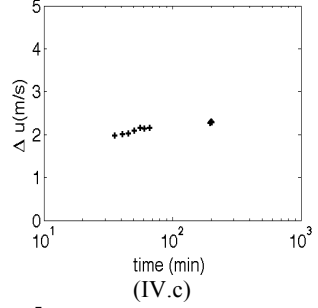
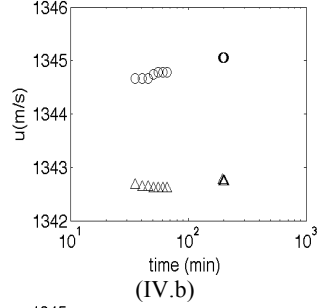
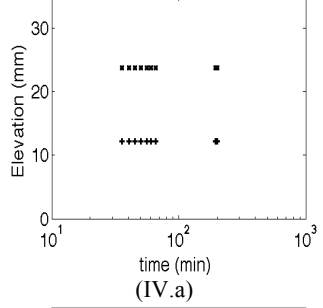
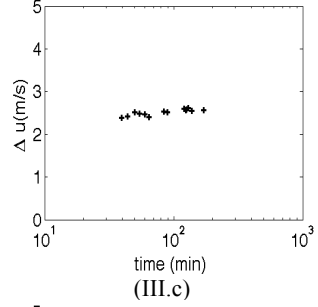
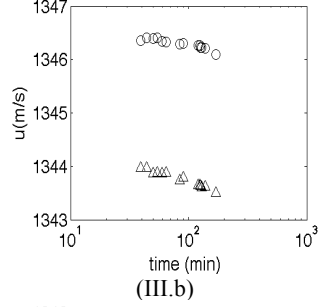
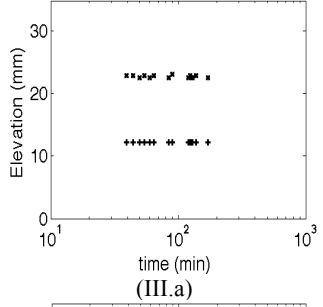
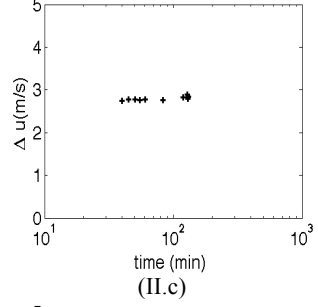
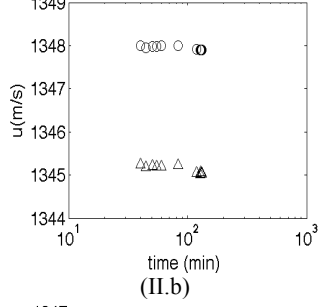
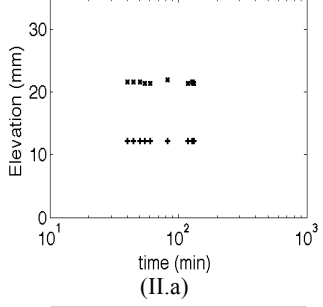
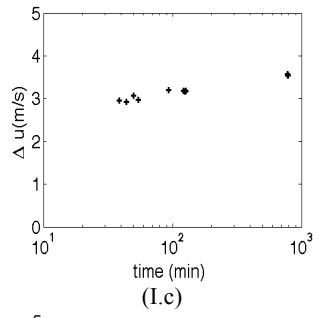
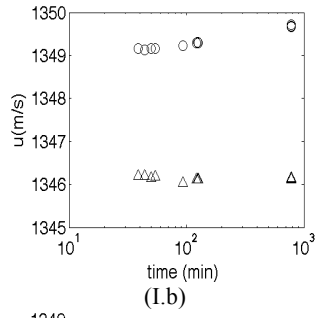
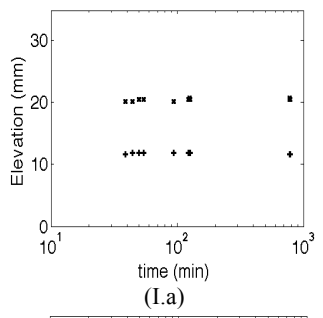


Figure A.4.1. (a) Speed of sound profile, (b) attenuation spectra profile, (c) attenuation at $f=7.9$ MHz for mixtures along dilution line q. Roman symbols refer to mixture numbers in Table 4.4.



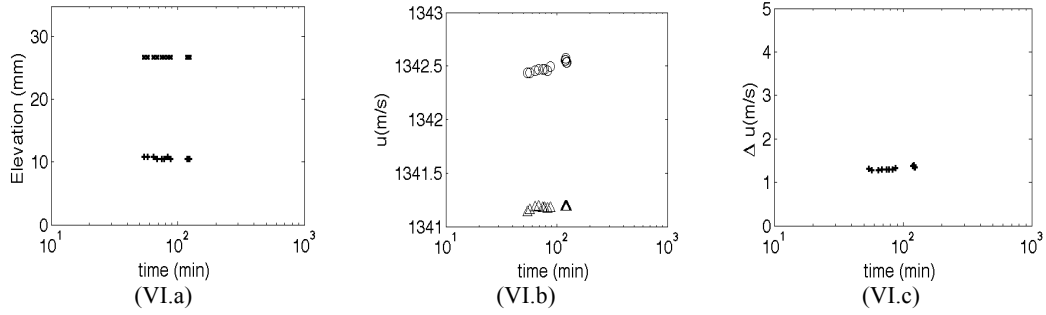


Figure A.4.2. (a) Variations of the liquid-liquid and liquid-air interfaces, (b) Speeds of sound in the separated phases: (triangle): upper phase, (circle): lower phase, (c) Speed of sound difference between the separated phases (c), for dilution line q. Roman symbols refer to mixture numbers in Table 4.4.

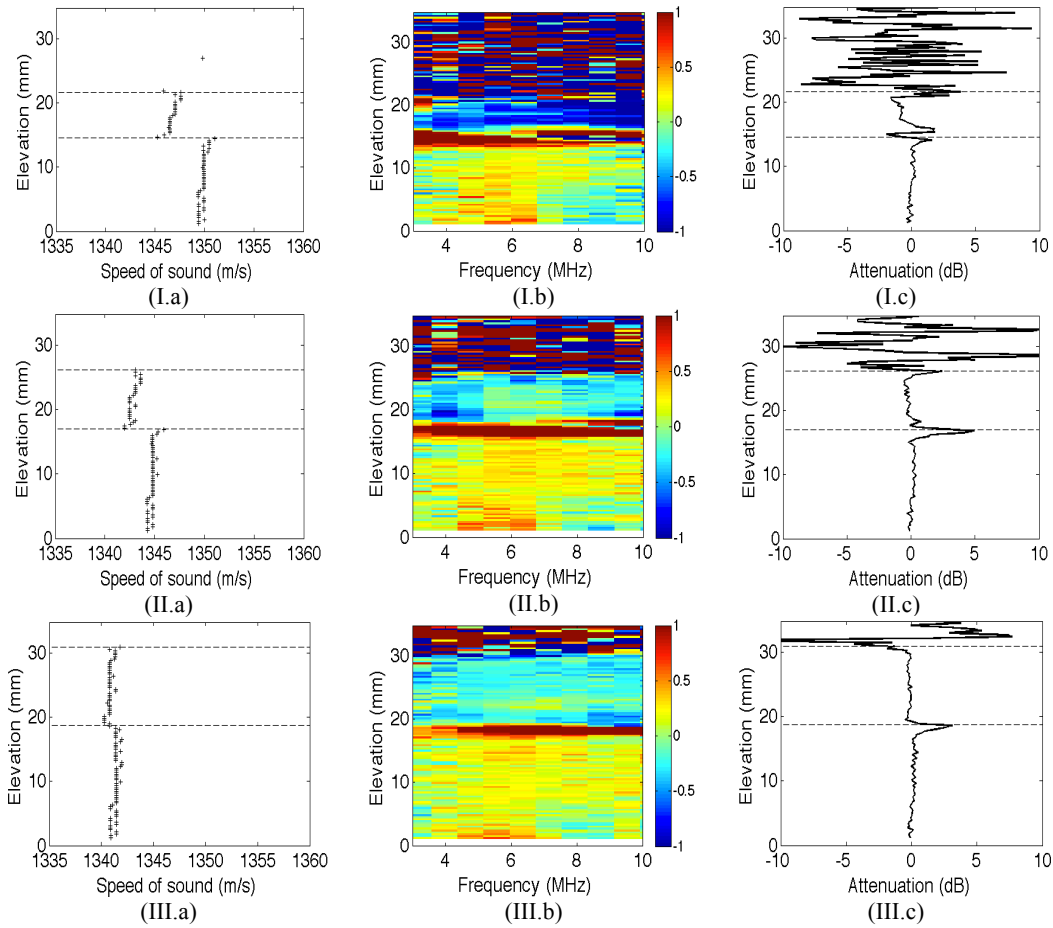


Figure A.5.1. (a) Speed of sound profile, (b) attenuation spectra profile, (c) attenuation at $f=7.9$ MHz for mixtures along line V. Roman symbols refer to mixture numbers in Table 4.4.

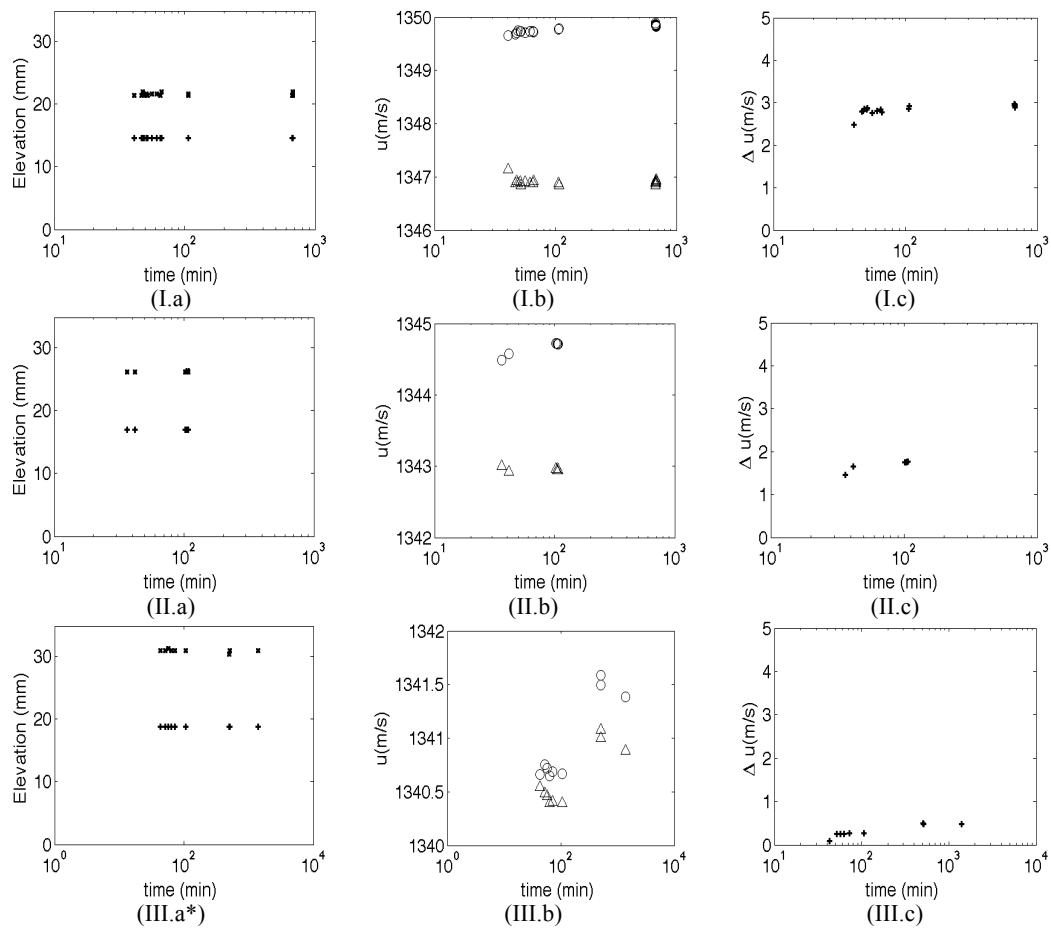


Figure A.5.2. (a) Variations of the liquid-liquid and liquid-air interfaces , (b) Speeds of sound in the separated phases: (triangle): upper phase, (circle): lower phase, (c) Speed of sound difference between the separated phases (c), for line V. Roman symbols refer to mixture numbers in Table 4.4. (*) The position of the liquid-liquid interface for mixture with composition 3 in Figure (III.a*) is fixed.

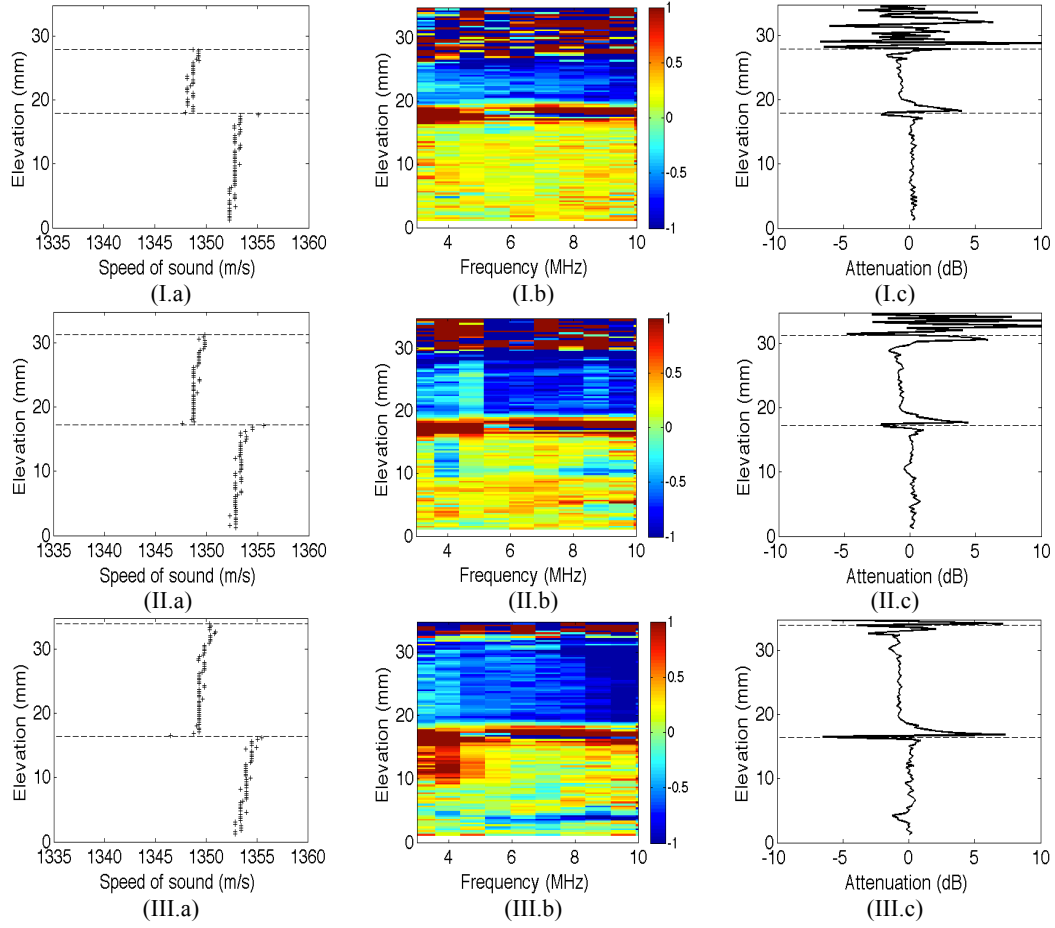


Figure A.6.1. (a) Speed of sound profile, (b) attenuation spectra profile, (c) attenuation at $f=7.9$ MHz for mixtures along line W. Roman symbols refer to mixture numbers in Table 4.4.

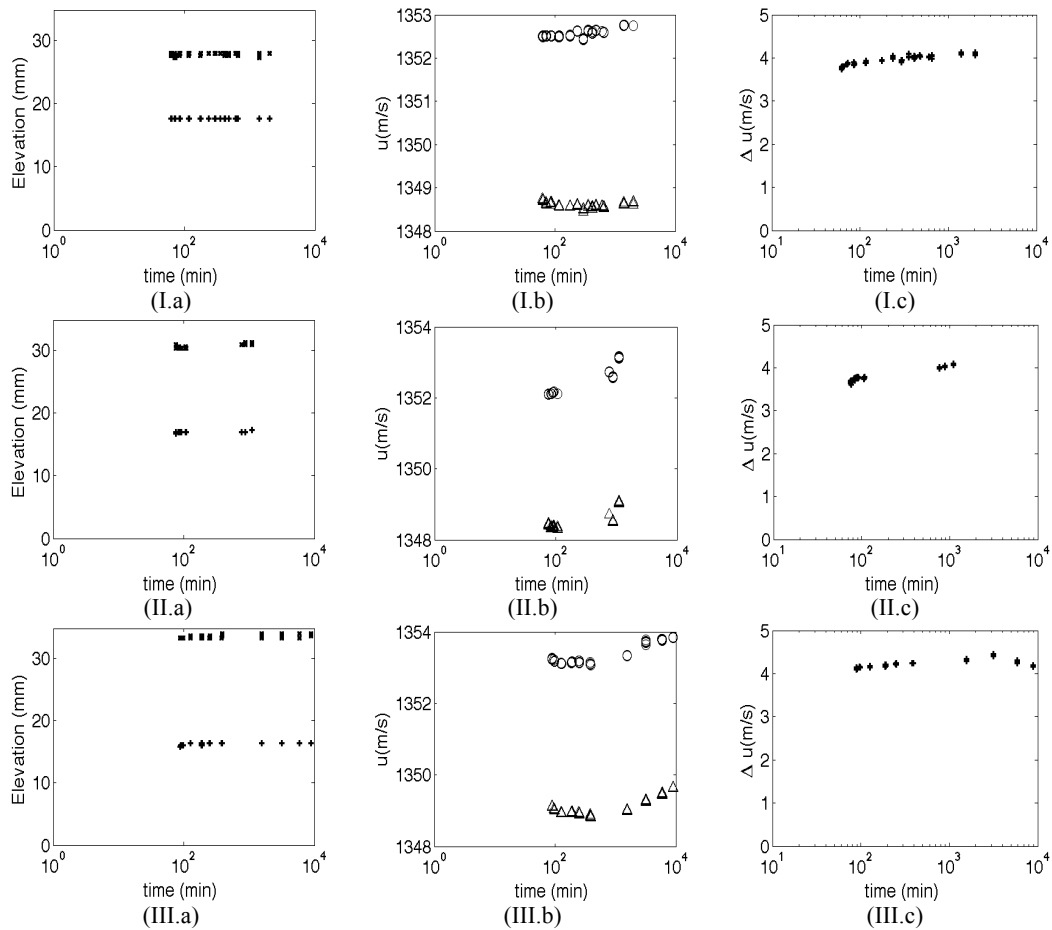


Figure A.6.2. (a) Variations of the liquid-liquid and liquid-air interfaces, (b) Speeds of sound in the separated phases: (triangle): upper phase, (circle): lower phase, (c) Speed of sound difference between the separated phases (c), for line W. Roman symbols refer to mixture numbers in Table 4.4.

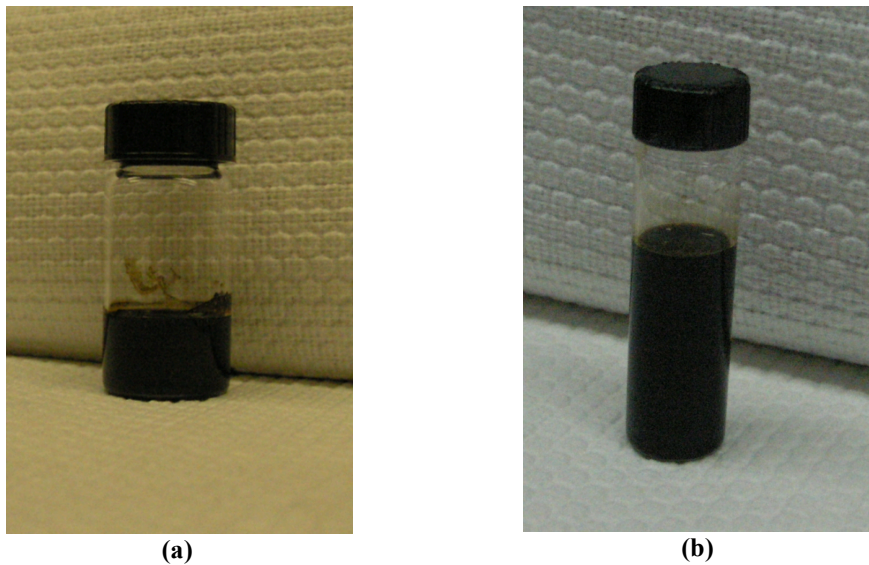


Figure A.6.3. Mixture 3 in line W is extracted with a needle and mixed for 5 minutes in a vial: (a) 268 minutes after mixing (b) 203 minutes after mixing.

A.2. Measurements of mixtures of asphaltene + polystyrene ($M_w=700,000$ g/mol) + toluene (Figures for data in Table 4.5)

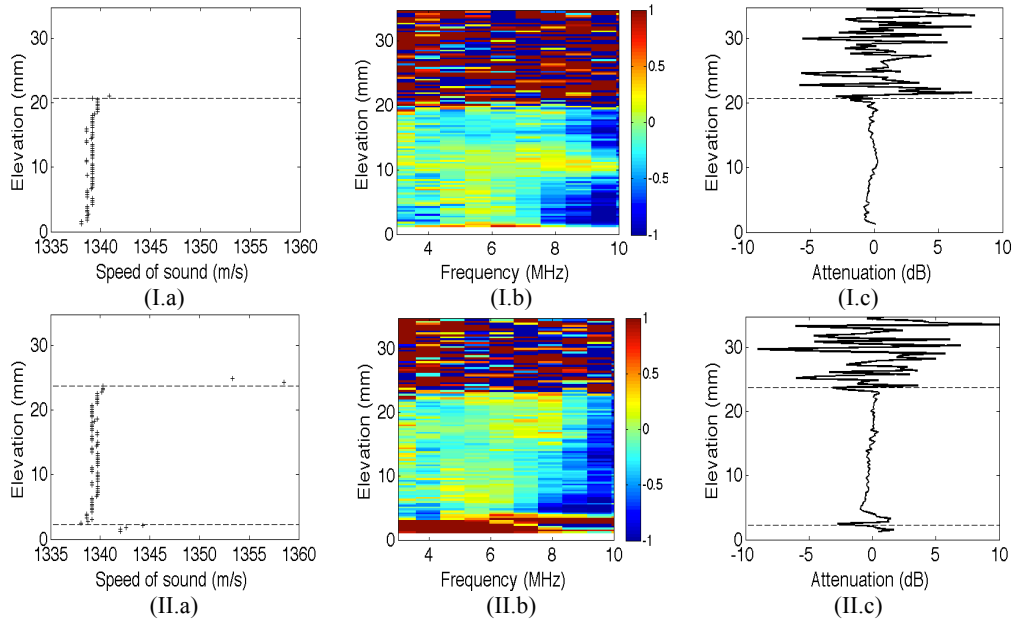


Figure A.7.1. (a) Speed of sound profile, (b) attenuation spectra profile, (c) attenuation at $f=7.9$ MHz for mixtures: (I) P_1 , (II) P_2 of Table 4.5.

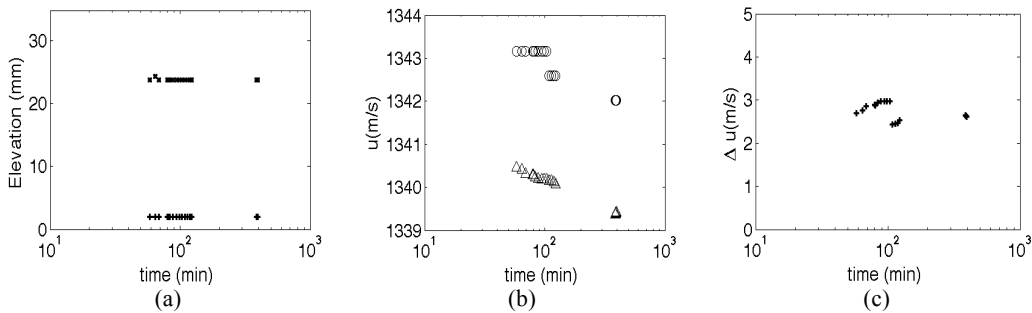
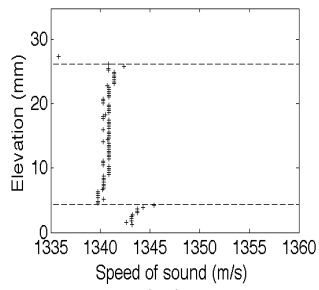
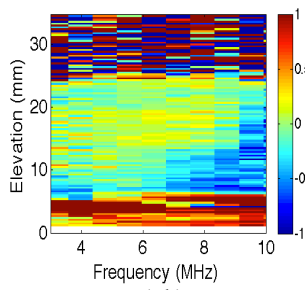


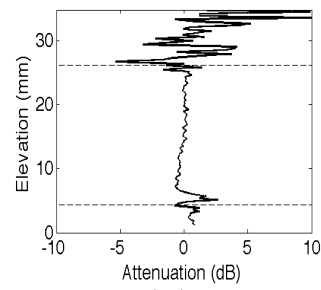
Figure A.7.2. (a) Evolution with time of the liquid-liquid and liquid-air interfaces, (b) speed of sound in the separated phases: (triangle): upper phase, (circle): lower phase, (c) speed of sound difference between the separated phases for mixture P_2 of Table 4.5.



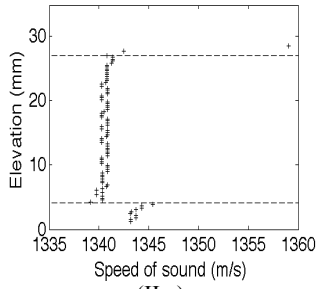
(I.a)



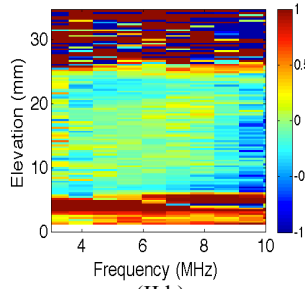
(I.b)



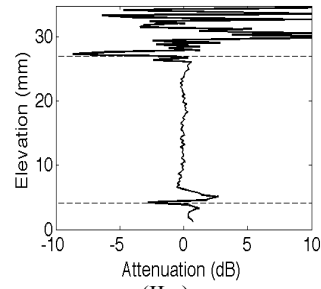
(I.c)



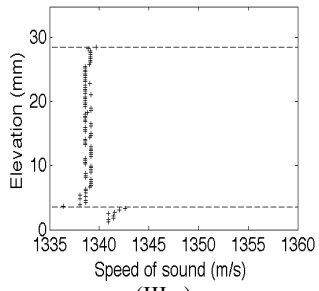
(II.a)



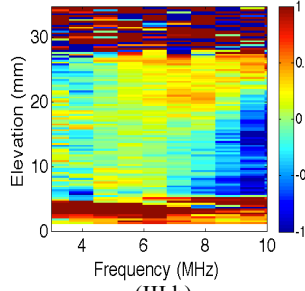
(II.b)



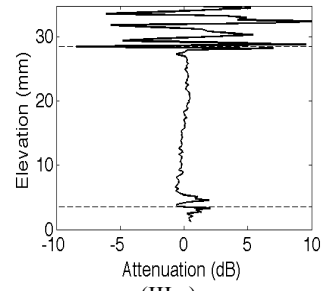
(II.c)



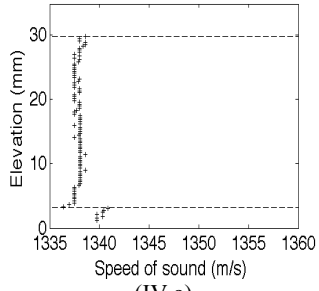
(III.a)



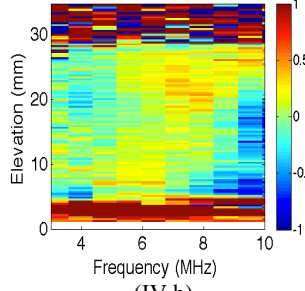
(III.b)



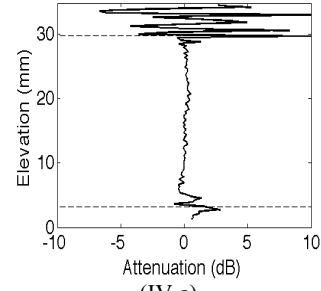
(III.c)



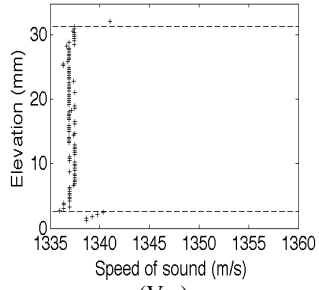
(IV.a)



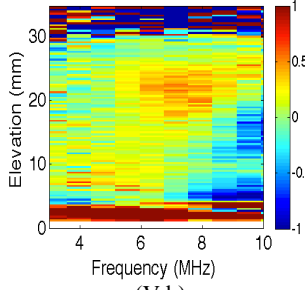
(IV.b)



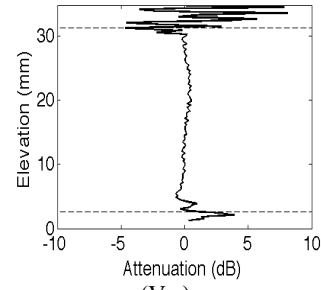
(IV.c)



(V.a)



(V.b)



(V.c)

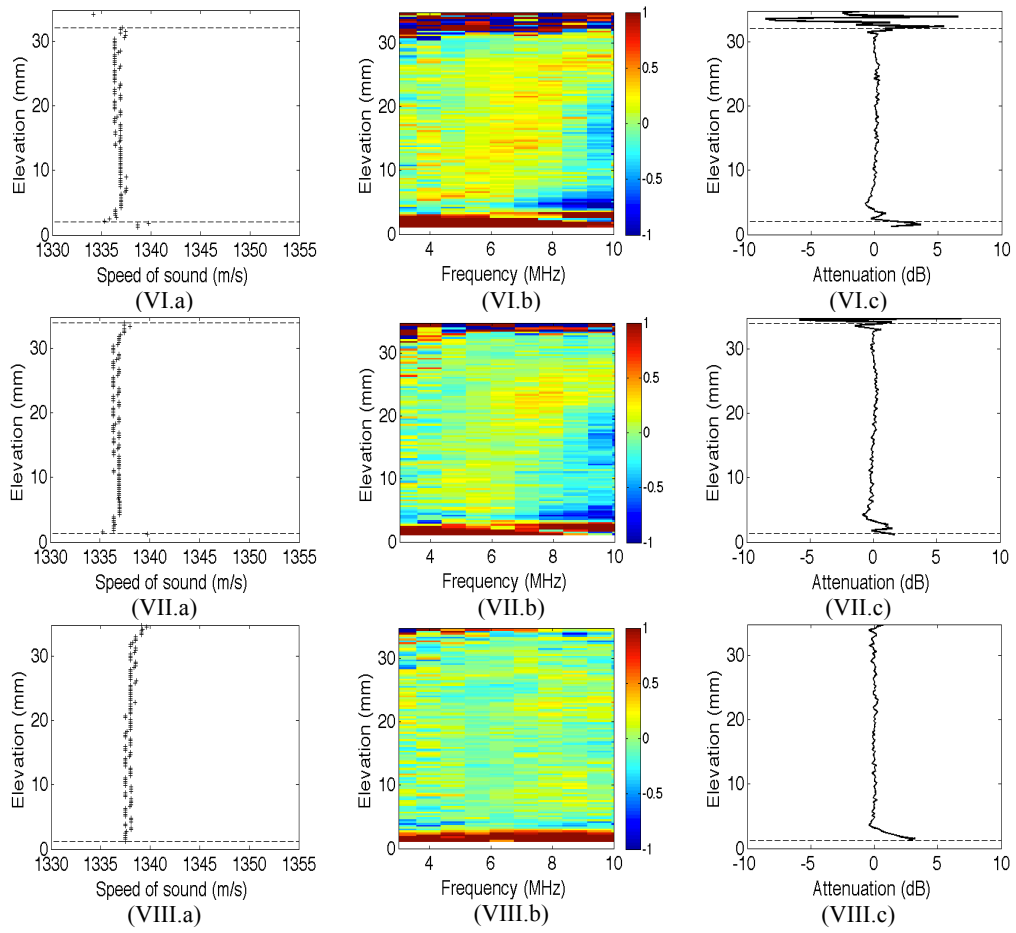
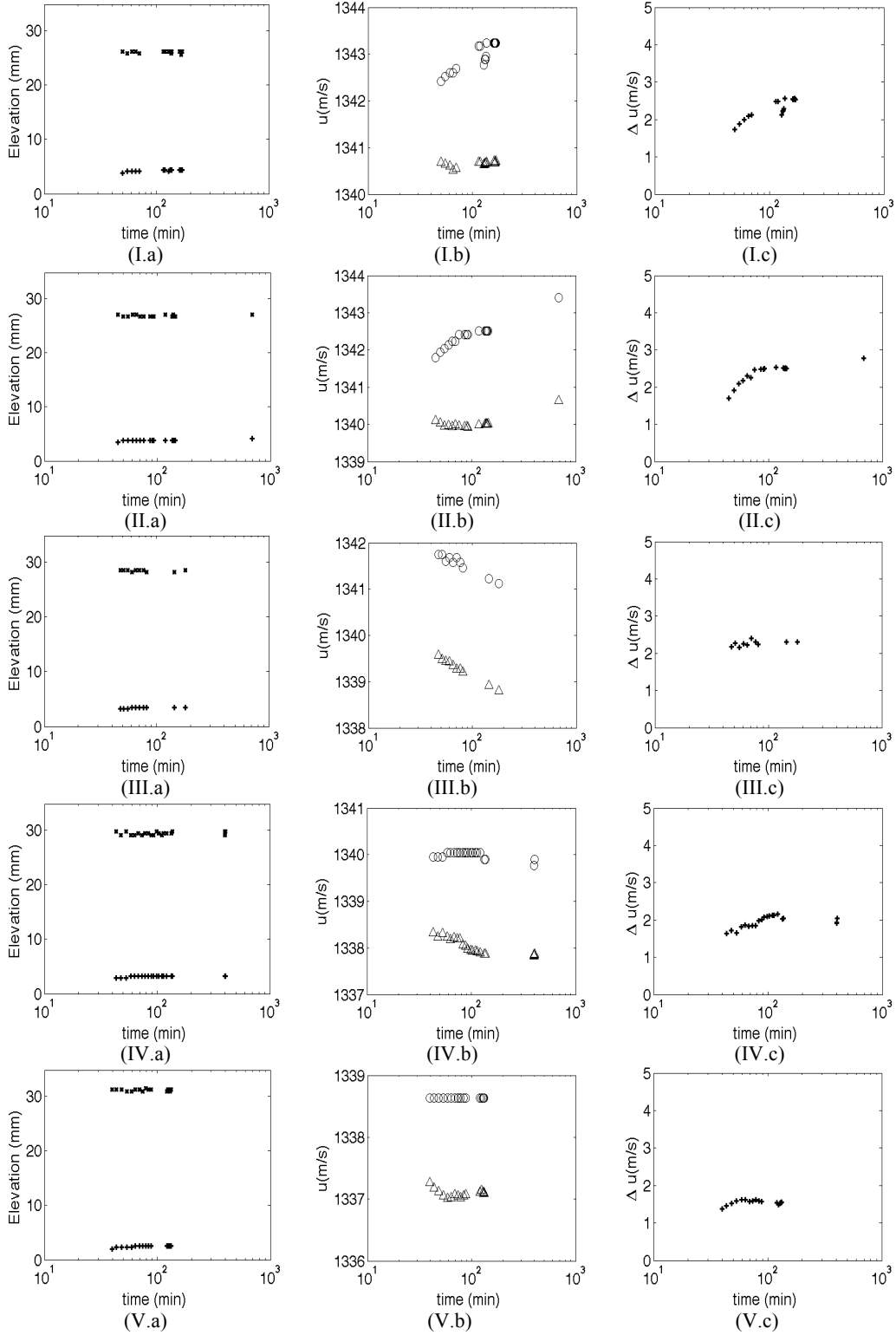


Figure A.8.1. (a) Speed of sound profile, (b) attenuation spectra profile, (c) attenuation at $f=7.9$ MHz for mixtures along dilution line p. Roman symbols refer to mixture numbers in Table 4.5.



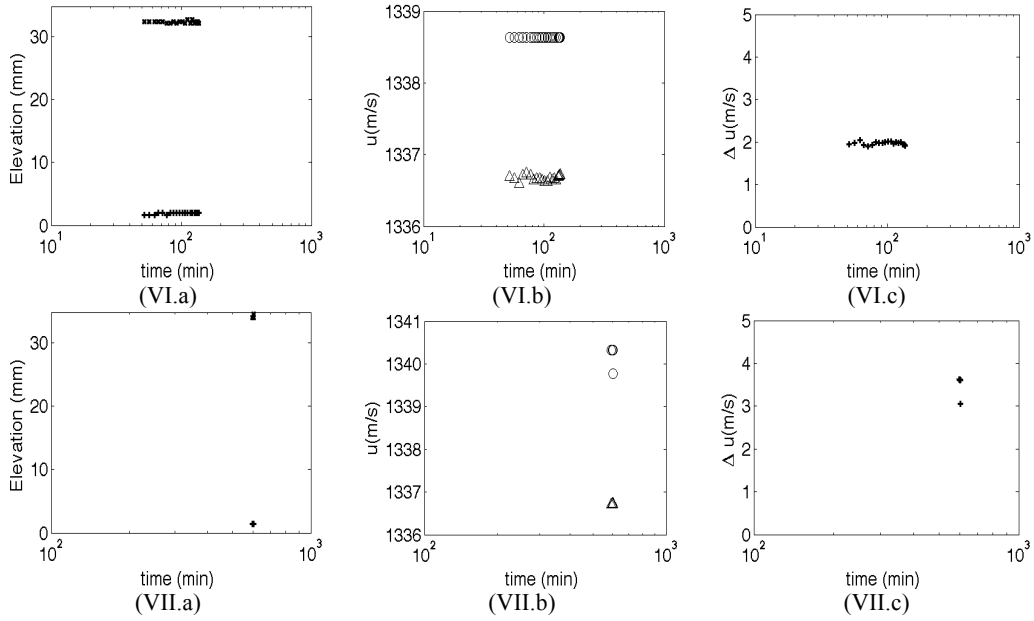
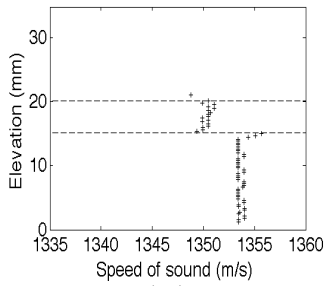
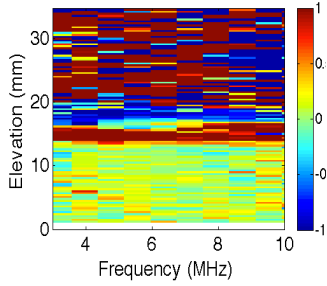


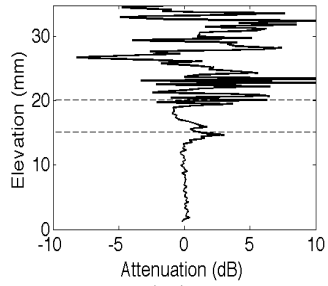
Figure A.8.2. (a) Variations of the liquid-liquid and liquid-air interfaces, (b) Speeds of sound in the separated phases: (triangle): upper phase, (circle): lower phase, (c) Speed of sound difference between the separated phases (c), for dilution line p. Roman symbols refer to mixture numbers in Table 4.5.



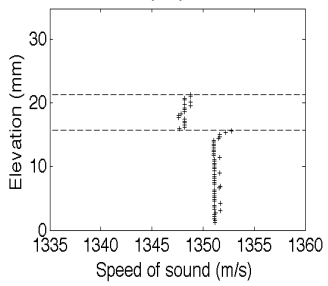
(I.a)



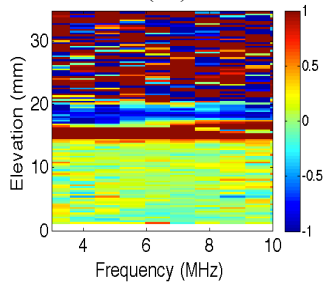
(I.b)



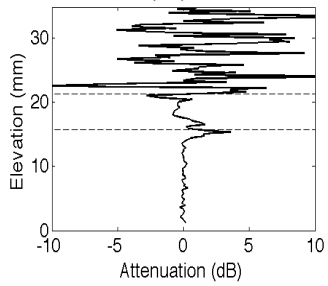
(I.c)



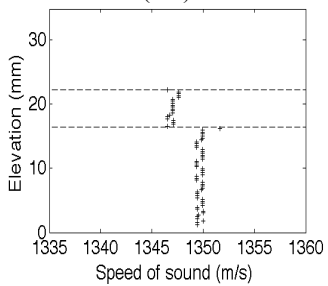
(II.a)



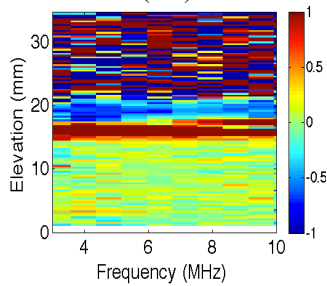
(II.b)



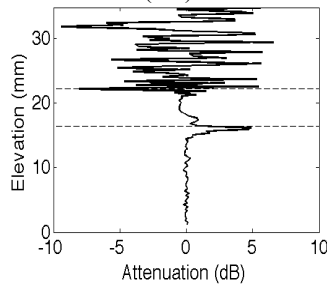
(II.c)



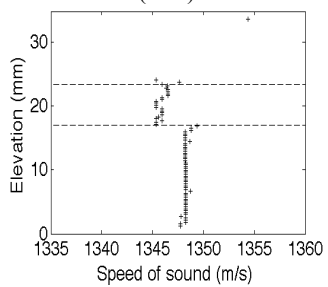
(III.a)



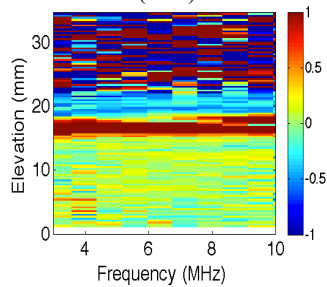
(III.b)



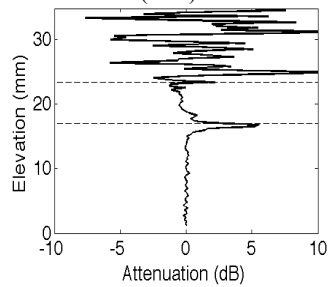
(III.c)



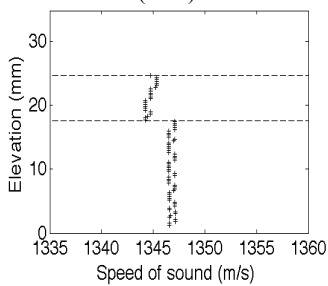
(IV.a)



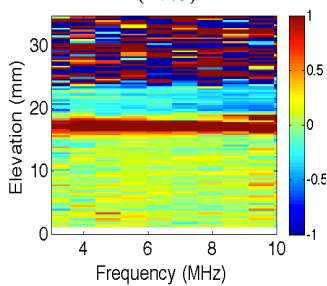
(IV.b)



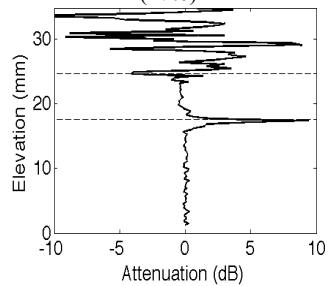
(IV.c)



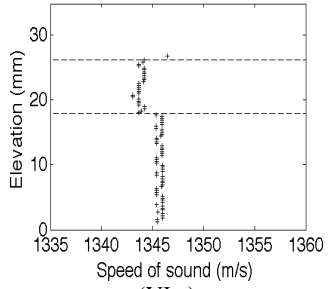
(V.a)



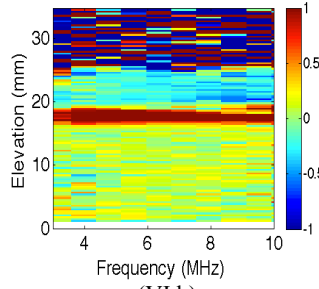
(V.b)



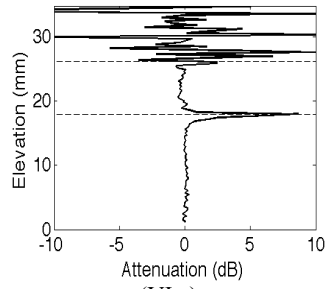
(V.c)



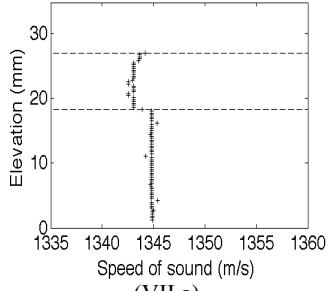
(VI.a)



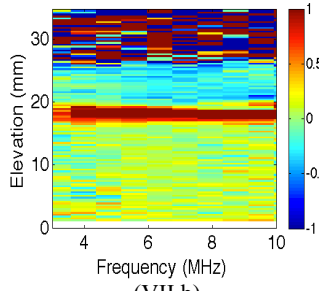
(VI.b)



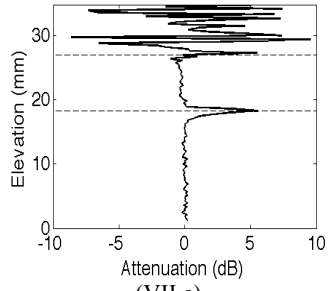
(VI.c)



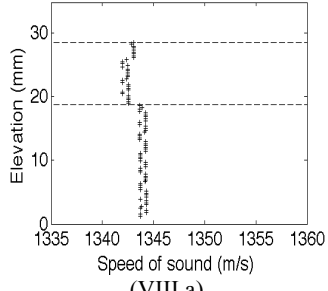
(VII.a)



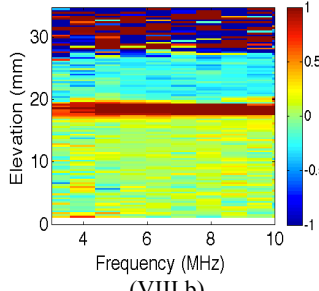
(VII.b)



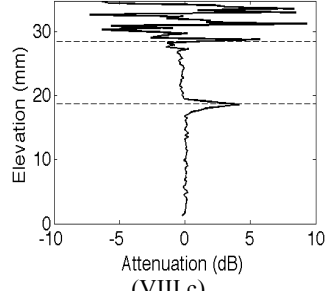
(VII.c)



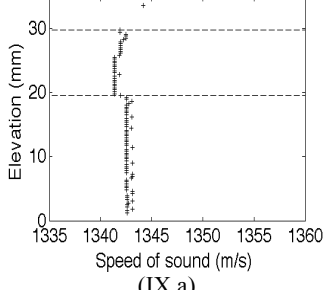
(VIII.a)



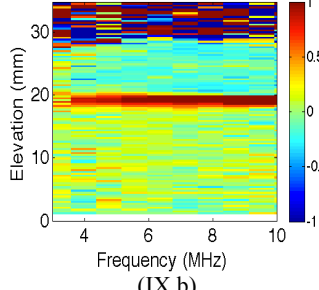
(VIII.b)



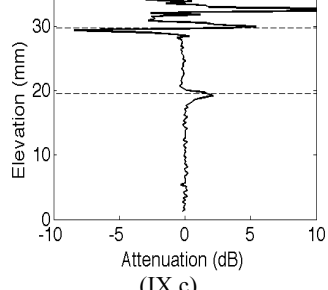
(VIII.c)



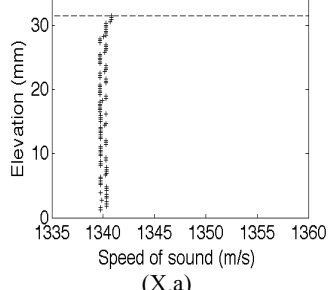
(IX.a)



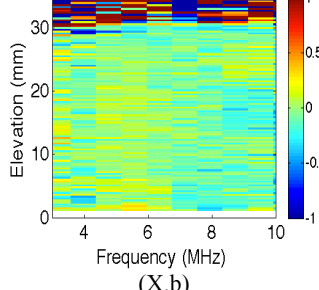
(IX.b)



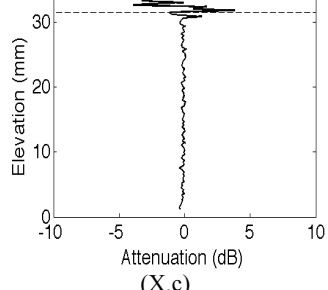
(IX.c)



(X.a)



(X.b)



(X.c)

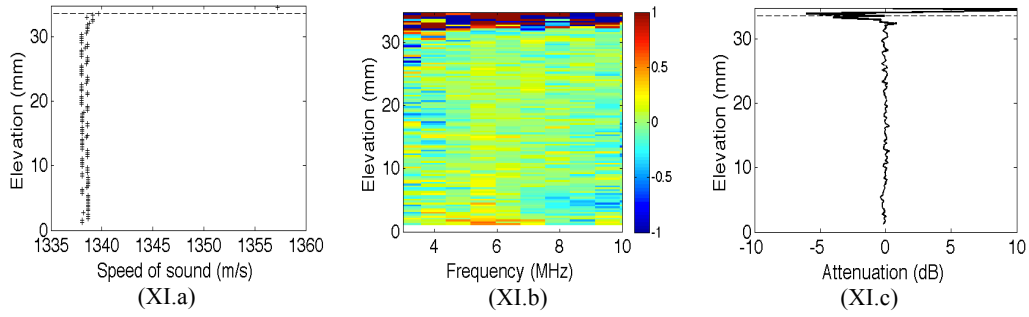
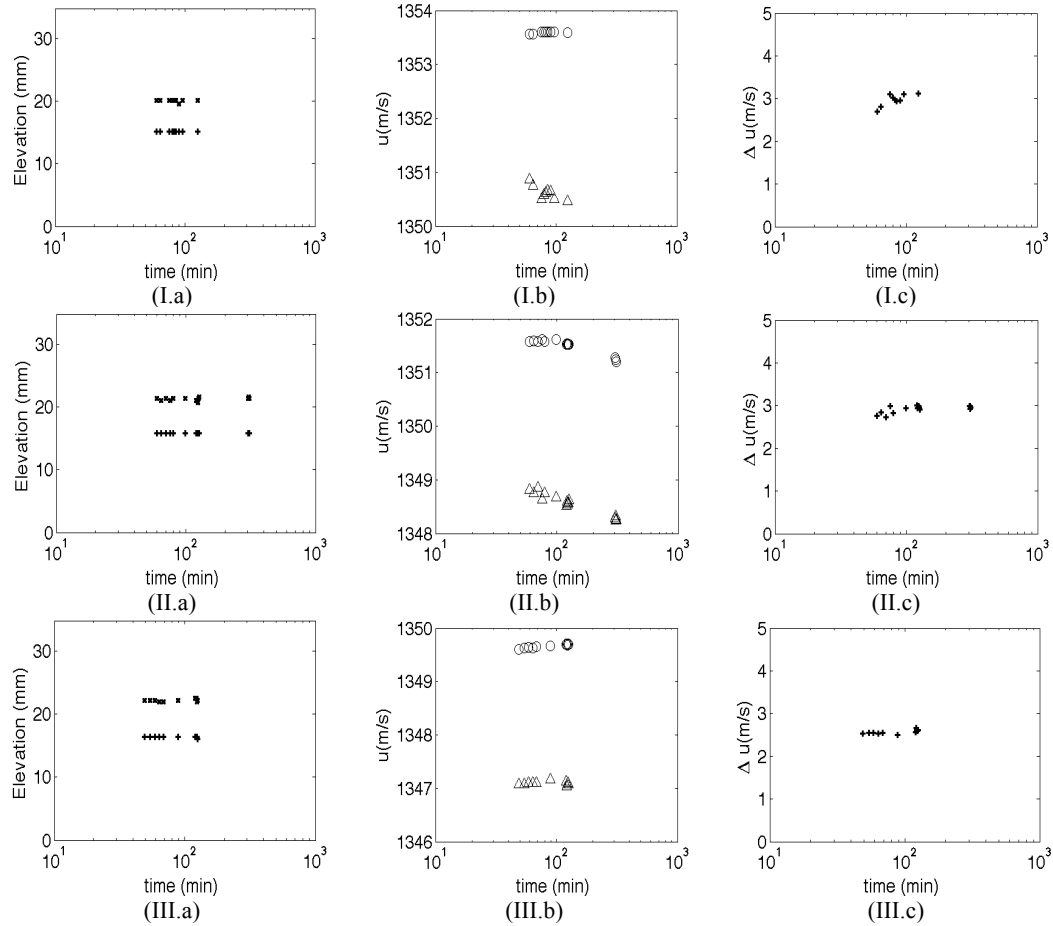


Figure A.9.1. (a) Speed of sound profile, (b) attenuation spectra profile, (c) attenuation at $f=7.9$ MHz for mixtures along dilution line r. Roman symbols refer to mixture numbers in Table 4.5.



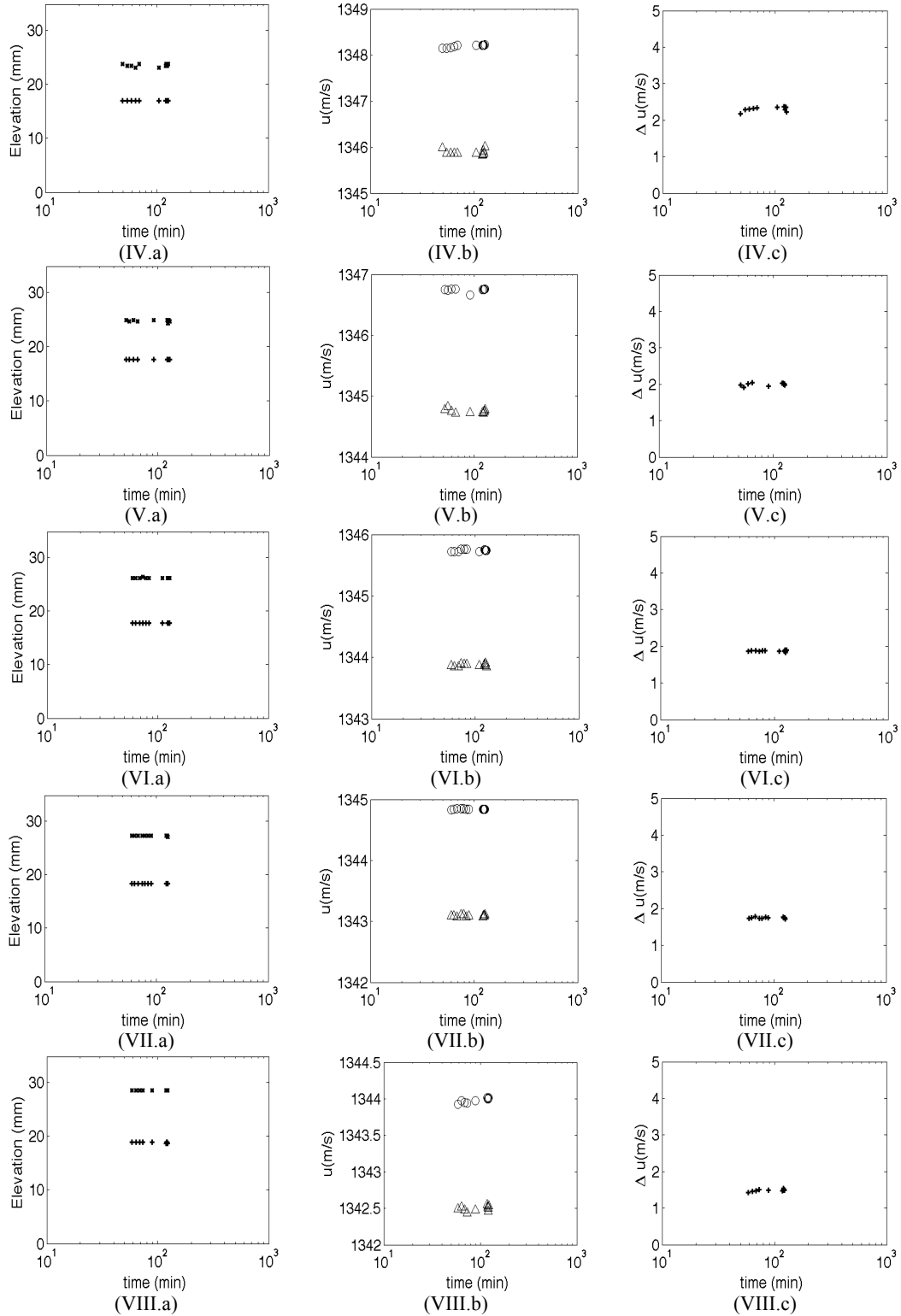
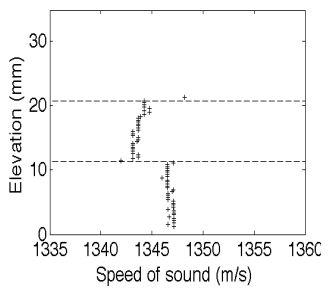
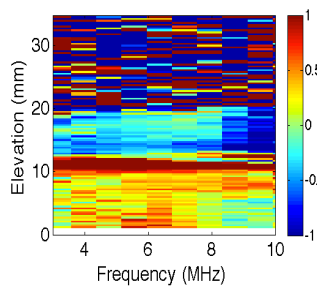


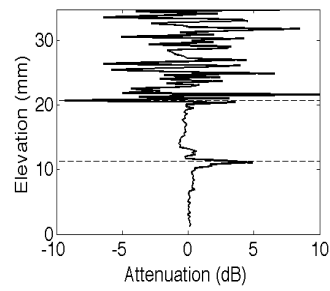
Figure A.9.2. (a) Variations of the liquid-liquid and liquid-air interfaces, (b) Speeds of sound in the separated phases: (triangle): upper phase, (circle): lower phase, (c) Speed of sound difference between the separated phases (c), for dilution line r. Roman symbols refer to mixture numbers in Table 4.5.



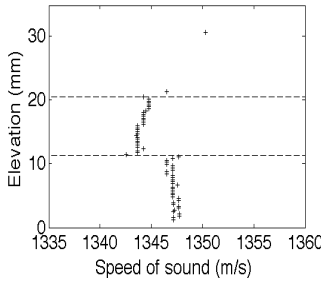
(I.a)



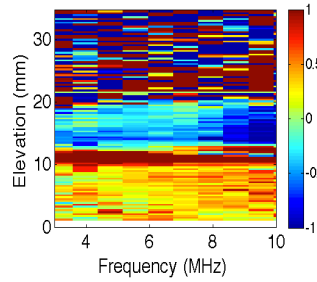
(I.b)



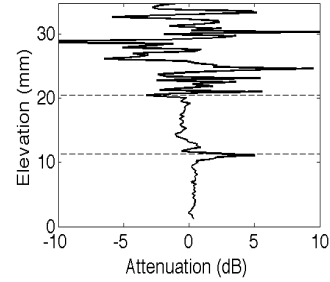
(I.c)



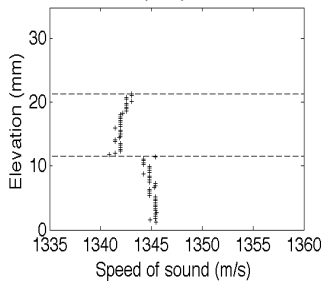
(I'.a)



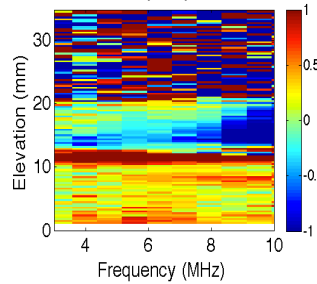
(I'.b)



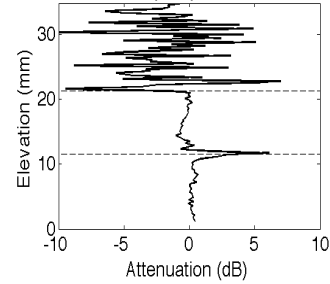
(I'.c)



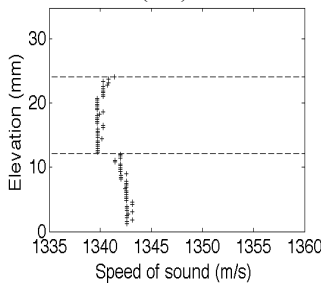
(II.a)



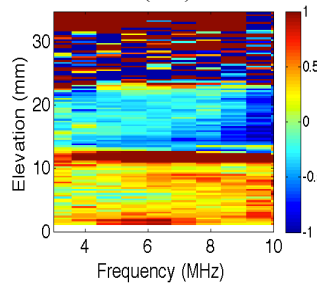
(II.b)



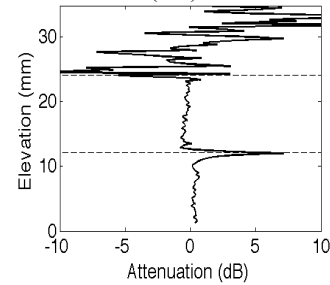
(II.c)



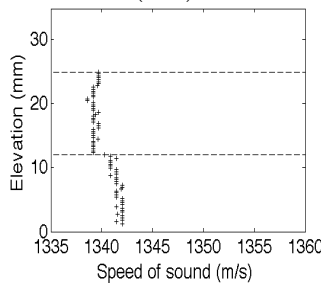
(III.a)



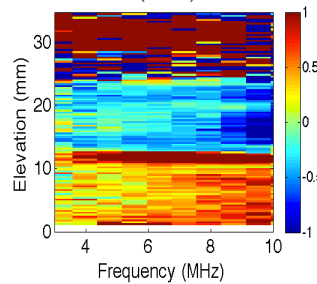
(III.b)



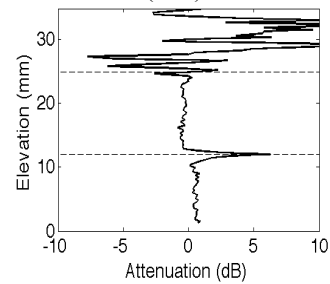
(III.c)



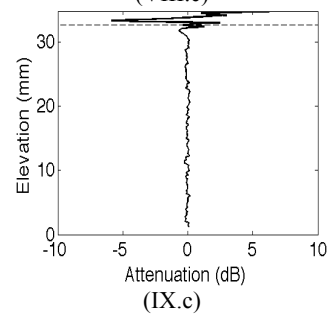
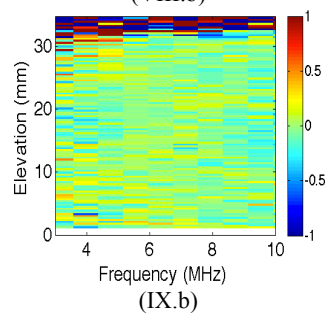
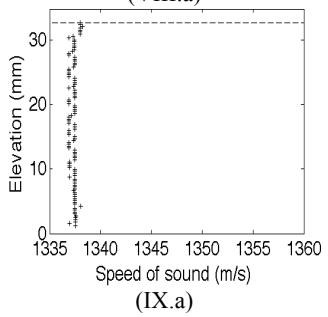
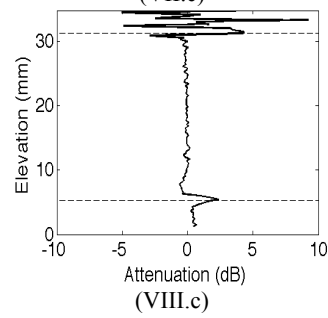
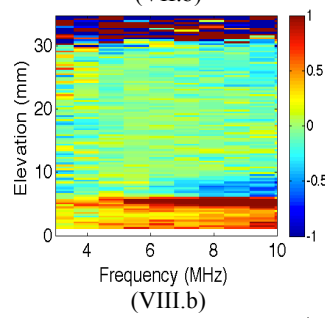
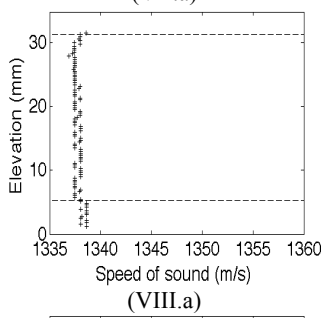
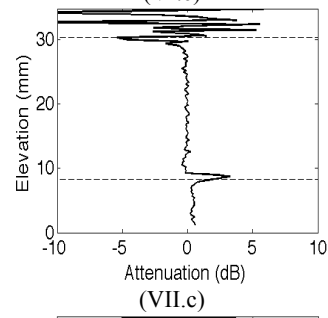
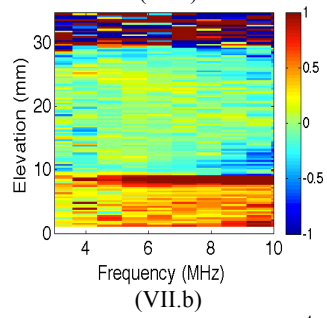
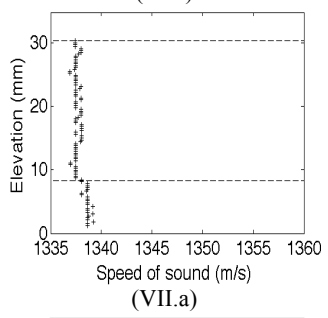
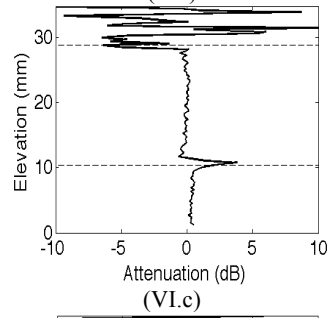
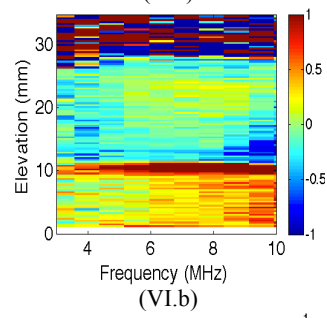
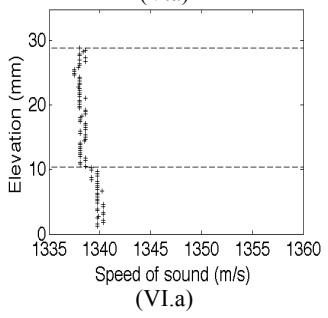
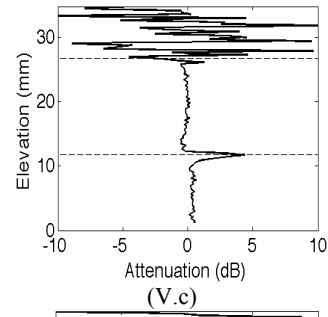
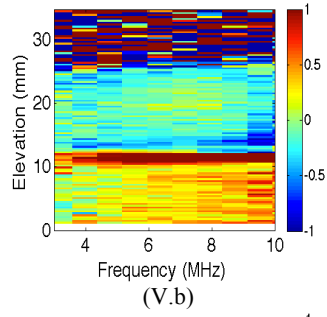
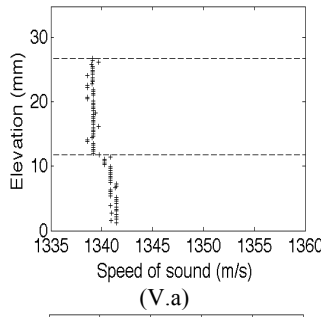
(IV.a)



(IV.b)



(IV.c)



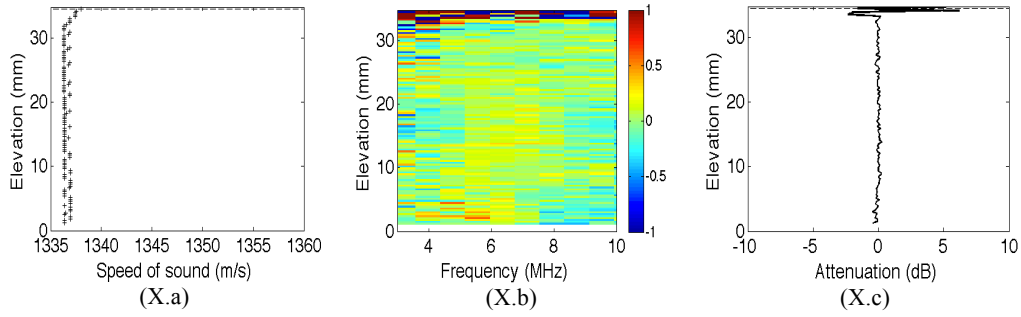
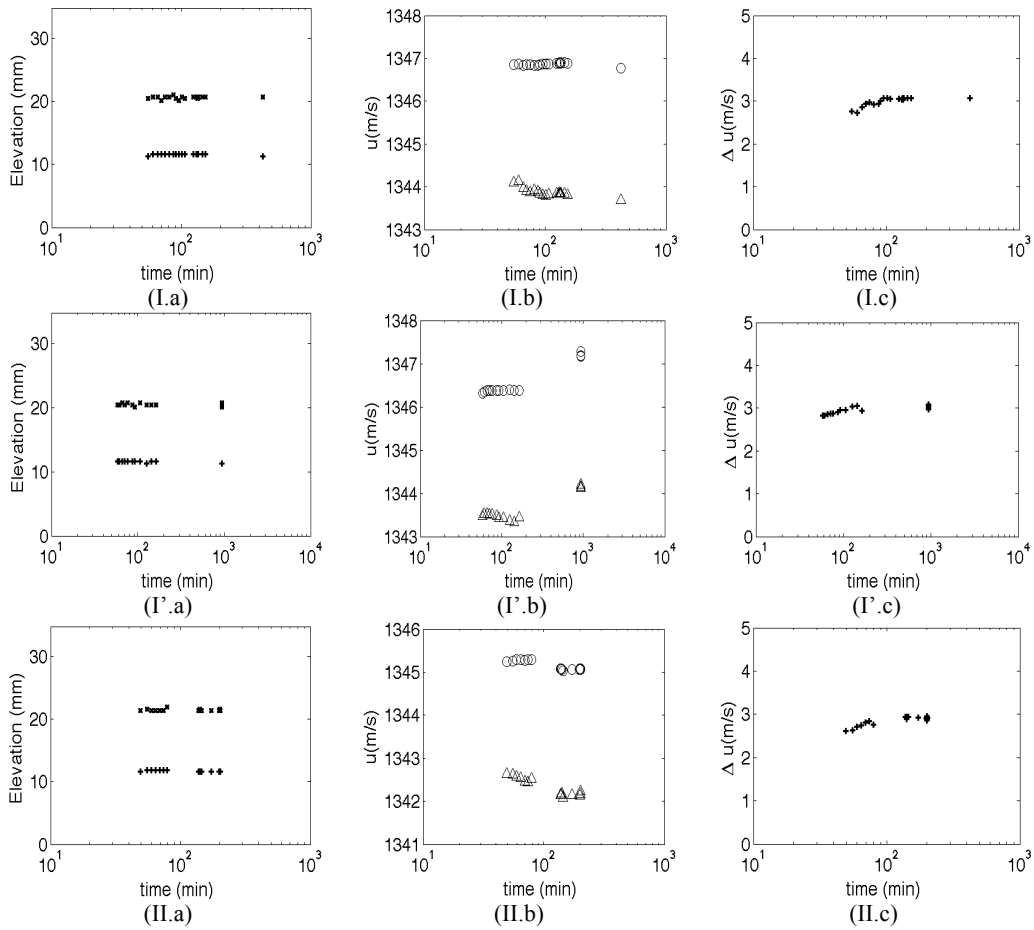
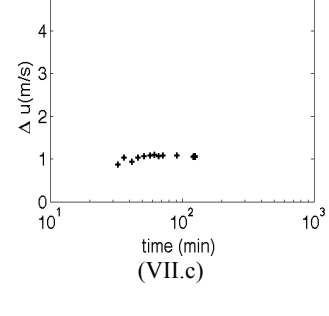
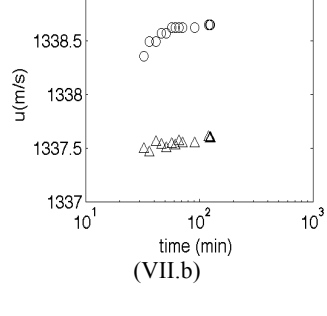
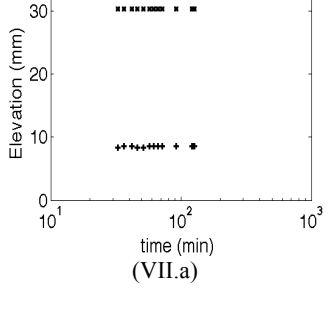
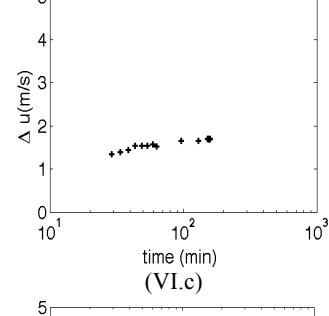
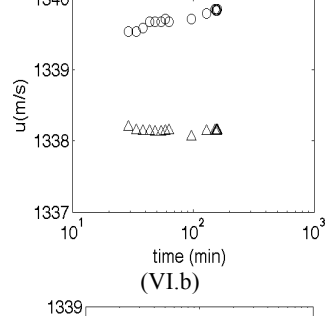
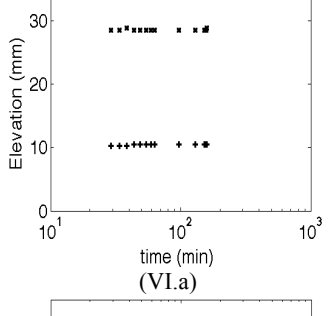
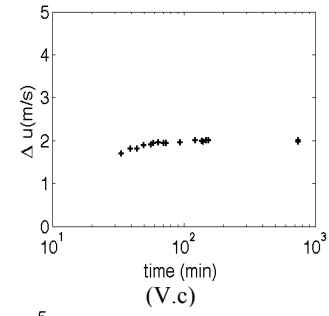
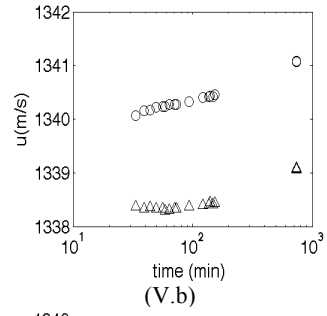
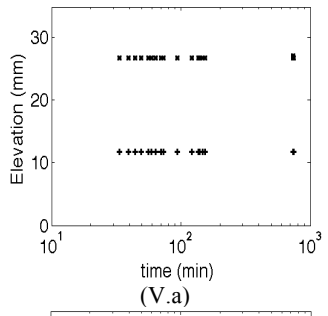
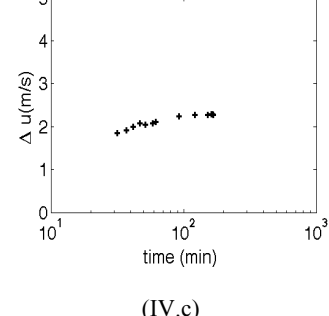
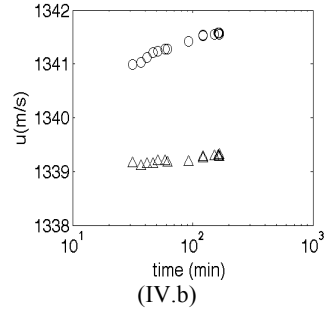
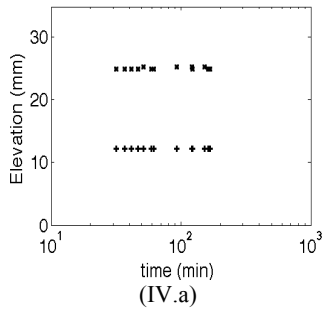
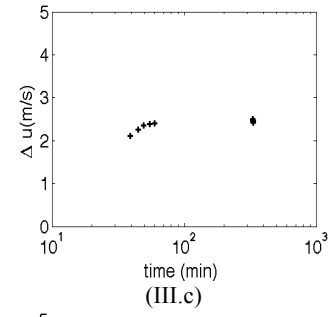
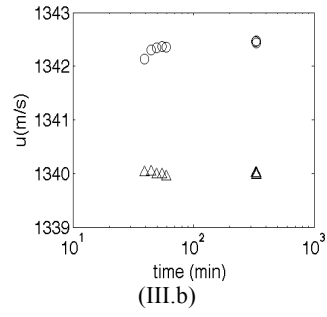
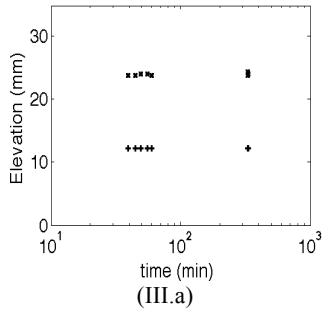


Figure A.10.1. (a) Speed of sound profile, (b) attenuation spectra profile, (c) attenuation at $f=7.9$ MHz for mixtures along dilution line q. Roman symbols refer to mixture numbers in Table 4.5. (I'): refers to mixture 1 after the second mixing.





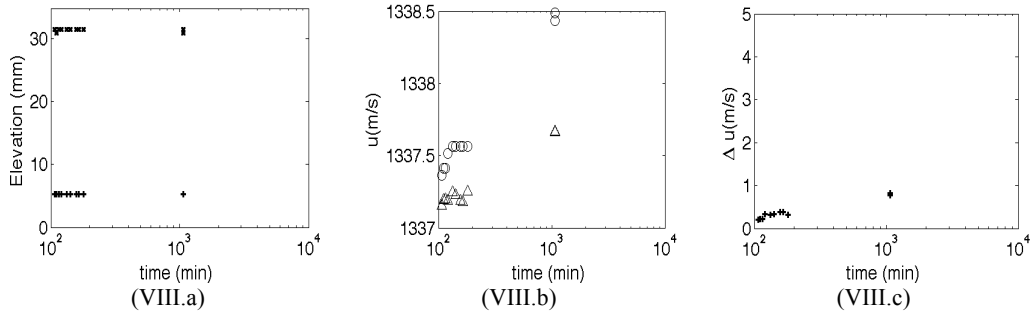


Figure A.10.2. (a) Variations of the liquid-liquid and liquid-air interfaces, (b) Speeds of sound in the separated phases: (triangle): upper phase, (circle): lower phase, (c) Speed of sound difference between the separated phases (c), for dilution line q. Roman symbols refer to mixture numbers in Table 4.5. (I'): refers to mixture 1 after the second mixing.

Appendix B. Calculation of Asphaltene and Polystyrene Volume Fractions in The Separated Phases

The concentrations of asphaltene in the diluted samples obtained from UV-Visible spectrophotometry measurements are $C_{\text{asph0}}|_{\text{Lower}} = 938.7 \pm 8.53$ mg/L and $C_{\text{asph0}}|_{\text{Upper}} = 346.4 \pm 3.15$ mg/L in the lower and upper phases respectively. The concentration of asphaltene in the original lower and upper phases are:

$$C_{\text{asph}}|_{\text{Lower}} = C_{\text{asph0}}|_{\text{Lower}} \times (V_{\text{tot}}/V_0) = 234.67 \pm 6.84 \text{ mg/ml}, \quad (\text{B.1})$$

$$C_{\text{asph}}|_{\text{Upper}} = C_{\text{asph0}}|_{\text{Upper}} \times (V_{\text{tot}}/V_0) = 86.61 \pm 3.02 \text{ mg/ml}, \quad (\text{B.2})$$

where: $V_{\text{tot}} = 100 \pm 0.08$ ml is the volume of the diluted sample and $V_0 = 0.4 \pm 0.01$ ml is the volume of the original sample.

The volume fractions of asphaltene in the original phases are:

$$\eta_{\text{Lower}} = C_{\text{Lower}} \times (1/\rho_{\text{asph}}) = 20.06 \pm 0.58 \text{ vol}\% \quad (\text{B.3})$$

$$\eta_{\text{Upper}} = C_{\text{Upper}} \times (1/\rho_{\text{asph}}) = 7.40 \pm 0.26 \text{ vol}\% \quad (\text{B.4})$$

The concentrations of polystyrene in the phases were obtained by evaporating toluene from two vials containing samples from the original upper and lower phases. The weights of the empty vials, with original samples from the upper and lower phases, and after toluene evaporation are shown in Table B.1.

The masses of toluene and asphaltene + polystyrene, in the vials, are calculated by subtracting the mass of the vials after drying from their mass before drying. Results are reported in Table B.1.

The masses of asphaltene and polystyrene in the vials is calculated using the following equations:

$$m_{asph} = \frac{\left[\left(\frac{m_{asph} + m_{polyst}}{\rho_{polyst}} \right) + \left(\frac{m_{tol}}{\rho_{tol}} \right) \right] C_{asph}}{\left[1 - C_{asph} \left(\frac{1}{\rho_{asph}} + \frac{1}{\rho_{polyst}} \right) \right]}, \quad (B.5)$$

$$m_{polyst} = (m_{asph} + m_{polyst}) - \frac{\left[\left(\frac{m_{asph} + m_{polyst}}{\rho_{polyst}} \right) + \left(\frac{m_{tol}}{\rho_{tol}} \right) \right] C_{asph}}{\left[1 - C_{asph} \left(\frac{1}{\rho_{asph}} + \frac{1}{\rho_{polyst}} \right) \right]}, \quad (B.6)$$

The total volume of the sample in the vials is given by:

$$V_{tot} = \frac{m_{asph}}{\rho_{asph}} + \frac{m_{polyst}}{\rho_{polyst}} + \frac{m_{tol}}{\rho_{tol}}, \quad (B.7)$$

The volume fraction of polystyrene in each vial is calculated using the following equation:

$$\phi = \frac{(m_{polyst} / \rho_{polyst})}{V_{tot}}, \quad (B.8)$$

Calculation results for the upper and lower phase samples are summarized in Table B.1.

Table B.1. Weights of vials empty, with original sample from upper and lower phases and after toluene evaporation.

	Lower phase	Upper phase
Empty vial weight (mg)	8133.05 ± 0.01	8041.09 ± 0.01
Vial with original sample (mg)	9347.81 ± 0.01	8709.39 ± 0.01
Vial with dried sample (mg)	8438.5 ± 0.01	8152.23 ± 0.01
$m_{asph} + m_{polyst}$ (mg)	305.45 ± 0.02	111.13 ± 0.02
m_{tol} (mg)	909.31 ± 0.02	557.16 ± 0.02
m_{asph} (mg)	307.90 ± 9.18	64.41 ± 2.27
m_{polyst} (mg)	-2.45 ± 9.20	46.72 ± 2.29
V_{tot} (ml)	1.312 ± 0.017	0.744 ± 0.004
ϕ (%)	-0.18 ± 0.67	6.00 ± 0.33

Appendix C. Linear Fit Plots of Speed of Sound vs Concentration in the Binary Mixtures of Asphaltene + Toluene and Polystyrene + Toluene

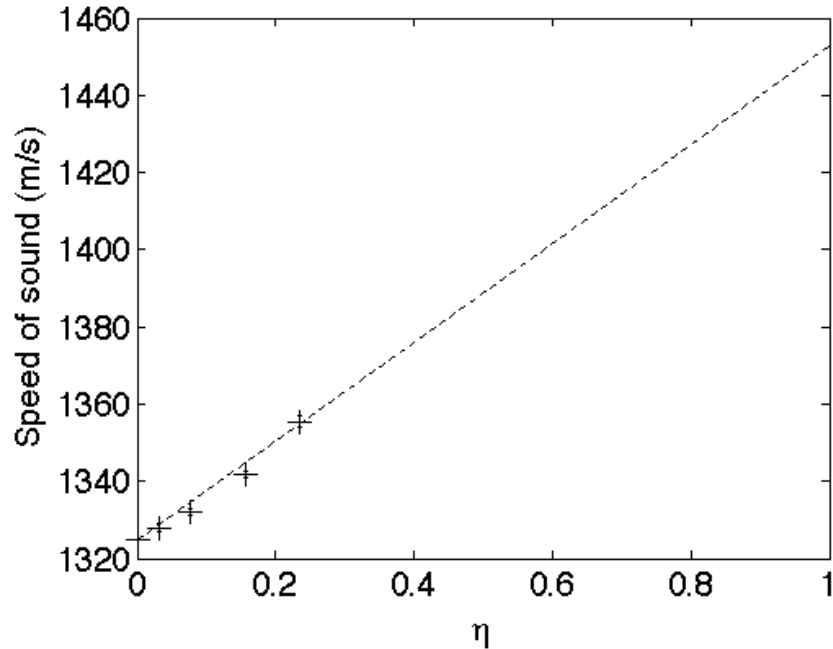


Figure C.1. Linear fit of speed of sound vs asphaltene volume fraction. $u_{\text{asph}}=1452.7$ m/s. $u(\text{m/s})=129.35 \eta+1323.39$. $R^2=0.991635717160612$.

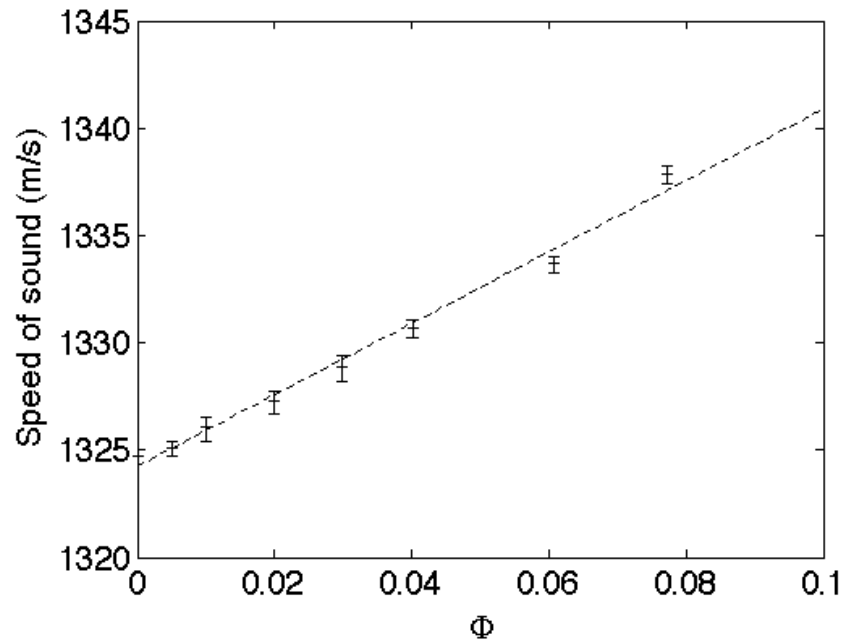


Figure C.2. Linear fit of speed of sound vs polystyrene volume fraction in binary mixtures of polystyrene ($M_w=390,000$ g/mol) + toluene, $u(\text{m/s})=166.41 \phi + 1324.25$. $u_{\text{polyst}}=1490.65$ m/s. $R^2=0.9949222931158359$.

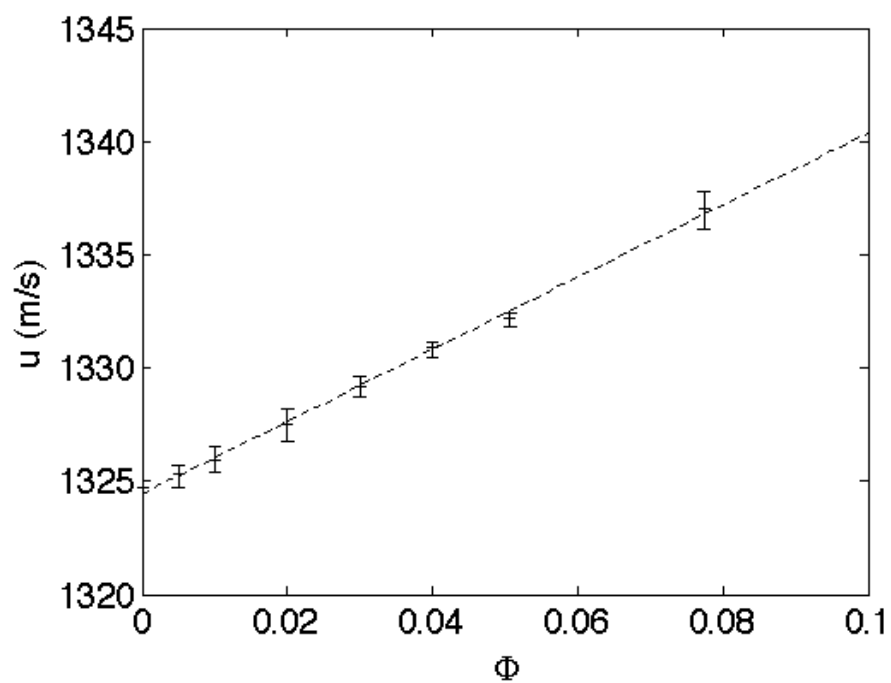


Figure C.3. Linear fit of speed of sound vs polystyrene volume fraction in binary mixtures of polystyrene ($M_w=700,000$ g/mol) + toluene, $u(\text{m/s})= 159.26 \phi + 1324.45$. $u_{\text{polyst}}=1483.7$ m/s. $R^2=0.9989073340684618$.

Appendix D. Scaling Geometric Transformation of Dilution Lines p , q and r and the Tie Line $[\alpha \beta]$

When only a fraction γ of asphaltene particles are active (large enough) in the phase separation. The composition of the separated phases can be estimated using a scaling geometric transformation of the tie lines p , q and r by γ in η -direction and by 1 in ϕ -direction to obtain the scaled dilution lines p^* , q^* and r^* . In this case, the components active in the phase separation are the polystyrene in toluene and the fraction γ of asphaltenes. p^* , q^* and r^* are the dilution lines of the colloidal particles participating in the phase separation.

In this appendix, it will be proven that the line $[\alpha^* \beta^*]$, the scaled transformation of the tie line $[\alpha \beta]$ (Fig.D.1.b) crossing dilution lines p , q and r at compositions P, Q and R (Fig.D1.a), is the tie line crossing dilution lines p^*, q^* and r^* at compositions P^*, Q^* and R^* (Fig.D.1.c).

From equation (2.23) in Chapter 2, the tie line equation is given by:

$$\phi = d + n\eta \quad (D.1)$$

From equation (D.1) the following equation can be obtained:

$$\phi^\beta - \phi^P = n(\eta^\beta - \eta^P) \quad (D.2)$$

The scaling transformation equations are given by:

$$\begin{cases} \eta^* = \gamma \eta \\ \phi^* = \phi \end{cases} \quad (D.3)$$

The equation of the line $[\alpha^* \beta^*]$, the scaled transformation of the tie line $[\alpha \beta]$, is obtained from equations (D.1) and (D.3), as follows:

$$\phi = \phi^* = d + \left(\frac{n}{\gamma}\right)\eta^* \quad (D.4)$$

Thus, the slope of the line $[\alpha^* \beta^*]$ increases by a factor of $(1/\gamma)$ when compared to the slope of the original tie line $[\alpha \beta]$.

From equation (2.25) in Chapter 2, the volume fraction of the upper phase at point P in dilution line p is given by:

$$\begin{aligned} R^P &= \frac{\sqrt{(\eta^\beta - \eta^P)^2 + (\phi^\beta - \phi^P)^2}}{\sqrt{(\eta^\beta - \eta^\alpha)^2 + (\phi^\alpha - \phi^\beta)^2}} = \frac{\sqrt{(\eta^\beta - \eta^P)^2 + n^2(\eta^\beta - \eta^P)^2}}{\sqrt{(\eta^\beta - \eta^\alpha)^2 + n^2(\eta^\beta - \eta^\alpha)^2}} \\ &= \frac{(\eta^\beta - \eta^P)}{(\eta^\beta - \eta^\alpha)} = \frac{(\phi^\beta - \phi^P)}{(\phi^\beta - \phi^\alpha)} \end{aligned} \quad (D.5)$$

If the line $[\alpha^* \beta^*]$, the scaling transformation of the tie line $[\alpha \beta]$, is used to calculate the volume fraction of the upper phase for a mixture with composition P^* in dilution line p^* , the following equation is obtained:

$$\begin{aligned} R^{P^*} &= \frac{\sqrt{(\eta^{\beta^*} - \eta^{P^*})^2 + (\phi^{\beta^*} - \phi^{P^*})^2}}{\sqrt{(\eta^{\beta^*} - \eta^{\alpha^*})^2 + (\phi^{\alpha^*} - \phi^{\beta^*})^2}} = \frac{\sqrt{(\eta^{\beta^*} - \eta^{P^*})^2 + \left(\frac{n}{\gamma}\right)^2 (\eta^{\beta^*} - \eta^{P^*})^2}}{\sqrt{(\eta^{\beta^*} - \eta^{\alpha^*})^2 + \left(\frac{n}{\gamma}\right)^2 (\eta^{\beta^*} - \eta^{\alpha^*})^2}} \\ &= \frac{(\eta^{\beta^*} - \eta^{P^*})}{(\eta^{\beta^*} - \eta^{\alpha^*})} = \frac{\gamma(\eta^\beta - \eta^P)}{\gamma(\eta^\beta - \eta^\alpha)} = \frac{(\eta^\beta - \eta^P)}{(\eta^\beta - \eta^\alpha)} = \frac{(\phi^\beta - \phi^P)}{(\phi^\beta - \phi^\alpha)} = R^P \end{aligned} \quad (D.6)$$

Therefore:

$$R^{P*} = R^P \quad (D.7)$$

Similarly, the following equations can be obtained:

$$R^{Q*} = R^Q \quad (D.8)$$

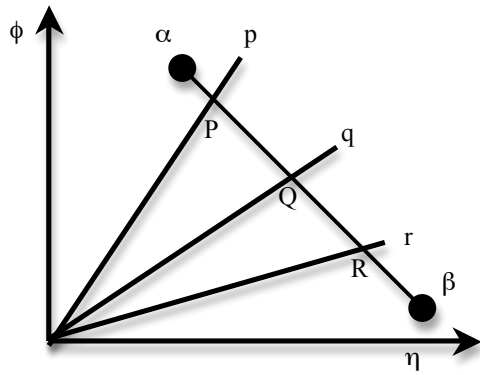
$$R^{R*} = R^R \quad (D.9)$$

Therefore, the volume fractions of the upper phases (R^P , R^Q and R^R) at the intersection of the tie line $[\alpha \beta]$ with dilution lines p,q and r in P, Q or R are equal to the volume fractions of the upper phases (R^{P*} , R^{Q*} and R^{R*}) at the intersection of the scaled line $[\alpha^* \beta^*]$ with the scaled dilution lines p^*, q^* and r^* . It can be concluded that the tie line that fits the variations of the upper phase volume fractions along the scaled dilution lines p^* , q^* and r^* is $[\alpha^* \beta^*]$, the scaled transformation of the tie line $[\alpha \beta]$.

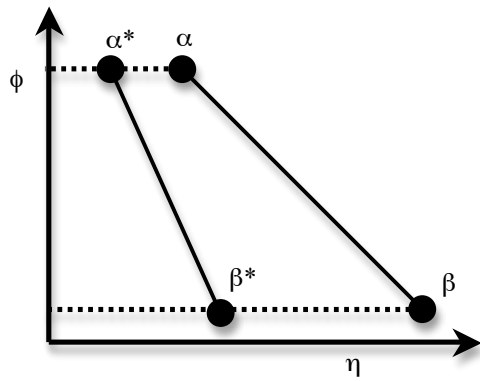
The volume fraction difference of asphaltenes between the separated phases in the tie line $[\alpha^* \beta^*]$ is related to the volume fraction difference of asphaltene between the separated phases in the original tie line $[\alpha \beta]$ by the following equation:

$$\Delta\eta^* = \eta^{\alpha^*} - \eta^{\beta^*} = \gamma(\eta^\alpha - \eta^\beta) = \gamma \Delta\eta \quad (D.10)$$

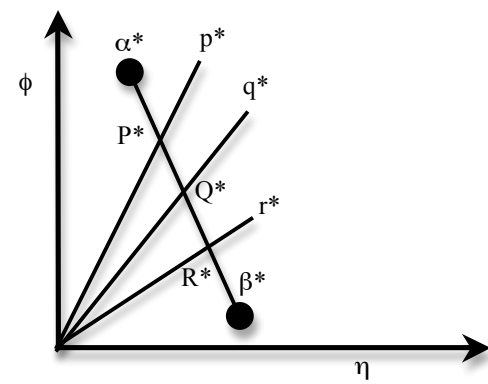
Therefore, when γ is reduced, the volume fraction difference between the separated phases decreases - at constant ϕ -. Consequently, the speed of sound difference between the separated phases decreases.



(a)



(b)



(c)

Figure D.1. (a) Original dilution lines p , q and r with tie line $[\alpha \beta]$, (b) Scaled line $[\alpha^* \beta^*]$ of tie line $[\alpha \beta]$ by γ in η direction and 1 in ϕ direction, (c) Intersection of scaled line $[\alpha^* \beta^*]$ with scaled dilution lines p^* , q^* and r^* .

Appendix E. Matlab Code for the Calculation of Speed of Sound and Attenuation Spectra Profiles from Recorded Waveforms

```
% This matlab file converts measured waveforms into
speed of sound and
% attenuation profiles videos and data for mixture 1 in
dilution line q for
% the case of mixtures of asphaltene + polystyrene
(Mw=393 400 g/mol) +
% toluene

% A similar file is used for every mixture in Tables
4.1-4.4.

clear all;
close all;

% Load waveforms pe recorded at different times

load Toluene_polyst_7vol_asphalt_april11_mix1_1.txt
pe(:, :, 1)=Toluene_polyst_7vol_asphalt_april11_mix1_1;

load Toluene_polyst_7vol_asphalt_april11_mix1_2.txt
pe(:, :, 2)=Toluene_polyst_7vol_asphalt_april11_mix1_2;

load Toluene_polyst_7vol_asphalt_april11_mix1_3.txt
pe(:, :, 3)=Toluene_polyst_7vol_asphalt_april11_mix1_3;

load Toluene_polyst_7vol_asphalt_april11_mix1_4.txt
pe(:, :, 4)=Toluene_polyst_7vol_asphalt_april11_mix1_4;

load Toluene_polyst_7vol_asphalt_april11_mix1_5.txt
pe(:, :, 5)=Toluene_polyst_7vol_asphalt_april11_mix1_5;

load Toluene_polyst_7vol_asphalt_april11_mix1_6.txt
pe(:, :, 6)=Toluene_polyst_7vol_asphalt_april11_mix1_6;

load Toluene_polyst_7vol_asphalt_april11_mix1_7.txt
pe(:, :, 7)=Toluene_polyst_7vol_asphalt_april11_mix1_7;

load Toluene_polyst_7vol_asphalt_april11_mix1_8.txt
pe(:, :, 8)=Toluene_polyst_7vol_asphalt_april11_mix1_8;

load Toluene_polyst_7vol_asphalt_april11_mix1_9.txt
pe(:, :, 9)=Toluene_polyst_7vol_asphalt_april11_mix1_9;
```

```
load Toluene_polyst_7vol_asphalt_april11_mix1_10.txt
pe(:, :, 10)=Toluene_polyst_7vol_asphalt_april11_mix1_10;

load Toluene_polyst_7vol_asphalt_april11_mix1_11.txt
pe(:, :, 11)=Toluene_polyst_7vol_asphalt_april11_mix1_11;

load Toluene_polyst_7vol_asphalt_april11_mix1_12.txt
pe(:, :, 12)=Toluene_polyst_7vol_asphalt_april11_mix1_12;

load Toluene_polyst_7vol_asphalt_april11_mix1_13.txt
pe(:, :, 13)=Toluene_polyst_7vol_asphalt_april11_mix1_13;

load Toluene_polyst_7vol_asphalt_april11_mix1_14.txt
pe(:, :, 14)=Toluene_polyst_7vol_asphalt_april11_mix1_14;

load Toluene_polyst_7vol_asphalt_april11_mix1_15.txt
pe(:, :, 15)=Toluene_polyst_7vol_asphalt_april11_mix1_15;

load Toluene_polyst_7vol_asphalt_april11_mix1_16.txt
pe(:, :, 16)=Toluene_polyst_7vol_asphalt_april11_mix1_16;

load Toluene_polyst_7vol_asphalt_april11_mix1_17.txt
pe(:, :, 17)=Toluene_polyst_7vol_asphalt_april11_mix1_17(
:, 1:4001);

load Toluene_polyst_7vol_asphalt_april11_mix1_18.txt
pe(:, :, 18)=Toluene_polyst_7vol_asphalt_april11_mix1_18;

load Toluene_polyst_7vol_asphalt_april11_mix1_19.txt
pe(:, :, 19)=Toluene_polyst_7vol_asphalt_april11_mix1_19;

load Toluene_polyst_7vol_asphalt_april11_mix1_20.txt
pe(:, :, 20)=Toluene_polyst_7vol_asphalt_april11_mix1_20;

load Toluene_polyst_7vol_asphalt_april11_mix1_21.txt
pe(:, :, 21)=Toluene_polyst_7vol_asphalt_april11_mix1_21;

load Toluene_polyst_7vol_asphalt_april11_mix1_22.txt
pe(:, :, 22)=Toluene_polyst_7vol_asphalt_april11_mix1_22;

load Toluene_polyst_7vol_asphalt_april11_mix1_23.txt
pe(:, :, 23)=Toluene_polyst_7vol_asphalt_april11_mix1_23;

load Toluene_polyst_7vol_asphalt_april11_mix1_24.txt
pe(:, :, 24)=Toluene_polyst_7vol_asphalt_april11_mix1_24;
```

```

for j=1:24

    b=['Toluene_polyst_7vol_asphalt_april11_mix1_'
int2str(j) '.txt'];

    try_file(j)=dir(fullfile(b));
    vec(j,:)=try_file(j).date; % load the date and time
when the file was recorded.

end
%-----
load dist_T197Cave0.txt -ASCII % load the variations of
the acoustic path
                                % with elevation

distance=dist_T197Cave0;% variation of the acoustic
path with elevation

[m n]=size(pe(:,:,1));

nFrames=24;

dx=0.3; % elevation between two successive waveforms
L=1:m;
L=dx*(L-1)+1.243; % Elevation vector

ni1=35;
ni2=36;
nf=65;

Hinterface=0.5*(L(ni1)+L(ni2)); % Elevation of the
liquid-liquid interface
Hf=L(nf); % Elevation of the air-
liquid interface

R=1-Hinterface/Hf; % Upper phase volume
fraction

aviobj=avifile('Speed_April11_mix1.avi','fps',2);
%creates AVI file, test.avi
hf= figure('color',[1 1 1],'visible','off'); %turns
visibility of figure off
hax=axes;

```

```

% This loop produces a video of the variations of the
speed of sound
% profile with time

for j=1:nFrames %numframes
    matrix=pe(:, :, j);

    % Determine the speed of sound and the time
    difference between the first and second reflected
    waveforms at any elevation and time

    [c(:, j) To(:, j)]=speedofsound_Time(matrix,distance);

    % Plot the speed of sound with the position of the
    liquid-liquid and
    % air-liquid interfaces
    plot(c(:, j), L, 'k+');hold on;
    plot([1335 1360],[Hinterface Hinterface], 'k:');hold
on;
    plot([1335 1360],[Hf Hf], 'k:');

    xlim([1335 1360])
    ylim([0. L(length(L))])
    set(gca, 'FontSize', 16)
    ylabel('Elevation (mm) ')
    xlabel('Speed of sound (m/s) ')
    % Display the date and time of the measurement
    title(num2str(vec(j, :)));hold off;

    aviobj=addframe(aviobj, hf); %adds frames to the AVI
file
    hold off;
end

aviobj=close(aviobj); %closes the AVI file
close(hf); %closes the handle to invisible figure

% Calculate the speed of sound just after mixing at t=0
min
format bank
plot(c(1:nf-3, 1), 'k+');hold on;
umix=mean(c(1:nf-3, 1));

%%-- Attenuation -----
%---Calculate the attenuation spectra at time t=0 min:
npos_final=length(L);

```

```

    dt1=To(:,1);
    pe1=pe(:, :,1);
    T=1.e-8;
    Fs=1/T;
    [attenuation_frame1 f Imax1 fmax_frame1
attenuationmax_frame1]=...

Attenuation_formovie2_testfig(npos_final,T,Fs,dt1,pe1);
%-----

aviobj=avifile('Attenuation_April11_mix1_without.avi','
fps',2); %creates AVI file, test.avi
hf=figure('color',[1 1 1],'visible','off'); %turns
visibility of figure off
hax=axes;

% This loop produces a video of the variations of the
attenuation spectra
% with time

for j=1:nFrames
    dt1=To(:,j);% Time difference between first and
second echoes
    pe1=pe(:, :,j); % Waveform at time corresponding to
index j

    % Calculation of the attenuation spectra
    [attenuation f Imax fmax
attenuationmax]=Attenuation_formovie2_testfig...
        (npos_final,T,Fs,dt1,pe1);

    % Elevation (mm)
    x=L;

    % Frequency (MHz)
    y=f(1,:)*1e-6;

    % Calculation of the attenuation difference spectra
    z=attenuation'-attenuation_frame1';

    clim = [-1.0 1.0];
    imagesc(y,x,z',clim);hold on;

    set(gca,'ydir','normal','FontSize',16)

    title(num2str(vec(j,:)));

```

```

axis([3 10 0 x(length(x))])
ylabel('Elevation (mm) ');
xlabel('Frequency (MHz) ');
colorbar;
% Display the date and time of the measurement
title(num2str(vec(j,:)));
colormap(jet)

for k=1:113
    zf(j,k)=z(11,k);
end

aviobj=addframe(aviobj,hf); %adds frames to the AVI
file
hold off;
end

aviobj=close(aviobj); %closes the AVI file
close(hf); %closes the handle to invisible figure

%---
aviobj=avifile('Attenuation_April11_mix1_freq.avi','fps
',2); %creates AVI file, test.avi
hf2=figure('color',[1 1 1],'visible','off'); %turns
visibility of figure off
hax=axes;

for j=1:nFrames %numframes
    plot(zf(j,:),L,'k','Linewidth',2);hold on;
    plot([-10 10],[Hinterface Hinterface],'k:');hold on;
    plot([-10 10],[Hf Hf],'k:');

    set(gca,'ydir','normal','FontSize',16)

    xlabel('Attenuation (dB) ');
    ylabel('Elevation (mm) ');
    title(num2str(vec(j,:)));
    xlim([-10 10]);
    ylim([0 L(length(L))])
    aviobj=addframe(aviobj,hf2); %adds frames to the AVI
file
    hold off;

end

aviobj=close(aviobj); %closes the AVI file
close(hf2); %closes the handle to invisible figure

```

```

%-----
%-----

n_ps=11;% time index at which complete phase separation
was obtained

% This loop determine the variations of the liquid-
liquid interface and
% air-liquid interfaces with time

for j=n_ps:nFrames

% look for liquid-liquid interface
for k=ni1-5:ni2+5
    if abs(c(k,j)-c(k-1,j))>1.5
        nit1=k-1;
        nit2=k;
        H_interfacetime(j)=0.5*(L(nit1)+L(nit2));
        break
    end
end

% look for air-liquid interface
for k=nf-5:nf+5

    if abs(c(k,j)-c(k-1,j))>2.
        nft=k-1;
        H_ftime(j)=L(nft);
        break
    end

end

% Calculate the speed of sound in the separated
phases and the speed of
% sound difference between the separated phases

delta_c(j)=mean(c(1:nit1-3,j))-mean(c(nit2+3:nft-
1,j));
V1(j)=mean(c(1:nit1-3,j));
V2(j)=mean(c(nit2+3:nft-1,j));

end
%---

```

```

% Convert the time of the first measurement to minutes
V0=datevec(vec(1,:));
time0=V0(4)*60+V0(5)+(V0(6)/60);

% Converts all times to minutes
time=zeros(1,nFrames);

for j=1:nFrames

    V=datevec(vec(j,:));
    time(j)=V(4)*60+V(5)+(V(6)/60);
end

time(20:nFrames)=time(20:nFrames)+24*60;

% Calculate the relative time in minutes from the first
measurement
%at t=0 min

dtime=time-time0;

% Plot the variations of the liquid-liquid and air-
liquid interfaces with time:

figure('color',[1 1 1]);
semilogx(dtime(n_ps:nFrames),H_interfacetime(n_ps:nFrames),
'k+', 'Linewidth',2);hold on;
semilogx(dtime(n_ps:nFrames),H_ftime(n_ps:nFrames),'kx'
, 'Linewidth',2);hold on;
ylim([0. L(length(L))]);
set(gca,'FontSize',16);
ylabel('Elevation (mm) ');
xlabel('time (min) ')

% Plot the variations of the speed of sound difference
between the separated phases with time:

figure('color',[1 1 1]);
semilogx(dtime(n_ps:nFrames),delta_c(n_ps:nFrames),'k+'
, 'Linewidth',2),hold on;
set(gca,'FontSize',16);
ylabel('\Delta u(m/s)');
xlabel('time (min) ')
ylim([0 5]);

```

```

% Plot the variations of the speeds of sound in the
separated phases with
% time:

figure('color',[1 1 1]);
semilogx(dtime(n_ps:nFrames),V1(n_ps:nFrames),'ko','Lin
ewidth',1.),hold on;
semilogx(dtime(n_ps:nFrames),V2(n_ps:nFrames),'k^','Lin
ewidth',1.),hold on;
set(gca,'FontSize',16);
ylabel('u(m/s)');
xlabel('time (min) ');

% This function calculates the speed of sound and time
difference between
% the first and second reflected waveforms

function [c,To]=speedofsound_Time(pe,distance)

% Input parameters:
% pe: waveform at fixed elevation
% distance: acoustic path at fixed elevation

% Output parameters:
% c: speed of sound
% To: time difference between the first and the second
echoes

Fs = 100e6; % Sampling frequency
T = 1/Fs; % Sample time

for k=1:113

[ACF,Lags,Bounds]=autocorr(pe(k,:),length(pe(k,:))-1);
istart=2000;
[v,index]=max(ACF(istart:length(ACF)));
index=index+istart-2; % Lags start by 0
To(k)=Lags(index)*T;
c(k)=2*distance(k)/To(k);

end

return

```

```

% This function calculates the attenuation spectra

function [attenuation frequency I_max fmax
attenuationmax]=...

Attenuation_formovie2_testfig(npos_final,T,Fs,dt1,pe1)

% Input parameters:

% npos_final total number of waveforms at any given
time
% Fs : frequency of the recording (100 MHz)
% T: time difference between two data point (1/Fs)
% dt1: time difference between two reflections
% pe1: waveform

% Output parameters:
% attenuation: attenuation
% frequency: frequency
% I_max: index at maximum spectra of the first
reflection
% fmax: frequency at maximum spectra of the first
reflection
% attenuationmax: attenuation at fmax

for npos=1:npos_final

dty1=floor(dt1(npos)*Fs); % estimates the time index
difference
                                % between two successive
reflections

y1=pe1(npos,:); %

%-----

[pemax Imax]=max(abs(y1(1:length(y1))));

% Identify the first reflected waveform and its
duration between time1 and
% time2

for kk=1:length(y1)
    if abs(y1(kk))>1000
        break
    end
end

```

```

end

time1=kk-5;
time2=time1+90;

if (time1<=0) || (time2>=length(y1))
    time1=800;
    time2=time1+90;
end

% First reflected waveform:
w11=y1(time1:time2);%

% Second reflected waveform:
w21=y1(time1+dtY1:min(time2+dtY1,length(y1)));% Echo

% This is useful when the signal is noise
if time2+dtY1>length(y1)
    w21=w11
end

time=1:length(w11);
T=1/Fs;
time=T*time;

%*****
%*****
L = length(w11);           % Length of signal
t = (0:L-1)*T;           % Time vector

NFFT = 2^nextpow2(L);% Next power of 2 from length of
Y

f = Fs/2*linspace(0,1,NFFT/2);% Frequency vector
%-----
coefficent=(10.);

u=w11; % first reflection
y=w21; % second reflection

W11_ = fft(w11,NFFT)/L;
W21_ = fft(w21,NFFT)/L;

W11=abs(W11_(1:NFFT/2)); % Frequency spectra of first
reflection
W21=abs(W21_(1:NFFT/2)); % Frequency spectra of the

```

```
second reflection
```

```
% Calculation of the attenuation spectra
```

```
attenuation1=-
```

```
coefficent.*(log10(abs(W21(1:NFFT/2)./W11(1:NFFT/2))));
```

```
[W11max Imax]=max(W11);
```

```
I_max(npos)=Imax;
```

```
attenuation(npos,:)=attenuation1;
```

```
frequency(npos,:)=f;
```

```
%-----
```

```
fmax(npos)=f(Imax);
```

```
attenuationmax(npos)=attenuation(npos,Imax);
```

```
end
```

Appendix F. Matlab Code for the Calculation of the Composition and the Speed of Sound in the Separated Phases

```
% This code calculates the composition of the separated
phases using the variations of the upper phase volume
fraction along the three dilution lines

clear all;
close all;

% load experimental dilution lines:

load mydilution1_philphi2.txt -ASCII
load mydilution2_philphi2.txt -ASCII
load mydilution3_philphi2.txt -ASCII

mydilution1_philphi2=mydilution1_philphi2';
mydilution2_philphi2=mydilution2_philphi2';
mydilution3_philphi2=mydilution3_philphi2';

% perform scaling transformation of the dilution lines
by gama in eta direction:

mydilution1_philphi2(:,1)=mydilution1_philphi2(:,1);
mydilution2_philphi2(:,1)=mydilution2_philphi2(:,1);
mydilution3_philphi2(:,1)=mydilution3_philphi2(:,1);

% Load experimental variations of the volume fraction
of the upper phase along the three dilution lines

load R_mydilution1.txt -ASCII
load R_mydilution2.txt -ASCII
load R_mydilution3.txt -ASCII

R_mydilution1=R_mydilution1';
R_mydilution2=R_mydilution2';
R_mydilution3=R_mydilution3';

% perform scaling transformation of the dilution lines
by gama in eta direction:

R_mydilution1(:,1)=R_mydilution1(:,1);
R_mydilution2(:,1)=R_mydilution2(:,1);
R_mydilution3(:,1)=R_mydilution3(:,1);

% Calculation of the ratio polystyrene/asphaltene
volume fractions along the dilution lines:
```

```

cp=max(mydilution1_philphi2(:,2))./max(mydilution1_phi1
phi2(:,1));
cq=max(mydilution2_philphi2(:,2))./max(mydilution2_phi1
phi2(:,1));
cr=max(mydilution3_philphi2(:,2))./max(mydilution3_phi1
phi2(:,1));

% Discretize the interfaces along the dilution lines in
eta direction
vecphi_1P=min(R_mydilution1(:,1)):0.001:max(R_mydilutio
n1(:,1));
vecphi_1Q=min(R_mydilution2(:,1)):0.001:max(R_mydilutio
n2(:,1));
vecphi_1R=min(R_mydilution3(:,1)):0.001:max(R_mydilutio
n3(:,1));

% Fit the variations of the volume fraction of the
upper phase with a first order exponential function:

xdata1=R_mydilution1(:,1);ydata1=R_mydilution1(:,2);
[estimates1, model] = fitcurvedemo(xdata1, ydata1);
[sse, FittedCurve1] = model(estimates1);

xdata2=R_mydilution2(:,1);ydata2=R_mydilution2(:,2);
[estimates2, model] = fitcurvedemo(xdata2, ydata2);
[sse, FittedCurve2] = model(estimates2);

xdata3=R_mydilution3(:,1);ydata3=R_mydilution3(:,2);
[estimates3, model] = fitcurvedemo(xdata3, ydata3);
[sse, FittedCurve3] = model(estimates3);

vecR_phi_P=spline(R_mydilution1(:,1),FittedCurve1,vecph
i_1P);
vecR_phi_Q=spline(R_mydilution2(:,1),FittedCurve2,vecph
i_1Q);
vecR_phi_R=spline(R_mydilution3(:,1),FittedCurve3,vecph
i_1R);

figure('color',[1 1 1]);
plot(R_mydilution1(:,1),R_mydilution1(:,2),'k+');hold
on;

plot(vecphi_1P,vecR_phi_P,'k--');hold on;

```

```

plot(R_mydilution2(:,1),R_mydilution2(:,2),'k+');hold
on;
plot(vecphi_1Q,vecR_phi_Q,'k--');hold on;

plot(R_mydilution3(:,1),R_mydilution3(:,2),'k+');hold
on;
plot(vecphi_1R,vecR_phi_R,'k--');hold on;

set(gca,'FontSize',16);
ylim([0 1])
xlabel('\eta','FontSize',16);
ylabel('R','FontSize',16);

%-----
% parameters of the minimization procedure for the
objective function:
opts.tol=1.e-8;
opts.maxevals=61000;%maximum number of function
evaluations
opts.maxits=2000;%number of iterations
opts.maxdeep=100;%
opts.globalmin=0.;

% Lower and upper bounds for n: the slope and L: the
length of the tie lines:

lb=[-10. 0.];
ub=[0. 1.];

bounds(:,1)=lb;
bounds(:,2)=ub;

% Define vector eta along which the loop is performed
along dilution line p:

vector_phil_P=0.080:0.0034:0.097;
vector_phil_P=vector_phil_P;

% Loop moving along dilution line p to calculate
binodal points

for j=1:length(vector_phil_P)

% Coordonates of point P in dilution line p:
phil_P=vector_phil_P(j);

```

```

eta_P(j)=phil_P;

% Minimize the objective function defined in equation
(2.40) to obtain the
% length L and slope n of the tie line:

myfunc=@(x)
object_function2(x,phil_P,cp,vecphi_1P,vecR_phi_P,...
    cq,vecphi_1Q,vecR_phi_Q,cr,vecphi_1R,vecR_phi_R)

Problem.f=myfunc;
[ret_minval(j),final_xatmin,history] =
Direct(Problem,bounds,opts);

    n(j)=final_xatmin(1) ;
    L=final_xatmin(2);

    d(j)=(cp-n(j))*phil_P;
%-----
----

% Calculate eta at the binodal for the three different
dilution lines:

%-- Dilution line p:
[vec indexp]=min(abs(vecphi_1P-phil_P))
fpP=vecR_phi_P(indexp);
phil_betaI(j)=phil_P+((fpP*L)/sqrt(n(j)^2+1));
phil_alfaI(j)=phil_P-((1-fpP)*L/sqrt(n(j)^2+1));

%-- Dilution line q:

phil_Q=((cp-n(j))/(cq-n(j)))*phil_P;

eta_Q(j)=phil_Q;

[vec indexq]=min(abs(vecphi_1Q-phil_Q));
fqQ=vecR_phi_Q(indexq);

phil_betaII(j)=phil_P*((cp-n(j))/(cq-
n(j)))+(fqQ*L/sqrt(n(j)^2+1));
phil_alfaII(j)=phil_P*((cp-n(j))/(cq-n(j)))-((1.-
fqQ)*L/sqrt(n(j)^2+1));

%-- Dilution line r:

phil_R=((cp-n(j))/(cr-n(j)))*phil_P;

eta_R(j)=phil_R;

```

```

[vec indexr]=min(abs(vecphi_1R-phil_R));
frR=vecR_phi_R(indexr);

phil_betaIII(j)=phil_P*((cp-n(j))/(cr-
n(j)))+(frR*L/sqrt(n(j)^2+1));
phil_alfaIII(j)=phil_P*((cp-n(j))/(cr-n(j)))-((1.-
frR)*L/sqrt(n(j)^2+1));

%---

phil_alfa_mean(j)=(phil_alfaI(j)+phil_alfaII(j)+phil_al
faIII(j))/3.;
phil_beta_mean(j)=(phil_betaI(j)+phil_betaII(j)+phil_be
taIII(j))/3.;

end
%-----
-----% plot the phase diagram:

figure('color',[1 1 1])

for j=1:length(phil_alfa_mean)

plot([phil_alfa_mean(j) phil_beta_mean(j)],...
      [d(j)+n(j)*phil_alfa_mean(j)
d(j)+n(j)*phil_beta_mean(j)], 'ko', ...
      'Linewidth',2);hold on;

plot([phil_alfa_mean(j) phil_beta_mean(j)],...
      [d(j)+n(j)*phil_alfa_mean(j)
d(j)+n(j)*phil_beta_mean(j)], 'k:');

Xmean(j)=0.5*(phil_alfa_mean(j)+phil_beta_mean(j));
Ymean(j)=0.5*(d(j)+n(j)*phil_alfa_mean(j)+d(j)+n(j)*phi
l_beta_mean(j));

      hold on;

plot([phil_alfaI(j) phil_betaI(j)],...
      [d(j)+n(j)*phil_alfaI(j)
d(j)+n(j)*phil_betaI(j)], 'kx');...
      hold on;

plot([phil_alfaII(j) phil_betaII(j)],...
      [d(j)+n(j)*phil_alfaII(j)
d(j)+n(j)*phil_betaII(j)], 'kx');...

```

```

    hold on;

    plot([phi1_alfaII(j) phi1_alfaIII(j)],...
         [d(j)+n(j)*phi1_alfaII(j)
          d(j)+n(j)*phi1_alfaIII(j)], 'k:');...
    hold on;

    plot([phi1_betaII(j) phi1_betaIII(j)],...
         [d(j)+n(j)*phi1_betaII(j)
          d(j)+n(j)*phi1_betaIII(j)], 'k:');...
    hold on;

    plot([phi1_alfaIII(j) phi1_betaIII(j)],...
         [d(j)+n(j)*phi1_alfaIII(j)
          d(j)+n(j)*phi1_betaIII(j)], 'kx');...
    hold on;

end

hold on;

% plot median of tie lines:
p=polyfit(Xmean,Ymean,1);
xmean=0.12:0.001:0.2;
plot(xmean,p(1)*xmean+p(2), 'k--');hold on;

% plot experimental phase diagram:
Experimental_phase_diagram_final_MW390000_withrrorbars
hold on;

% plot dashed lines along the dilution lines:
plot([0 max(mydilution1_philphi2(:,1))],[0
max(mydilution1_philphi2(:,2))], 'k--');hold on;
plot(mydilution1_philphi2(:,1),mydilution1_philphi2(:,2)
), 'k. ');hold on;

plot([0 max(mydilution2_philphi2(:,1))],[0
max(mydilution2_philphi2(:,2))], 'k--');hold on;
plot(mydilution2_philphi2(:,1),mydilution2_philphi2(:,2)
), 'k. ');hold on;

plot([0 max(mydilution3_philphi2(:,1))],[0
max(mydilution3_philphi2(:,2))], 'k--');hold on;
plot(mydilution3_philphi2(:,1),mydilution3_philphi2(:,2)
), 'k. ');hold on;

set(gca, 'FontSize', 16);

```

```

xlabel( '\eta', 'FontSize', 16);
ylabel( '\Phi', 'FontSize', 16);

%-----
-----% Calculated and plot results corresponding to the
case where only a fraction of asphaltene are colloidal
particles:

fraction=1.;
[www]=ploting_binodals_speeds_Mw390000(fraction,eta_alf
a,fi_alfa,eta_beta,fi_beta,eta_Q,eta_P,eta_R,cq,cp,cr,e
ta_alfaI,fi_alfaI,eta_alfaII,fi_alfaII,eta_alfaIII,fi_a
lfaIII,eta_betaI,fi_betaI,eta_betaII,fi_betaII,eta_beta
III,fi_betaIII)

```

```
% This function was used in the minimization procedure
for the calculation of the binodal points
```

```
Function
```

```
[Obj]=object_function2(x,phil_P,cp,vecphi_1P,vecR_phi_P
, ...
    cq,vecphi_1Q,vecR_phi_Q,cr,vecphi_1R,vecR_phi_R)
```

```
% Objective function (eq.2.40).
```

```
% Input parameters:
```

```
n=x(1); % slope of tie line
```

```
L=x(2); % length of tie line
```

```
% phil_P: eta coordonate along dilution line p
```

```
% cp: ratio polystyrene/asphaltene volume fraction
```

```
% vecphi_1P: discretized vector eta along dilution line
```

```
p
```

```
% vecR_phi_P: Volume fraction of upper phase along
dilution line p
```

```
% cq: ratio polystyrene/asphaltene volume fraction
```

```
% vecphi_1Q: discretized vector eta along dilution line
```

```
q
```

```
% vecR_phi_Q: Volume fraction of upper phase along
dilution line q
```

```
% cr: ratio polystyrene/asphaltene volume fraction
```

```
% vecphi_1R: discretized vector eta along dilution line
```

```
r
```

```
% vecR_phi_R: Volume fraction of upper phase along
dilution line r
```

```
%-- Dilution line p:
```

```
% eta coordonates at the binodal:
```

```
[vec indexp]=min(abs(vecphi_1P-phil_P));
```

```
fpP=vecR_phi_P(indexp);
```

```
phil_betaI=phil_P+((fpP*L)/sqrt(n^2+1));
```

```
phil_alfaI=phil_P-((1-fpP)*L/sqrt(n^2+1));
```

```
%-- Dilution line q:
```

```
% eta coordonates at the binodal:
```

```
phil_Q=((cp-n)/(cq-n))*phil_P;
```

```
[vec indexq]=min(abs(vecphi_1Q-phil_Q));
```

```
fqQ=vecR_phi_Q(indexq);
```

```
phil_betaII=phil_P*((cp-n)/(cq-n))+(fqQ*L/sqrt(n^2+1));
```

```

phil_alfaII=phil_P*((cp-n)/(cq-n))-((1.-
fqQ)*L/sqrt(n^2+1));

%-- Dilution line r:
% eta coordonates at the binodal:

phil_R=((cp-n)/(cr-n))*phil_P;
[vec indexr]=min(abs(vecphi_1R-phil_R));
frR=vecR_phi_R(indexr);

phil_betaIII=phil_P*((cp-n)/(cr-
n))+(frR*L/sqrt(n^2+1));
phil_alfaIII=phil_P*((cp-n)/(cr-n))-((1.-
frR)*L/sqrt(n^2+1));

% -- Calculate average eta at binodal points:

phil_alfa_mean=(phil_alfaI+phil_alfaII+phil_alfaIII)/3.
;%
phil_beta_mean=(phil_betaI+phil_betaII+phil_betaIII)/3.
;%

% Calculate the objective function:

Obj_alfaI=((n^2+1)*(phil_alfaI-phil_alfa_mean))^2.;
Obj_alfaII=((n^2+1)*(phil_alfaII-phil_alfa_mean))^2.;
Obj_alfaIII=((n^2+1)*(phil_alfaIII-phil_alfa_mean))^2.;

Obj_alfa=Obj_alfaI+Obj_alfaII+Obj_alfaIII;%+Obj_alfaIV;

Obj_betaI=((n^2+1)*(phil_betaI-phil_beta_mean))^2.;
Obj_betaII=((n^2+1)*(phil_betaII-phil_beta_mean))^2.;
Obj_betaIII=((n^2+1)*(phil_betaIII-phil_beta_mean))^2.;

Obj_beta=Obj_betaI+Obj_betaII+Obj_betaIII;%+Obj_betaIV;

Obj=Obj_alfa+Obj_beta;

d=(cp-n)*phil_P;

% Phi coordonates at binodal points:

phi2_alfaI=d+n*phil_alfaI;
phi2_alfaII=d+n*phil_alfaII;
phi2_alfaIII=d+n*phil_alfaIII;

```

```

phi2_betaI=d+n*phi1_betaI;
phi2_betaII=d+n*phi1_betaII;
phi2_betaIII=d+n*phi1_betaIII;

if
((phi1_betaI<=0)|| (phi1_alfaI<=0)|| (phi1_betaII<=0)|| (p
hi1_alfaII<=0)...
    || (phi1_betaIII<=0)|| (phi1_alfaIII<=0))
    Obj=1000000;
elseif
((phi2_betaI<=0)|| (phi2_alfaI<=0)|| (phi2_betaII<=0)|| ..
.

(phi2_alfaII<=0)|| (phi2_betaIII<=0)|| (phi2_alfaIII<=0))
    Obj=1000000;
end

return

```

```

% This function was used for the calculation of the
coefficients A's in the binary mixtures by minimizing
the standard deviation

function
[w]=Objective_function(A,frac1,frac2,speed_asph_tol,spe
ed_asph,speed_tol)

A0=A(1);
A1=A(2);
A2=A(3);
A3=A(4);

y_RK=(frac1.*frac2).*(A0+A1.*(frac1-frac2)+A2.*(frac1-
frac2).^2+A3.*(frac1-frac2).^3);

N=length(speed_asph_tol);

% standard deviation
w=(sum((speed_asph_tol-frac1.*speed_asph-
frac2*speed_tol-y_RK).^2)/N).^(0.5);

% This function calculates the difference between
calculated speed of sound and volume average speed of
sound

function [y_RK]=Redlich_Kister(A,frac1,frac2)

A0=A(1);
A1=A(2);
A2=A(3);
A3=A(4);

y_RK=(frac1.*frac2).*(A0+A1.*(frac1-frac2)+A2.*(frac1-
frac2).^2+A3.*(frac1-frac2).^3);%

```

```

% This function was used for the calculation of the
coefficients B's in the binary mixtures by minimizing
the standard deviation
function
[w]=Objective_function_ternary(B,Abin12,Abin13,Abin23,f
rac1,frac2,u_asph_polyst_tol,u_asph,u_polyst,u_tol)
% 1: asphaltene
% 2: polystyrene
% 3: toluene
frac3=1.-frac1-frac2;

B1=B(1);
B2=B(2);
B3=B(3);

A0_12=Abin12(1);
A1_12=Abin12(2);
A2_12=Abin12(3);
A3_12=Abin12(4);

A0_13=Abin13(1);
A1_13=Abin13(2);
A2_13=Abin13(3);
A3_13=Abin13(4);

A0_23=Abin23(1);
A1_23=Abin23(2);
A2_23=Abin23(3);
A3_23=Abin23(4);

uE_bin12=(frac1.*frac2).*(A0_12+A1_12*(frac1-
frac2)+A2_12*(frac1-frac2).^2+A3_12*(frac1-frac2).^3);

uE_bin13=(frac1.*frac3).*(A0_13+A1_13*(frac1-
frac3)+A2_13*(frac1-frac3).^2+A3_13*(frac1-frac3).^3);

uE_bin23=(frac2.*frac3).*(A0_23+A1_23*(frac2-
frac3)+A2_23*(frac2-frac3).^2+A3_23*(frac2-frac3).^3);

uE_bin=uE_bin12+uE_bin13+uE_bin23;

uE_ternary=uE_bin+(frac1.*frac2).*(1.-frac1-
frac2).*(B1+B2*frac1+B3*frac2);

u_ternary=frac1.*(u_asph)+frac2.*(u_polyst)+frac3.*(u_tol
)+uE_ternary;
N=length(u_asph_polyst_tol);
w=(sum((u_asph_polyst_tol-u_ternary).^2)/N).^0.5);

```

```
% This function calculates the speed of sound in the
ternary mixtures of asphaltene + polystyrene + toluene
```

```
function
```

```
[u_ternary]=Ternary_speed_sound(B,Abin12,Abin13,Abin23,
frac1,frac2,u_asph,u_polyst,u_tol)
```

```
% 1: asphaltene
% 2: polystyrene
% 3: toluene
```

```
frac3=1.-frac1-frac2;
```

```
B1=B(1);
B2=B(2);
B3=B(3);
```

```
A0_12=Abin12(1);
A1_12=Abin12(2);
A2_12=Abin12(3);
A3_12=Abin12(4);
```

```
A0_13=Abin13(1);
A1_13=Abin13(2);
A2_13=Abin13(3);
A3_13=Abin13(4);
```

```
A0_23=Abin23(1);
A1_23=Abin23(2);
A2_23=Abin23(3);
A3_23=Abin23(4);
```

```
uE_bin12=(frac1.*frac2).*(A0_12+A1_12*(frac1-
frac2)+A2_12*(frac1-frac2).^2+A3_12*(frac1-frac2).^3);
```

```
uE_bin13=(frac1.*frac3).*(A0_13+A1_13*(frac1-
frac3)+A2_13*(frac1-frac3).^2+A3_13*(frac1-frac3).^3);
```

```
uE_bin23=(frac2.*frac3).*(A0_23+A1_23*(frac2-
frac3)+A2_23*(frac2-frac3).^2+A3_23*(frac2-frac3).^3);
```

```
uE_bin=uE_bin12+uE_bin13+uE_bin23;
```

```
uE_ternary=uE_bin+(frac1.*frac2).*(1.-frac1-
frac2).*(B1+B2*frac1+B3*frac2);
u_ternary=frac1.*u_asph+frac2.*u_polyst+frac3.*u_tol+uE_t
ernary;
```

```

function [www]=ploting_binodals_speeds_Mw390000
(fraction,eta_alfa,fi_alfa,eta_beta,fi_beta,eta_Q1,et
a_P1,eta_R1,cq,cp,cr,eta_alfaI1,fi_alfaI,eta_alfaII1,fi
_alfaII,eta_alfaIII1,fi_alfaIII,...
eta_betaI1,fi_betaI,eta_betaIII1,fi_betaII,eta_betaIII1,
fi_betaIII)

% This function calculates and plots phase compositions
and speed of sound per phase for the case where only a
fraction of asphaltene are colloidal particles

%=====
% Experimental Global Composition:
eta_exp=1.472e-01;
phi_exp=2.88e-02;

%Experimental Lower phase composition:
etaI=2.005777624579399e-01;
DetaI=0.58*1e-2;
phiI=0.*1e-2;
DphiI=0.67*1e-2;

% Experimental Upper phase composition
etaII=7.402337674553910e-02;
DetaII=0.26*1e-2;
phiII=6.0*1.e-2;
DphiII=0.33*1e-2;
%=====
% Calculation of asphaltene colloidal volume fraction
from the overall asphaltene volume fraction
% Binodal points:

eta_alfa=fraction*eta_alfa1;%
eta_beta=fraction*eta_beta1;%

eta_alfaI=fraction*eta_alfaI1;
eta_alfaII=fraction*eta_alfaII1;
eta_alfaIII=fraction*eta_alfaIII1;

eta_betaI=fraction*eta_betaI1;
eta_betaII=fraction*eta_betaII1;
eta_betaIII=fraction*eta_betaIII1;

% Dilution lines:

% (fraction) of asphaltene colloidal particles
participating in the phase separation mechanism along
the tie lines:

```

```

eta_P=(fraction)*eta_P1; % Colloidal dilution line p
eta_Q=(fraction)*eta_Q1; % Colloidal dilution line q
eta_R=(fraction)*eta_R1; % Colloidal dilution line r

% (1.-fraction) of asphaltene not participating in
the phase separation
% mechanism along the dilution lines:

eta0P=(1.-fraction)*eta_P1; % Dilution line p
eta0Q=(1.-fraction)*eta_Q1; % Dilution line q
eta0R=(1.-fraction)*eta_R1; % Dilution line r

figure('color',[1 1 1]);

for j=1:length(eta_Q)

plot(eta_alfa(j)+eta0Q(j),fi_alfa(j),'ko','LineWidth',1
.);hold on;

plot(eta_beta(j)+eta0Q(j),fi_beta(j),'ko','LineWidth',1
.);hold on;

plot(eta_alfa(j),fi_alfa(j),'ksq','LineWidth',1.);hold
on;

plot(eta_beta(j),fi_beta(j),'ksq','LineWidth',1.);hold
on;
    plot([eta_alfa(j) eta_alfa(j)+eta0Q(j)],[fi_alfa(j)
fi_alfa(j)],'k:');hold on;
    plot([eta_beta(j) eta_beta(j)+eta0Q(j)],[fi_beta(j)
fi_beta(j)],'k:');hold on;
    plot([eta_alfa(j) eta_beta(j)],...
        [fi_alfa(j) fi_beta(j)],'k:');hold on;

    plot([eta_Q(j) eta_Q(j)+eta0Q(j)],[cq*eta_Q1(j)
cq*eta_Q1(j)],'k:');hold on;
    plot([eta_Q(j) eta_Q(j)+eta0Q(j)],[cq*eta_Q1(j)
cq*eta_Q1(j)],'k.','LineWidth',1.5);hold on;

plot([eta_Q(j)+eta0Q(j)],[cq*eta_Q1(j)],'kx','LineWidth
',2);hold on;
end

plot([0. fraction*max(eta_Q1)],[0. cq*max(eta_Q1)],'k--
');hold on;

```

```

plot([0. fraction*max(eta_P1)], [0. cp*max(eta_P1)], 'k--');hold on;
plot([0. fraction*max(eta_R1)], [0. cr*max(eta_R1)], 'k--');hold on;

plot(eta_P, cp*eta_P1, 'k.', 'LineWidth', 1.5);hold on;
plot(eta_R, cr*eta_R1, 'k.', 'LineWidth', 1.5);hold on;

HERRORBAR([etaI etaII], [phiI phiII], [DetaI DetaII], 'b--');hold on;
plot(eta_exp, phi_exp, 'b*', 'Markersize', 12);hold on;
errorbar(etaI, phiI, DphiI, 'b+');hold on;
errorbar(etaII, phiII, DphiII, 'b+');hold on;

HERRORBAR([eta_exp etaI], [phi_exp phiI], [0.58e-2 DetaI], 'b. ');hold on;

errorbar([eta_exp], [phi_exp], [0.25e-2], 'b*', 'Markersize', 12);hold on;

set(gca, 'FontSize', 16);
xlabel('\eta', 'FontSize', 16);
ylabel('\Phi', 'FontSize', 16);
xlim([0 0.25]);
ylim([0 0.06]);
ylim([-0.0005 0.075]);

%----- Coexistence points along dilution line p:

figure('color', [1 1 1]);

for j=1:length(eta_P)

plot(eta_alfa(j)+eta0P(j), fi_alfa(j), 'ko', 'LineWidth', 1.);hold on;

plot(eta_beta(j)+eta0P(j), fi_beta(j), 'ko', 'LineWidth', 1.);hold on;

plot(eta_alfa(j), fi_alfa(j), 'ksq', 'LineWidth', 1.);hold on;
plot(eta_beta(j), fi_beta(j), 'ksq', 'LineWidth', 1.);hold on;
plot([eta_alfa(j) eta_alfa(j)+eta0P(j)], [fi_alfa(j) fi_alfa(j)], 'k:');hold on;

```

```

    plot([eta_beta(j) eta_beta(j)+eta0P(j)], [fi_beta(j)
fi_beta(j)], 'k:');hold on;

    plot([eta_alfa(j) eta_beta(j)], ...
    [fi_alfa(j) fi_beta(j)], 'k:');hold on;

    plot([eta_P(j) eta_P(j)+eta0P(j)], [cp*eta_P1(j)
cp*eta_P1(j)], 'k:');hold on;
    plot([eta_P(j) eta_P(j)+eta0P(j)], [cp*eta_P1(j)
cp*eta_P1(j)], 'k.', 'LineWidth', 1.5);hold on;

plot([eta_P(j)+eta0P(j)], [cp*eta_P1(j)], 'kx', 'LineWidth
', 2);hold on;

end

plot([0. fraction*max(eta_Q1)], [0. cq*max(eta_Q1)], 'k--
');hold on;
plot([0. fraction*max(eta_P1)], [0. cp*max(eta_P1)], 'k--
');hold on;
plot([0. fraction*max(eta_R1)], [0. cr*max(eta_R1)], 'k--
');hold on;

plot(eta_Q, cq*eta_Q1, 'k.', 'LineWidth', 1.5);hold on;
plot(eta_R, cr*eta_R1, 'k.', 'LineWidth', 1.5);hold on;

set(gca, 'FontSize', 16);

xlabel('\eta', 'FontSize', 16);
ylabel('\Phi', 'FontSize', 16);
xlim([0 0.25]);
ylim([0 0.06]);

%%-----
%%----- Coexistence points along dilution line r:

figure('color', [1 1 1]);

for j=1:length(eta_R)

plot(eta_alfa(j)+eta0R(j), fi_alfa(j), 'ko', 'LineWidth', 1
.);hold on;

plot(eta_beta(j)+eta0R(j), fi_beta(j), 'ko', 'LineWidth', 1

```

```

.);hold on;
plot(eta_alfa(j),fi_alfa(j),'ksq','LineWidth',1.);hold
on;
plot(eta_beta(j),fi_beta(j),'ksq','LineWidth',1.);hold
on;
plot([eta_alfa(j) eta_alfa(j)+eta0R(j)],[fi_alfa(j)
fi_alfa(j)],'k:');hold on;
plot([eta_beta(j) eta_beta(j)+eta0R(j)],[fi_beta(j)
fi_beta(j)],'k:');hold on;
plot([eta_alfa(j) eta_beta(j)],...
[fi_alfa(j) fi_beta(j)],'k:');hold on;
plot([eta_R(j) eta_R(j)+eta0R(j)],[cr*eta_R1(j)
cr*eta_R1(j)],'k:');hold on;
plot([eta_R(j) eta_R(j)+eta0R(j)],[cr*eta_R1(j)
cr*eta_R1(j)],'k.','LineWidth',1.5);hold on;
plot([eta_R(j)+eta0R(j)],[cr*eta_R1(j)],'kx','LineWidth
',2);hold on;

end

plot([0. fraction*max(eta_Q1)],[0. cq*max(eta_Q1)],'k--
');hold on;
plot([0. fraction*max(eta_P1)],[0. cp*max(eta_P1)],'k--
');hold on;
plot([0. fraction*max(eta_R1)],[0. cr*max(eta_R1)],'k--
');hold on;

plot(eta_Q,cq*eta_Q1,'k.','LineWidth',1.5);hold on;
plot(eta_P,cp*eta_P1,'k.','LineWidth',1.5);hold on;

set(gca,'FontSize',16);

xlabel('\eta','FontSize',16);
ylabel('\Phi','FontSize',16);
xlim([0 0.25]);
ylim([0 0.06]);

www=0.;

%%%%%%%%%%%%%%%%%%%%%%%%%%%%%%%%%%%%%%%%%%%%%%%%%%%%%%%%%%%%%%%%%%%%%%%%
%%%%%%%%%%%%%%%%%%%%%%%%%%%%%%%%%%%%%%%%%%%%%%%%%%%%%%%%%%%%%%%%%%%%%%%%
%----- Binary asphaltene in toluene:

V_mean=mean([1356.4 1353.4 1357.2 1356.89 1353.57
1354.8]);
eta_mean=mean([23.43 23.43 23.347 23.3475 23.446
23.389]*1.e-2);

```

```

eta=[0 0.0330 0.0765 0.1576 eta_mean];%
speed_asph_tol=[1324.7 1327.9 1332.0 1341.8 V_mean];%

sigma=std([1356.4 1353.4 1357.2 1356.89 1353.57
1354.8],1);

P=polyfit(eta,speed_asph_tol,1); %

speed_asph_fit=P(1)*eta+P(2);

u_asph=P(1)*1+P(2);% Estimate the apparent speed of
sound in asphaltene
u_tol=1324.7;

frac1=eta;
frac2=1.-eta;

% Estimate the coefficient A's for the speed of sound
correlation
Ain=1.*ones(1,4);
myfunc2= @(A)
Objective_function(A,frac1,frac2,speed_asph_tol,u_asph,
u_tol);
[AA
f_minasph]=fminsearch(myfunc2,Ain,optimset('TolX',1.e-
8,'MaxFunEvals',...
1000000,'MaxIter',1000000));
[y_RK]=Redlich_Kister(AA,frac1,frac2);

figure('color',[1 1 1]);

xx=0:0.001:1.;
plot(xx,(xx.*(u_asph)+(1-xx).*(u_tol)),'k--');hold on;

errorbar(eta,speed_asph_tol,[ones(1,length(speed_asph_t
ol)-1) sigma],'k+','markersize',12);hold on;

set(gca,'FontSize',16);
xlabel('\eta');
ylabel('Speed of sound (m/s)');
xlim([0. 1.]);

% Coefficients used for the speed of sound correlation
in the binary
% mixtures of asphaltene in toluene:

Abin13(1)=AA(1);

```

```

Abin13(2)=AA(2);
Abin13(3)=AA(3);
Abin13(4)=AA(4);

%----- Binary Polystyrene in toluene:

Ain=1.*ones(1,4);

phi=[0. 0.0050 0.0100 0.0199 0.0299 0.0401 0.0607
0.0773];
speed_polyst_tol=[1324.1 1324.5 1325.5 1326.7 1328.3
1330.1 1333.1 1337.3]+0.6;

P=polyfit(phi,speed_polyst_tol,1);
%polyfit(eta,(1./speed_asph_tol),1);
speed_polyst_fit=P(1)*phi+P(2);

Output = polyval(P,phi);
Correlation=corrcoef(speed_polyst_tol,Output)

u_polyst=P(1)*1.+P(2);% Apparent speed of sound in
polystyrene

frac1=phi;
frac2=1-phi;

% Estimate the coefficient A's for the speed of sound
correlation

myfunc2 = @(A)
Objective_function(A,frac1,frac2,speed_polyst_tol,u_pol
yst,u_tol);

[AA2
f_minpolyst]=fminsearch(myfunc2,Ain,optimset('TolX',1.e
-8,'MaxFunEvals',1000000,'MaxIter',1000000));

[y_RK2]=Redlich_Kister(AA2,frac1,frac2);

figure('color',[1 1 1]);

plot(phi,speed_polyst_tol,'+');hold on;
plot(phi,frac1.*u_polyst+frac2.*u_tol+y_RK2,'k-');hold
on;

plot(phi,frac1.*u_polyst+frac2.*u_tol,'k--');hold on;

set(gca,'FontSize',16);

```

```

xlabel('\Phi');
ylabel('Speed of sound (m/s)');

% Coefficients used for the speed of sound correlation
in the binary mixtures of asphaltene in toluene:

Abin23(1)=AA2(1);
Abin23(2)=AA2(2);
Abin23(3)=AA2(3);
Abin23(4)=AA2(4);

%-----
%--- Experimental speed of sound data before and after
phase separation:

% dilution line p
eta_p=[0.0978 0.0932 0.0890 0.0852 0.0785 0.0770];
phi_p=[0.0450 0.0429 0.0410 0.0392 0.0361 0.0354];

u_pI=[1346.0 1344.7 1343.4 1342.6 1342.0 1342.4];
u_pII=[1342.7 1341.6 1340.6 1339.7 1339.0 1338.7];

u_p=[1345.0 1343.5 1342.3 1341.3 1340.7 1339.7];

% dilution line r
eta_r=[0.1965 0.1848 0.1673 0.1529 0.1457];
phi_r=[0.0123 0.0115 0.01045 0.0095 0.0091];

u_rI=[1353.6 1351.3 1348.6 1346.8 1344.9];
u_rII=[1349.4 1348.4 1345.9 1344.6 1342.8];

u_r=[1354.2 1351.5 1348.8 1346.6 1345.2];
% dilution line q
eta_q=[0.1478 0.1416 0.1340 0.1273 0.1183 0.1130];

phi_q=[0.0284 0.0272 0.0258 0.0245 0.0227 0.0217];

u_qI=[1349.7 1347.9 1346.1 1345.0 1343.9 1342.5];
u_qII=[1346.1 1345.0 1343.5 1342.7 1342.0 1341.2];

u_q=[1348.6 1347.5 1345.9 1344.6 1343.5 1342.3];

%-----
% Speed of sound data in the ternary asphaltene +
polystyrene + toluene before phase separation:

frac1=[eta_r eta_q eta_p];

```

```

frac2=[phi_r phi_q phi_p];

u_asph_polyst_tol=[u_r u_q u_p];

%-----
% Asphaltene polystyrene:
Abin12(1)=0.;
Abin12(2)=0.;
Abin12(3)=0.;
Abin12(4)=0.;

%-----
% Calculation of the coefficient B's used in the
ternary mixture of asphaltene + polystyrene + toluene
by fitting the speeds of sound before phase separation:

Bin=10.*ones(1,3);
myfunc3=@(B)
Objective_function_ternary(B,Abin12,Abin13,Abin23,frac1
,frac2,u_asph_polyst_tol,u_asph,u_polyst,u_tol);
[BB f_minB]=fminsearch(myfunc3,Bin,optimset('TolX',1.e-
8,'MaxFunEvals',...
10000000,'MaxIter',1000000));

% Calculation of the speed of sound before phase
separation:

[u_ternary_p]=Ternary_speed_sound(BB,Abin12,Abin13,Abin
23,eta_p,phi_p,u_asph,u_polyst,u_tol);
[u_ternary_q]=Ternary_speed_sound(BB,Abin12,Abin13,Abin
23,eta_q,phi_q,u_asph,u_polyst,u_tol);
[u_ternary_r]=Ternary_speed_sound(BB,Abin12,Abin13,Abin
23,eta_r,phi_r,u_asph,u_polyst,u_tol);

% 1: asphaltene
% 2: polystyrene
% 3: toluene

%=====
% Calculation of the speed of sound after phase
separation along dilution line p:

%[umix_P]=Ternary_speed_sound(BB,Abin12,Abin13,Abin23,e
ta0P+eta_P,cp*eta_P1,u_asph,u_polyst,u_tol);

[umix_alfaP]=Ternary_speed_sound(BB,Abin12,Abin13,Abin2
3,eta0P+eta_alfa,fi_alfa,u_asph,u_polyst,u_tol);

```

```

[umix_alfaPI]=Ternary_speed_sound(BB,Abin12,Abin13,Abin
23,eta0P+eta_alfaI,fi_alfaI,u_asph,u_polyst,u_tol);
[umix_alfaPII]=Ternary_speed_sound(BB,Abin12,Abin13,Abi
n23,eta0P+eta_alfaII,fi_alfaII,u_asph,u_polyst,u_tol);
[umix_alfaPIII]=Ternary_speed_sound(BB,Abin12,Abin13,Abi
n23,eta0P+eta_alfaIII,fi_alfaIII,u_asph,u_polyst,u_tol
);

%
[umix_betaP]=Ternary_speed_sound(BB,Abin12,Abin13,Abin2
3,eta0P+eta_beta,fi_beta,u_asph,u_polyst,u_tol);

[umix_betaPI]=Ternary_speed_sound(BB,Abin12,Abin13,Abin
23,eta0P+eta_betaI,fi_betaI,u_asph,u_polyst,u_tol);
[umix_betaPII]=Ternary_speed_sound(BB,Abin12,Abin13,Abi
n23,eta0P+eta_betaII,fi_betaII,u_asph,u_polyst,u_tol);
[umix_betaPIII]=Ternary_speed_sound(BB,Abin12,Abin13,Ab
in23,eta0P+eta_betaIII,fi_betaIII,u_asph,u_polyst,u_tol
);

%Speed of sound difference between the separated phases:

diff_umixP=(umix_betaP-umix_alfaP);

diff_umixPI=(umix_betaPI-umix_alfaPI);
diff_umixPII=(umix_betaPII-umix_alfaPII);
diff_umixPIII=(umix_betaPIII-umix_alfaPIII);

for j=1:length(umix_betaPI)

umix_betaPmax(j)=max([umix_betaPI(j) umix_betaPII(j)
umix_betaPIII(j)]);
umix_betaPmin(j)=min([umix_betaPI(j) umix_betaPII(j)
umix_betaPIII(j)]);
umix_alfaPmin(j)=min([umix_alfaPI(j) umix_alfaPII(j)
umix_alfaPIII(j)]);
umix_alfaPmax(j)=max([umix_alfaPI(j) umix_alfaPII(j)
umix_alfaPIII(j)]);

end

diff_umixPmax=(umix_betaPmax-umix_alfaPmin);
diff_umixPmin=(umix_betaPmin-umix_alfaPmax);

% Calculation of the speed of sound after phase

```

separation along dilution line q:

```
 %[umix_Q]=Ternary_speed_sound(BB,Abin12,Abin13,Abin23,eta0Q+eta_Q,cq*eta_Q1,u_asph,u_polyst,u_tol);
```

```
 [umix_alfaQ]=Ternary_speed_sound(BB,Abin12,Abin13,Abin23,eta0Q+eta_alfa,fi_alfa,u_asph,u_polyst,u_tol);
```

```
 [umix_alfaQI]=Ternary_speed_sound(BB,Abin12,Abin13,Abin23,eta0Q+eta_alfaI,fi_alfaI,u_asph,u_polyst,u_tol);
```

```
 [umix_alfaQII]=Ternary_speed_sound(BB,Abin12,Abin13,Abin23,eta0Q+eta_alfaII,fi_alfaII,u_asph,u_polyst,u_tol);
```

```
 [umix_alfaQIII]=Ternary_speed_sound(BB,Abin12,Abin13,Abin23,eta0Q+eta_alfaIII,fi_alfaIII,u_asph,u_polyst,u_tol);
```

```
 [umix_betaQ]=Ternary_speed_sound(BB,Abin12,Abin13,Abin23,eta0Q+eta_beta,fi_beta,u_asph,u_polyst,u_tol);
```

```
 [umix_betaQI]=Ternary_speed_sound(BB,Abin12,Abin13,Abin23,eta0Q+eta_betaI,fi_betaI,u_asph,u_polyst,u_tol);
```

```
 [umix_betaQII]=Ternary_speed_sound(BB,Abin12,Abin13,Abin23,eta0Q+eta_betaII,fi_betaII,u_asph,u_polyst,u_tol);
```

```
 [umix_betaQIII]=Ternary_speed_sound(BB,Abin12,Abin13,Abin23,eta0Q+eta_betaIII,fi_betaIII,u_asph,u_polyst,u_tol);
```

```
 diff_umixQ=(umix_betaQ-umix_alfaQ);
```

```
 diff_umixQI=(umix_betaQI-umix_alfaQI);
```

```
 diff_umixQII=(umix_betaQII-umix_alfaQII);
```

```
 diff_umixQIII=(umix_betaQIII-umix_alfaQIII);
```

```
 for j=1:length(umix_betaQI)
```

```
 umix_betaQmax(j)=max([umix_betaQI(j) umix_betaQII(j) umix_betaQIII(j)]);
```

```
 umix_betaQmin(j)=min([umix_betaQI(j) umix_betaQII(j) umix_betaQIII(j)]);
```

```
 umix_alfaQmin(j)=min([umix_alfaQI(j) umix_alfaQII(j) umix_alfaQIII(j)]);
```

```
 umix_alfaQmax(j)=max([umix_alfaQI(j) umix_alfaQII(j) umix_alfaQIII(j)]);
```

```
 end
```

```

diff_umixQmax=(umix_betaQmax-umix_alfaQmin);
diff_umixQmin=(umix_betaQmin-umix_alfaQmax);

% Calculation of the speed of sound after phase
separation along dilution line r:

%[umix_R]=Ternary_speed_sound(BB,Abin12,Abin13,Abin23,e
ta0R+eta_R,cr*eta_R1,u_asph,u_polyst,u_tol);

[umix_alfaR]=Ternary_speed_sound(BB,Abin12,Abin13,Abin2
3,eta0R+eta_alfa,fi_alfa,u_asph,u_polyst,u_tol);

[umix_alfaRI]=Ternary_speed_sound(BB,Abin12,Abin13,Abin
23,eta0R+eta_alfaI,fi_alfaI,u_asph,u_polyst,u_tol);
[umix_alfaRII]=Ternary_speed_sound(BB,Abin12,Abin13,Abi
n23,eta0R+eta_alfaII,fi_alfaII,u_asph,u_polyst,u_tol);
[umix_alfaRIII]=Ternary_speed_sound(BB,Abin12,Abin13,Ab
in23,eta0R+eta_alfaIII,fi_alfaIII,u_asph,u_polyst,u_tol
);

[umix_betaR]=Ternary_speed_sound(BB,Abin12,Abin13,Abin2
3,eta0R+eta_beta,fi_beta,u_asph,u_polyst,u_tol);

[umix_betaRI]=Ternary_speed_sound(BB,Abin12,Abin13,Abin
23,eta0R+eta_betaI,fi_betaI,u_asph,u_polyst,u_tol);
[umix_betaRII]=Ternary_speed_sound(BB,Abin12,Abin13,Abi
n23,eta0R+eta_betaII,fi_betaII,u_asph,u_polyst,u_tol);
[umix_betaRIII]=Ternary_speed_sound(BB,Abin12,Abin13,Ab
in23,eta0R+eta_betaIII,fi_betaIII,u_asph,u_polyst,u_tol
);

diff_umixR=(umix_betaR-umix_alfaR);
diff_umixRI=(umix_betaRI-umix_alfaRI);
diff_umixRII=(umix_betaRII-umix_alfaRII);
diff_umixRIII=(umix_betaRIII-umix_alfaRIII);

```

```

for j=1:length(umix_betaRI)

umix_betaRmax(j)=max([umix_betaRI(j) umix_betaRII(j)
umix_betaRIII(j)]);
umix_betaRmin(j)=min([umix_betaRI(j) umix_betaRII(j)
umix_betaRIII(j)]);
umix_alfaRmin(j)=min([umix_alfaRI(j) umix_alfaRII(j)
umix_alfaRIII(j)]);
umix_alfaRmax(j)=max([umix_alfaRI(j) umix_alfaRII(j)
umix_alfaRIII(j)]);

eta_betamax(j)=max([eta_betaI(j) eta_betaII(j)
eta_betaIII(j)]);
eta_betamin(j)=min([eta_betaI(j) eta_betaII(j)
eta_betaIII(j)]);

eta_alfamax(j)=max([eta_alfaI(j) eta_alfaII(j)
eta_alfaIII(j)]);
eta_alfamin(j)=min([eta_alfaI(j) eta_alfaII(j)
eta_alfaIII(j)]);

end

diff_umixRmax=(umix_betaRmax-umix_alfaRmin);
diff_umixRmin=(umix_betaRmin-umix_alfaRmax);

% Volume fraction difference of asphaltene between the
separated phases:

delta_eta=eta_beta-eta_alfa;
delta_etamax=eta_betamax-eta_alfamin;
delta_etamin=eta_betamin-eta_alfamax;

figure('color',[1 1 1]);
plot(eta_P+eta0P,delta_etamin,'k--
','MarkerFaceColor','k');hold on;
plot(eta_P+eta0P,delta_etamax,'k--
','MarkerFaceColor','k');hold on;
plot(eta_P+eta0P,delta_eta,'k-
^','MarkerFaceColor','k');hold on;

plot(eta_Q+eta0Q,delta_etamin,'k--
','MarkerFaceColor','k');hold on;
plot(eta_Q+eta0Q,delta_etamax,'k--
','MarkerFaceColor','k');hold on;
plot(eta_Q+eta0Q,delta_eta,'k-
v','MarkerFaceColor','k');hold on;

```

```

plot(eta_R+eta0R,delta_etamin,'k--
','MarkerFaceColor','k');hold on;
plot(eta_R+eta0R,delta_etamax,'k--
','MarkerFaceColor','k');hold on;
plot(eta_R+eta0R,delta_eta,'k-
sq','MarkerFaceColor','k');hold on;

set(gca,'FontSize',16);

xlabel('\eta','FontSize',16);
ylabel('\Delta \eta','FontSize',16);
legend('Dilution line p','Dilution line q','Dilution
line r');
xlim([0.05 0.25]);
ylim([0. 0.16]);

%-----
load delta_u_aprill_.txt
load delta_u_april7_.txt
load delta_u_aprill1_.txt

eta_aprill=delta_u_aprill_(1,:);
delta_u_aprill=delta_u_aprill_(2,:);

eta_april7=delta_u_april7_(1,:);
delta_u_april7=delta_u_april7_(2,:);

eta_aprill1=delta_u_aprill1_(1,:);
delta_u_aprill1=delta_u_aprill1_(2,:);

%---- Speed of sound difference between the phases:

figure('color',[1 1 1]);

plot(eta_aprill,delta_u_aprill,'k-^',
'MarkerSize',7);hold on;
plot(eta_aprill1,delta_u_aprill1,'k-v',
'MarkerSize',7);hold on;
plot(eta_april7,delta_u_april7,'k-sq',
'MarkerSize',7);hold on;

plot(eta_P1,diff_umixP,'k-
^','MarkerFaceColor','k','Linewidth',1.25);hold on;
plot(eta_P1,diff_umixPmin,'k--
','MarkerFaceColor','k','Linewidth',1.);hold on;
plot(eta_P1,diff_umixPmax,'k--
','MarkerFaceColor','k','Linewidth',1.);hold on;

```

```

plot(eta_Q1,diff_umixQ,'k-
v','MarkerFaceColor','k','Linewidth',1.25);hold on;
plot(eta_Q1,diff_umixQmin,'k--','Linewidth',1.);hold
on;
plot(eta_Q1,diff_umixQmax,'k--','Linewidth',1.);hold
on;

plot(eta_R1,diff_umixR,'k-
sq','MarkerFaceColor','k','Linewidth',1.25);hold on;
plot(eta_R1,diff_umixRmin,'k--','Linewidth',1.);hold
on;
plot(eta_R1,diff_umixRmax,'k--','Linewidth',1.);hold
on;

set(gca,'FontSize',16);

xlabel('\eta','FontSize',16);
ylabel('\Delta u (m/s)','FontSize',16);
legend('Dilution line p','Dilution line q','Dilution
line r');
xlim([0.05 0.25]);
ylim([0. 14.]);

% dilution line p
eta_p=[0.0978 0.0932 0.0890 0.0852 0.0785 0.0770];
phi_p=[0.0450 0.0429 0.0410 0.0392 0.0361 0.0354];

u_pI=[1346.0 1344.7 1343.4 1342.6 1342.0 1342.4];
u_pII=[1342.7 1341.6 1340.6 1339.7 1339.0 1338.7];

u_p=[1345.0 1343.5 1342.3 1341.3 1340.7 1339.7];

% dilution line r
eta_r=[0.1965 0.1848 0.1673 0.1529 0.1457];
phi_r=[0.0123 0.0115 0.01045 0.0095 0.0091];

u_rI=[1353.6 1351.3 1348.6 1346.8 1344.9];
u_rII=[1349.4 1348.4 1345.9 1344.6 1342.8];

u_r=[1354.2 1351.5 1348.8 1346.6 1345.2];

% dilution line q
eta_q=[0.1478 0.1416 0.1340 0.1273 0.1183 0.1130];

phi_q=[0.0284 0.0272 0.0258 0.0245 0.0227 0.0217];

u_qI=[1349.7 1347.9 1346.1 1345.0 1343.9 1342.5];

```

```

u_qII=[1346.1 1345.0 1343.5 1342.7 1342.0 1341.2];
u_q=[1348.6 1347.5 1345.9 1344.6 1343.5 1342.3];

% Plot experiment and calculated speed of sound in the
separated phases
% Along dilution line p:

figure('color',[1 1 1]);
% Experimental speeds of sound in the separated phases:
plot(eta_p,u_pI,'ko',
'MarkerSize',12,'LineWidth',1);hold
on;%, 'MarkerFaceColor','k');hold on;
errorbar(eta_p,u_pI,ones(1,length(eta_p)), 'ko',
'MarkerSize',12);hold on;

plot(eta_p,u_pII,'k^','MarkerSize',12,'LineWidth',1);
hold on;
errorbar(eta_p,u_pII,ones(1,length(eta_p)), 'k^','Marker
Size',12);hold on;
[u_calp]=Ternary_speed_sound(BB,Abin12,Abin13,Abin23,et
a_p,phi_p,u_asph,u_polyst,u_tol);

% Caclulated speed of sound in the separated phases
plot(eta_P+eta0P,umix_alfaP,'k-', 'LineWidth',1.25);hold
on;plot(eta_P+eta0P,umix_alfaPmin,'k--
','LineWidth',1.);hold on;
plot(eta_P+eta0P,umix_alfaPmax,'k--
','LineWidth',1.);hold on;
plot(eta_P+eta0P,umix_betaP,'k', 'LineWidth',1.25);hold
on;
plot(eta_P+eta0P,umix_betaPmin,'k', 'LineWidth',1.);hold
on;
plot(eta_P+eta0P,umix_betaPmax,'k', 'LineWidth',1.);hold
on;

set(gca,'FontSize',16);
xlabel('\eta','FontSize',16);
ylabel('u (m/s)','FontSize',16);
xlim([0.07 0.11])

% Plot experiment and calculated speed of sound in the
separated phases
% Along dilution line r:

```

```

figure('color',[1 1 1]);
% Experimental speeds of sound in the separated phases:
plot(eta_r,u_rI,'ko',
'MarkerSize',12,'LineWidth',1);hold on;
errorbar(eta_r,u_rI,ones(1,length(eta_r)),'ko',
'MarkerSize',12);hold on;

plot(eta_r,u_rII,'k^','MarkerSize',12,'LineWidth',1);hold
on;
errorbar(eta_r,u_rII,ones(1,length(eta_r)),'k^','Marker
Size',12);hold on;

[u_calr]=Ternary_speed_sound(BB,Abin12,Abin13,Abin23,et
a_r,phi_r,u_asph,u_polyst,u_tol);

% Caclulated speed of sound in the separated phases:

plot(eta_R+eta0R,umix_alfaR,'k--
','LineWidth',1.25);hold on;
plot(eta_R+eta0R,umix_alfaRmin,'k--');hold on;
plot(eta_R+eta0R,umix_alfaRmax,'k--');hold on;

plot(eta_R+eta0R,umix_betaR,'k','LineWidth',1.25);hold
on;
plot(eta_R+eta0R,umix_betaRmin,'k');hold on;
plot(eta_R+eta0R,umix_betaRmax,'k');hold on;

set(gca,'FontSize',16);
xlabel('\eta','FontSize',16);
ylabel('u (m/s)','FontSize',16);

% Plot experiment and calculated speed of sound in the
separated phases
% Along dilution line q:

figure('color',[1 1 1]);
% Experimental speeds of sound in the separated phases:

plot(eta_q,u_qI,'ko',
'MarkerSize',12,'LineWidth',1.);hold
on;%, 'MarkerFaceColor','k');hold on;
errorbar(eta_q,u_qI,ones(1,length(eta_q)),'ko',
'MarkerSize',12);hold on;

plot(eta_q,u_qII,'k^','MarkerSize',12,'LineWidth',1.);h
old on;
errorbar(eta_q,u_qII,ones(1,length(eta_q)),'k^',

```

```

'MarkerSize',12);hold on;

[u_calq]=Ternary_speed_sound(BB,Abin12,Abin13,Abin23,et
a_q,phi_q,u_asph,u_polyst,u_tol);

% Caclulated speed of sound in the separated phases
plot(eta_Q+eta0Q,umix_alfaQ,'k--
','LineWidth',1.25);hold on;
plot(eta_Q+eta0Q,umix_alfaQmin,'k--
','LineWidth',1.);hold on;
plot(eta_Q+eta0Q,umix_alfaQmax,'k--
','LineWidth',1.);hold on;

plot(eta_Q+eta0Q,umix_betaQ,'k','LineWidth',1.25);hold
on;
plot(eta_Q+eta0Q,umix_betaQmin,'k','LineWidth',1);hold
on;
plot(eta_Q+eta0Q,umix_betaQmax,'k','LineWidth',1);hold
on;

set(gca,'FontSize',16);
xlabel('\eta','FontSize',16);
ylabel('u (m/s)','FontSize',16);

%=====
% Calculate the speed of sound based from experimental
phase compositions
% and the effect of phase composition error on the
speed of sound:

Ddelta_eta=DetaII+DetaI;

delta_eta=etaI-etaII;

[u_ternary]=Ternary_speed_sound(BB,Abin12,Abin13,Abin23
,eta_exp,phi_exp,u_asph,u_polyst,u_tol)

[u_ternary_Lower]=Ternary_speed_sound(BB,Abin12,Abin13,
Abin23,etaI,phiI,u_asph,u_polyst,u_tol)
[u_ternary_Lower_max]=Ternary_speed_sound(BB,Abin12,Abi
n13,Abin23,etaI+DetaI,phiI+DphiI,u_asph,u_polyst,u_tol)
[u_ternary_Lower_min]=Ternary_speed_sound(BB,Abin12,Abi
n13,Abin23,etaI-DetaI,phiI,u_asph,u_polyst,u_tol)

[u_ternary_Upper]=Ternary_speed_sound(BB,Abin12,Abin13,
Abin23,etaII,phiII,u_asph,u_polyst,u_tol)
[u_ternary_Upper_max]=Ternary_speed_sound(BB,Abin12,Abi
n13,Abin23,etaII+DetaII,phiIII+DphiII,u_asph,u_polyst,u_

```

```

tol)
[u_ternary_Upper_min]=Ternary_speed_sound(BB,Abin12,Abi
n13,Abin23,etaII-DetaII,phiII-
DphiII,u_asph,u_polyst,u_tol)

difference_u=u_ternary_Lower-u_ternary_Upper
difference_u_max=u_ternary_Lower_max-
u_ternary_Upper_min
difference_u_min=u_ternary_Lower_min-
u_ternary_Upper_max
delta_u=u_ternary_Lower-u_ternary_Upper;

h=errorbar([eta_exp],[u_ternary_Lower],[u_ternary_Lower
-u_ternary_Lower_min],[u_ternary_Lower_max-
u_ternary_Lower],'kx','LineWidth',1.1,
'MarkerSize',12);hold on;
errorbar_tick(h,160)

h=errorbar([eta_exp],[u_ternary_Upper],[u_ternary_Upper
-u_ternary_Upper_min],[u_ternary_Upper_max-
u_ternary_Upper],'k*','LineWidth',1.1,
'MarkerSize',12);hold on;
errorbar_tick(h,160)

plot([eta_exp],[u_ternary_Lower],'kx','LineWidth',1.2,
'MarkerSize',12);hold on;
plot([eta_exp],[u_ternary_Upper],'k*','LineWidth',1.2,
'MarkerSize',12);hold on;

%=====

U_upper_exp=1344.9;%m/s
U_lower_exp=1349.1;%m/s
U_mix=1349.6;% m/s

h=errorbar([eta_exp],[U_lower_exp],[1],[1],'ko','LineWi
dth',1., 'MarkerSize',12);hold on;
errorbar_tick(h,60)

h=errorbar([eta_exp],[U_upper_exp],[1],[1],'k^','LineWi
dth',1., 'MarkerSize',12);hold on;
errorbar_tick(h,60)

www=0.;

return

```

Appendix G. Matlab Code for the Calculation of the Phase Diagram of Colloidal Particles + non-adsorbing Polymer

```
close all;
clear all;

% This code calculates the phase diagram for mixtures
of colloidal
% particles and non-adsorbing polymer in good solvent
% using Fleer et al model.

Mw=393400;% Polystyrene molecular weight (g/mol)
a=23.;% Colloidal particle radius(nm)
Rg=0.012*(Mw^0.595);% Radius of giration of the polymer
(nm)
NA=6.0221417930e23; % Avogrado number
Cp_over=3*Mw/(4.*pi*((Rg*1.e-9)^3)*NA);% Polymer
overlap concentration
phi_over=Cp_over/(1.047e6);% Polymer overlap volume
fraction

qR=Rg/a;
qR_star=0.388;
qR_tilda=qR/qR_star;

Y_star=1.464;
eta_star=0.317;
f_star=eta_star/(1-eta_star);
eta_stars=0.594;
f_stars=eta_stars/(1-eta_stars);
    %----- parameters for minimization:
opts.tol=1.e-8;
opts.maxevals=100;
opts.maxits=100;
opts.maxdeep=100;
opts.globalmin=0.;

fs_star=1.465;

%----- Critical Point Calculation -----

myfunc_crit = @(vec)integ_object_critical(vec,qR);

X0=[Y_star f_star];
```

```

[X
f_valX]=fminsearch(myfunc_crit,X0,optimset('TolX',1e-
8,'MaxFunEvals',...
    10000,'MaxIter',10000))

Yc=X(1);
fcritical=X(2);

%-----
%----- Triple Point Calculation -----

%fcritical=fc;

lb=[Y_star 1.18 0. fcritical];
ub=[1.6*Y_star fs_star fcritical 0.97];
bounds_triple(:,1)=lb;
bounds_triple(:,2)=ub;

opts.tol=1.e-8;
opts.maxevals=10000;
opts.maxits=1000;
opts.maxdeep=100;
opts.globalmin=0.;

myfunc_triple = @(vec)Obj_triple_integr(vec,qR);
Problem.f=myfunc_triple;

[ret_minval,final_xatmin,history_triple]=Direct(Problem
,bounds_triple,opts)

history_triple(:,3)
Y_trip=final_xatmin(1);
fs_trip=final_xatmin(2)
fg_trip=final_xatmin(3)
fl_trip=final_xatmin(4)

fL2triple=fl_trip;
fL1triple=fg_trip;

%----- LS calculations -----
gama=0.77;
etasmin=0.542;
fsmin=etasmin/(1.-etasmin);
opts.maxevals=1000;

fs=fsmin:0.05:1.6;

```

```

if (abs(fL2triple-fL1triple)>0.001) % If there is
triple point

    lb=[0.4*Y_star fL2triple];
    ub=[1.6*Y_star 0.970];
    bounds_L(:,1)=lb;
    bounds_L(:,2)=ub;

for j=1:length(fs)

    fsj=fs(j)

    if (fs(j)>fs_trip)
        lb=[0.4*Y_star 0.0000000001];
        ub=[1.6*Y_star fL1triple];
        bounds_L(:,1)=lb;
        bounds_L(:,2)=ub;
    end

    myfunc_LS=@(vec) Obj_LS_integr(vec,fs(j),qR);

    Problem.f=myfunc_LS;

[ret_minval,final_xatmin,history]=Direct(Problem,bounds
_L,opts)

    Y_LS(j)=final_xatmin(1);
    y_LS(j)=Y_LS(j)./(qR^(-1./gama));
    fLeq(j)=final_xatmin(2);

end

else % No triple point

    lb=[0.4*Y_star 0.];
    ub=[1.6*Y_star 0.970];
    bounds_L(:,1)=lb;
    bounds_L(:,2)=ub;

    for j=1:length(fs)
        fsj=fs(j)
        myfunc_LS=@(vec) Obj_LS_integr(vec,fs(j),qR);
        Problem.f=myfunc_LS;

[ret_minval,final_xatmin,history]=Direct(Problem,bounds
_L,opts)

```

```

        Y_LS(j)=final_xatmin(1);
        y_LS(j)=Y_LS(j)./(qR^(-1./gama));
        fLeq(j)=final_xatmin(2);

    end

end

%-----
%-- Colloidal Gas- Colloidal Liquid calculations:

if (abs(fL2triple-fL1triple)>0.001)

    lb=[0.4*Y_star 0.];
    ub=[1.6*Y_star fcritical];

    bounds(:,1)=lb;
    bounds(:,2)=ub;

    opts.tol=1.e-8;
    opts.maxevals=5000;
    opts.maxits=5000;
    opts.maxdeep=50;
    opts.globalmin=0.;

    etasmin=0.542;

    fsmin=etasmin/(1.-etasmin);

    fLvec2=fcritical:0.01:fL2triple;

    for j=1:length(fLvec2)

        myfunc_LL= @(vec)
Obj_LL_integr(vec,fLvec2(j),qR);

        Problem.f=myfunc_LL;

[ret_minval,final_xatmin,history]=Direct(Problem,bounds
,opts)

        Y_LG(j)=final_xatmin(1);
        y_LG(j)=Y_LG(j)./(qR^(-1./gama));

        fLvec1(j)=final_xatmin(2);

    end

end

```

```

%-----
yc=Yc./(qR^(-1./gama));
y_trip=Y_trip./(qR^(-1./gama));

%*****
% plotting phase diagram in coordonates
(eta,y=phi/phi_over)
% where phi is the volume fraction of polystyrene in
the free volume
%*****
*****

figure('color',[1 1 1]);
%---- Solid Liquid -----

plot(fs,y_LS,'r.');
```

hold on;

```
plot(fLeq,y_LS,'b.');
```

hold on;

```
if (abs(fL2triple-fL1triple)>0.001)
  %---- Liquid Gas -----
  plot(fLvec1,y_LG,'r.','Linewidth',2);hold on;
  plot(fLvec2,y_LG,'b.','Linewidth',2);hold on;

  plot([0. 1.6],[y_trip y_trip],'k:');
```

hold on;

```
plot([fL1triple fL1triple],[0 y_trip],'k:');
```

hold on;

```
plot([fL2triple fL2triple],[0 y_trip],'k:');
```

hold on;

```
plot([fs_trip fs_trip],[0 y_trip],'k:');
```

hold on;

```
plot([fcritical fcritical],[0. y_trip],'g:');
```

end

```
  xlabel('f');
  ylabel('y');
```

%*****

```
*****
% plotting phase diagram in coordonates
(eta,w=fi/phi_over)
% where fi is the "real" volume fraction of polysytrene
%*****
*****

[alphas]=cal_alpha_y(fs,qR,Y_LS);
[alphaLeq]=cal_alpha_y(fLeq,qR,Y_LS);

phi_LS=y_LS.*phi_over;
fi_LS_S=alphas.*phi_LS;
fi_LS_Leq=alphaLeq.*phi_LS;
```

```

%-----
-----
figure('color',[1 1 1]);
%---- Solid Liquid -----
plot(fs./(fs+1),fi_LS_S,'r.-','Linewidth',2);hold on;
plot(fLeq./(fLeq+1),fi_LS_Leq,'b.','Linewidth',2);hold
on;

if (abs(fL2triple-fL1triple)>0.001) % If there is
triple point

    %---- Liquid Gas -----
    etaLvec1=fLvec1./(1+fLvec1);
    etaLvec2=fLvec2./(1+fLvec2);

    [alphaG]=cal_alpha_y(fLvec1,qR,Y_LG);
    [alphaL]=cal_alpha_y(fLvec2,qR,Y_LG);

    phi_LG=y_LG.*phi_over;
    fi_LG_G=alphaG.*phi_LG;
    fi_LG_L=alphaL.*phi_LG;

    %---- LG TIE LINE CALCULATION ---
    nf=1000;

    for j=1:length(etaLvec1)
        dV=(etaLvec2(j)-etaLvec1(j))/nf;
        V=etaLvec1(j):dV:etaLvec2(j);
        eta_LG_tie_line(:,j)=V;
        P(:,j)=polyfit([etaLvec1(j) etaLvec2(j)],[fi_LG_G(j)
fi_LG_L(j)],1);

        fi_LG_tie_line(:,j)=P(1,j)*eta_LG_tie_line(:,j)+P(2,j);
    end

%-----

[alphaL1triple]=cal_alpha_y(fL1triple,qR,Y_trip);
[alphaL2triple]=cal_alpha_y(fL2triple,qR,Y_trip);
[alphaStriple]=cal_alpha_y(fs_trip,qR,Y_trip);
[alphacritical]=cal_alpha_y(fcritical,qR,Yc);

```

```

phi_L1triple=y_trip*phi_over;
fi_L1triple=alphaL1triple*phi_L1triple;

phi_L2triple=y_trip*phi_over;
fi_L2triple=alphaL2triple*phi_L2triple;

phi_Striple=y_trip*phi_over;
fi_Striple=alphaStriple*phi_Striple;

phi_crit=yc*phi_over;
fi_critical=alphacritical*phi_crit;

plot(etaLvec1,fi_LG_G,'r.-','LineWidth',2);hold on;
plot(etaLvec2,fi_LG_L,'b.-','LineWidth',2);hold on;

plot([fL1triple./(fL1triple+1)
fL2triple./(fL2triple+1) fs_trip./...
(fs_trip+1)
fL1triple./(fL1triple+1)],[fi_L1triple fi_L2triple...
fi_Striple fi_L1triple],'k','LineWidth',2);hold
on;

plot([fLeq(1:3)./(fLeq(1:3)+1)
fL2triple./(fL2triple+1)],...
[fi_LS_Leq(1:3) fi_L2triple],'b.-
','LineWidth',2);hold on;

end

hold on;

for j=1:10:length(etaLvec1)
plot([etaLvec1(j) etaLvec2(j)],[fi_LG_G(j)
fi_LG_L(j)],'k:');hold on
end

% plot experimental phase diagram:

Experimental_phase_diagram_final_MW390000_fraction_Nov

plot(fcritical./(fcritical+1),fi_critical,'kp','Markers
ize'...
,12,'LineWidth',2.);hold on;

```

```

set(gca,'FontSize',16)

xlabel('\eta^*', 'FontSize',16);
ylabel('\it{\Phi}  ', 'FontSize',16);
xlim([0 0.2]);
ylim([0 0.06]);

%=====
% plotting phase diagram in coononates
(eta,w=fi/phi_over)
%-----
-----

figure('color',[1 1 1]);
%---- Solid Liquid -----
plot(fs./(fs+1),fi_LS_S/phi_over,'r. ');hold on;
plot(fLeq./(fLeq+1),fi_LS_Leq/phi_over,'b. ');hold on;

if (abs(fL2triple-fL1triple)>0.001) % If there is
triple point

%---- Liquid Gas -----
etaLvec1=fLvec1./(1+fLvec1);
etaLvec2=fLvec2./(1+fLvec2);

[alphaG]=cal_alpha_y(fLvec1,qR,Y_LG);
[alphaL]=cal_alpha_y(fLvec2,qR,Y_LG);

phi_LG=y_LG.*phi_over;
fi_LG_G=alphaG.*phi_LG;
fi_LG_L=alphaL.*phi_LG;

[alphaL1triple]=cal_alpha_y(fL1triple,qR,Y_trip);
[alphaL2triple]=cal_alpha_y(fL2triple,qR,Y_trip);
[alphaStriple]=cal_alpha_y(fs_trip,qR,Y_trip);
[alphacritical]=cal_alpha_y(fcritical,qR,Yc);

phi_L1triple=y_trip*phi_over;
fi_L1triple=alphaL1triple*phi_L1triple;

phi_L2triple=y_trip*phi_over;
fi_L2triple=alphaL2triple*phi_L2triple;

```

```

phi_Striple=y_trip*phi_over;
fi_Striple=alphaStriple*phi_Striple;

phi_crit=yc*phi_over;
fi_critical=alphacritical*phi_crit;

    plot(etaLvec1,fi_LG_G/phi_over,'r.');
```

hold on;

```

    plot(etaLvec2,fi_LG_L/phi_over,'b.');
```

hold on;

```

    plot([fL1triple./(fL1triple+1)
fL2triple./(fL2triple+1) ...
        fs_trip./(fs_trip+1)
fL1triple./(fL1triple+1)],...
        [fi_L1triple/phi_over fi_L2triple/phi_over
fi_Striple/phi_over...
        fi_L1triple/phi_over],'k','LineWidth',2);
```

hold on;

end

```

    xlabel('\eta^*', 'FontSize', 16);
    ylabel('\y_i', 'FontSize', 16);

    eta_critical=(fcritical/(fcritical+1))
```

function [Obj]=Obj_triple_integr(vec,qR,fcritical)

```

Y=vec(1);
fs=vec(2);
fL1=vec(3);
fL2=vec(4);

[pvs mus]=cal_pv_mu(Y,fs,qR,1);
[pvL1 muL1]=cal_pv_mu(Y,fL1,qR,0);
[pvL2 muL2]=cal_pv_mu(Y,fL2,qR,0);

Obj=abs((pvs-pvL1)/pvL1)+abs((pvs-pvL2)/pvL2)+abs((mus-
muL2)/muL2)+abs((mus-muL1)/muL1);
```

Return

```

function [Obj]=Obj_LS_integr(vec,fs,qR)

Y=vec(1);
fL1=vec(2);

[pvs mus]=cal_pv_mu(Y,fs,qR,1);
[pvL1 muL1]=cal_pv_mu(Y,fL1,qR,0);

Obj=abs((pvs-pvL1)/pvL1)+abs((mus-muL1)/muL1);

Return

function [pv mu]=cal_pv_mu(Y,f,qR,flag)

[mu0,pv0]=f_mupv0_int(f,flag);
YY=0:0.001*Y:Y;
myfunc_pv =fun_pvp(YY,f,qR);
integral_pv= trapz(YY,myfunc_pv);
pv=pv0+integral_pv;
myfunc_mu =fun_mup(YY,f,qR);
integral_mu=trapz(YY,myfunc_mu);
mu=mu0+integral_mu;

return

function [Obj]=Obj_LL_integr(vec,fL2,qR)
Y=vec(1);
fL1=vec(2);

[pvL1 muL1]=cal_pv_mu(Y,fL1,qR,0);
[pvL2 muL2]=cal_pv_mu(Y,fL2,qR,0);

Obj=abs((pvL2-pvL1)/pvL1)+abs((muL2-muL1)/muL1);

return

```

```

function [alpha]=cal_alpha_y(f,qR,Y)

c1=3.95;
gama=0.77;

q=0.865*((qR.^(-2.))+c1*(Y.^(2*gama))).^(-0.44));

A=3*q+3*(q.^2)+(q.^3);
B=3*(q.^2).*(q+(3/2));
C=3*(q.^3);
Q=A.*f+B.*(f.^2)+C.*(f.^3);

eta=(f./(1+f));
beta=exp(-Q);
alpha=(1.-eta).*beta;

return

```